Master Thesis

Influence of jointing and joint properties on blast fragmentation in model scale blasting

Ilke Alp Özer

Chair of Mining Engineering and Mineral Economics
Department Mineral Resources and Petroleum Engineering
Montanuniversitaet Leoben

A-8700 LEOBEN, Franz Josef Straße 18
Phone: +43/(0)3842-402-2001
Fax: +43/(0)3842-402-2002
bergbau@unileoben.ac.at

DECLARATION OF AUTHORSHIP

„I declare in lieu of oath that this thesis is entirely my own work except where otherwise indicated. The presence of quoted or paraphrased material has been clearly signaled and all sources have been referred. The thesis has not been submitted for a degree at any other institution and has not been published yet.”

PREFACE, DEDICATION, ACKNOWLEDGEMENT

Firstly, I would like to express my thanks to Prof. Carsten Drebenstedt, Prof. Peter Moser for giving me this opportunity to study such a program and their interest. Furthermore I would like to thank all the Professors who were involved in the AMRD master program at TU Freiberg, National Mining University Ukraine, and Montanuniversität Leoben.

I owe a debt of great gratitude to Prof. Finn Ouchterlony for his great contribution to this thesis as well as his sharing of valuable knowledge and I would like to thank him for his mentoring, advices and corrections in this thesis.

I also acknowledge to Peter Schimek and Radoslava Ivanova for their help and contribution.

Finally, I want to say my thanks to colleagues Orhan Altürk and Jonas Hyldahl for their great effort in the work behind this thesis and I would like to mention them additionally in the name of the times we worked together.

ABSTRACT

The purpose of this project is to observe how the joints affect rock fragmentation. In order to see the influence of the joints, the properties of the mortar blocks used in the testing were kept similar as well as delay times, explosives, detonators but not the joint families in the blocks.

In order to succeed, different types of jointed lab-scale blocks were prepared by Jonas Hyldahl. These blocks were measured, weighed and volumes were calculated. The hole lengths and widths, and the P-S wave speeds of the blocks were measured.

The blocks were blasted as 3 single rows under the similar circumstances. Right after blasting the rows, photographs were taken in order to make roughness calculations in Blast Matrix by Orhan Altürk. After the each row was blasted, the fragments and dust were carefully collected into the buckets for sieving tests in the laboratory. The remaining parts of the blocks which were left after blasting were then extracted carefully and sliced into 4 equal parts. These slices were subjected to dye penetrants to make the cracks on the slice faces visible. Afterwards, the slice faces were photographed (the most suitable upper or lower faces were always chosen). These photographs were used for crack detection and AutoCAD 3D modelling.

In the modelling sequence, the crack families were identified and cracks were counted with the help of AutoCAD. The data of the crack families were used for comparison and analysis with statistical methods. Outputs of the analysis were interpreted in terms of if joints possibly influence the fragmentation.

In addition, the sieving data was also analyzed, the K_{30}, K_{50} and K_{80} fragment sizes of the different jointed blocks were compared and graphed.

Results show that, different crack families occur in the jointed blocks and in some cases these cracks lead to large breakage behind the line of drill holes in the blocks. On the JS1, JS2 and JS4 blocks, these cracks occur at the end of the joints and form a bow shape between joints. On the other hand, in JS3 blocks these joint related cracks were following a path from the borehole to the end of the joint.

Furthermore, the obtained K_{30}, K_{50} and K_{80} results show that the fragmentation of the jointed blocks is finer than the fragmentation of the reference blocks.

TABLE OF CONTENTS

1. INTRODUCTION

Improvements in blasting, determining the best rock fragmentation with the lowest costs is essential for the sake of the mining sector and others involved in the blasting process. Since every blast has its own properties like rock properties, used material and amount, blasting pattern, delay times and many other properties, making full scale tests are too hard, too time consuming and too expensive. Model scale tests might eliminate most of the disadvantages while giving an opportunity to measure the effects of a single variable by holding other variables stable.

At the Chair of Mining Engineering, model scale blasts have been made by dal Farra (2012), Morros (2013), Navarro (2014), Schimek (2015) and Ivanova (2015). The purpose of their work was to determine effects of delay times or drilling errors on rock fragmentation, research of the crack families and interpretation the results obtained after blasting to improve the efficiency of rock blasting.

Even though different variables were tested, their works were following the same procedure. After the first row of the block blasted, fragments were collected to determine sieving parameters and sieving curves.

The following part after the collection of blasted particles, is the detection of cracks with surface analysis which is done both observing and photographing the surface and having slices of the post blasting block remains to observe what kind of cracks occurred inside the block after blasting by using photographs in cooperation with different computer programs.

In our work, we carried out model scale blasts with the purpose of determination of influence of pre-made joints on rock fragmentation by using a similar methodology.

Hyldahl (2015) focused on building the model specimens with different jointing and analyzing the resulting fragmentation.

My aim was to work on crack detection, characterization and distinguishing the crack families.

Orhan Altürks´ main focus was exterior blast damage and surface roughness analysis with Blast Matrix and stereophotography.

2. LITERATURE STUDY

2.1 Rock Fragmentation

All of the processes in mining are somehow related to the rock fragmentation, so that it is essential to assess the fragmentation behavior of the rocks in order to make the processes describable, controllable. This will hopefully lead to a cost efficient production, side effect reductions, and process improvements.

It needs to be considered that, there is no really reliable method that assesses the efficiency of mechanical rock breakage and blasting.

The basics of rock breakage is to exceed the rock strength with induced stresses by blasting or mechanical methods. This leads to rock fragmentation.

In the mining industry, it is very important to have optimum fragmentation. When we say optimum fragmentation, it generally means to:

- Minimize oversize boulders (less secondary breakage)
- Minimize production of very fine materials
- Maximize lump-pellet products
- Obtain suitable particle sizes to ensure efficient excavation and loading

The other term issue to be discussed is how to quantify the rock fragmentation.

A commonly used method to quantify the rock fragmentation is to use percentile passing fragment sizes which obtained from the fragments that pass through certain sieves. These numbers are mostly indicated with K_{30}-K_{50}-K_{80}. When we have a high value, this implies that we have a coarse fragmentation. When we have low value, it means that we have a fine fragmentation.

K_{30} represents the screen size which the 30% of the loose rock can pass after screening process is done. K_{50} and K_{80} represent 50% and 80% in following order.

A representative Grain-Size distribution can be seen in Figure 2-1.

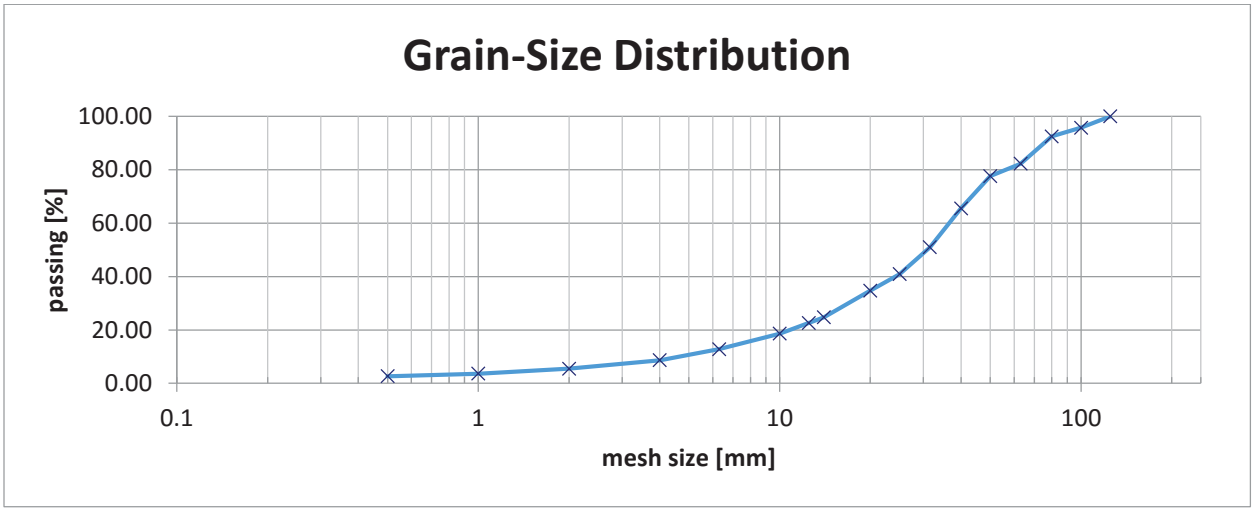

Figure 2-1 A representative grain-size distribution curve

To have the optimum fragmentation, it is essential to know the effects of different factors for the rock fragmentation.

2.2 Parameters Influencing Rock Fragmentation

To predict the fragmentation behavior, there are three general groups of factors which should be considered;

1) Geological Conditions
   a) Rock and Rock Mass Properties
      i) Compressive Strength of the rock
      ii) Tensile Strength of the rock
      iii) Density
      iv) Young`s modulus
2) Machine Parameters
   a) Machine Properties
   b) Explosive Properties
   c) Operational Characteristics
3) Test Methods
   a) Strength of the rock
   b) Elastic and Plastic Properties of the rock
   c) Abrasivity of the tools
   d) Breakability of the rock

2.3 Rock Fragmentation – Fragmentation Prediction Methods

Figure 2-2 Rock blasting (www.mining-technology.com)

There are many evaluation methods, attempting to predict the rock fragmentation using different parameters. As indicated on the previous pages, calculation of K_{50} (median fragment size) is one of the most common ways to evaluate fragmentation. There are a few ways to evaluate K_{50} with different evaluation models using different parameters and equations.

The Kuz-Ram model and Swebrec functions are two different methods to estimate K_{50} which will be explained in the next section.

2.3.1 Kuz-Ram Model

Introduced by Cunningham (1983), the Kuz-Ram model is the most used fragmentation model and it is based on Rosin-Rammler distribution. It has a Russian origin (Kuznetsov 1973). It was first presented at the 1983 Lulea Conference on Fragmentation by Blasting. It is a set of empirical formulas which includes the Kuznetsov and Rosin-Rammler equations. It also includes the exponent of uniformity “n”, which is needed in the Rosin-Rammler equation.

The Kuz-Ram model expresses that, a better fragmentation requires higher energy and occurs more easily in weaker rock types for smaller holes diameters.

To obtain a more regular sizing, there should be a uniform distribution of explosives in the rock body, a smaller burdens and larger spacing/burden ratio.

Some problems of the blasting models are

- Defining the related rock properties
- Selection of a convenient explosive performance index
- Determination of actual blasting fragmentation

Ouchterlony & Moser (2013-2014) gave the equations of the Kuz-Ram Model as;

$$A = 0,06 \cdot (RMD + (JF) + RDI + HF)$$

Equation 1 Rock mass factor

A= Rock mass factor ranging between 0.8 -21
RMD= rock mass description (10 if powdery, JF if vertically jointed, 50 if massive rock)
JF = Joint Factor = JPS+ JPA
JPS = Joint Plane Spacing (10 if mean joint spacing S_j<0.1m, 20 if 0,1m<S_j<oversize x_o, 50 if S_j>x_o)
JPA= Joint Plane Angle (varying from 20 for dip from the face to 40 for dip into the face)
RDI = Rock Density Influence
HF= Hardness factor

Rosin-Rammler Equation

The symbols x and K basically denote the same quantity. K, with or without subscript, refers to mesh sizes of actual sieves and interpolated values like K_{50} etc. The symbol x, with or without subscript, refers to continuous sieve size distribution functions.

$$P(x) = 1 - e^{-ln2 \cdot (x/x_{50})^n} = 1 - 2^{-(x/x_{50})^n}$$

Equation 2 Rosin Rammler P(x) equation

Where the 50% passing mesh size

$$\mathrm{x}_{50} = \mathrm{A} \cdot \mathrm{Q}_e{}^{0.167} \cdot \frac{\left(\frac{115}{S_{ANFO}}\right)^{\frac{19}{30}}}{q^{0.8}}$$

Equation 3 Rosin Rammler x_{50} equation

where

Q_e =total charge weight per borehole [kg]
S_{ANFO}= weight strength, 115 for TNT
q = specific charge of ANFO [kg/m^3]

The uniformity index in the Rosin Rammler equation is calculated as;

$$\mathrm{n} = (2,2 - 0,014 \cdot \mathrm{B}/\emptyset) \cdot (1 - \mathrm{SD}/\mathrm{B}) \cdot \sqrt{[(1 + \mathrm{S}/\mathrm{B})/2]} \cdot [|\mathrm{L}_b - \mathrm{L}_c|/\mathrm{L}_{tot} + 0,1]^{0,1} \cdot (\mathrm{L}_{tot}/\mathrm{H})$$

Equation 4 Uniformity Index

where

B = burden [m]
S = spacing [m]
Ø = drill-hole diameter [m]
L_b = length of bottom charge [m]
L_c = length of column charge [m]
L_{tot} = total charge length [m]

H = bench height [m]
SD = standard deviation of drilling accuracy [m]

Disadvantages of Kuz-Ram

The Kuz-Ram is not complete because;

- It will not predict true amount of fines.
- It is useless for large fragment sizes.
- It doesn`t reckon the influence of velocity of detonation, initiation delay times or initiation pattern.

2.3.2 Swebrec Function

Regarding the disadvantages of Kuz-Ram model, there is another fragment size distribution called “Swebrec Function” which covers the particles sizes between 0,5 mm and 500 mm and which also has boulder size involved. It reproduces fines well down to 1 mm. It has 2 obvious parameters that are x_{50}- x_{max}. The Swebrec function (see Equation 5) can also be extended to include the ultrafine particles range. (Ouchterlony, 2014).

Its advantages are listed as;

- Prediction of fines from coarse range data.
- Prediction of coarse fractions from the fines sample.
- Extended measuring range from image analysis.
- Prediction for blast fragmentation.

Swebrec Function

$$P(x) = \frac{1}{1 + \left[\frac{\ln(\frac{x_{max}}{x})}{\ln(x_{max}/x_{50}}\right]^{b}}$$

Equation 5 Swebrec function

Here according to Ouchterlony (2014)

$$b = 0.5 \cdot {x_{50}}^{0.25} \cdot \ln(\frac{x_{max}}{x_{50}})$$

Equation 6 Swebrec function, calculation of the parameter “b”

2.4 Crack Types, Joints and Faults

In order to understand the crack behavior, it is essential to understand basic differences between the geological terms.

In geology, cracks and joints are generally considered under the name of fractures or discontinuities. In order to simplify, it can be said that cracks and joints are spaces or gaps that occur in the rock bodies. However they have characteristics that set them apart from one another.

The most significant difference between a joint and a fault is the size of the crack. Joints are narrower compared to the faults. Joints can be observed in almost every kind of rock formation. They are mostly too narrow to be observed from a distance unlike faults, which are much wider and can extend for much longer distances.

Rather than the size difference of joints and faults, it is better to categorize the displacement that resulted in movement in or of the side rocks to judge if the crack type is a joint or a fault. Joints have very little or no associated displacement in the side rock for they usually don't entirely separate the rock formations.

Faults are different because they tend to include lateral movement caused by tectonic forces, which is why they occur through cuts between rock formations.

Joints are formed in a rock mass which is stretched to its breaking point.

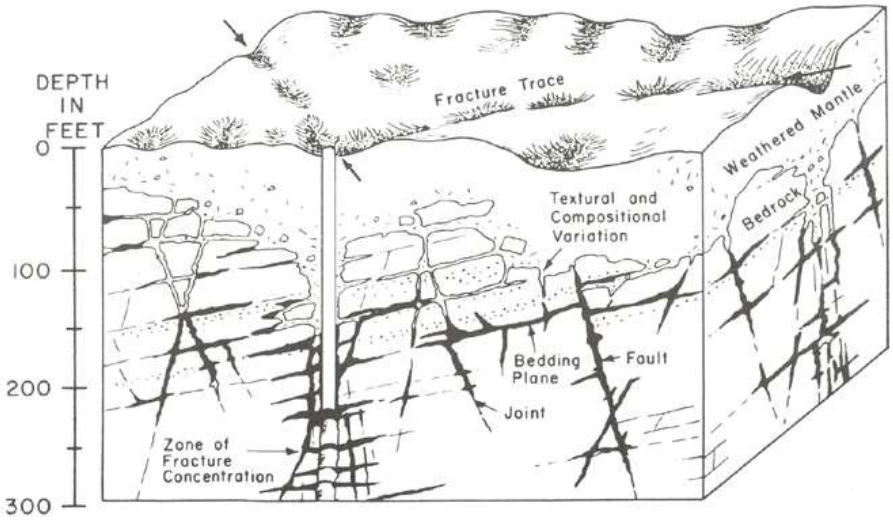

Figure 2-3 Joint formations in earth crust (Lattman and Parizek 1964)

According to Hariri (2011), fractures can be identified as three types which are;

a) Mode 1 fractures (joints) which are called extensional fractures and they are formed by opening with no displacement parallel to the fracture surface,
b) Mode 2 shear fractures,
c) Mode 3 shear fractures. Type b and c are the faults which are formed like fractures, type b is called strike-slip and type c is dip-slip.

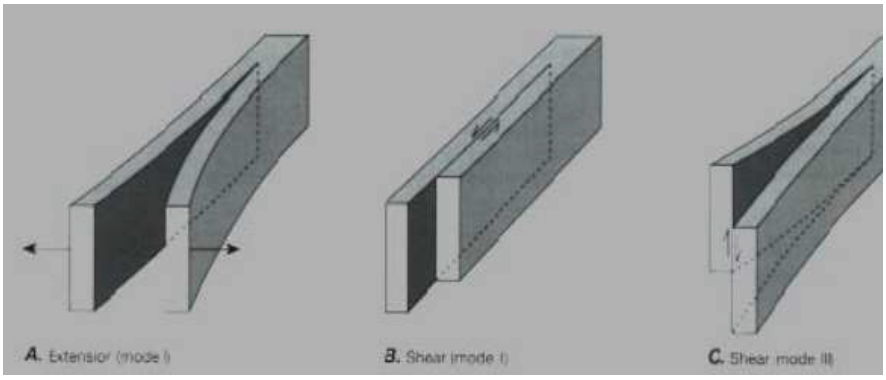

Figure 2-4 Fracture Types

As Hariri (2011) indicated, the types of joints can be classified in 4 groups

1. Systematic joints: They have a subparallel orientation and regular spacing.
2. Joint sets: Joints that share a similar orientation in the same area.
3. Joint system: Two or more joint sets in the same area
4. Nonsystematic joints: Joints that don't share a common orientation and that have highly curved and irregular fracture surfaces. They occur in most areas but are not easily related to the recognizable stresses.

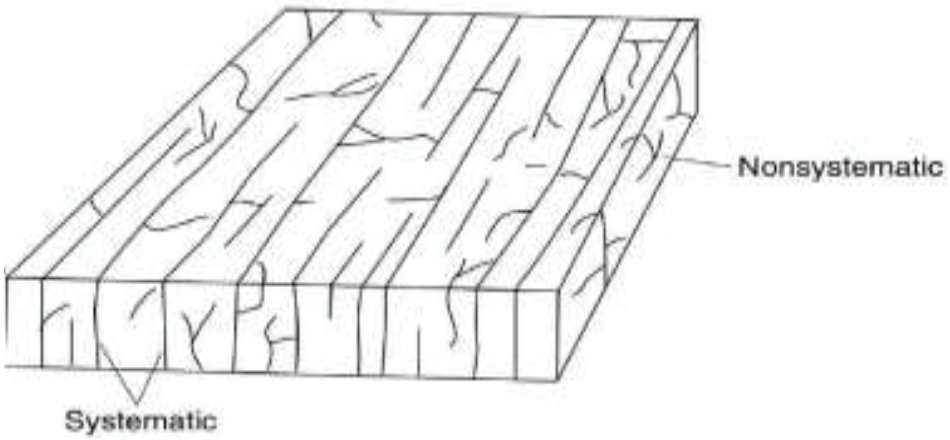

Figure 2-5 Systematic and nonsystematic cracks (Hariri 2011)

The crack initiation and propagation is explained at ANNEX I.

2.5 Crack Detection Methods

Structures and objects that are subjected to stresses may develop cracks. These cracks can develop and potentially lead to failure. According to Wishaw (2001), the reasons for crack development can vary. Components working at high cyclic stress levels will suffer from cyclic fatigue and fail. In many cases this process aided by discontinuities at welds or inclusions.

The demand in the industry to inspect failures and cracks, started a technology branch commonly called as Non-Destructive Testing (NDT), setting it apart from the destructive materials testing. This also indicates that these testing methods do not damage the structural components.

There are different kinds of NDT methods used in industry.

2.5.1 NDT Methods

According to Güven (2015), there are five different common types of NDT methods used in industry. The most common methods of NDT are, Radiography(Nuclear Methods) (RT), Ultrasonics (UT), Dye Penetrant Method (DPI), Magnetic Particle Inspection (MPI) and Eddy Current Testing (ECT).

2.5.1.1 Radiography

Alekseychuk (2006) explained the radiography method as; *"This is very analogous to the medical X-ray technology that we are all familiar with. A beam of radiation is released from a source point and transmitted through the object being inspected. An X-ray sensitive film on the other side records a single-plane image representing the varying densities of absorption of the radiation."*

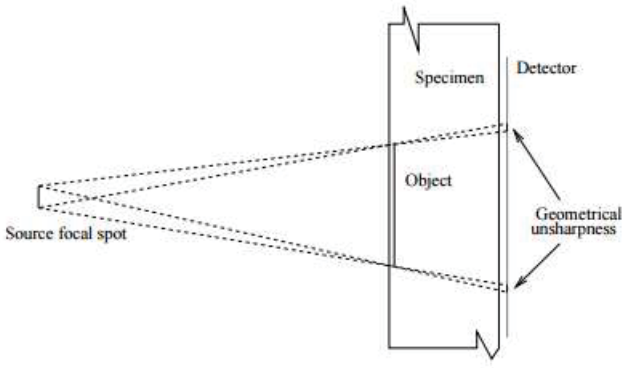

Figure 2-6 Radiography

Common applications are:

• Pipeline weld quality inspections.

• Castings.

• Checking inaccessible components.

• Conveyor belt internal condition.

The advantages of the system are that it can produce a permanent record of the inspection for future reference if required. It can be reasonably automated and has some real-time

capabilities. Disadvantages are that there are safety issues, the equipment is cumbersome, it requires multiple operators, a film processing facility is usually required before results can be seen, and it is not good at defining the presence or dimensions of small cracks.

2.5.1.2 Ultrasonics (UT)

Wishaw (2001) explained the Ultrasonics method as "*High frequency sound waves (typically around 1 MHz) have the ability to transmit through solids and liquids and the associated technologies are known as 'ultrasonics'. A very useful feature is that any discontinuity or change of density produces a reflection and this can be turned into an 'image' by measuring the time between transmission of an ultrasonic pulse and the various return signals received. The equipment measures the time delays in nanoseconds!*

The method is analogous to the 'echo-sounder' used on boats to display reflections from anything in the water (fish) and the bottom. The UT method is very commonly used for precise crack detection in relatively small items. Note that it cannot be used to detect cracks on the surface – a minimum depth of around 3 mm is required to get within the 'focal length' of the sensor.

Transmission losses typically limit its use to a transmission path of around 300 mm. Most portable equipment displays an image from which the operator is able to determine a finding. Some newer equipment is able to digitize the image for computer analysis.

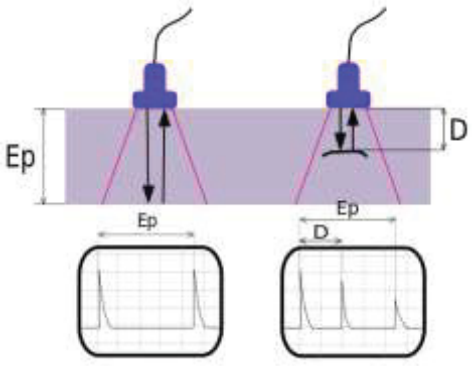

Figure 2-7 Ultrasonic Device

A significant disadvantage is that there is quite a degree of operator skill required and consequently the industry requires formal qualifications for UT operators. There are also some limitations in its ability to detect certain kinds of cracks but a good operator will be able to indicate the requirement for other techniques to be used.

A variation on the UT method is the use of the technology to measure wall thickness of tanks, pipes and the like. This is a very simple adaption of the technique and requires very little operator skill."

Advantages of UT

1. High penetrating power, which allows of flaws detection of flows deep in the part.
2. High sensitivity, permitting the detection of extremely small cracks and flows.
3. Only two nonparallel surfaces need to be accessible.

4. Greater accuracy than other nondestructive methods in determining the depth of internal cracks and the thickness of parts with parallel surfaces.
5. Some capability of estimating the size, orientation, shape and nature of defects.
6. Non-hazardous to operations or to nearby personnel and has no effect on equipment and materials in the vicinity.
7. Capable of portable or highly automated operation.

Disadvantages of UT

1. Manual operation requires careful attention by experienced technicians. The transducers alert to both normal structure of some materials, tolerable anomalies of other specimens (both termed “noise”) and to faults therein severe enough to compromise specimen integrity. These signals must be distinguished by a skilled technician, possibly requiring follow up with other nondestructive testing methods. (McNulty 1962)
2. Extensive technical knowledge is required for the development of inspection procedures.
3. Parts that are rough, irregular in shape, very small or thin, or not homogeneous are difficult to inspect.
4. Surface must be prepared by cleaning and removing loose scale, paint, etc., although paint that is properly bonded to a surface need not be removed.
5. Couplants are needed to provide effective transfer of ultrasonic wave energy between transducers and parts being inspected unless a non-contact technique is used. Non-contact techniques include Laser and Electro Magnetic Acoustic Transducers.
6. Inspected items must be water resistant, when using water based couplants that do not contain rust inhibitors.

2.5.1.3 Dye Penetrant Method (DPI)

The Dye Penetrant method was used by Navarro (2014), and Schimek (2015) as well as in this research for it is the most suitable and cost effective method due to the laboratory and sample conditions. This method can sometimes be called as liquid penetrant inspection (LPI) or penetrant testing (PT), and it is used to locate surface-breaking defects in all non-porous materials. The penetrant may be applied to all non-ferrous materials and ferrous materials, although for ferrous components magnetic-particle inspection is often used instead for its subsurface detection capability. LPI is used to detect casting, forging and welding surface defects such as hairline cracks, surface porosity, leaks in new products, and fatigue cracks on in-service components.

Working Procedure of Dye Penetrant Inspection;

Pre-Cleaning

The surface that is going to be tested is cleaned from any dirt or from any kind of material that can keep the penetrant out of a defect. The aim of this step is to clean the surface near any defects, and free it out of contamination.

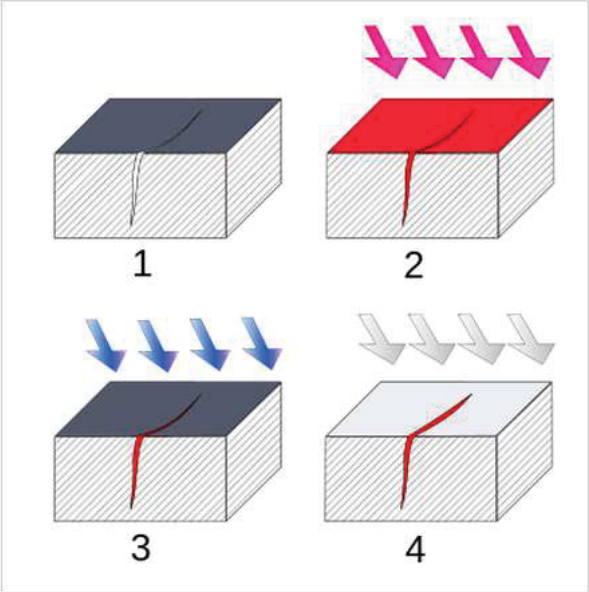

1. Section of material with a surface-breaking crack that is not visible to the naked eye.
2. Penetrant is applied to the surface.
3. Excess penetrant is removed.
4. Developer is applied, rendering the crack visible.

Figure 2-8 Penetrant application

Application of Penetrant

After cleaning of the surface is done, then the penetrant is applied to the item that is going to be tested. The penetrant is allowed some time (5 to 30 min, in our case it was 5 minutes) to flow and soak into the cracks. The dwell time depends on the penetrant being used and material being tested (Items with bigger cracks require more time).

Excessive Penetrant Cleaning

The excess penetrant is removed from the surface. In this test paper towels and napkins were suitable to use. In other cases water-washable, solvent-removable, lipophilic post-emulsifiable, or hydrophilic post-emulsifiable are the common choices. Emulsifiers represent the highest sensitivity level, and chemically interact with the oily penetrant to make it removable with a water spray. When using solvent remover and lint-free cloth it is important to not spray the solvent on the test surface directly, because this can remove the penetrant from the flaws. If excess penetrant is not properly removed, once the developer is applied, it may leave a background in the developed area that can mask indications or defects. In addition, this may also produce false indications therefore reducing the ability to do a proper inspection. Also, the removal of excessive penetrant is done towards one direction either vertically or horizontally as the case may be.

Developer Application

After excess penetrant has been removed, a white developer is applied to the sample. Several developer types are available, including: non-aqueous wet developer, dry powder, water-suspendable, and water-soluble. Choice of developer is governed by penetrant compatibility (one can't use water-soluble or -suspendable developer with water-washable penetrant), and by inspection conditions. When using non-aqueous wet developer (NAWD) or dry powder, the sample must be dried prior to application, while soluble and suspendable developers are applied with the part still wet from the previous step. NAWD is commercially available in aerosol spray cans, and may employ acetone, isopropyl alcohol, or a propellant that is a combination of the two. Developer should form a semi-transparent, even coating on the surface.

The developer draws penetrant from defects out onto the surface to form a visible indication, commonly known as bleed-out. Any areas that bleed out can indicate the location, orientation and possible types of defects on the surface. Interpreting the results and characterizing defects from the indications found may require some training and/or experience [the indication size is not the actual size of the defect.

Inspection

Inspection of the test surface should take place after 10- to 30-minute development time, depends of product kind. This time delay allows the blotting action to occur. The inspector may observe the sample for indication formation when using visible dye. It is also good practice to observe indications as they form because the characteristics of the bleed out are a significant part of interpretation characterization of flaws.

Post Cleaning

The test surface is often cleaned after inspection and recording of defects, especially if post-inspection coating processes are scheduled.

Advantages and Disadvantages of DPI;

According to Kohan (1997), DPI method is very fast and very cost effective. However, the detection is possible only for surface cracks. Clean and smooth surface are necessities for this method. Rough and porous surfaces will make the method application difficult and may cause false indications.

According to Rummel and Matzkanin (1996), another advantage is that, the method user doesn’t have to be heavily trained, although experience can be counted as an asset. Proper cleaning is necessary to assure that surface contaminants have been removed

and any defects present are clean and dry. Some cleaning methods have been shown to be detrimental to test sensitivity, so acid etching to remove metal smearing and re-open the defect may be necessary.

2.5.1.4 Magnetic Particle Inspection

This method is similar in application to the Dye Penetrant method however it gives more reliable results and is the most widely used in industry. In this method, magnetic featured ink or powder applied to the subject and then a powerful magnetic field is applied .If a crack or discontinuity exists on or near the surface, the magnetic featured ink fills that line. So that it will be suitable to inspect the cracks and discontinuities.

This technique is simple like the DPI method but there is more technique required than for Dye Penetrant. The surface must be cleaned well before the test and the method can only work on magnetic materials. A photo should be taken to make the inspection.

2.5.1.5 Eddy Current Test

Buckley (2015) explained the ECT as;

"Eddy-current testing (ECT) is one of many electromagnetic testing methods used in nondestructive testing (NDT) making use of electromagnetic induction to detect and characterize surface and sub-surface flaws and cracks in conductive materials.

In its most basic form, the single-element ECT probe and a coil of conductive wire are excited with an alternating electrical current. This wire coil produces an alternating magnetic field around itself in the direction ascertained by the right-hand rule. The magnetic field oscillates at the same frequency as the current running through the coil. When the coil approaches a conductive material, currents opposed to the ones in the coil are induced in the material.

Variations in the electrical conductivity and magnetic permeability of the test object, and the presence of defects causes a change in eddy current and a corresponding change in phase and amplitude that can be detected by measuring the impedance changes in the coil, which is a telltale sign of the presence of defects. This is the basis of standard (pancake coil) ECT.

ECT has a very wide range of applications. Because ECT is electrical in nature, it is limited to conductive material. There are also physical limits to generating eddy currents and depth of penetration."

3. TEST FIELD AND SET-UP

3.1 Test Place

The Blasting site of the Chair of Mining Engineering at MUL is located at the Styrian Erzberg. It was constructed as part of a master thesis work (Maierhofer 2011). In the test site, there is a yoke placed within the concrete walls with a purpose of letting the blast waves spread outside of the specimen.

Figure 3-1 Blast Site

Figure 3-2 Cemented block

The space between blast walls and yoke is filled with compacted sand which lets 70% of the blasting waves propagate into the surrounding rocks. As can be seen from the Figure 3-2 and Figure 3-3, the yoke has a place for smaller blocks to fit in. The testing blocks were grouted into this place with fast hardening cement from the sides and back to keep it stable and let the waves pass to the yoke. The fast hardening cement has similar material properties as the block material. The blocks were placed on a rubber mat to make their extraction easier and to prevent them from sliding during blasting.

Figure 3-3 Block installation and test specimens and procedure

The tests were carried out with 11 test blocks which were prepared by Hydahl (2015) for the master theses of Hyldahl, Altürk and Özer. The blocks had 4 different type of joint sets, and 3 reference blocks without any joints in them. Even though they have different joint sets, the mortar was mixed according to the same recipe.

The recipe is shown in the Table 3-1;

CONTENT	%
Quartz sand	31.71
Magnetite powder	29.65
Portland cement	25.62
Water	12.64
Glenium 51 (plasticizer)	0.25
Tributylphosfate (defoamer)	0.13

Table 3-1 Recipe of the blocks

The dimension of the blocks are shown in the Table 3-2;

Length L	**660 mm**
Width W	280 mm
Height H	210 mm

Table 3-2 Dimension of the blocks

The blocks were carrying 21 blast holes that had 10.5 mm diameter, 7 holes in each of 3 rows. The hole spacing is 95 mm and the burden length is 70 mm. The holes were made by inserting dowels during the pouring of the mortar and withdrawing them relatively soon.

The dimensions of the testing blocks used in this project were 660×280×210 mm (L×H×W) – the same as Johansson & Ouchterlony (2012).

The designs of the blocks which have been prepared by Hyldahl (2015) can be seen in the section 3.1.1.

3.1.1 Design of the Blocks

Reference Blocks

Reference blocks are given the acronym “Ref” in this report. They don’t have joint systems in them and they were made for comparison. Top, front and end views of the reference blocks are shown in the Figure 3-4 to Figure 3-6.

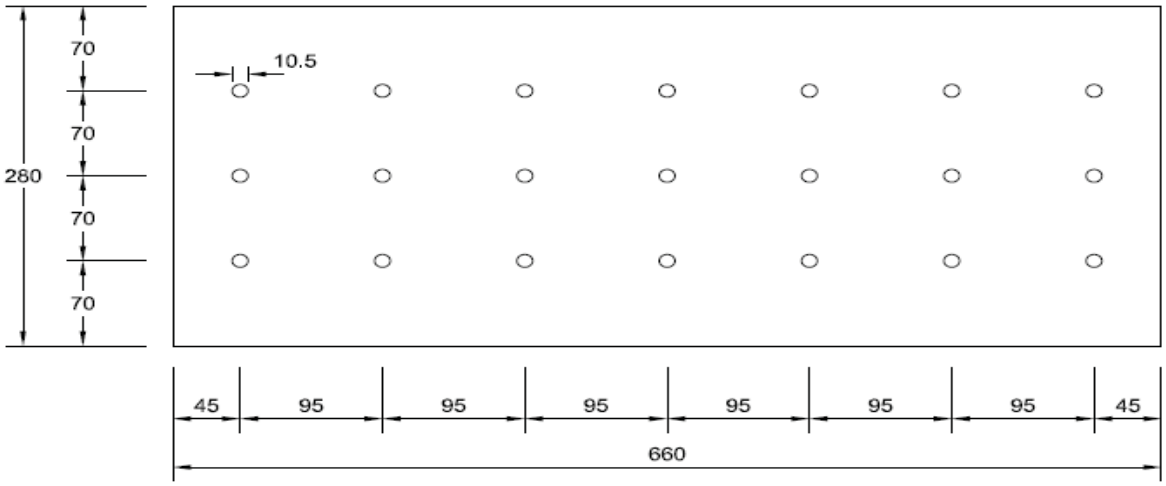

Figure 3-4 Top view of Reference blocks

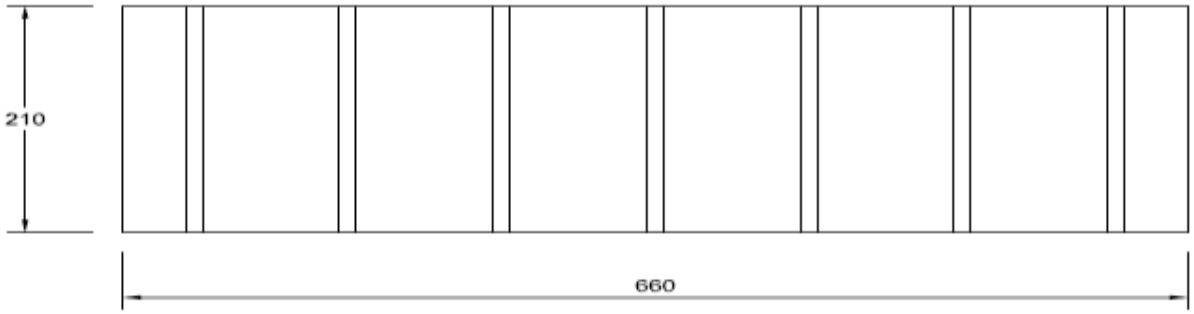

Figure 3-5 Front view of Reference blocks

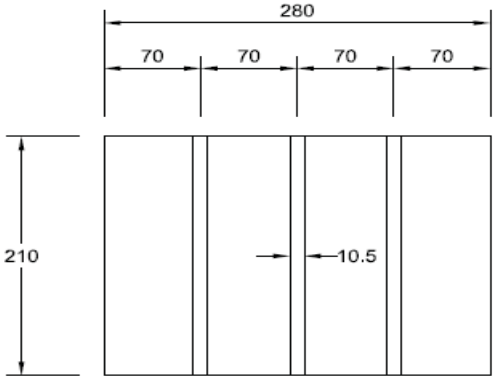

Figure 3-6 End view of Reference blocks

Joint System 1 blocks (JS1)

Joint System 1 blocks are denoted JS1 in our works. They have joints with dip 90° and strike 90°, i.e. perpendicular to the bench face. The distance between two joints is 95 mm. As can be seen from the Figure 3-7, 25 mm space is left between end of the joints and the edge of the test specimen. This 25 mm is required to avoid the block failure and separation during handling. Top, front and end views of JS1 blocks are shown in Figure 3-7 to Figure 3-8.

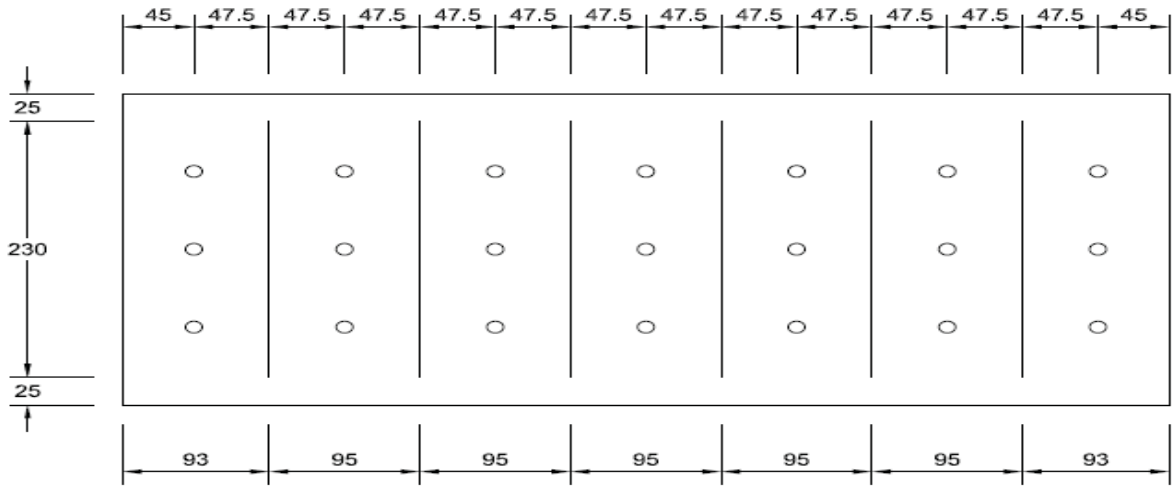

Figure 3-7 Top view of JS1 blocks

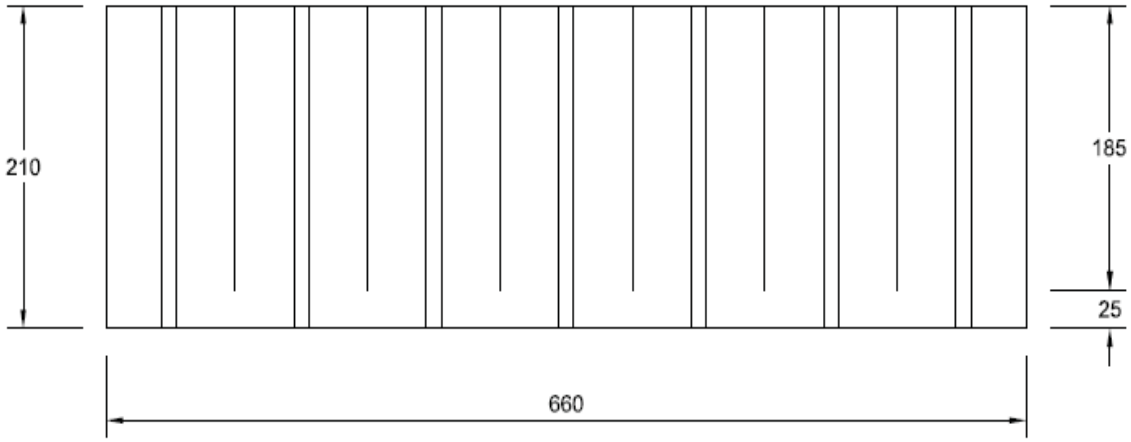

Figure 3-8 Front view of JS1 blocks

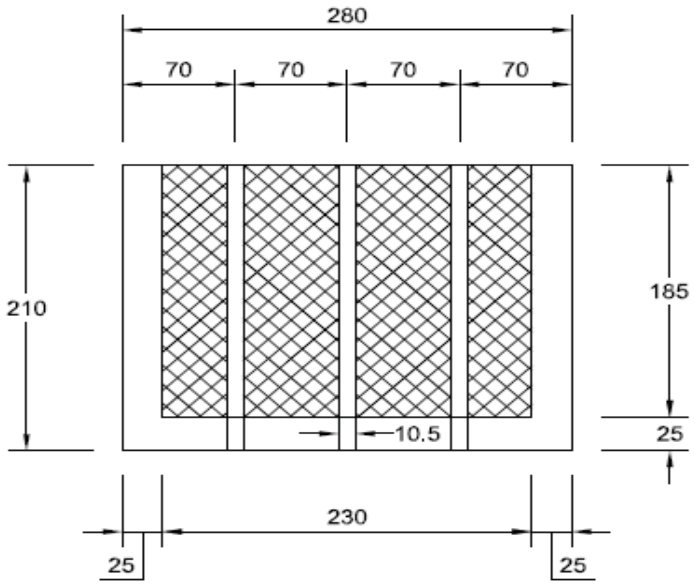

Figure 3-9 End view of JS1 blocks

Join System 2 Blocks (JS2)

Joint System 2 blocks are denoted JS2 blocks. They have joints dipping 90° and striking 90° just as the JS1 blocks. However the spacing between joints is half of that in the JS1 block, i.e. 47.5 mm. See top view in Figure 3-10.

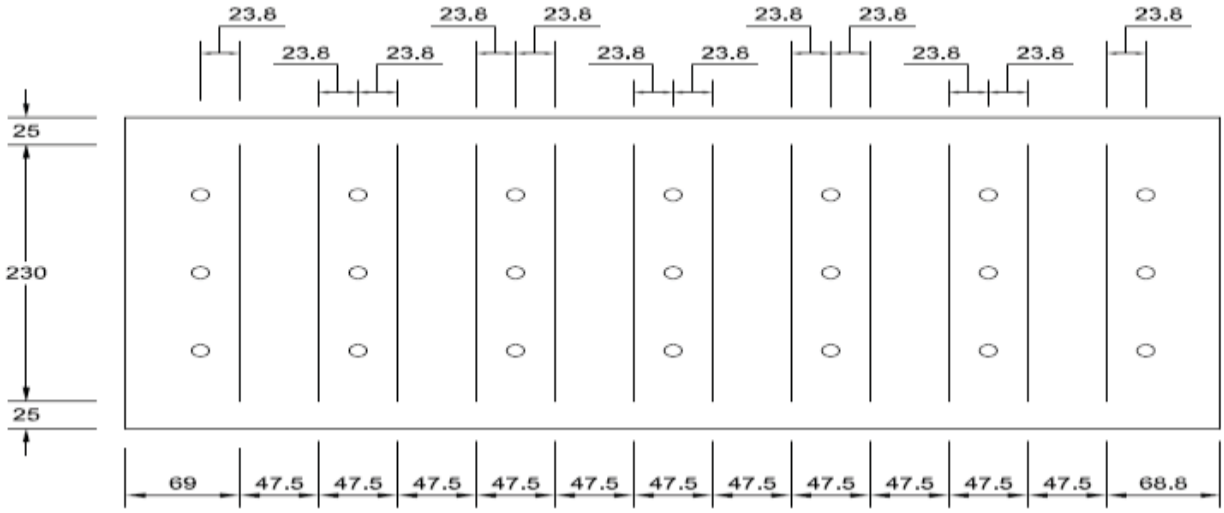

Figure 3-10 Top view of JS2 blocks

The distances between the joints and the holes are 23.8 mm unlike in the JS1 set blocks and the distance between two joints is 47.5 mm. The distance from the end of the joints to the back and front of the block is 25 mm in JS2 blocks. Influence of the smaller joint spacing is studied in the analysis part.

Join System 3 Blocks (JS3)

Joint System 3 blocks are denoted JS3 blocks. They have joints dipping 90° and striking 30°. The strike angle differs from the JS1 and JS2 blocks. The spacing between the joints is the same as for JS2, i.e. 47.5 mm. See top view in Figure 3-11.

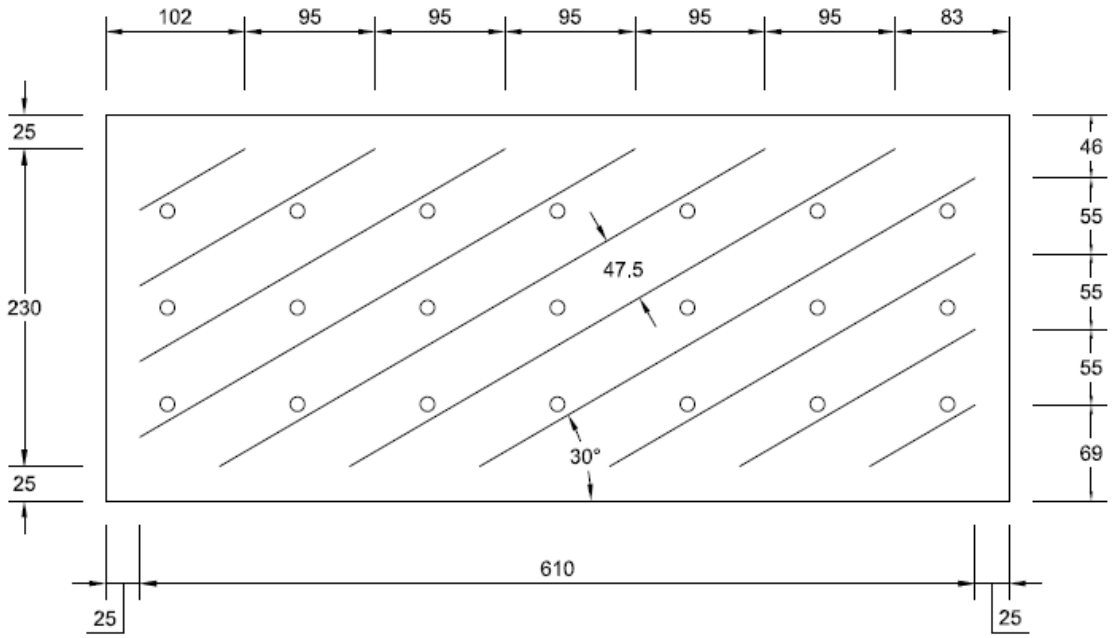

Figure 3-11 Top view of JS3 blocks

Join System 4 Blocks (JS4)

Joint System 4 blocks are denoted JS4 blocks. They have joints dipping 70° and striking 90°. These type of blocks were the only ones where the joints had a dip different than 90°. The spacing between the joints is 95×cos(20°) = 89 mm. Top and front views of the JS4 blocks are shown in Figure 3-12 to Figure 3-13.

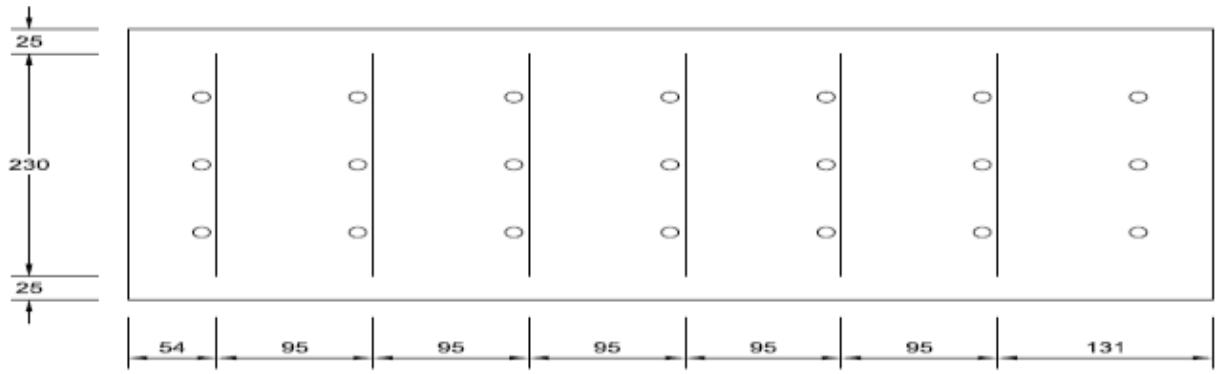

Figure 3-12 Top view of JS4 blocks

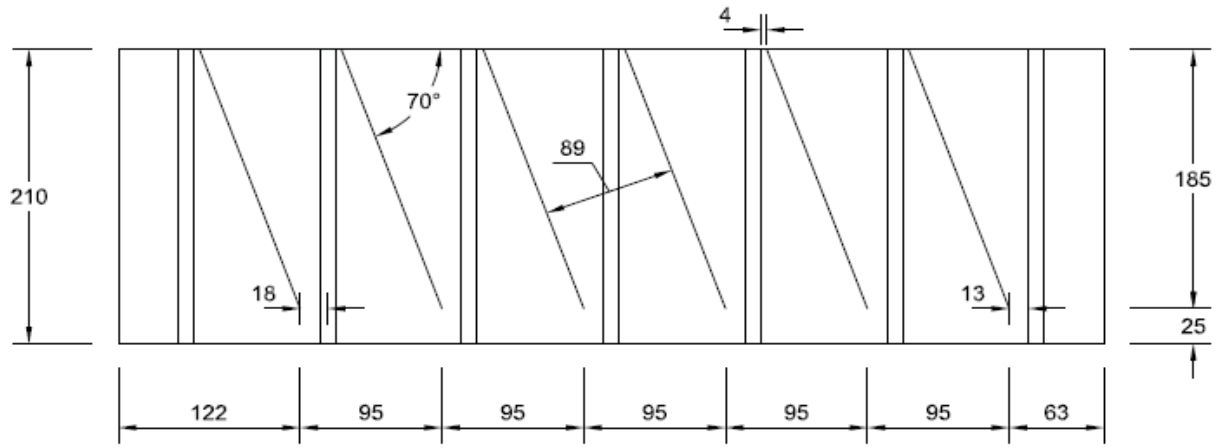

Figure 3-13 Front view of JS4 blocks

3.1.2 Properties of Blocks

Before starting the blasting process size, weight, P wave and S wave velocities of the blocks were measured.

3.1.2.1 Block Dimensions

The planned block dimensions were L×W×H= 660×280×210 mm, see Table 3-2. The measured values for the 11 blocks are given in Table 3-3 to Table 3-13.

To be sure about the dimensions, every axis (L, H, W) were measured from three points that has equal distances to each other. The mean size was used for calculation of volume. However it should be noted that drill hole volumes and weights were ignored because their influence on the final result was so low (0.5%- 0.1%) that they could be disregarded. Measurements of the blocks are shown at the Table 3-3 to Table 3-13.

JS1 Alpha				Mean(mm)
L(mm)	665	664	665	665
H(mm)	210	211	211	211
W(mm)	282	282	282	282
Weight(kg)	94			
Density(kg/m³)	2380			

Table 3-3 Properties of block JS1 Alpha

JS1 Beta				Mean(mm)
L(mm)	664	664	664	664
H(mm)	214	214	214	214
W(mm)	281	281	281	281
Weight(kg)	94			
Density(kg/m³)	2353			

Table 3-4 Properties of block JS1 Beta

JS1 Gamma				Mean(mm)
L(mm)	660	660	660	660
H(mm)	210	212	210	210
W(mm)	282	281	284	282
Weight(kg)	94.50			
Density(kg/m³)	2408			

Table 3-5 Properties of block JS1 Gamma

JS2 Beta				Mean(mm)
L(mm)	660	660	660	660
H(mm)	214	212	210	212
W(mm)	280	280	280	280
Weight(kg)	94.7			
Density(kg/m³)	2415			

Table 3-6 Properties of block JS2 Beta

JS3 Alpha				Mean(mm)
L(mm)	660	660	660	660
H(mm)	210	210	210	210
W(mm)	280	280	280	280
Weight(kg)	98.4			
Density(kg/m³)	2537			

Table 3-7 Properties of block JS3 Alpha

JS3 Beta				Mean(mm)
L(mm)	663	663	664	660
H(mm)	212	211	210	210
W(mm)	280	280	281	280
Weight(kg)	96.5			
Density(kg/m³)	2462			

Table 3-8 Properties of block JS3 Beta

JS4 Alpha				Mean(mm)
L(mm)	660	660	660	660
H(mm)	202	200	200	200
W(mm)	280	280	280	280
Weight(kg)	90.2			
Density(kg/m³)	2436			

Table 3-9 Properties of block JS4 Alpha

JS4 Beta				Mean(mm)
L(mm)	663	663	663	660
H(mm)	209	209	209	209
W(mm)	280	280	280	280
Weight(kg)	93.5			
Density(kg/m³)	2412			

Table 3-10 Properties of block JS4 Beta

Reference 1				Mean(mm)
L(mm)	663	664	661	663
H(mm)	214	214	214	212
W(mm)	282	282	282	282
Weight(kg)	94.1			
Density(kg/m³)	2353			

Table 3-11 Properties of block Reference 1

Reference 2				Mean(mm)
L(mm)	663	663	663	663
H(mm)	212	212	205	209
W(mm)	282	282	282	282
Weight(kg)	95.2			
Density(kg/m³)	2428			

Table 3-12 Properties of block Reference 2

Reference 3				Mean(mm)
L(mm)	660	660	660	660
H(mm)	208	208	210	209
W(mm)	284	282	283	283
Weight(kg)	94.5			
Density(kg/m³)	2424			

Table 3-13 Properties of block Reference 3

3.1.2.2 P and S Waves Measurements

After the size measurements were taken, the next step was the calculation of P and S wave measurements. A special equipment and a related computer program designed for seismic wave measurements were used. This device sends signals through the object using two probes. One is the transmitter while the other is the receiver.

In order to take the measurements, the first step was the application of a coupling gel on the probes. Then probes were held across each other for the first measurement. Afterwards, one probe rotated reversely while the other one was kept stable to take second measurement. The measurement points were chosen carefully to eliminate the problems and false results which may be caused from probe position errors. This work was done for each of the axes two times, to obtain more reliable results statistically.

The subsequent work was to choose best related data from the seismic graph which is drawn by the program.

The Table 3-14 shows the individual P-S wave measurements for the blocks.

Block Names		P- Waves	S-Waves	Block Names		P- Waves	S-Waves
JS1 Alpha	L	3408	1995	JS4 Alpha	L	3313	2205
	H	3068	2012		H	3098	2117
	W	3073	1968		W	3154	2221
JS1 Beta	L	3012	1917	JS4 Beta	L	3326	2169
	H	2823	1846		H	3354	2204
	W	2791	1959		W	3587	2173
JS2 Alpha	L	3171	2396	JS1 Gamma	L	3266	2139
	H	3075	2076		H	3367	2099
	W	3071	2063		W	3290	2057
JS2 Beta	L	3423	2139	Ref1	L	3025	1933
	H	3367	2099		H	3150	2059
	W	3290	2057		W	2886	1988
JS3 Alpha	L	3421	2237	Ref2	L	2980	2106
	H	3306	2189		H	2950	2044
	W	3407	2189		W	3141	1949
JS3 Beta	L	3143	2149	Ref3	L	3164	2205
	H	3176	2099		H	3112	2093
	W	3164	2147		W	3143	2099

Table 3-14 P-S wave measurements of the blocks

3.1.3 Blasting Sequence and Delay Times

Navarro (2014), Schimek (2015) and Ivanova (2015) made block tests with different aims. In the year 2013, Schimek (2015) shot 8 blocks. Seven of them had 5 holes per row, a total number of 15 holes per block. Only 1 block had 7 blast holes per row, or a total of 21 holes. Navarro (2014) did the crack detection work for these specimens. Their purpose was to observe the effect of delay times on rock fragmentation.

All our blocks had 7 holes per row, total of 21 holes. Since the aim was to observe the influence of joints on rock fragmentation, the nominal delay times were kept the same, 73 (μs) as Ivanovas (2015). Figure 3-14 and Figure 3-15 show specimen JS1 Alpha before and after blasting.

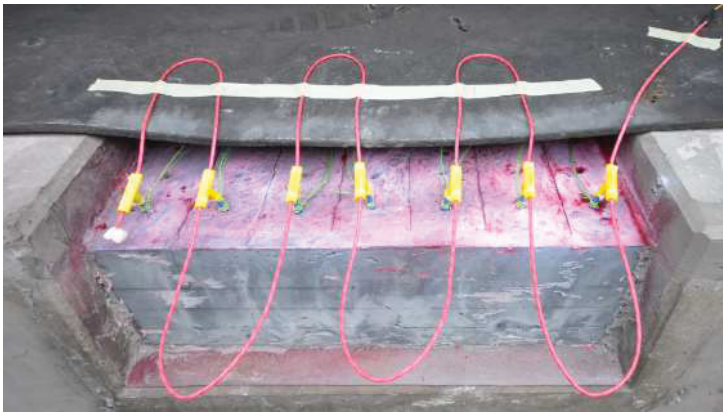

Figure 3-14 Implementation of explosives into the JS1 Alpha block

Figure 3-15 Alpha block surfaces after blasting of 1st, 2nd and 3rd rows

The initiation sequence was from top to the bottom of the borehole, and from right to left for all of the blocks. For the blasting, Austin Powder PETN cord was used. Respectively 20 g/m, article no. 300.003, and 3 g/m (another unknown producer) for blast holes respectively delay timing. The velocity of detonation of the 20 g/m is 7500 m/s and for 3 g/m it is 7200 m/s according to the manufacturer. The relative explosive strength of the PETN is 1.43 compared to ANFO (Persson et al. 1994). Figure 3-16 shows the manufacturer data.

The main reason that PETN was used instead of another explosive is that PETN cord can be used in boreholes smaller than 11 mm.

Art.-Nr.	Type	Laufmetergewicht in Gramm	Angaben pro Verpackungseinheit		
			Spulen	Meter/Spule	Meter insgesamt
301.567	Nitrocord	6	2	250	500
300.002	Detonex	12	2	250	500
300.001	Detonex	12	5	100	500
300.003	Detonex	20	2	250	500
300.242	Rowocord	25	2	150	300
300.004	Detonex	40	2	125	250
301.351	Detonex	100	1	75	75

Figure 3-16 PETN Cord properties

As detonators, both electric and Nonel types were used.

Delay times used for the blocks are shown in Table 3-15. The figures are mean values for each row, and they are aligned corresponding to the row order. JS2 Alpha was not blasted due to the wrong construction of burden distance in first row. Each block had 3 rows and 7 holes per row. The initiation sequence was from right to left.

Specimen	Mean delay times (µs)		
	Row 1	Row 2	Row 3
JS1 Alpha	73.0	73.0	73.2
JS1 Beta	72.4	72.6	72.5
JS1 Gamma	73.0	72.7	73.3
JS2 Beta	73.0	72.7	73.3
JS3 Alpha	73.1	72.4	72.83
JS3 Beta	73.1	73.5	73.0
JS4 Alpha	72.0	72.7	72.6
JS4 Beta	73.1	72.9	73.0
Reference 1	72.3	73.1	72.7
Reference 2	73.0	73.3	72.4
Reference 3	73.0	73.0	73.0

Table 3-15 Delay times of the blocks

3.1.4 Preparation before Analysis

The blocks were blasted row by row. After blasting each row, the mortar fragments were collected carefully into buckets in order to make sieving test afterwards. The buckets were numbered and named. Figure 3-17 shows the block JS3 Alpha after blasting of the 3rd row.

After the collection of the fragments, the remaining block was sprayed with dye penetrant, and photographs were taken to carry out crack analysis later.

In the final stage of the blast work, the remaining mass (back side of the blocks) was extracted by breaking it out from the left side or the right side (depending on the suitability). This remaining part is influenced by cracks which has been generated during the blasting

and have become fragile. Thus extracting it directly might cause it to break. To avoid that, fast hardening cement was poured in front of it.

Figure 3-17 JS3 Alpha after 3rd row blast

Figure 3-18 JS3 Alpha after fast hardening cement was poured.

After at least 24 hours passed from the pouring, the remaining blocks were ready for extraction. They were taken to the laboratory for the slicing procedure described below in order to subject them to crack detection analysis and 3D modelling via AutoCAD.

4. DATA ANALYSIS

4.1 Steps of the Analysis

4.1.1 Block Slicing

The blocks were extracted from the yoke, and brought to the laboratory for further analysis. There, the blocks were cut horizontally into 4 slices in order to carry out the crack detection analysis.

1) Before beginning to cutting procedure, visible cracks were traced with a pen in order to mark the significant cracks on the face.
2) After this, slicing procedure carried out with a GÖLZE diamond wheel saw, ST-100A with a blade with 5 mm width in the laboratory (see Figure 4-1).

Figure 4-1 ST100-A type of saw

Since the block heights were about 21 cm, it was convenient to slice the blocks as;

1st Slice 6cm from top surface

2nd Slice 5cm below slice 1

3rd Slice 5cm below slice 2

4th Slice 5cm below slice 3

See Figure 4-2;

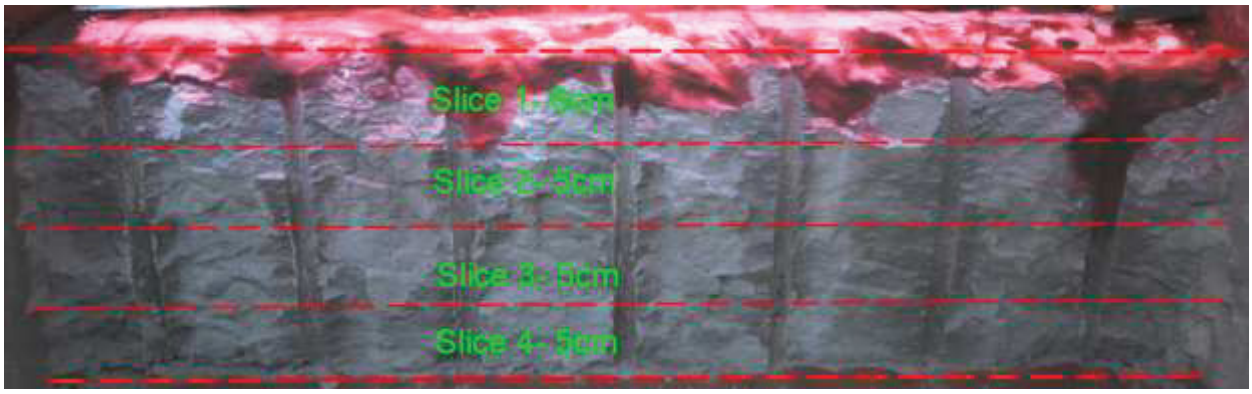

Figure 4-2 Illustration of slice widths

Differing from the work of Navarro (2014) and Zhu (2015), dye penetration method was only applied to the faces of the horizontal slices in this research. (Navarro´s work includes vertical slices as well as horizontal slices). When the crack visualization was not so good, the other side of the slice was sprayed and photographed in order to catch the suitability of AutoCAD drawing. Top and bottom faces of the slices are indicated in the Figure 4-3.

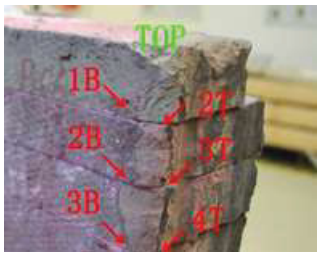

Figure 4-3 Designation of slice names **(Zhu 2015)**

In total, 11 blocks were blasted. Since the blocks JS1 Beta and JS3 Beta didn't have their 3rd rows blasted, their remaining width was larger than that of the other blocks. They couldn't be sliced as the depth of the saw cut was not large enough even we tried to cut the remains from both sides.

4.1.2 Dye Penetrant Application

After the slicing was done, the Dye Penetrant Method was applied to all of the selected slice faces, which were then used for crack detection analysis by photographing the faces. The steps of the DPM were;

- Cleaning the face of the slices
- Applying dye penetrant
- Suction time of 5 minutes
- Applying cleaner and wiping the surface
- Applying developer.
- Bleeding time of 5 minutes

Figure 4-4 Dye penetrant spray

4.1.3 Photographing

For the photographing, a Nikon D60 camera was used. In order to take suitable pictures, the following steps were taken;

The block slices were put on a table. The camera was positioned at a suitable place at a constant distance from the slices. A ruler was placed on the slices for the purpose of image scaling in AutoCAD.

Examples of the photographs of the faces are presented in the Figure 4-5 to Figure 4-8. A full set is given at ANNEX II.

JS1 Alpha- 1B

Figure 4-5 Bottom view of 1st slice, JS1 Alpha-1B

JS1 Alpha- 2B

Figure 4-6 Bottom view of 2nd slice, JS1 Alpha-2B

JS1 Alpha- 3T

Figure 4-7 Top view of 3rd slice, JS1 Alpha-3T

JS1 Alpha- 4T

Figure 4-8 Top view of 4th slice, JS1 Alpha-4T

4.1.4 Crack Tracing

After the pictures were taken, the photographs were imported into AutoCAD as backgrounds in different layers. Paper properties were set to centimeters. The ruler in the picture provided the scaling so that all of the slice layers would be in the same scale. The procedure of crack tracing in AutoCAD is as follows:

1- Good quality pictures belonging to the same block and in which the cracks can be identified easily were chosen.
2- The chosen pictures were imported into AutoCAD under the insert picture tab. This is recommended to be done in a separate layer since it will be necessary to hide the picture in following steps.
3- Scaling must be done according to the ruler on the picture, so that the slices will be in the same size and correctly positioned in relation to each other. Otherwise it won´t be possible to create a correct 3D model. A 1cm error can e.g. cause the drill hole half casts to shift too much when they should be underneath each other.
4- Under a new layer, the borders of the blocks need to be drawn with a specific color. It is important that borders don't include the fast hardening cement but only the block itself. The border points shouldn't overlap each other in order to avoid problems in the next steps. Before drawing the borders, it is important to mark them and drill holes with a pen to avoid any problem during AutoCAD drawing. It is an experience that the fast hardening cement and the block remains may be hard to distinguish from each other.
5- Cracks are traced carefully for each of the slices under a new layer with a color distinguishable from that of the borders. There is an option to mark those cracks which could be seen without dye penetrant with a different color, to recognize the difference between cracks. However, it was not done in this work unlike Navarro (2014).

While drawing the cracks, attention must be paid in order to not to miss the crack directions and their intersections. In the analysis of these data, the results may otherwise change.

6- Final stage of this step is to, check the crack drawings by copying the drawings into another AutoCAD file with another picture of the same slice to avoid mistakes and false interpretation.

After the drawings are done, the next step is 3D modelling of the block.

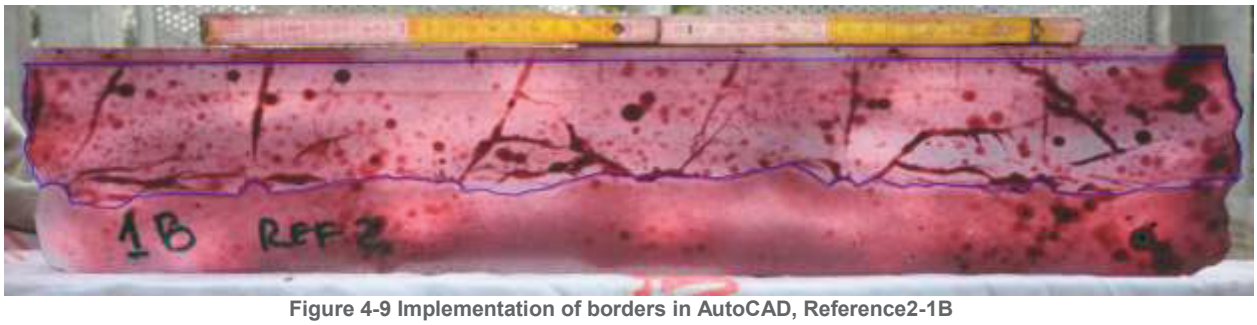

Figure 4-9 Implementation of borders in AutoCAD, Reference2-1B

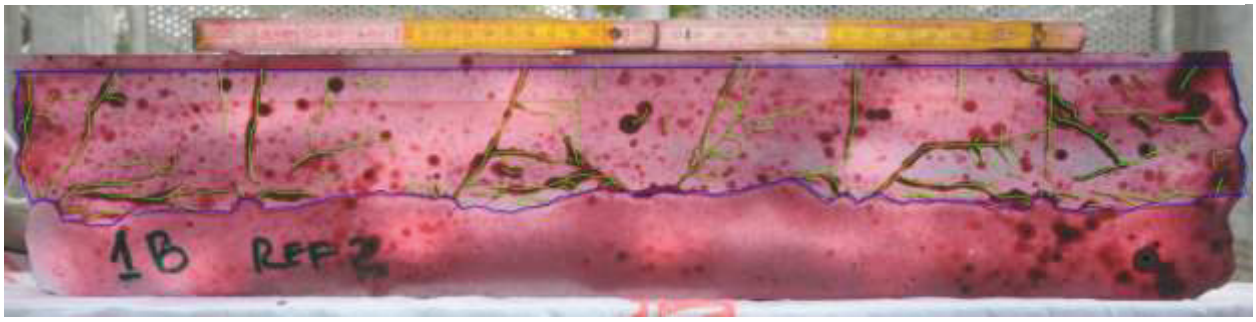

Figure 4-10 Crack drawing in AutoCAD, Reference 2-1B

4.1.5 3D Modelling

After completing the crack-border drawings, the next step is to form 3D models of the blocks. There are different ways to manage 3D Modelling of the blocks. Another method without side pictures of the blocks than Navarro´s (2014) and Zhu´s (2015) who made similar analyses before, was followed.

In order to make the 3D models results, the following steps were followed;

1- Open the slice drawings which belong to the same block in AutoCAD. The slice pictures should be hidden from the layer options. Border and crack drawings must be copied into a new AutoCAD sheet.
2- After copying the drawings, we need to ensure that slice scales are the same and they are correctly positioned at the top of or under each other.

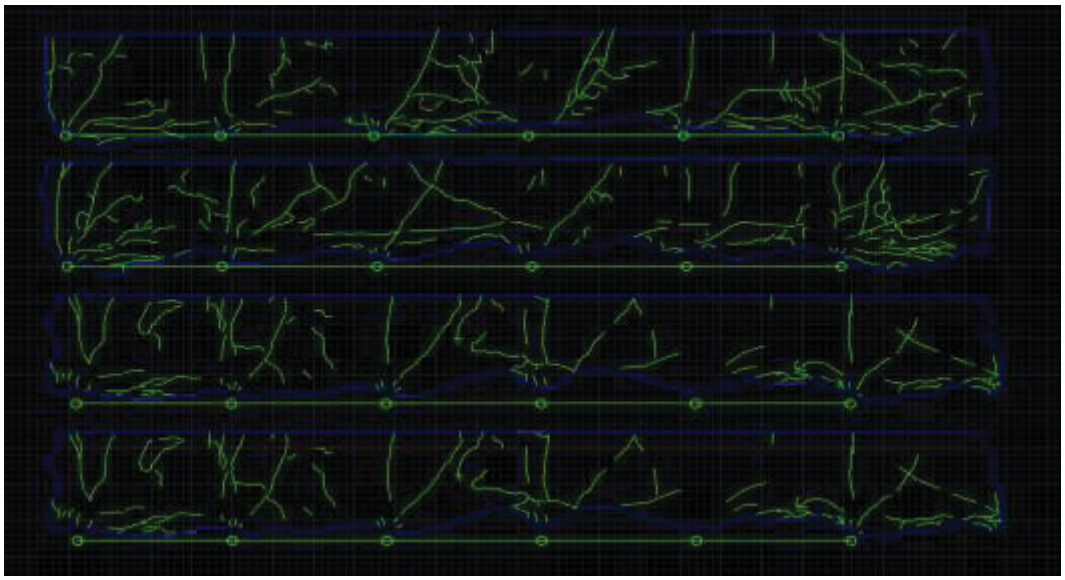

Figure 4-11 Top view of the cracks in AutoCAD

3- Then put the drawings in the right orientation, considering x-y-z axis in AutoCAD. When putting the slices in the right orientation, the slice distances must be correct. (They were 6-5-5-5 cm respectively from top to bottom.)

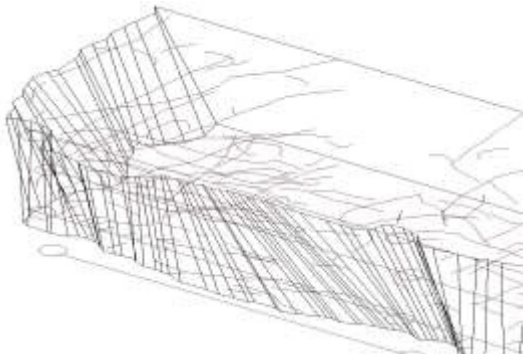

Figure 4-12 Step before 3D solid formation

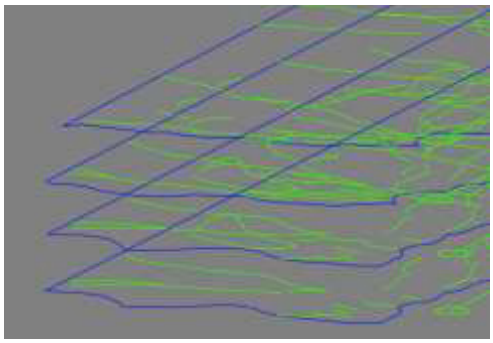

Figure 4-13 Part of the 3D illustration of the block

4- When the arrangement of the slice layers has been done, then the top face drawing of the block was put just above the others. After this has been done, regions of the top side and the bottom side were created.
5- The last step is to solidify and connect the slice layers each other using the Loft command. The first and last layers of the slice were selected for the Loft process, and a solid object can be created.

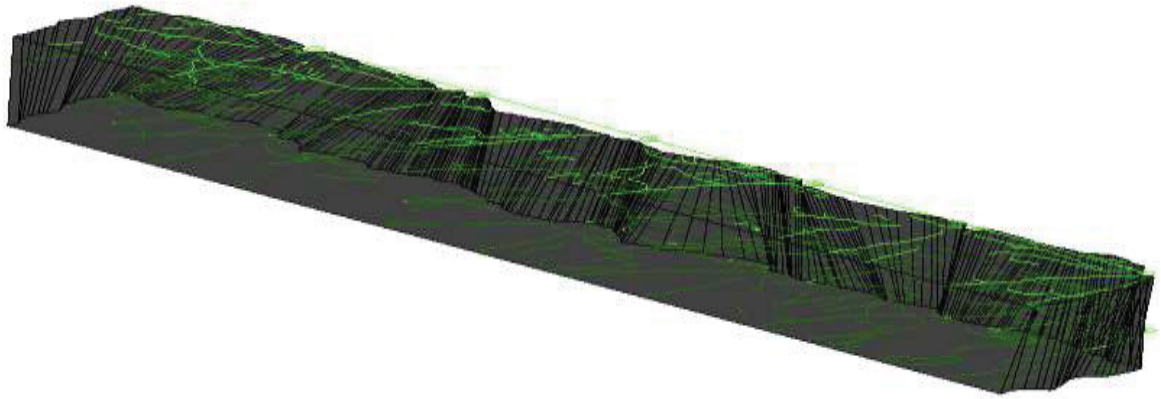

Figure 4-14 3D view of the block from back with angle

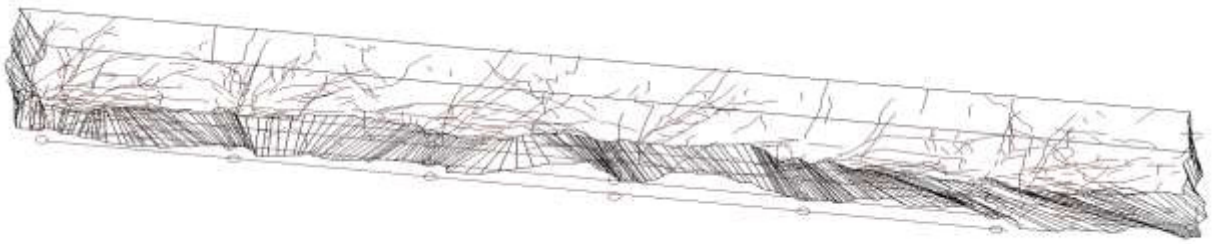

Figure 4-15 3D view of the block formation in AutoCAD

When the solid object has been created, with changing the view options, one may see the cracks and their positions in the solid block better. Figure 4-14 and Figure 4-15 shows the Reference 2 Solid Model. The Figure 4-16 shows the top part of the block model.

Figure 4-16 3D view of the block model from top

4.2 Crack Classification and Sieving

4.2.1 Introduction to Crack Classification

With the 3D models constructed, the cracks occurring on the slice faces were counted and classified using the crack families defined in the previous work (Navarro 2014, Zhu 2015). The steps of this procedure are explained under the section 4.2.4. The results of the crack counting and classification were used for a comparison of influence of the different types of joints.

4.2.2 Crack Families

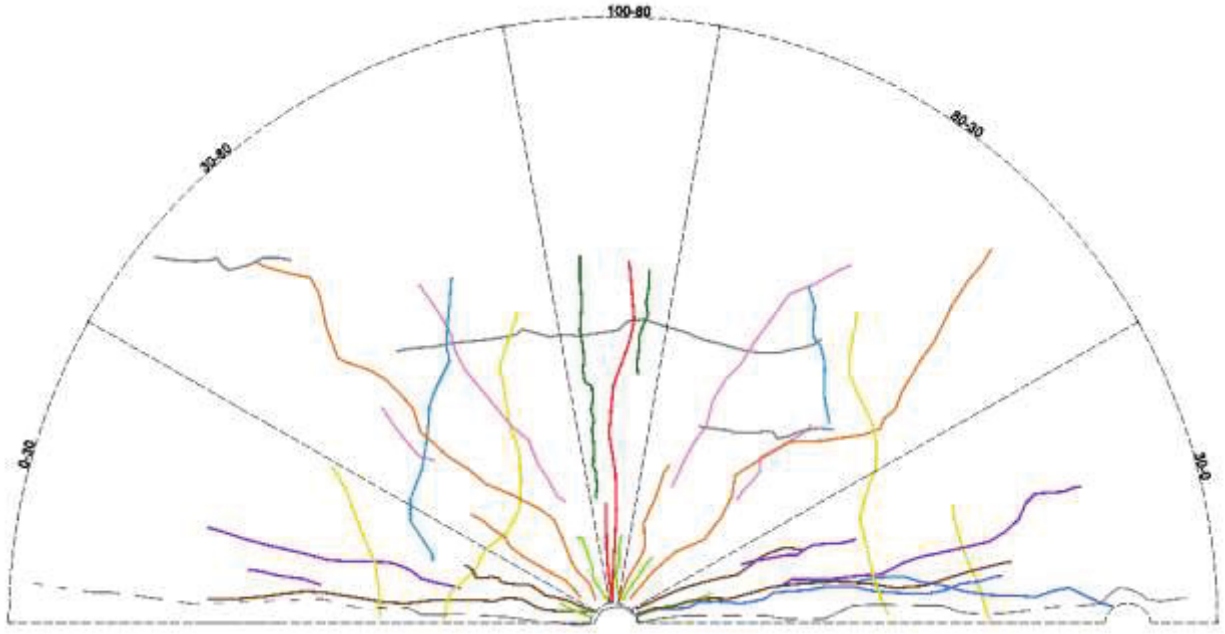

Figure 4-17 Illustration of existing crack families

The crack families were defined due to their length, shape, direction, angle and their starting positions. All the crack families can be seen in Figure 4-17.

As can be seen from the following explanations, the crack families were distinguished by different colors. The figure above represents all of the crack families in one drawing.

Cracks of type DIR and CB90-80 were divided into 3 groups according the their angles, namely cracks in sectors between 0°-30°, cracks in sectors between 30°- 80°, and cracks in sectors between 80°-90° in order to do a better analysis of their behaviors.

All crack families except the SC family are divided into short and long ones according to their lengths. Long cracks are longer than 3cm, short cracks are between 1cm and 3cm. Cracks shorter than 1 cm are not included in the crack counting, because they are not representative considering the dimensions of the specimens.

4.2.2.1 Cracks from borehole in sectors between 90°-80°

They have the abbreviation CB90-80. This family of cracks start at the boreholes. They tend to develop a path between 90° and 80° including the mirror sector 90° to 100° on the other side of the normal to the bore hole line. See Figure 4-18. When they are shorter than 3cm, they are considered under the SC family.

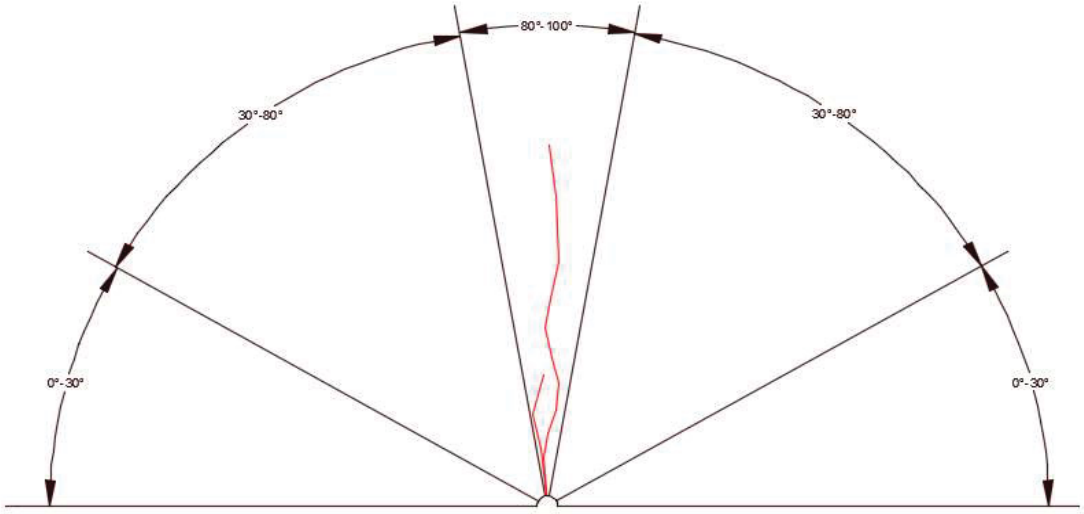

Figure 4-18 Cracks from the borehole between sectors 90° and 80°

4.2.2.2 Cracks from borehole in sectors between 80-30

They have the abbreviation CB80-30. This family of cracks also start from the borehole and they develop and follow a path between the angles 80° and 30° or in the mirror sector. See Figure 4-19. When they are shorter than 3cm, they are considered under the SC family.

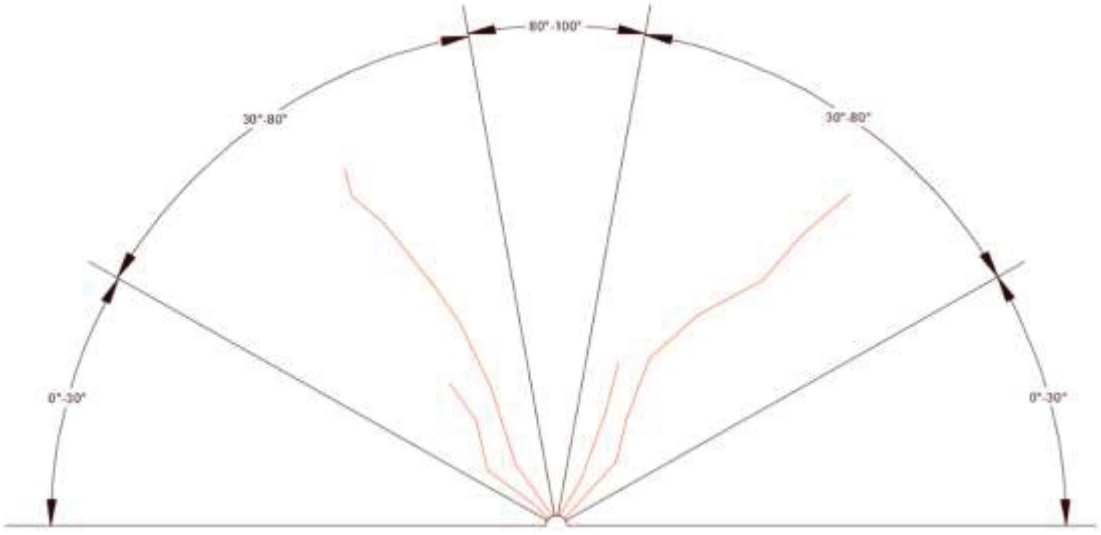

Figure 4-19 Cracks from the borehole between sectors 80° and 30°

4.2.2.3 Cracks from borehole in sectors between 0° and 30°

They have abbreviation CB0-30. This family of cracks also start from the borehole and they develop and follow a path between the angles 0° and 30° or in the mirror sector. See Figure 4-20.

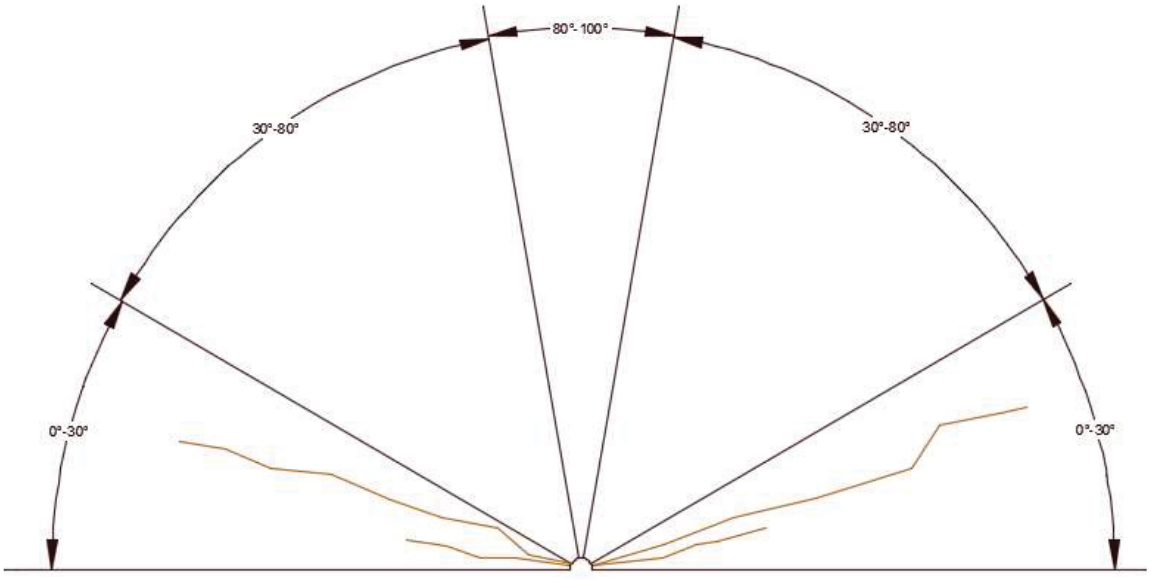

Figure 4-20 Cracks from the borehole between sectors 0° and 30°

4.2.2.4 Straight cracks from back side

They have the abbreviation SCB. These are the cracks which start from the back side of the slice and they develop along a trajectory that is not directed to the boreholes. See Figure 4-21.

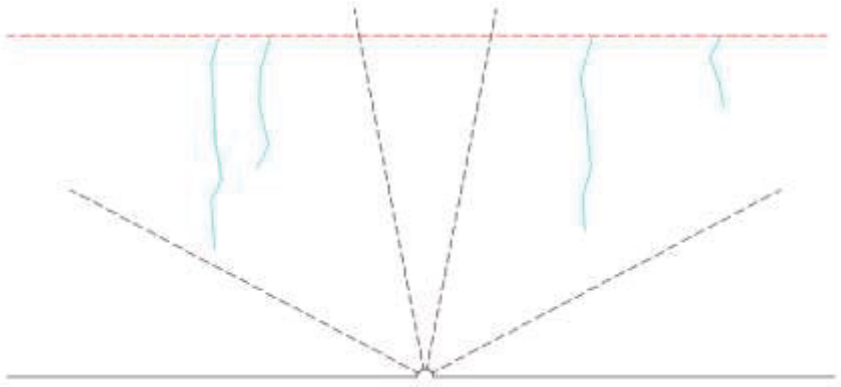

Figure 4-21 Straight cracks from the back (SCB)

4.2.2.5 Connections between boreholes

They have the abbreviation Connect. In many of the blocks, it is observed that the cracks taking place between 0° and 30° connects the two boreholes with each other. See Figure 4-22. They are occasionally forming an arc shape, basically in the shape of banana.

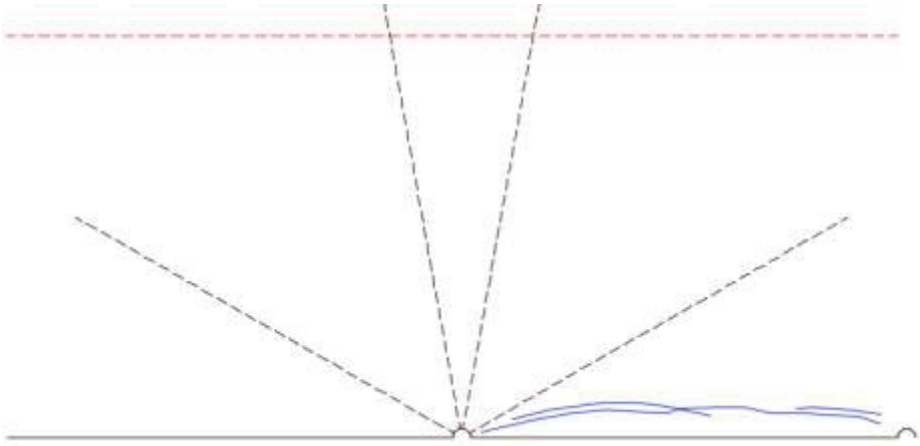

Figure 4-22 Connection between boreholes (Connect)

4.2.2.6 Parallel cracks to the surface

They have the abbreviation Parallel. This family of cracks are laying along the slice. They follow a parallel line to the boreholes. See Figure 4-23.

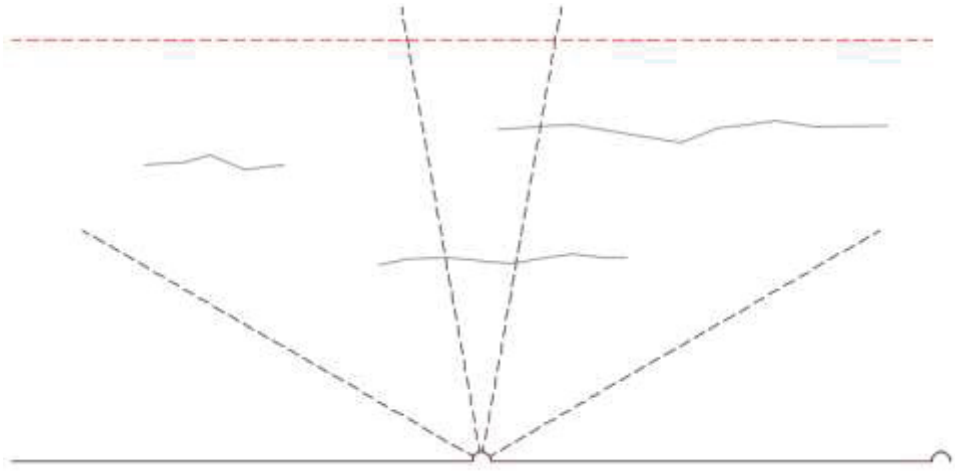

Figure 4-23 Parallel cracks to the surface (Parallel)

4.2.2.7 Cracks with direction to the boreholes in sectors between 90-80

They have the abbreviation DIR90-80. This family of cracks basically look like the CB90-80 cracks. The difference is that they don't start from the borehole but they follow a path towards the borehole. They are found between the sectors 90° and 80°. If we consider the both sides of the borehole, it could be said that they are found in the sector 100°-80°. See Figure 4-24.

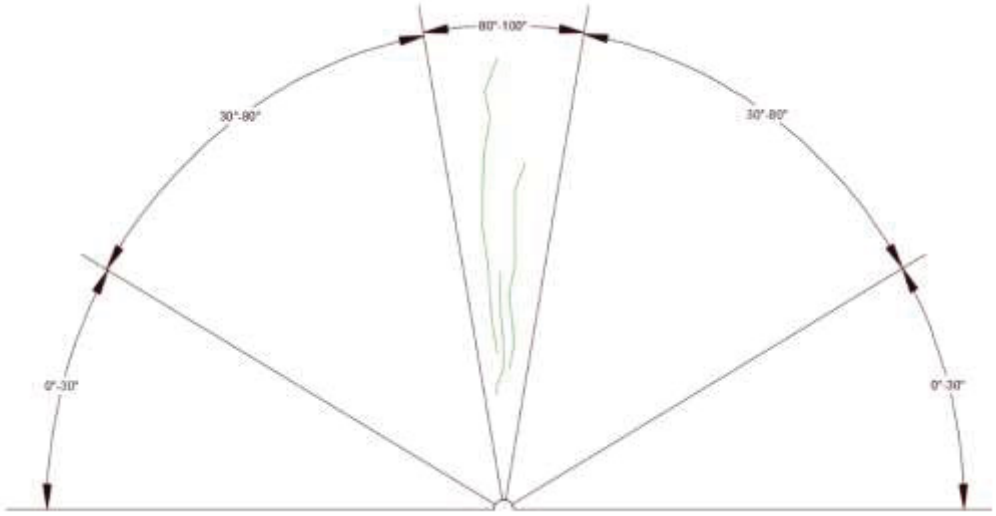

Figure 4-24 Cracks with direction to the boreholes in sectors 90°-80°

4.2.2.8 Cracks with direction to the boreholes in sectors between 80°-30°

They have the abbreviation DIR80-30. This family of cracks like DIR90-80 cracks don't start from the boreholes but follow a trajectory in direction towards the boreholes. They are found between the sectors 80° and 30° and in the mirror sector. See Figure 4-25.

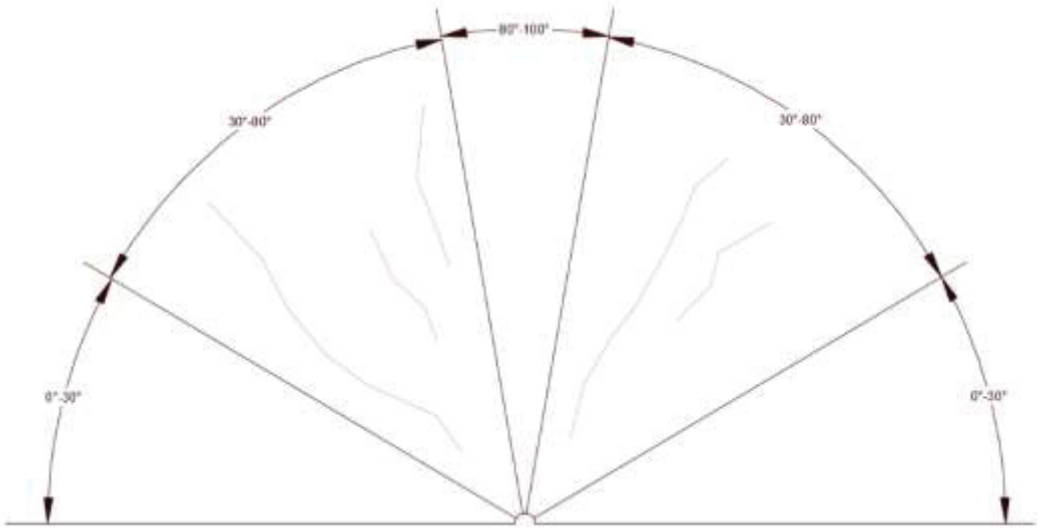

Figure 4-25 Cracks with direction to the boreholes in sectors 80°-30°

4.2.2.9 Cracks with direction to the boreholes in sectors between 30°-0°

They have the abbreviation DIR30-0. Like DIR90-80 and DIR80-30 these DIR30-0 cracks follow a trajectory in direction towards the boreholes. They are found between the sectors 30° and 0°. See Figure 4-26.

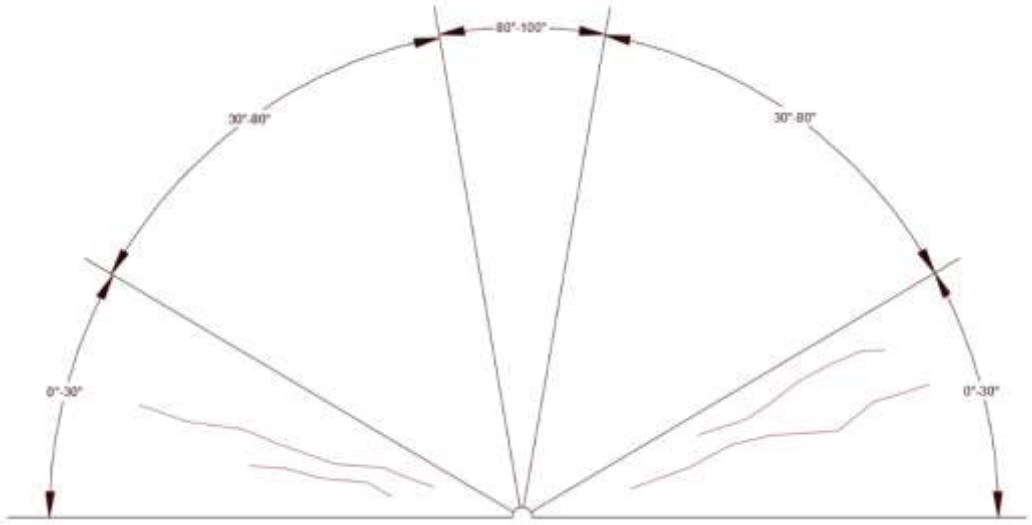

Figure 4-26 Cracks with direction to the boreholes in sectors 30°-0°

4.2.2.10 Short cracks from borehole

They have the abbreviation SC. These family of cracks are only found at the boreholes. They surround the borehole and form a sun like shape. Their length is less than 3cm. The longer cracks are correlated to other crack groups. See Figure 4-27.

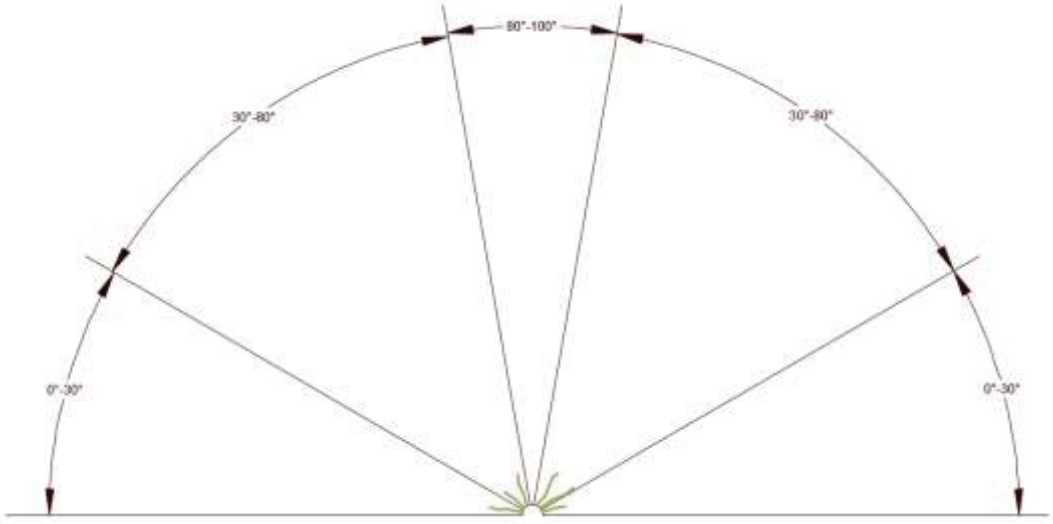

Figure 4-27 Short cracks from borehole

4.2.2.11 Vertical cracks between boreholes

They have the abbreviation VCB. These cracks run perpendicular to the bench face. They have a starting point between the boreholes. See Figure 4-28.

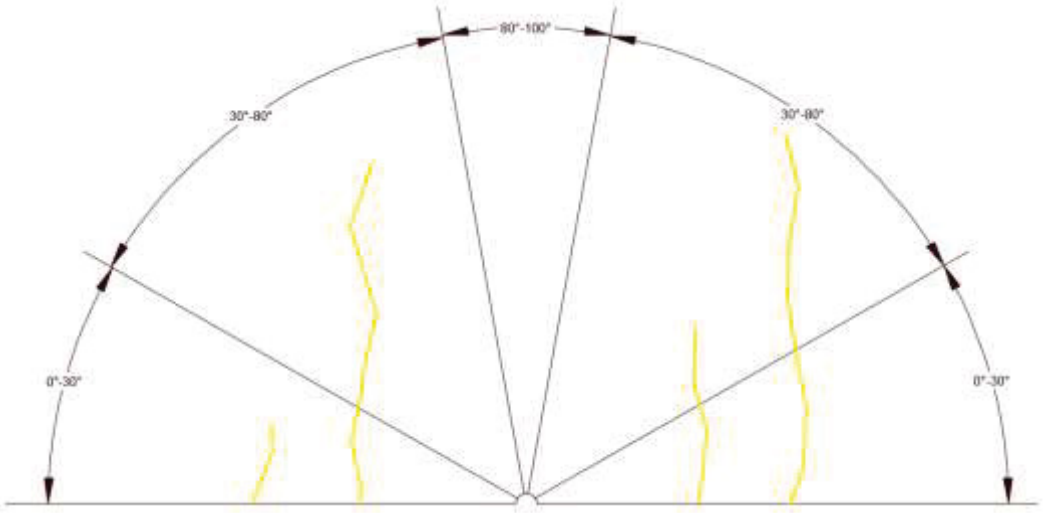

Figure 4-28 Vertical cracks between boreholes

In addition the crack families above, different family of cracks related with the joints were observed during the analysis. There are also some additional crack families defined in the section 4.2.3 in order to make the classification of the cracks easier.

4.2.3 Joint Related Cracks (JRC)

In addition to the eleven crack families which are defined in Ivanova (2015) (section 4.2.2), new crack families were observed in the jointed blocks. These cracks are completely related with the joint formations in the blocks and they don't occur in the Reference blocks. Although these cracks were classified under the name of a different family group (JRC), the calculation was made using only original crack families because they were already containing the new crack families within.

The JRC group of cracks consists of the following 4 different crack families.

- Joint 90°End Cracks (J90C)
- Cracks Connecting Joints to the Boreholes (CJB)
- Combination of CJB and J90C cracks (CC)
- Other families

4.2.3.1 Cracks Connecting Joints to the Boreholes (CJB)

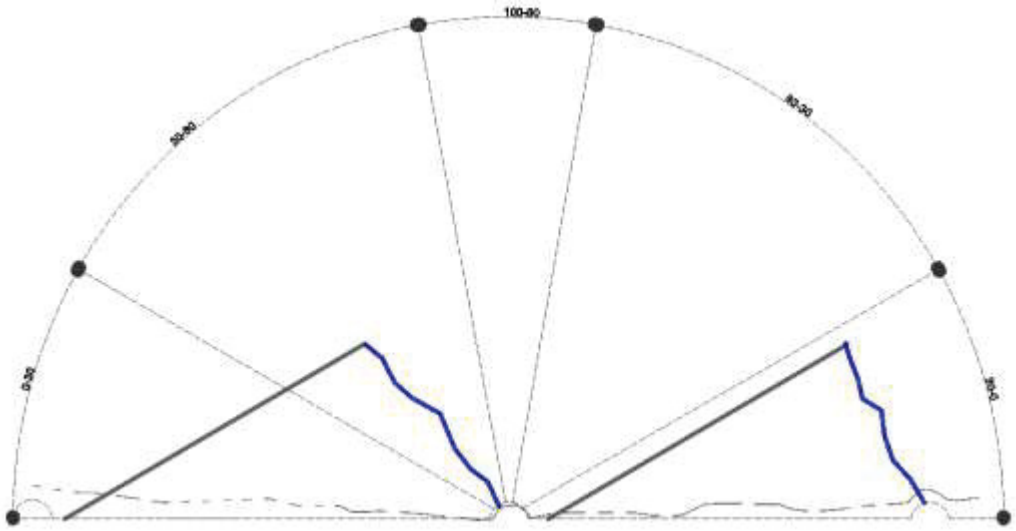

Figure 4-29 Representation of CJB

CJB cracks occur in the JS3 blocks in which the joints strike 30° from the line of the boreholes. See Figure 4-29.They start from boreholes and follow a straight path until the end of a joint. Regardless of the jagged path, these cracks always end up at the end of a joint. This often causes a wedge break out after blasting of the second or third rows because this blast damage at the same place is repeated for every row. The CJB cracks are longer than 3cm due to the place of the joints.

The CJB cracks can also be considered to belong to the CB80-30 family if the end points of CJB cracks are ignored. In the calculations, CJB cracks are considered under the CB80-30 family. An example of CJB can be seen on Figure 4-30.

Figure 4-30 JS3 Alpha- CJB

4.2.3.2 Joint 90°End Cracks (J90C)

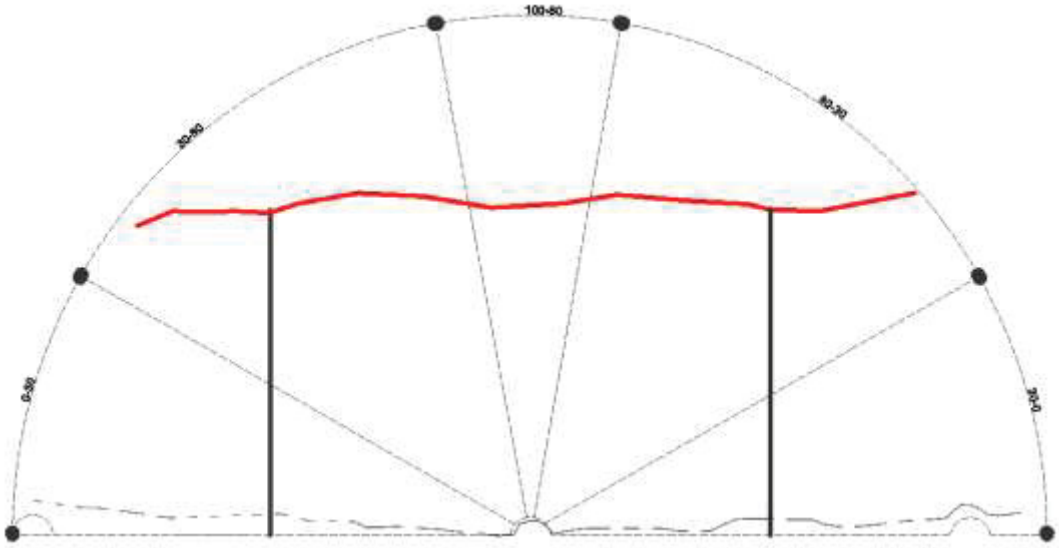

Figure 4-31 Representation of J90C

J90C cracks can be observed in the blocks which have joints that are perpendicular joints to the line of boreholes. See Figure 4-33. JS1, JS2 and JS4 blocks have such joints. The J90C cracks follow a straight path between ends of the joints, connecting them to each other. Like the CJB cracks, these wide and thick cracks have a destructive influence on the blocks.

In the analysis chapter, they were considered under the parallel cracks family because of their similar form. The difference is that they start from the end of the first joint and finish at the end of the last joint. See Figure 4-32 and Figure 4-33.

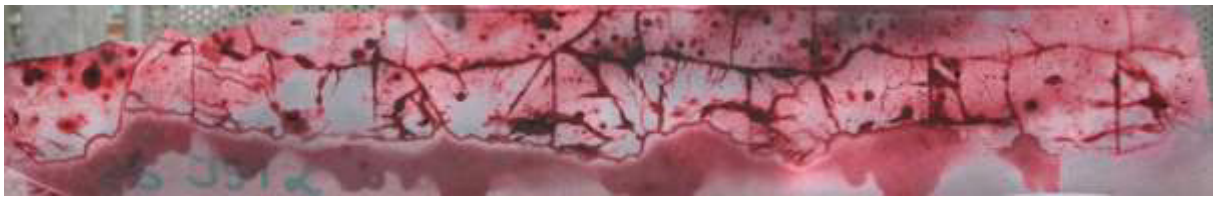

Figure 4-32 JS1 Alpha J90C

Figure 4-33 JS1 Gamma J90C

4.2.3.3 Combination of CJB and J90C Cracks (CC)

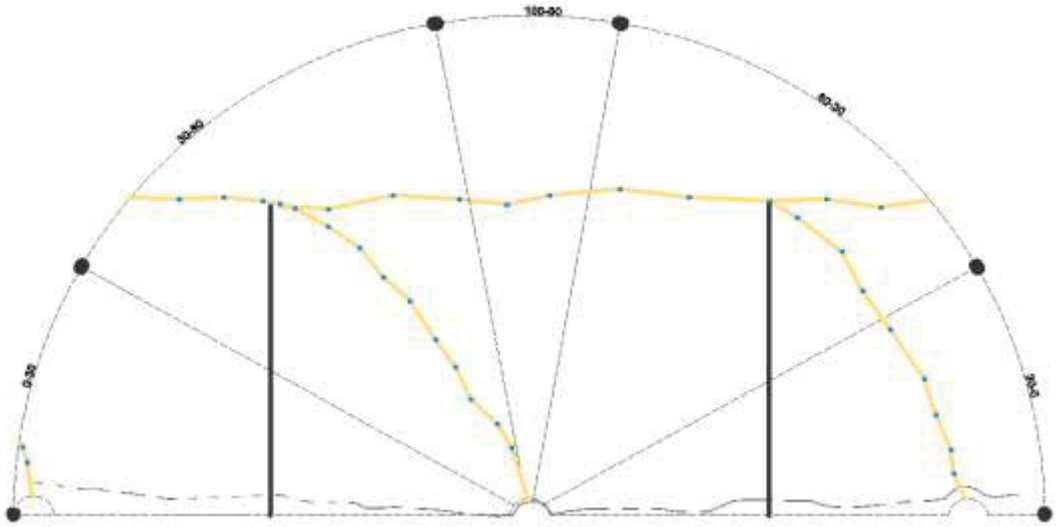

Figure 4-34 Representation of CC

The so-called Combination or CC cracks are observed in the JS1 and JS4 blocks. See Figure 4-34. Distances between joints and to the boreholes are sufficient for CC cracks to occur. A long crack starting from the boreholes follows a half curved path to the end of the joint and then follows a straight path to the end of the next joint. The cracks´ direction is dependent on the blasting sequence and starts from borehole and veers to the left in this case. CC cracks are long and highly visible. In the calculations chapter, they were not counted separately because the family of both parallel and CB80-30 cracks were already containing their two parts.

Figure 4-35 JS1 Gamma CC

4.2.3.4 Other Crack Families

Apart from the crack families defined above, two types of cracks fall outside the definitions of the former were identified.

1) CNU Shaped Cracks (CNU)
2) Inclined Cracks (IC)

CNU Shaped Cracks

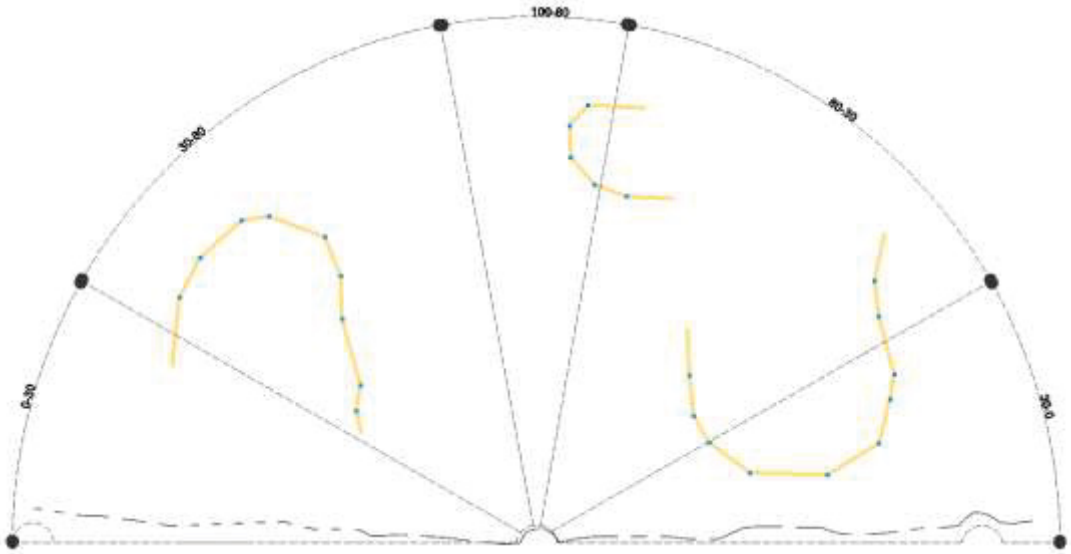

Figure 4-36 Illustration of C N U cracks

The CNU cracks can be found almost in every block. Their shapes look like c, n, u. These cracks were separated into three parts in order to be able to put them into the current existing families. One long U shaped crack was defined as a parallel crack and two vertical cracks between boreholes. This eventually leads a change in the results of total crack numbers for one CNU crack was considered to consist of crack parts that belonged to three of the eleven standard families. See Figure 4-36.

Inclined Cracks

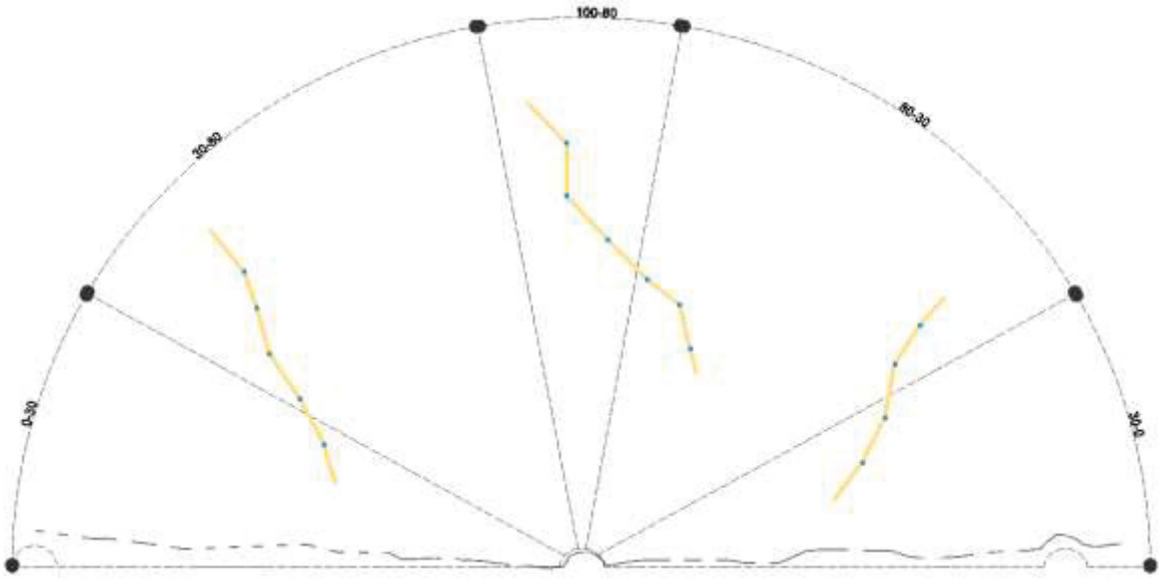

Figure 4-37 illustration of inclined cracks

They have the abbreviation IC. Inclined cracks occur in all blocks. In many cases, these cracks are directed to the boreholes and then belong to DIR80-30 or DIR30-0 families, depending on their angle. When they are not directed towards the boreholes, either a related family must be expanded or a new family should be defined. See Figure 4-37.

In the calculations, the cracks of these families were considered to the belong the closest looking standard crack families, sometimes defining them as two or three cracks.

4.2.4 Crack Density Analysis

In the crack density analysis, counting the numbers of the cracks and estimating their concentration is done.

In order to get the results, we needed to make a model to see how intensely the cracks were distributed on the slices. To achieve the desired results, a 2×2cm grid is superposed on the crack drawings in AutoCAD.

After the grid is made, numbers were entered into the boxes according to how many cracks there are in each box. Every number had a different color so that they could be used to create a damage map (Navarro 2014). Damage maps were not constructed in this thesis.

These crack numbers data obtained from the AutoCAD files were used to calculate the MCD and MCID values which are explained in section **MCD and MCID calculations**.

4.2.4.1 Design of the Grid

The slice models were superposed with a grid in order to carry out crack counting and the related analysis. The grid is formed from boxes or cells with dimensions 2×2cm which cover the slice. The reasons to use 2×2cm cells were explained by Navarro (2014) as;

"*According to the figures presented in this section, it can be seen that the grid with cells of 2 x 2 cm represents the best distribution of crack density. That means: sufficiently large difference between cell crack numbers to identify areas with large damage, like areas around boreholes, and areas with small damage.*

Due to the smaller size of the cell in the grid of 1 x 1 cm, a lower number of cracks can be counted in each cell; therefore, a representation of the individual cracks network can be done. However, this makes it harder to identify crack concentration areas, like directly behind a blast hole.

On the other hand, the grid of 4 x 4 cm gives a more general view about crack density. Due to its size, a larger number of cracks is counted in each cell, creating greater crack

concentration areas. In this situation, identification with more detail of specific crack concentration areas in the slice can be difficult.

Following the best representation possible, the grid of 2x2 cm cell size was chosen to represent crack density maps."

As the grid is formed, the points representing the crack numbers in the boxes were set into the grids. The boxes which have no cracks inside were indicated by 0. Outside of the slice borders, the area with fast hardening cement was excluded.

In order to superpose these grids onto the slice drawings, this empty grid template had to be adjusted according to the block slice drawings. See Figure 4-38. The units of the slice drawings and the units of the template must be compatible otherwise 2×2cm wouldn't represent the real measure.

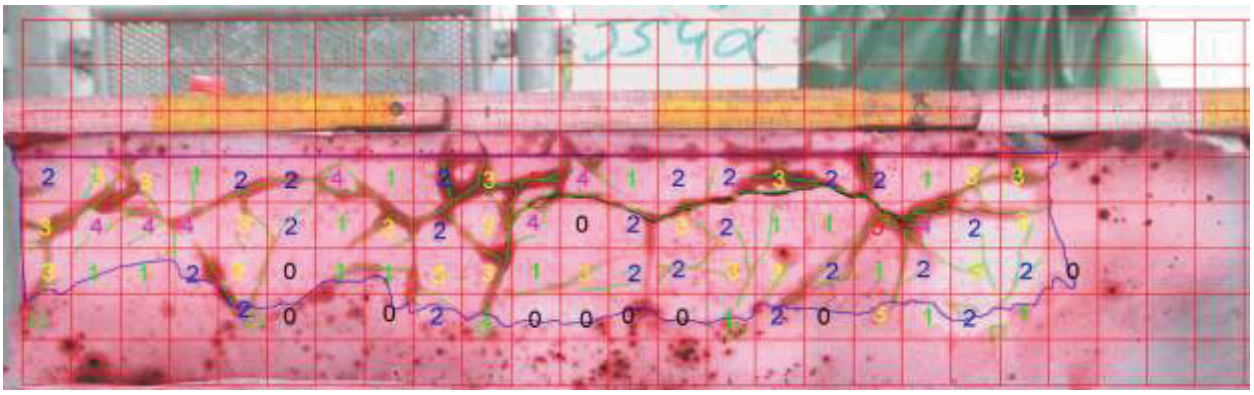

Figure 4-38 JS4 Alpha 1B drawing with grids.

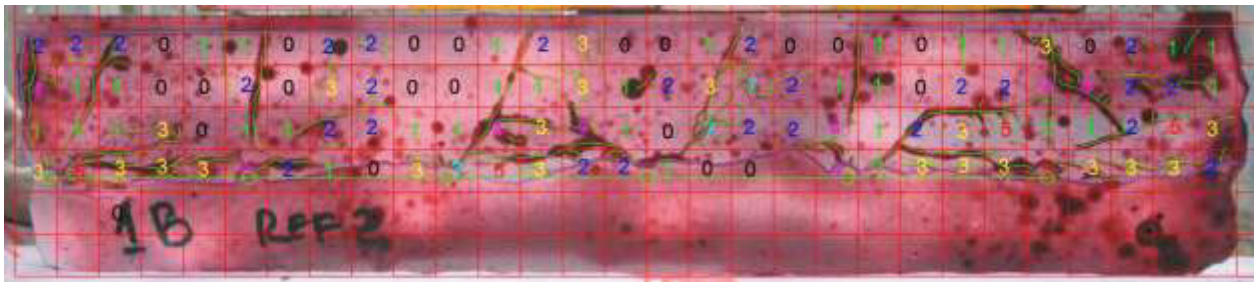

Figure 4-39 Reference 1 1B drawing with grids.

The 2×2 grids were used for all of the blocks except JS1 Beta and JS3 Beta. JS1 Beta was broken during the cutting and JS3 Beta was too large for the saw. Therefore these blocks were neither involved in MCD-MCID calculations nor in the statistical analysis.

MCD and MCID calculations

After the grids were drawn, the mean crack density (MCD) and the mean crack intersection density (MCID) were calculated.

The damage is not constant along the slices and directly comparable from slice to slice. These measures are based on the density of the cracks which are occurring in the grids. The crack numbers in the grids were used to determine MCD for that slice. The purpose of calculating MCD and MCD is a presentation of the damage dispersion in terms of numbers.

The mean crack density of the slices is calculated as:

$$MCD_{value} = \frac{\sum_{i=1}^{N} = Number\ of\ cracks\ in\ the\ cell(i)}{N}$$

Equation 7 **MCD calculation equation (Navarro 2014)**

Where N is the sum of the grid points or number of 2×2 boxes in other words and the sum of “i” is the number of the cracks in the cell.

The other method to illustrate the damage inside the blocks is defined as MCID, which its´ calculation is based on the crack intersections taking place in the grids. The more cracks intersecting each other in the slices means that the more damage was occurred inside the blocks. The logic of MCD and the logic of MCID are similar.

Mean crack intersection density (MCID) is calculated as:

$$MCID_{value} = \frac{\sum_{i=1}^{N} = Number\ of\ intersections\ in\ the\ cell}{N}$$

Equation 8 MCID calculation equation (Navarro 2014)

Where N is the number of the 2×2 boxes in slice and the sum of “i” is the number of cracks intersections occurred in the cell.

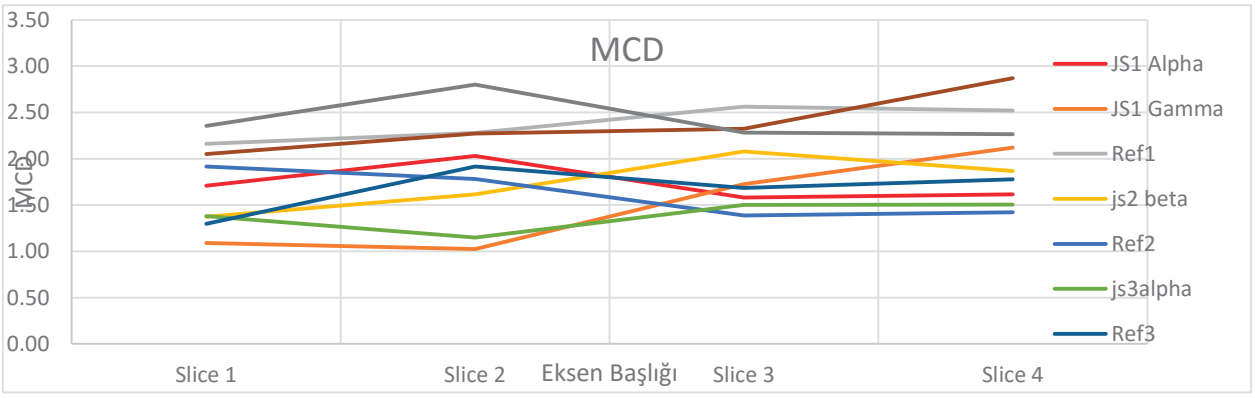

Figure 4-40 MCD comparison of the blocks

Figure 4-40 shows the mean crack density values of the 4 slices belonging to all blocks. Difference between MCD values for each slice and for each block can be observed from the graph. See Figure 4-40.

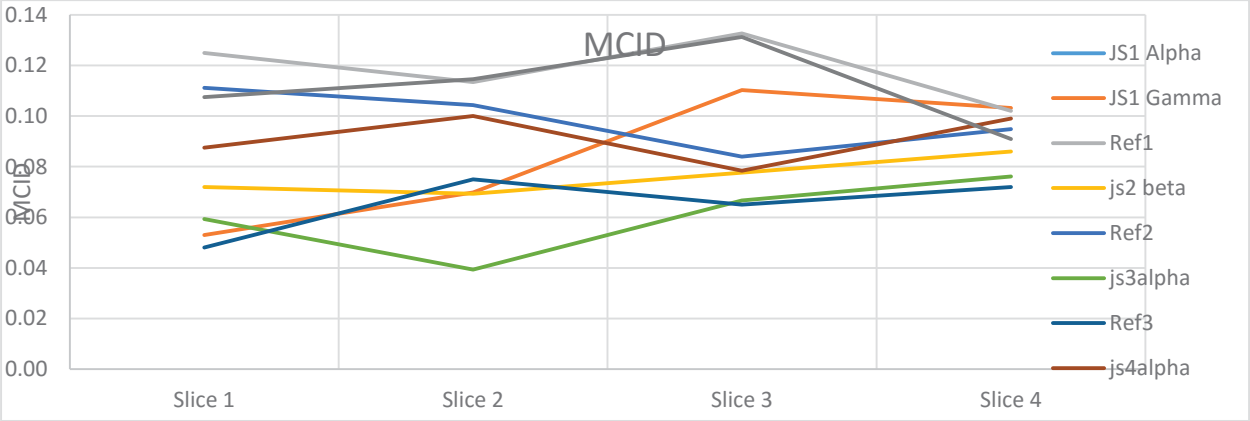

Figure 4-41 MCID comparison of the blocks

Figure 4-41 shows the MCID values. The values for the slices and the blocks can be observed and compared.

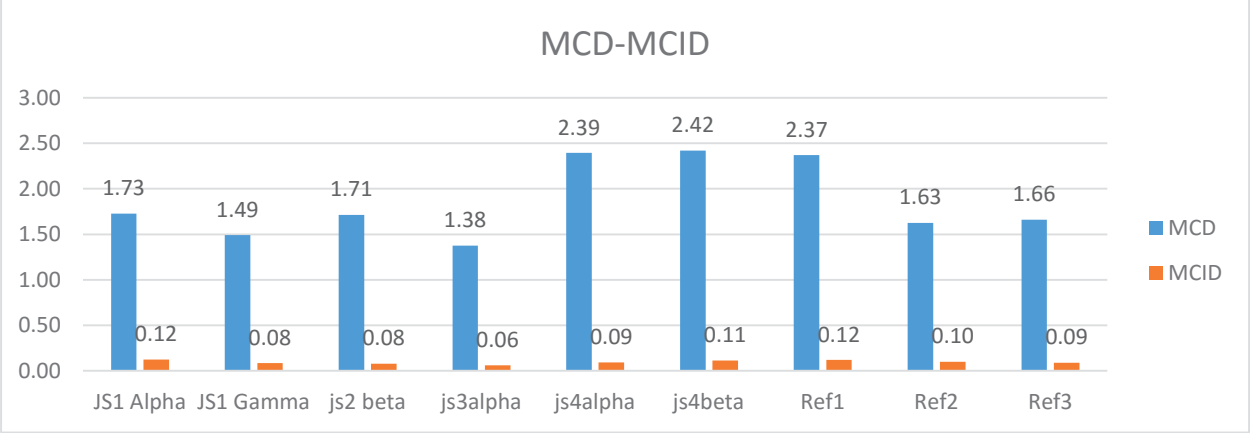

Figure 4-42 MCD and MCID comparison of the blocks

MCD and MCID values are related to each other. Figure 4-42 shows that the blocks which have higher MCD values in general also have higher MCID values but this is not the case for all individual blocks. Furthermore the blocks which belong to same joint family have different values. There might be other parameters which influence the MCD and MCID values. The complete set of MCD and MCID values are shown at ANNEX IV.

4.2.4.2 Crack Classification and Numbers

According to the length of cracks, location and occurrence, they were divided into different families. The data from each block are presented in the tables from Table 4-1 to Table 4-18.

JS1 ALPHA FAMILIES	LENGTH	S1	TOTAL	S2	TOTAL	S3	TOTAL	S4	TOTAL	SUM	%
CB90-80	Long	4	6	3	4	2	3	3	3	12	4.5
	Short	2		1		1		0		4	
CB80-30	Long	4	5	2	5	2	6	2	3	10	5.3
	Short	1		3		4		1		9	
CB30-0	Long	3	5	2	5	3	6	1	3	9	5.3
	Short	2		3		3		2		10	
SCB	Long	7	11	6	9	5	10	4	8	22	10.7
	Short	4		3		5		4		16	
CONNECT	Long	3	10	6	11	3	3	8	13	20	10.4
	Short	7		5		0		5		17	
PARALLEL	Long	8	15	7	12	4	15	8	16	27	16.3
	Short	7		5		11		8		31	
DIR90-80	Long	4	7	2	5	6	13	6	12	18	10.4
	Short	3		3		7		6		19	
DIR80-30	Long	3	11	8	13	4	7	3	6	18	10.4
	Short	8		5		3		3		19	
DIR30-0	Long	2	10	7	12	4	9	6	11	19	11.8
	Short	8		5		5		5		23	
SC	Short	2	2	4	4	3	3	1	1	10	2.8
VCB	Long	5	5	7	11	9	17	8	10	29	12.1
	Short	0		4		8		2		14	
TOTALS		87		91		92		86		356	

Table 4-1 JS1 Alpha crack quantification

JS1 ALPHA FAMILIES	LENGTH	S1	TOTAL	S2	TOTAL	S3	TOTAL	S4	TOTAL	SUM	%
CJB	Long	0	0	0	0	0	0	0	0	0	0.0
	Short	0		0	0		0		0		
J90C	Long	5	6	5	5	5	6	5	6	23	6.5
	Short	1		0		1		1			
CC	Long	1	1	1	1	2	2	2	2	6	1.7
	Short	0		0		0		0			
Other cracks											
CNU	Long	2	3	2	2	2	3	3	4	12	3.4
	Short	1		0		1		1			
IC	Long	2	4	3	4	3	3	2	3	14	3.9
	Short	2		1		0		1			
TOTALS		14		12		14		15		55	15.4

Table 4-2 JS1 Alpha new crack family numbers

JS1 GAMMA FAMILIES	LENGTH	S1	TOTAL	S2	TOTAL	S3	TOTAL	S4	TOTAL	SUM	%
CB90-80	Long	1	1	3	3	3	7	1	4	8	4.3
	Short	0		0		4		3		7	
CB80-30	Long	3	4	3	3	2	6	1	3	9	4.6
	Short	1		0		4		2		7	
CB30-0	Long	1	2	3	3	0	1	4	6	8	3.4
	Short	1		0		1		2		4	
SCB	Long	4	5	2	5	6	6	9	11	21	7.7
	Short	1		3		0		2		6	
CONNECT	Long	2	3	6	8	4	10	6	10	18	8.9
	Short	1		2		6		4		13	
PARALLEL	Long	7	16	9	11	6	14	12	26	34	19.1
	Short	9		2		8		14		33	
DIR90-80	Long	0	1	2	4	5	9	12	22	19	10.3
	Short	1		2		4		10		17	
DIR80-30	Long	1	4	2	4	4	11	13	24	20	12.3
	Short	3		2		7		11		23	
DIR30-0	Long	1	5	2	5	5	11	12	22	20	12.3
	Short	4		3		6		10		23	
SC	Short	1	1	0	0	9	9	5	5	15	4.3
VCB	Long	5	7	4	10	7	13	7	15	23	12.9
	Short	2		6		6		8		22	
TOTALS		49		56		97		148		350	

Table 4-3 JS1 Gamma crack quantification

JS1 GAMMA FAMILIES	LENGTH	S1	TOTAL	S2	TOTAL	S3	TOTAL	S4	TOTAL	SUM	%
CJB	Long	0	0	0	0	0	0	0	0	0	0.0
	Short	0		0	0		0		0		
J90C	Long	4	5	5	5	2	3	3	5	18	5.1
	Short	1		0		1		2			
CC	Long	3	3	3	3	4	4	4	4	14	4.0
	Short	0		0		0		0			
Other Cracks											
CNU	Long	0	0	0	0	0	2	2	3	5	1.4
	Short	0		0		2		1			
IC	Long	2	3	1	2	2	3	2	3	11	3.1
	Short	1		1		1		1			
TOTALS		11		10		12		15		48	13.7

Table 4-4 JS1 Gamma new crack family numbers

JS2 BETA FAMILIES	LENGTH	S1	TOTAL	S2	TOTAL	S3	TOTAL	S4	TOTAL	SUM	%
CB90-80	Long	2	3	3	5	5	8	3	5	13	6.6
	Short	1		2		3		2		8	
CB80-30	Long	1	1	3	6	5	7	3	6	12	6.3
	Short	0		3		2		3		8	
CB30-0	Long	2	2	3	3	3	4	0	2	8	3.4
	Short	0		0		1		2		3	
SCB	Long	5	8	2	6	4	7	5	11	16	10.0
	Short	3		4		3		6		16	
CONNECT	Long	6	8	5	7	3	5	4	11	18	9.7
	Short	2		2		2		7		13	
PARALLEL	Long	10	16	11	16	7	12	12	21	40	20.3
	Short	6		5		5		9		25	
DIR90-80	Long	3	5	2	3	0	1	2	3	7	3.8
	Short	2		1		1		1		5	
DIR80-30	Long	4	10	1	4	4	6	3	8	12	8.8
	Short	6		3		2		5		16	
DIR30-0	Long	5	8	3	4	1	2	2	4	11	5.6
	Short	3		1		1		2		7	
SC	Short	3	3	12	12	9	9	12	12	36	11.3
VCB	Long	4	11	7	15	3	7	7	13	21	14.4
	Short	7		8		4		6		25	
TOTALS		75		81		68		96		320	

Table 4-5 JS2 Beta crack quantification

JS2 BETA FAMILIES	LENGTH	S1	TOTAL	S2	TOTAL	S3	TOTAL	S4	TOTAL	SUM	%
CJB	Long	0	0	0	0	0	0	0	0	0	0.0
	Short	0		0	0		0		0		
J90C	Long	6	6	6	6	6	6	6	7	25	7.8
	Short	0		0		0		1			
CC	Long	3	3	5	5	4	4	2	2	14	4.4
	Short	0		0		0		0			
Other Cracks											
CNU	Long	0	2	1	1	1	1	0	1	5	1.6
	Short	2	0	0	0	0	0	1			
IC	Long	0	1	1	1	2	2	0	1	5	1.6
	Short	1	0	0	0	0	0	0			
TOTALS		12		13		13		11		49	15.3

Table 4-6 JS2 Beta new crack family numbers

JS3 ALPHA FAMILIES	LENGTH	S1	TOTAL	S2	TOTAL	S3	TOTAL	S4	TOTAL	SUM	%
CB90-80	Long	0	2	0	3	0	5	1	4	1	4.9
	Short	2		3		5		3		13	
CB80-30	Long	2	4	2	3	2	2	2	3	8	4.2
	Short	2		1		0		1		4	
CB30-0	Long	1	3	0	1	1	3	1	3	3	3.5
	Short	2		1		2		2		7	
SCB	Long	6	12	9	13	8	12	7	13	30	17.5
	Short	6		4		4		6		20	
CONNECT	Long	0	2	3	6	5	10	4	9	12	9.4
	Short	2		3		5		5		15	
PARALLEL	Long	3	9	1	6	3	12	3	11	10	13.3
	Short	6		5		9		8		28	
DIR90-80	Long	1	2	2	6	2	5	1	2	6	5.2
	Short	1		4		3		1		9	
DIR80-30	Long	3	8	6	8	4	7	5	7	18	10.5
	Short	5		2		3		2		12	
DIR30-0	Long	2	6	1	3	5	10	3	8	11	9.4
	Short	4		2		5		5		16	
SC	Short	5	5	6	6	10	10	6	6	27	9.4
VCB	Long	3	7	4	7	5	12	4	10	16	12.6
	Short	4		3		7		6		20	
TOTALS		60		62		88		76		286	

Table 4-7 JS3 Alpha crack quantification

JS3 ALPHA FAMILIES	LENGTH	S1	TOTAL	S2	TOTAL	S3	TOTAL	S4	TOTAL	SUM	%
CJB	Long	6	6	6	6	6	6	0	6	24	8.4
	Short	0		0		0			0		
J90C	Long	0	0	0	0	0	0	0	0	0	0.0
	Short	0		0		0		0			
CC	Long	0	0	0	0	0	0	0	0	0	0.0
	Short	0		0		0		0			
Other Cracks											
CNU	Long	2	3	0	1	1	2	2	3	9	3.1
	Short	1		1		1		1			
IC	Long	3	5	2	3	3	5	3	7	20	7.0
	Short	2		1		2		4			
TOTALS		14		10		13		16		53	18.5

Table 4-8 JS3 Alpha new crack family numbers

JS4 ALPHA FAMILIES	LENGTH	S1	TOTAL	S2	TOTAL	S3	TOTAL	S4	TOTAL	SUM	%
CB90-80	Long	3	3	4	5	3	4	4	6	14	5.7
	Short	0		1		1		2		4	
CB80-30	Long	3	4	3	8	3	8	4	9	13	9.2
	Short	1		5		5		5		16	
CB30-0	Long	0	1	1	2	2	2	3	7	6	3.8
	Short	1		1		0		4		6	
SCB	Long	2	9	1	4	3	10	4	12	10	11.1
	Short	7		3		7		8		25	
CONNECT	Long	0	0	4	9	8	13	7	13	19	11.1
	Short	0		5		5		6		16	
PARALLEL	Long	5	10	7	15	6	14	9	17	27	17.8
	Short	5		8		8		8		29	
DIR90-80	Long	2	3	2	7	2	7	3	9	9	8.3
	Short	1		5		5		6		17	
DIR80-30	Long	2	5	4	9	7	10	6	9	19	10.5
	Short	3		5		3		3		14	
DIR30-0	Long	0	1	3	6	3	5	2	6	8	5.7
	Short	1		3		2		4		10	
SC	Short	2	2	11	11	10	10	11	11	34	10.8
VCB	Long	3	8	1	2	1	2	2	6	7	5.7
	Short	5		1		1		4		11	
TOTALS		46		78		85		105		314	

Table 4-9 JS4 Alpha crack quantification

JS4 ALPHA FAMILIES	LENGTH	S1	TOTAL	S2	TOTAL	S3	TOTAL	S4	TOTAL	SUM	%
CJB	Long	0	0	0	0	0	0	0	0	0	0.0
	Short	0		0							
J90C	Long	3	3	5	5	5	5	5	5	18	5.7
	Short	0		0		0		0			
CC	Long	2	2	1	1	2	2	2	2	7	2.2
	Short	0		0		0		0			
Other Cracks											
CNU	Long	2	2	0	1	2	2	1	3	8	2.5
	Short	0		1		0		2			
IC	Long	2	2	4	6	5	5	4	9	22	7.0
	Short	0		2		0		5			
TOTALS		9		13		14		19		55	17.5

Table 4-10 JS4 Alpha new crack family numbers

JS4 BETA FAMILIES	LENGTH	S1	TOTAL	S2	TOTAL	S3	TOTAL	S4	TOTAL	SUM	%
CB90-80	Long	2	6	3	7	2	5	3	6	10	6.9
	Short	4		4		3		3		14	
CB80-30	Long	2	4	1	6	2	6	1	5	6	6.0
	Short	2		5		4		4		15	
CB30-0	Long	1	2	0	4	1	4	2	7	4	4.9
	Short	1		4		3		5		13	
SCB	Long	4	13	3	9	4	11	3	10	14	12.4
	Short	9		6		7		7		29	
CONNECT	Long	1	4	2	7	3	9	3	8	9	8.0
	Short	3		5		6		5		19	
PARALLEL	Long	11	21	9	17	7	12	9	19	36	19.8
	Short	10		8		5		10		33	
DIR90-80	Long	1	7	2	7	3	7	4	9	10	8.6
	Short	6		5		4		5		20	
DIR80-30	Long	5	10	4	8	5	7	3	6	17	8.9
	Short	5		4		2		3		14	
DIR30-0	Long	1	3	3	5	3	7	2	5	9	5.7
	Short	2		2		4		3		11	
SC	Short	12	12	15	15	9	9	11	11	47	13.5
VCB	Long	2	6	1	4	1	4	2	4	6	5.2
	Short	4		3		3		2		12	
TOTALS		88		89		81		90		348	

Table 4-11 JS4 Beta crack quantification

JS4 BETA FAMILIES	LENGTH	S1	TOTAL	S2	TOTAL	S3	TOTAL	S4	TOTAL	SUM	%
CJB	Long	0	0	0	0	0	0	0	0	0	0.0
	Short	0		0	0		0		0		
J90C	Long	8	8	8	8	7	9	7	8	33	9.5
	Short	0		0		2		1			
CC	Long	2	2	2	2	2	2	2	2	8	2.3
	Short	0		0		0		0			
Other Cracks											
CNU	Long	1	2	1	2	0	1	2	2	7	2.0
	Short	1		1		1		0			
IC	Long	3	6	3	5	3	4	4	4	19	5.5
	Short	3		2		1		0			
TOTALS		18		17		16		16		67	19.3

Table 4-12 JS4 Beta new crack family numbers

REF1 FAMILIES	LENGTH	S1	TOTAL	S2	TOTAL	S3	TOTAL	S4	TOTAL	SUM	%
CB90-80	Long	0	0	2	3	1	1	1	2	4	1.9
	Short	0		1		0		1		2	
CB80-30	Long	1	2	0	1	1	2	3	3	5	2.5
	Short	1		1		1		0		3	
CB30-0	Long	1	1	1	1	0	1	1	2	3	1.6
	Short	0		0		1		1		2	
SCB	Long	6	11	10	18	4	11	8	13	28	16.7
	Short	5		8		7		5		25	
CONNECT	Long	4	12	4	7	4	7	5	10	17	11.4
	Short	8		3		3		5		19	
PARALLEL	Long	8	14	7	13	9	21	7	13	31	19.2
	Short	6		6		12		6		30	
DIR90-80	Long	5	9	5	9	4	7	3	8	17	10.4
	Short	4		4		3		5		16	
DIR80-30	Long	2	7	2	6	3	10	3	7	10	9.5
	Short	5		4		7		4		20	
DIR30-0	Long	2	4	1	3	1	3	2	4	6	4.4
	Short	2		2		2		2		8	
SC	Short	11	11	13	13	5	5	10	10	39	12.3
VCB	Long	2	7	4	8	4	9	4	8	14	10.1
	Short	5		4		5		4		18	
TOTALS		78		82		77		80		317	

Table 4-13 Reference 1 crack quantification

REF1 FAMILIES	LENGTH	S1	TOTAL	S2	TOTAL	S3	TOTAL	S4	TOTAL	SUM	%
CJB	Long	0	0	0	0	0	0	0	0	0	0.0
	Short	0		0	0		0		0		
J90C	Long	0	0	0	0	0	0	0	0	0	0.0
	Short	0		0		0		0			
CC	Long	0	0	0	0	0	0	0	0	0	0.0
	Short	0		0		0		0			
Other Cracks											
CNU	Long	2	3	2	2	3	4	3	4	13	4.1
	Short	1		0		1		1			
IC	Long	4	6	3	4	4	6	3	4	20	6.3
	Short	2		1		2		1			
TOTALS		9		6		10		8		33	10.4

Table 4-14 Reference 1 new crack family numbers

REF2 FAMILIES	LENGTH	S1	TOTAL	S2	TOTAL	S3	TOTAL	S4	TOTAL	SUM	%
CB90-80	Long	0	0	1	1	1	1	1	1	3	1.1
	Short	0		0		0		0		0	
CB80-30	Long	2	3	2	2	2	2	1	1	7	2.9
	Short	1		0		0		0		1	
CB30-0	Long	2	3	1	2	1	1	0	0	4	2.2
	Short	1		1		0		0		2	
SCB	Long	7	10	6	7	4	4	7	12	24	12.1
	Short	3		1		0		5		9	
CONNECT	Long	6	10	4	8	3	9	4	7	17	12.5
	Short	4		4		6		3		17	
PARALLEL	Long	5	9	4	13	4	9	2	5	15	13.2
	Short	4		9		5		3		21	
DIR90-80	Long	2	3	3	6	2	2	5	8	12	7.0
	Short	1		3		0		3		7	
DIR80-30	Long	1	4	4	7	5	8	3	5	13	8.8
	Short	3		3		3		2		11	
DIR30-0	Long	3	4	4	9	4	9	2	4	13	9.5
	Short	1		5		5		2		13	
SC	Short	9	9	13	13	14	14	13	13	49	17.9
VCB	Long	1	11	5	12	4	8	1	4	11	12.8
	Short	10		7		4		3		24	
TOTALS		66		80		67		60		273	

Table 4-15 Reference 2 crack quantification

REF2 FAMILIES	LENGTH	S1	TOTAL	S2	TOTAL	S3	TOTAL	S4	TOTAL	SUM	%
CJB	Long	0	0	0	0	0	0	0	0	0	0.0
	Short	0		0	0		0		0		
J90C	Long	0	0	0	0	0	0	0	0	0	0.0
	Short	0		0		0		0			
CC	Long	0	0	0	0	0	0	0	0	0	0.0
	Short	0		0		0		0			
Other Cracks											
CNU	Long	1	3	2	2	2	3	2	2	10	3.7
	Short	2		0		1		0			
IC	Long	2	3	3	4	2	3	2	4	14	5.1
	Short	1		1		1		2			
TOTALS		6		6		6		6		24	8.8

Table 4-16 Reference 2 new crack family numbers

REF3 FAMILIES	LENGTH	S1	TOTAL	S2	TOTAL	S3	TOTAL	S4	TOTAL	SUM	%
CB90-80	Long	2	2	2	2	0	0	1	1	5	1.9
	Short	0		0		0		0		0	
CB80-30	Long	2	2	1	1	1	2	1	1	5	2.2
	Short	0		0		1		0		1	
CB30-0	Long	1	1	3	5	0	0	0	0	4	2.2
	Short	0		2		0		0		2	
SCB	Long	7	10	6	11	7	11	5	9	25	15.2
	Short	3		5		4		4		16	
CONNECT	Long	4	9	3	7	5	10	3	6	15	11.9
	Short	5		4		5		3		17	
PARALLEL	Long	4	7	7	15	7	18	4	10	22	18.6
	Short	3		8		11		6		28	
DIR90-80	Long	3	3	2	6	3	7	2	5	10	7.8
	Short	0		4		4		3		11	
DIR80-30	Long	4	5	1	6	2	7	2	6	9	8.9
	Short	1		5		5		4		15	
DIR30-0	Long	0	4	1	5	1	3	1	3	3	5.6
	Short	4		4		2		2		12	
SC	Short	5	5	13	13	23	23	10	10	51	19.0
VCB	Long	1	3	1	6	3	5	3	4	8	6.7
	Short	2		5		2		1		10	
TOTALS		51		77		86		55		269	

Table 4-17 Reference 3 crack quantification

REF3 FAMILIES	LENGTH	S1	TOTAL	S2	TOTAL	S3	TOTAL	S4	TOTAL	SUM	%
CJB	Long	0	0	0	0	0	0	0	0	0	0.0
	Short	0		0	0		0		0		
J90C	Long	0	0	0	0	0	0	0	0	0	0.0
	Short	0		0		0		0			
CC	Long	0	0	0	0	0	0	0	0	0	0.0
	Short	0		0		0		0			
Other Cracks											
CNU	Long	1	2	3	4	2	3	0	2	11	4.1
	Short	1		1		1		2			
IC	Long	1	2	1	4	1	3	2	5	14	5.2
	Short	1		3		2		3			
TOTALS		4		8		6		7		25	9.3

Table 4-18 Reference 3 new crack family numbers

4.2.4.3 Crack Classification Graphs and Comparisons

The data from crack counting were used to make graphs of the differences between blocks and slices. Graphs for the blocks are shown in Figure 4-43 to Figure 4-67;

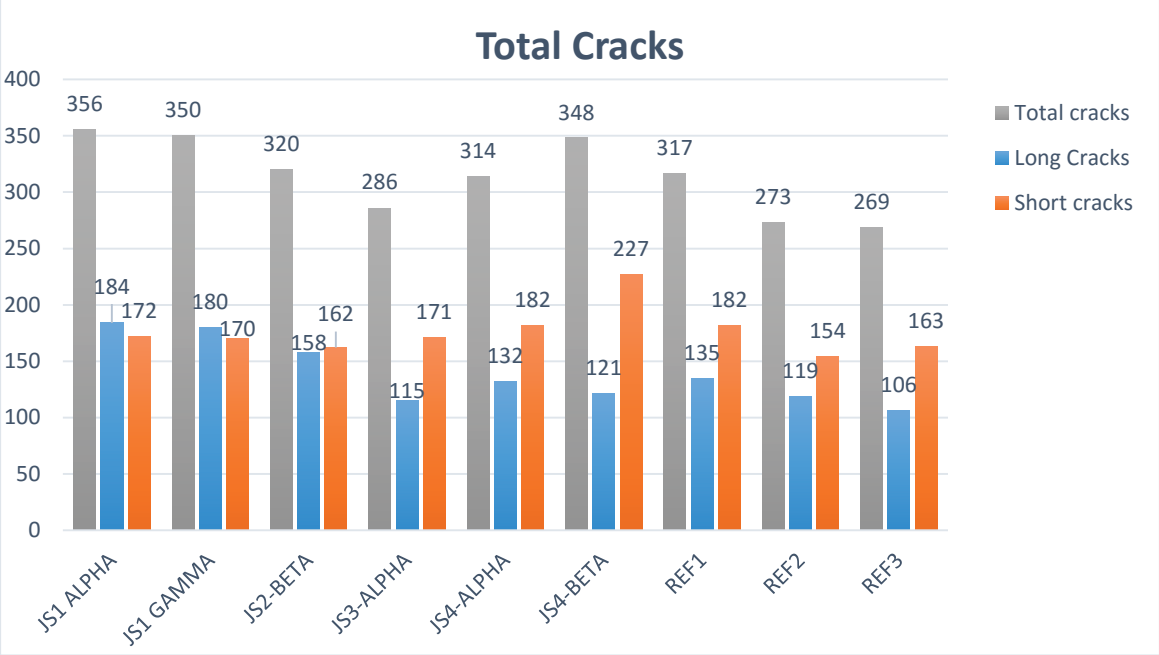

Figure 4-43 Comparison of total crack values

From the data in Figure 4-43, it can be observed that JS1 and JS4 blocks have the largest average number of cracks. In long cracks case, JS1 set contains the longest cracks. Short crack numbers are respectively same in every block except the JS4 beta block. This block has more short cracks than the averages of other blocks.

The Figure 4-44 shows the numbers of original crack families in the blocks. This figure gives the first impression about the crack numbers in the blocks. The crack families are discussed individually and detailed in the later sections.

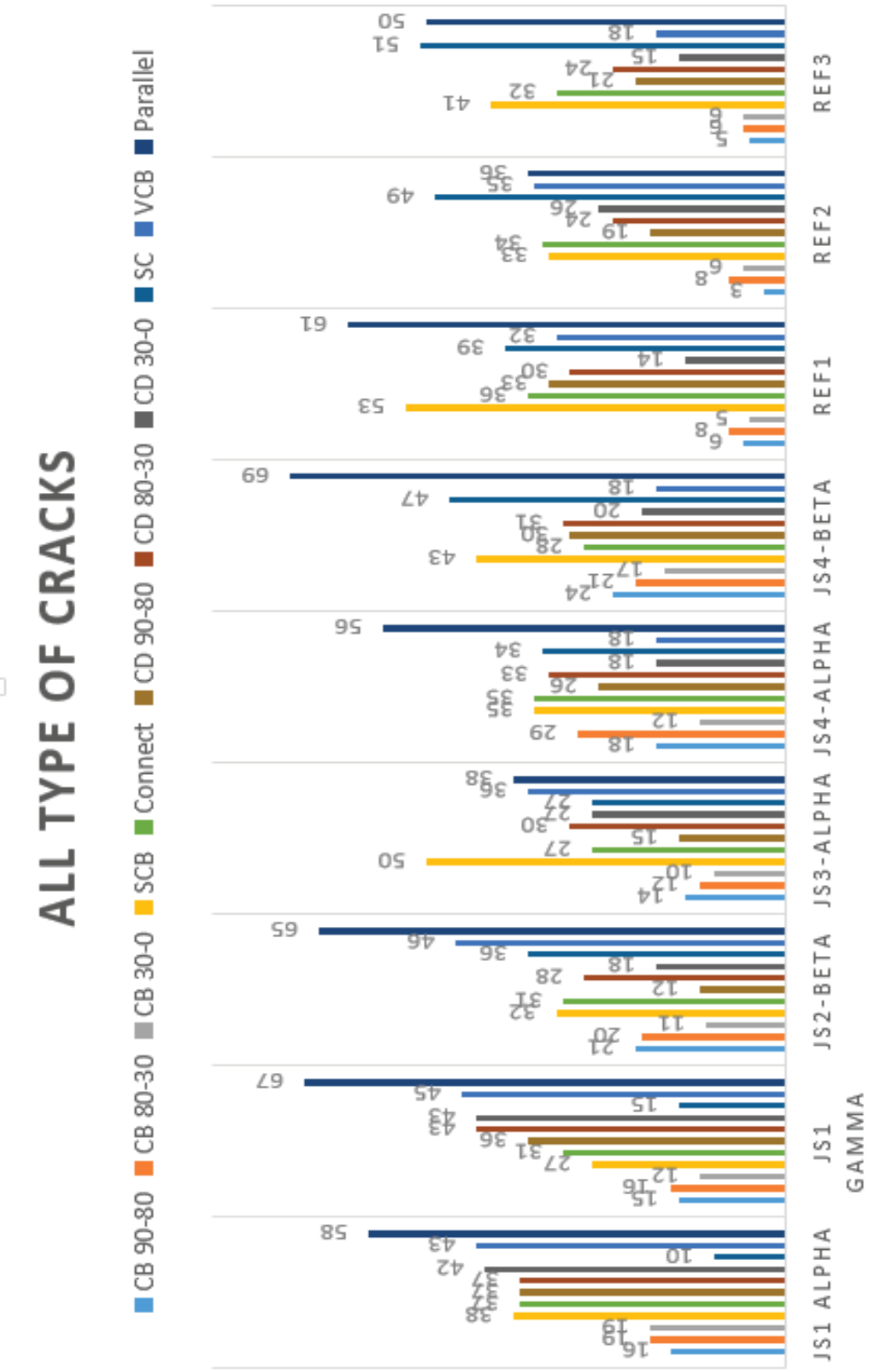

Figure 4-44 Comparison of all family of cracks in all blocks

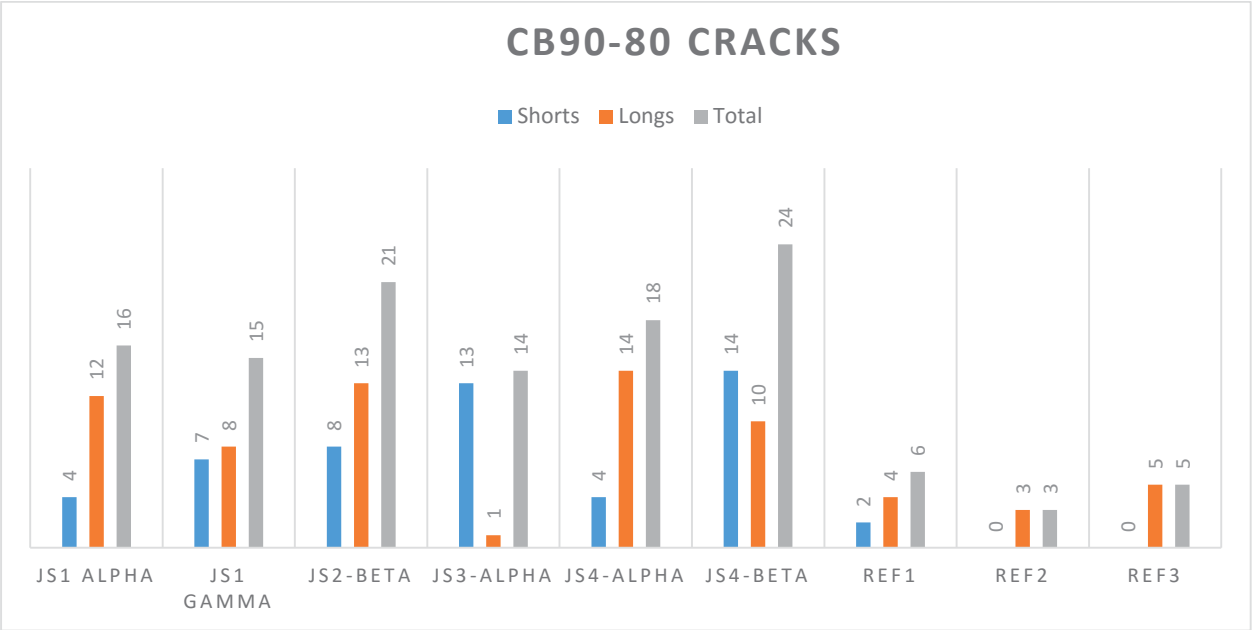

Figure 4-45 CB90-80 Cracks comparison

It can be observed from the Figure 4-45 that the reference blocks have the lowest number of CB90-80 family cracks. This family of cracks occurs more frequently in jointed blocks. The average crack number of JS4 blocks and JS2 blocks are about the same and the highest ones. JS1 blocks have the second smallest number of short cracks after the reference blocks.

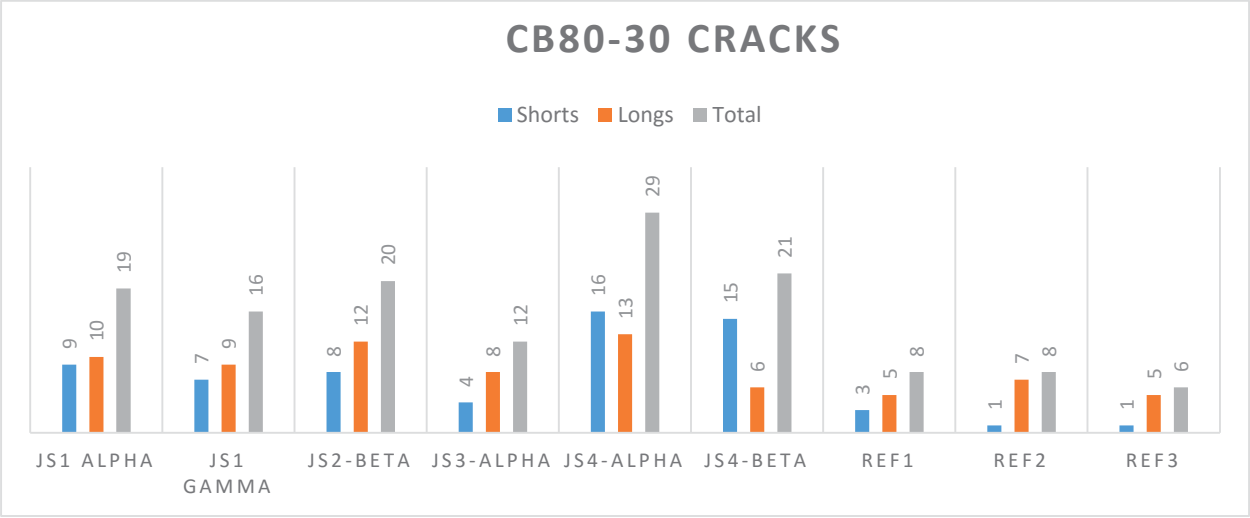

Figure 4-46 Comparison of CB80-30 family of cracks

Just like the CB90-80 crack comparison, Figure 4-46 shows that the reference blocks have the lowest number of CB80-30 family of cracks. Somehow, this family of cracks occur the most frequently in the blocks JS4 which has joints dipping with 70°. Furthermore, the JS4 family has also the largest short crack average.

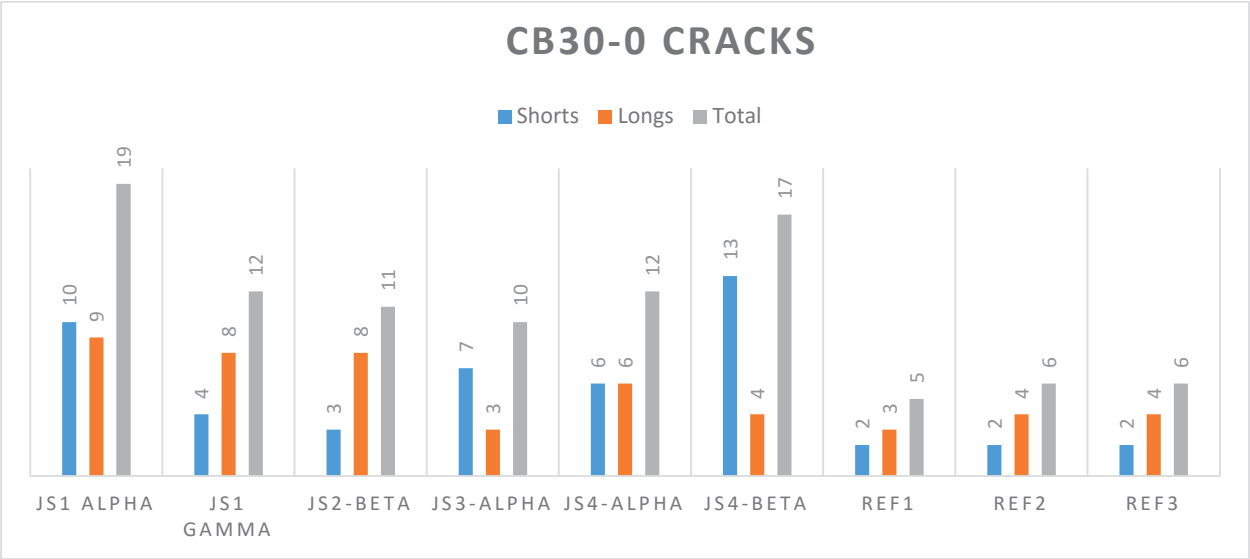

Figure 4-47 Comparison of CB30-0 family of cracks

Just like for the other CB family cracks, Figure 4-47 shows that the reference blocks have the lowest number of CB30-0 cracks. Differing from CB80-30 comparison, the JS1 blocks have the largest number of cracks in this case. However the JS4 set still has a high average number of cracks compared to the others.

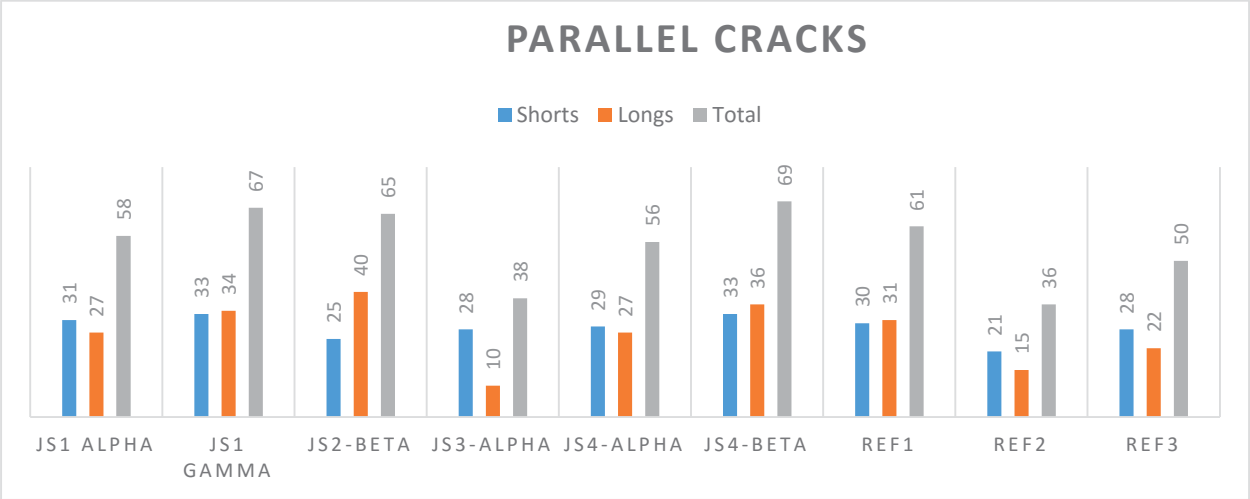

Figure 4-48 Comparison of Parallel family of cracks

Figure 4-44 and Figure 4-48 show that in nearly all cases the parallel cracks are the most abundant ones. The JS3 set has the smallest number of parallel cracks except block Reference 2. The average Reference block value is higher though. Minor changes during the blasting might influence this.

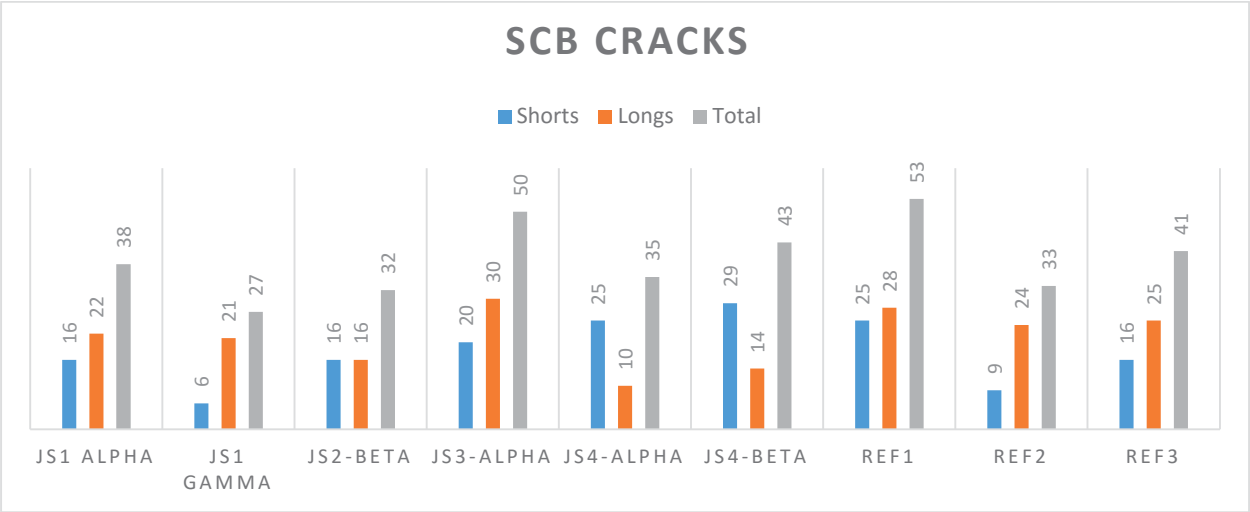

Figure 4-49 Comparison of Short cracks from the back

Figure 4-49 shows that the largest number of short cracks from the back is observed in blocks JS3 alpha and Ref 1. The other blocks don't show any significant differences in SCB crack numbers.

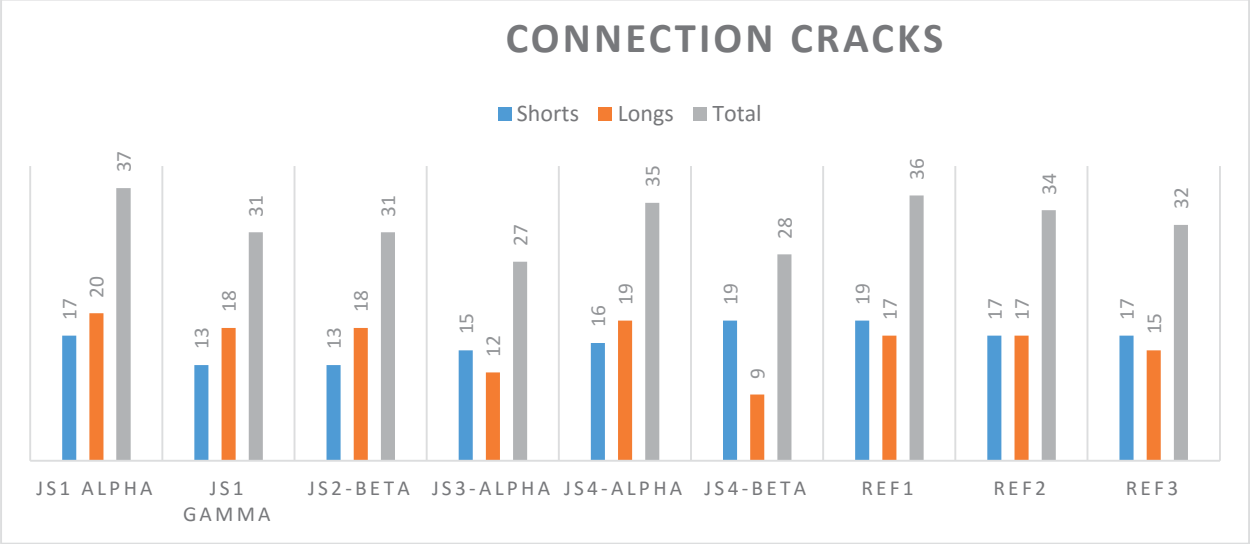

Figure 4-50 Comparison of Connection cracks

Figure 4-50 shows that no significant differences in crack numbers exist between the blocks. Neither long crack numbers, nor short crack numbers are very different. However block JS4 Beta has approximately 50% fewer long cracks than the other blocks.

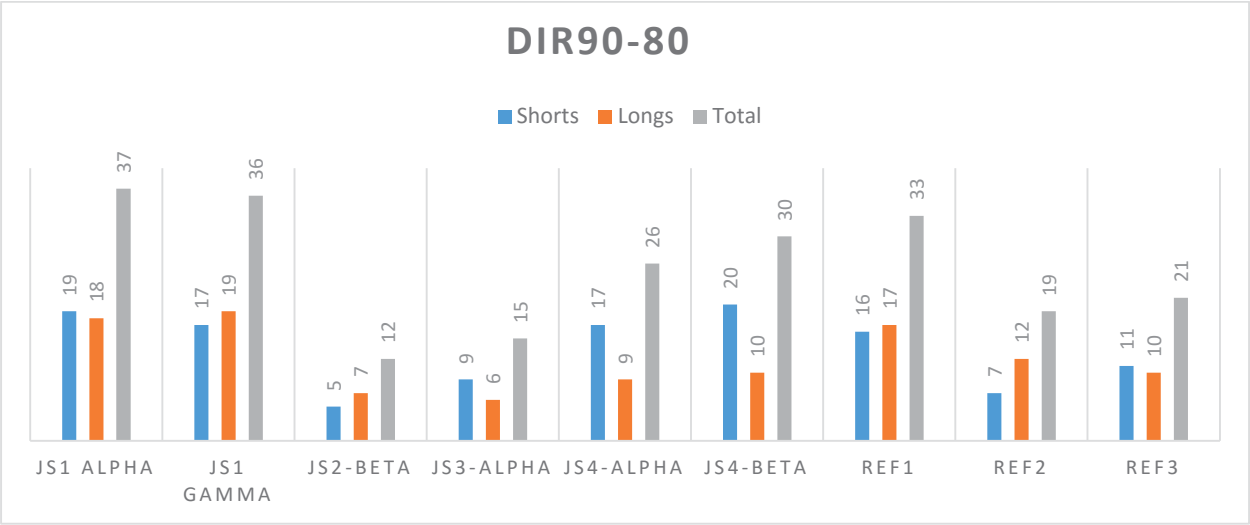

Figure 4-51 Comparison of DIR90-80 cracks

Figure 4-51 shows that joint set differences may have a strong effect on the formation of DIR90-80 family cracks. The JS1 blocks have large number of DIR90-80 family cracks while the JS2 and JS3 blocks have 60% fewer. Most of the blocks have almost equal number of short and long cracks while the JS4 blocks have much fewer long cracks.

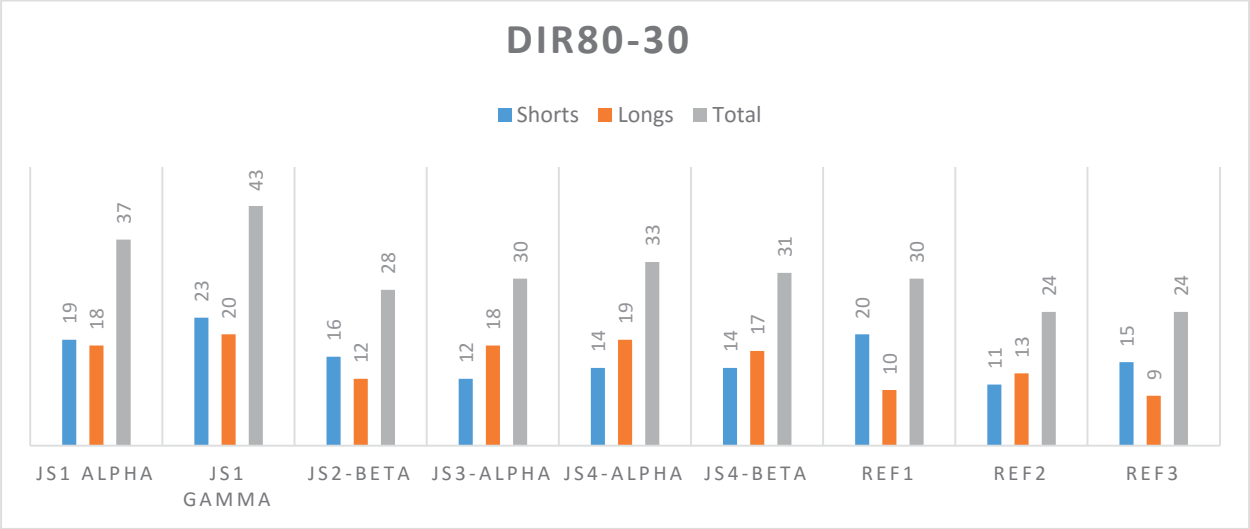

Figure 4-52 Comparison of DIR80-30 cracks

Figure 4-52 can be interpreted just as the DIR90-80 data in Figure 4-54 since two crack families are relatively similar. Different from the DIR90-80 cracks, the JS2 and JS3 sets have a relatively larger number of these cracks and the number of long cracks in JS4 blocks is higher in this case.

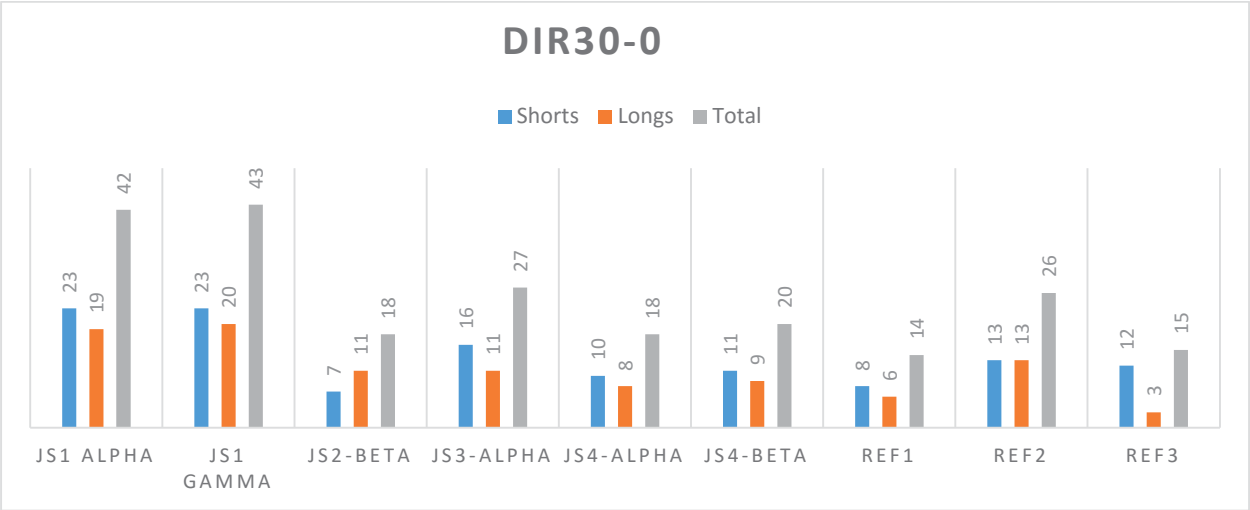

Figure 4-53 Comparison of DIR30-0 cracks

Figure 4-53 shows that the largest number of DIR30-0 family of cracks occur in the JS1 blocks. Furthermore the number of short cracks is with two exceptions larger than the number of long cracks in the blocks. In block JS2 Beta there are more long cracks than short ones. If we disregard the JS1 blocks, the number of DIR30-0 cracks in all other blocks is relatively constant.

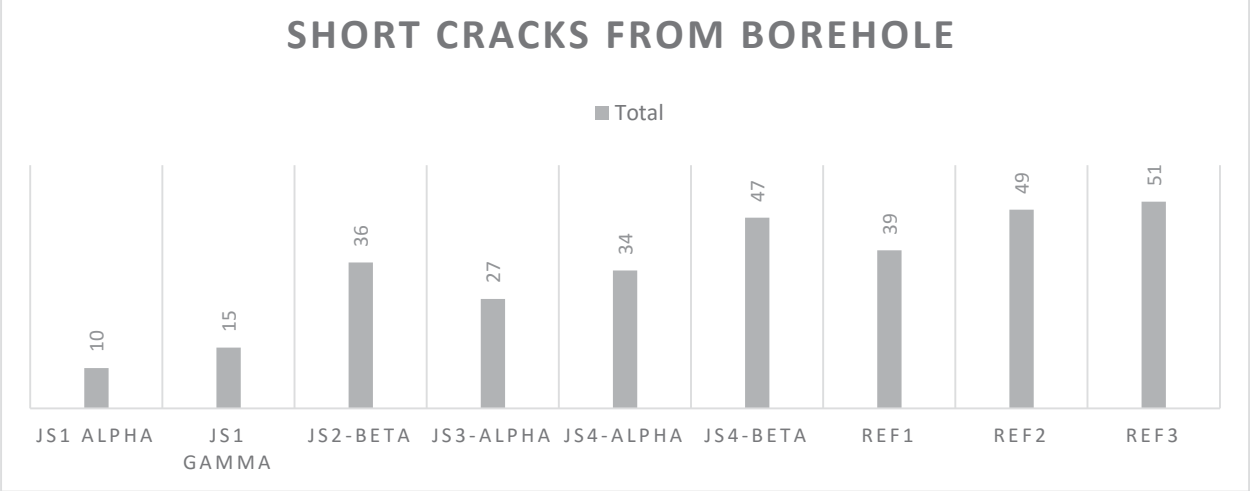

Figure 4-54 Comparison of SCB cracks

Figure 4-54 shows that the Reference and JS4 blocks have a relatively high number of SCB cracks compared to the other joint set blocks. The JS1 blocks have a substantially lower number of SCB cracks. Figure 4-36 on the other hand shows that the JS1 blocks has the largest number of cracks when all families are summed.

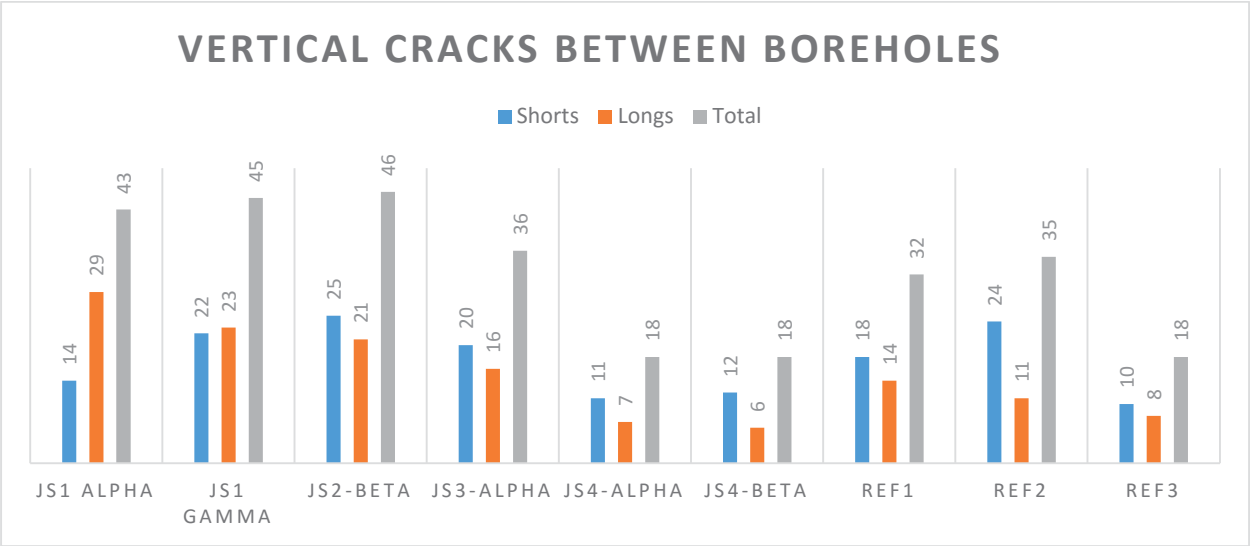

Figure 4-55 Comparison of vertical cracks between boreholes

Figure 4-55 shows that the largest number of vertical cracks between boreholes are observed in the JS1 and JS2 blocks while the JS4 blocks have the fewest number. Comparisons using statistical methods are made in the following sections.

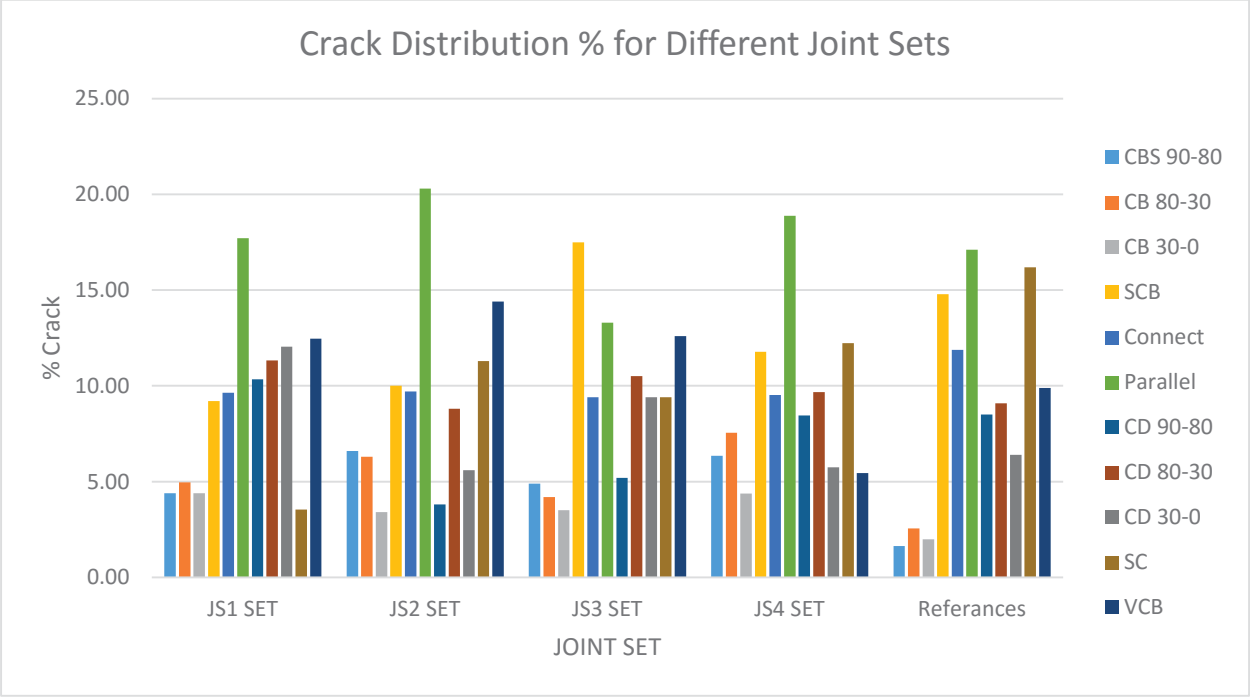

Figure 4-56 Crack distribution % for blocks

Figure 4-56 shows the percentage distribution of the crack families inside the blocks.

4.2.4.4 New Crack Family Graphs

The Figure 4-57 shows the total, long and short crack numbers of the new crack families for every block. As is indicated in section 4.2.3 they are considered under the original crack family numbers in the statistical analysis however they are calculated separately in this section. These graphs are to compare the new crack families and show their distribution.

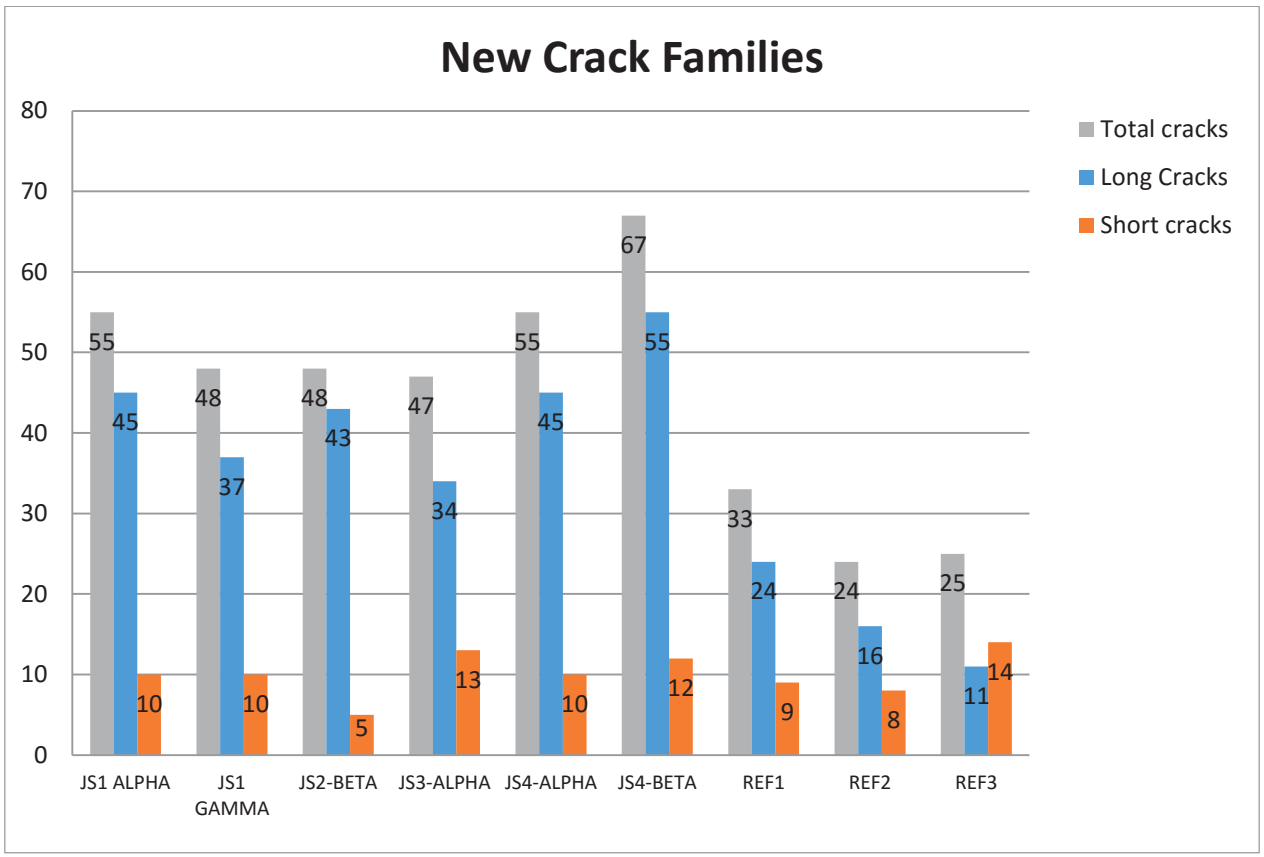

Figure 4-57 Total, long and short crack numbers of the new crack families

According to the Figure 4-57, the JS4 Beta block has the largest number of the new crack families. The reference blocks with no joints have the smallest number of new crack families as expected. These numbers includes only the CNU and IC crack families while all other blocks numbers include the JRC families.

The figures Figure 4-58 to Figure 4-66 show the percentages of the new crack families in the blocks.

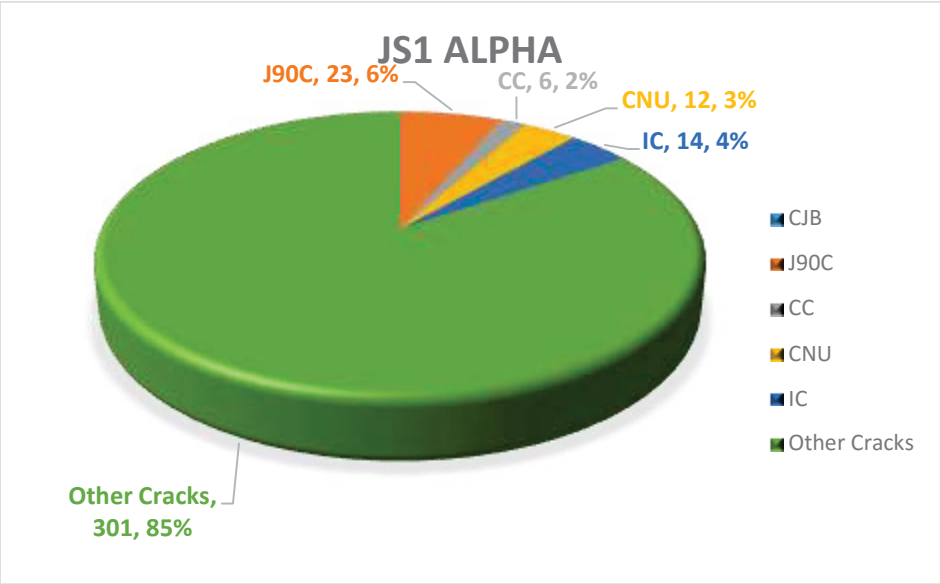

Figure 4-58 Specimen JS1 Alpha. New crack family values and percentages

As it is shown in the Figure 4-58, 85% of the cracks belong to the original crack families. 8% of the cracks in block JS1 Alpha are J90C and CC cracks and their formation is thought to be joint related. The joint related CJB cracks are not present in block JS1 Alpha due to the structure of the joints in the block. The new families CNU and IC make up 7% of the cracks.

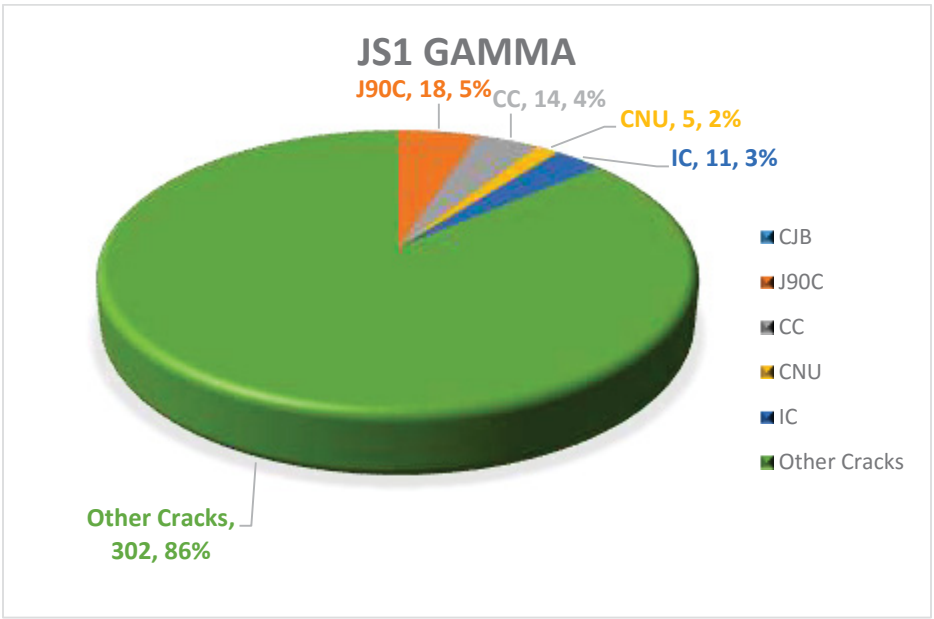

Figure 4-59 Specimen JS1 Gamma. New crack family values and percentages

The Figure 4-59 shows the numbers and percentages of the new crack families in the block JS1 Gamma. 9% of the cracks are joint related and 86% belong to original crack families while the 5% belong to the CNU and IC cracks.

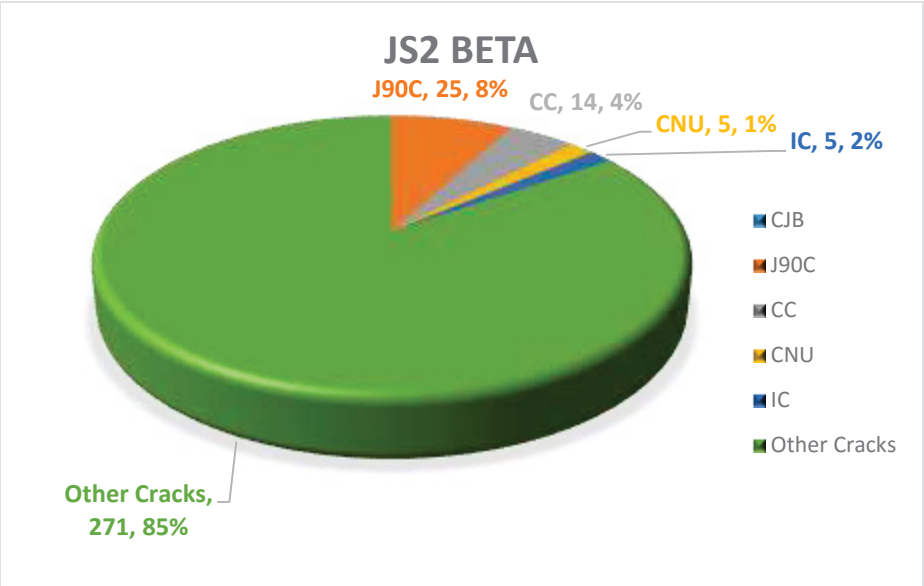

Figure 4-60 Specimen JS2 Beta. New crack family values and percentages

The Figure 4-60 shows the crack numbers and percentages of the new crack families in the JS2 block. 12% of the total cracks are joint related. Block JS2 Beta also has a small number of the new CNU and IC cracks with the percentage of 3%.

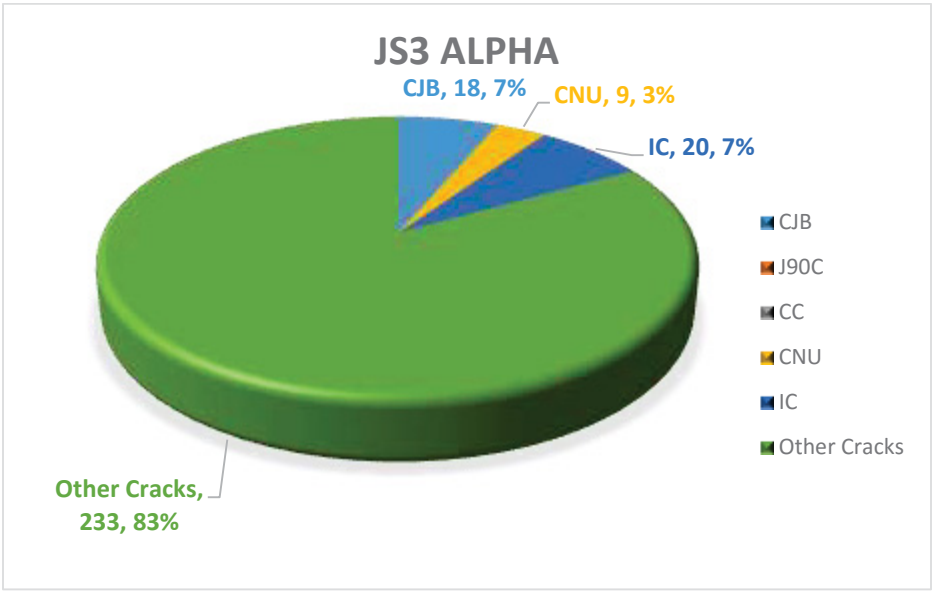

Figure 4-61 Specimen JS3 Alpha. New crack family values and percentages

The Figure 4-61 shows the numbers of the new crack families in block JS3 Alpha. This block has 7% of CJB cracks and it is the only block which has this family. It also has a relatively significant number of the new IC cracks within.

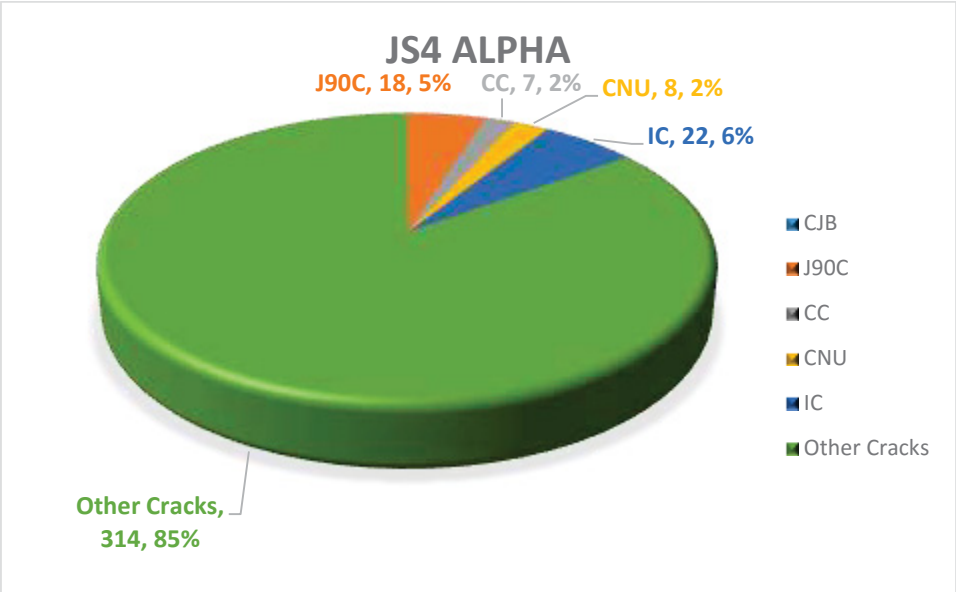

Figure 4-62 Specimen JS4 Alpha. New crack family values and percentages

The number of the joint related cracks are 7% in the JS4 Alpha block. As shown in the Figure 4-62, the total content of the new crack families in block JS4 Alpha is 15% of the total cracks.

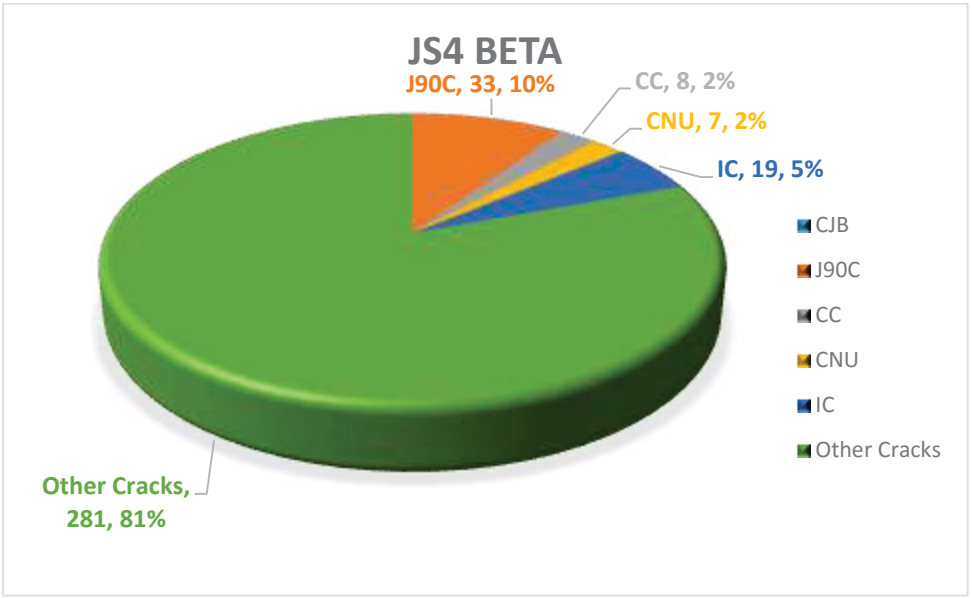

Figure 4-63 Specimen JS4 Beta. New crack family values and percentages

Block JS4 Beta has the largest J90C crack number compared to the other blocks. The total number of JRC cracks is 12% in this block. The percentage of the new crack families is 19% which is also the largest of all blocks. The Figure 4-63 shows the detailed information about block JS4 Beta.

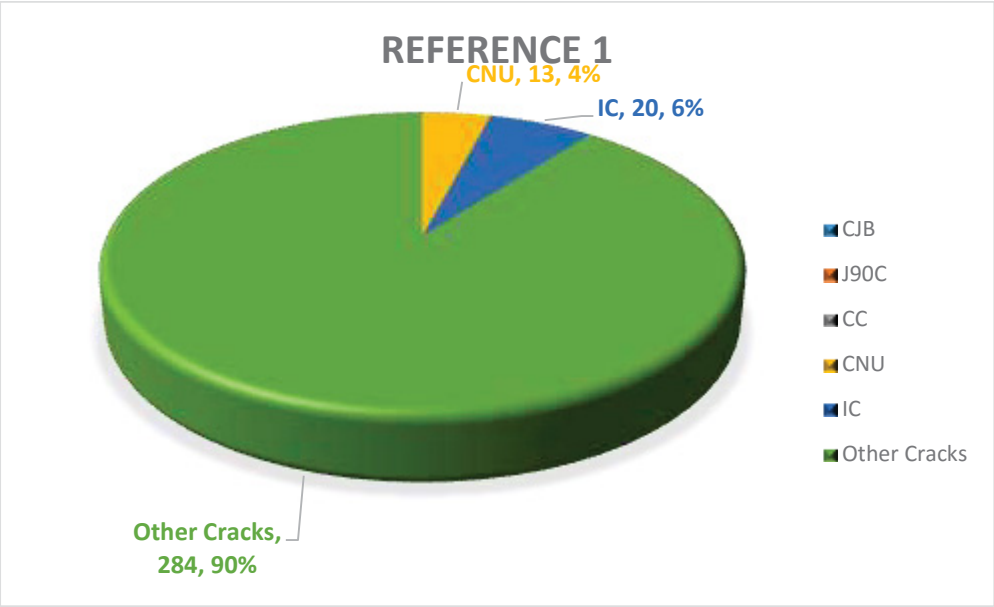

Figure 4-64 Specimen Reference 1. New crack family values and percentages

Reference 1 block has no JRC cracks. The CNU and IC cracks make up 10% of the total cracks. The Figure 4-64 shows a detailed crack numbers distribution for the Reference 1 block.

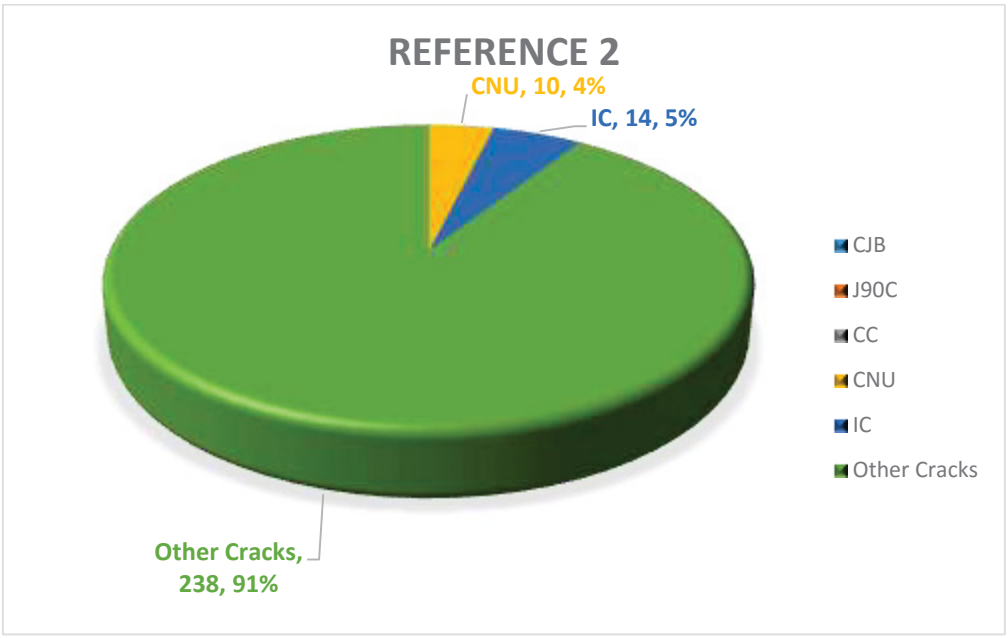

Figure 4-65 Specimen Reference 2. New crack family values and percentages

Just like the Reference 1 block, block Reference 2 has no JRC cracks within. The CNU and IC content in this block is 9%. The Figure 4-65 shows a detailed crack distribution for the Reference 2 block.

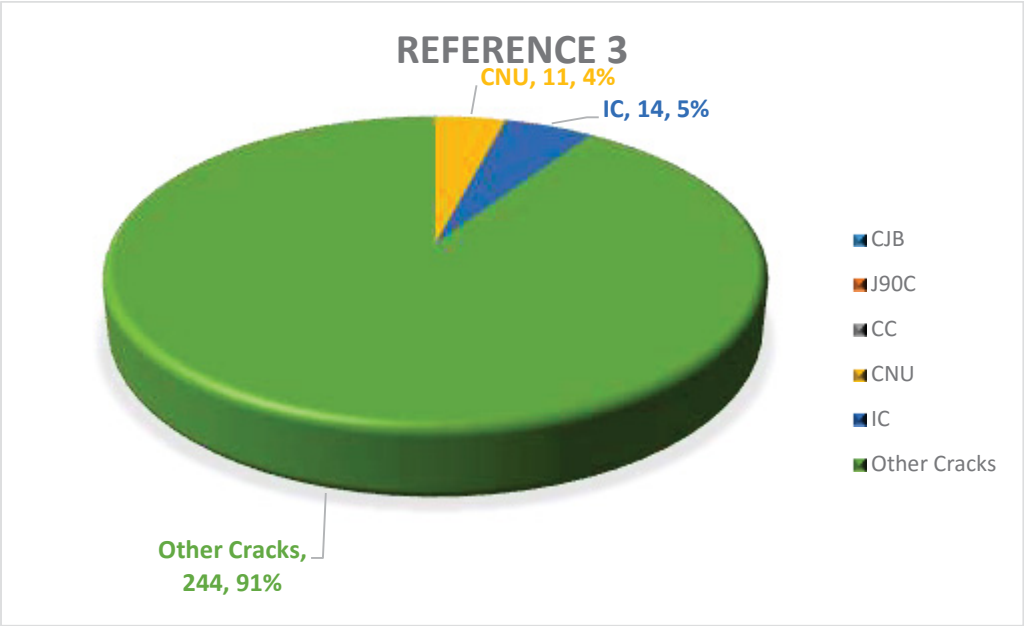

Figure 4-66 Specimen Reference 3. New crack family values and percentages

The Figure 4-66 shows the distribution of the crack numbers in the Reference 3 block. This block has 9% of CNU and IC cracks. The percentage of the original crack families is 91%.

The pie diagrams show that new crack families make up approximately 15% of the total cracks. This number is relatively important. The joint related JRC cracks in the blocks play an important role in the damaging the blocks. In practice they were also observed that they cause boulder breakages. This can be considered as an obvious proof of the influence of joints on the fragmentation. The summary of all analyses are furtherly discussed in the section 5.

4.2.4.5 Sieving Data

The fragments were collected after each row blasted. Sieving was done later in the Mineral Processing laboratory at the Montanuniversität Leoben. As a result of sieving we obtained particle size distributions for the individual rows of the blocks and from them some K values are calculated. The sieving work was done according to the sieving standards of the Chair of Mining Engineering.

The fragments were sieved in 2 steps, first the 125 mm-14 mm material and then the 14 mm-0.25 mm material. All the material was put into the sieves and was shaken by hand. The sieving machine was not used to avoid secondary breakage. The fragments larger than 20 mm were pushed through the mesh to achieve more correct results as the large particles occasionally don't pass the mesh even if they are able to. The mesh sizes that

were used are respectively 125, 100, 80, 63, 50, 40, 31.5, 25, 20, 14, 12.5, 10, 6.3, 4, 2, 1, 0.5 and 0.25 mm.

As we completed the sieving of the first part (125-14 mm), all fragments <14 mm were collected in a bucket and weighed. If they were heavier than 3kg, then the masses were split into two parts, and only one part was used for further sieving.

After all the sieving was completed, the particles on the large sieves were cleared from the waste materials by hand. For the particles on the smaller sieves, a magnet was used as our mortar material is magnetic.

All fragments from the sieves were collected in separate bags and weighed. These data are used to calculate K_{30}, K_{50} and K_{80}. After the fragmentation ratios are obtained, a sieving graph which consists of the cumulative percentage mass passing through the meshes of different sizes was constructed. The values of K_{30}, K_{50} and K_{80} are calculated by interpolation. The calculation formula is as follows:

$$K_{50} = K_L + \frac{K_U - K_L}{P_U - P_L} . (P_{50} - P_L)$$

Equation 9 K_{50} Calculation formula for K_{50} Values for K_{30} and K_{80} are obtained by replacing 50 by 30 or 80 respectively

Here;

K_{50}: calculated grain size at cumulative mass passing of 50%
K_L: lower screen size next to cumulative mass passing of 30%-50%-80%
K_U: upper screen size next to cumulative mass passing of 30%-50%-80%
P_L: cumulative mass passing at K_L
P_U: cumulative mass passing at K_U
P_{50}: cumulative mass passing at K_{50} (= 50%)
When the size distribution curves are observed, it can be seen that some of the lines don't reach to 100%. In those cases there was a boulder fragment involved which was not passing through any of the sieves. Since these cumulative graphs are based on undersize of the sieves, it was not possible to estimate the mesh size with current meshes without the help of a ruler where it reaches 100%. The numbers of the sieving results are shown at ANNEX III.

4.2.4.6 Size Distribution Graphs

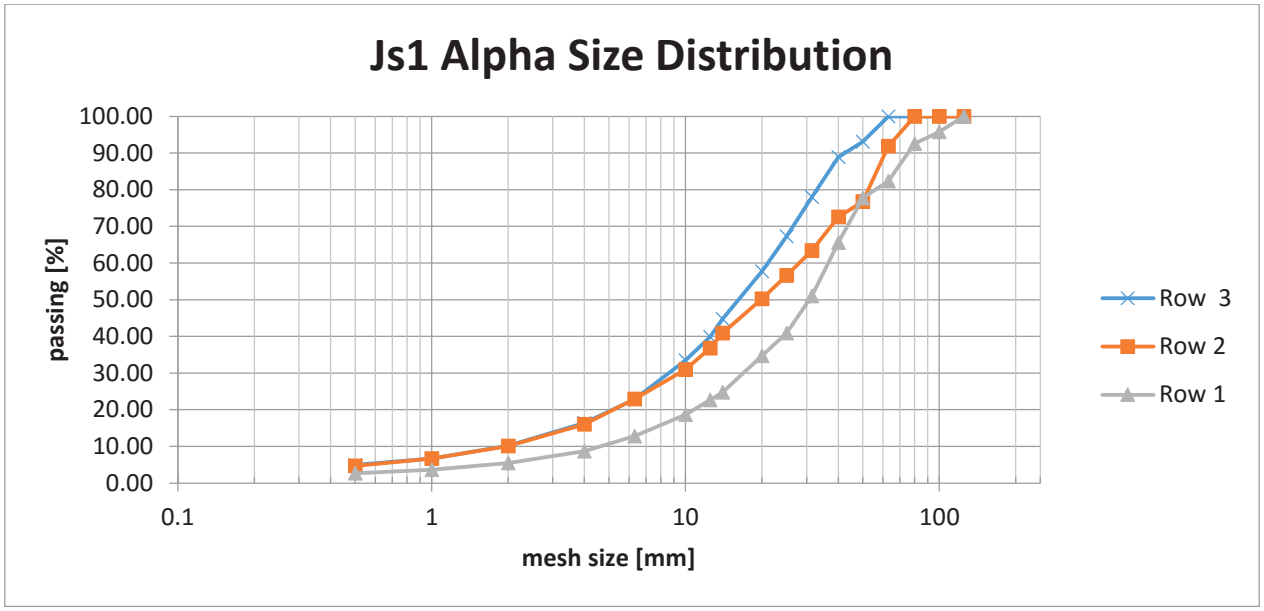

Figure 4-67 JS1 Alpha size distribution

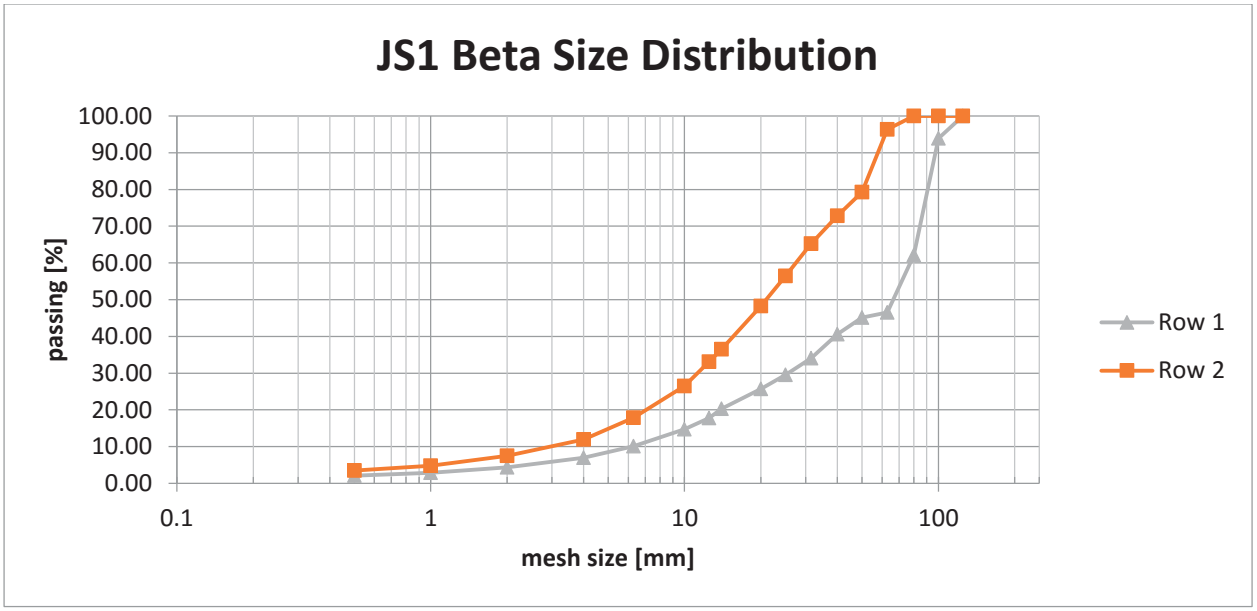

Figure 4-68 JS1 Beta size distribution

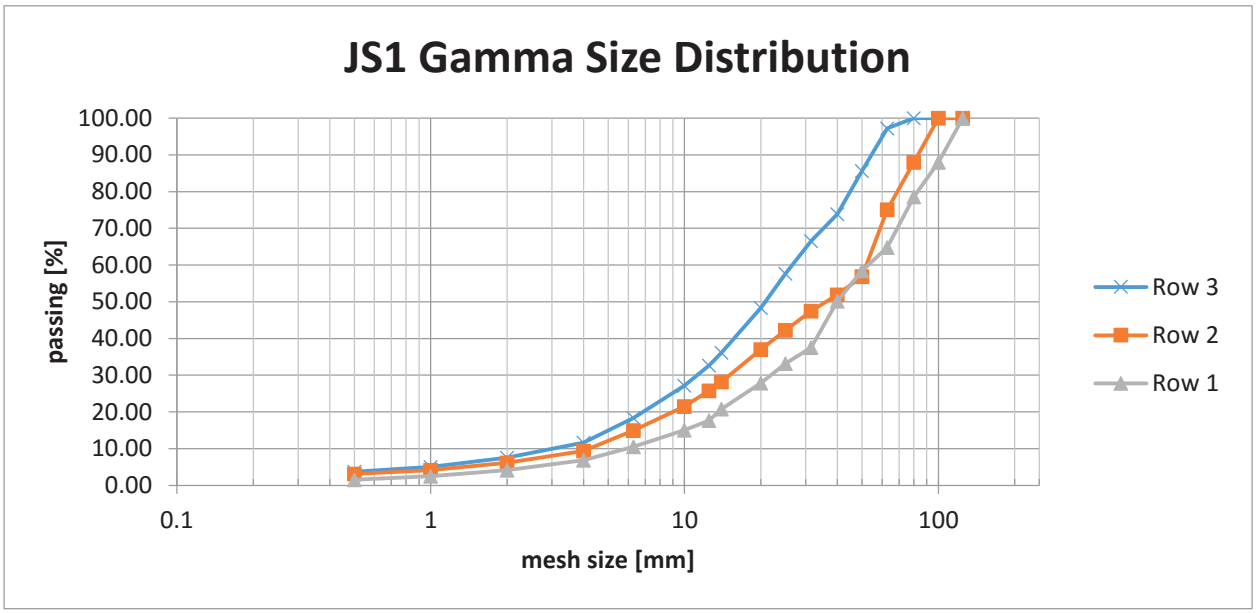

Figure 4-69 JS1 Gamma size distribution

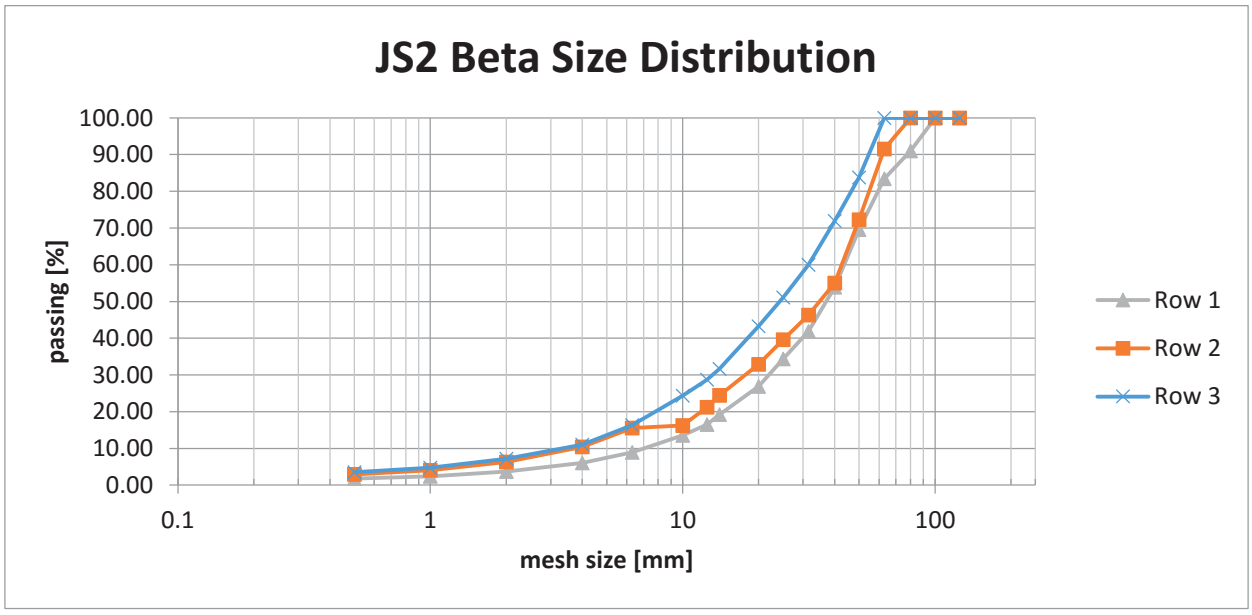

Figure 4-70 JS2 Beta size distribution

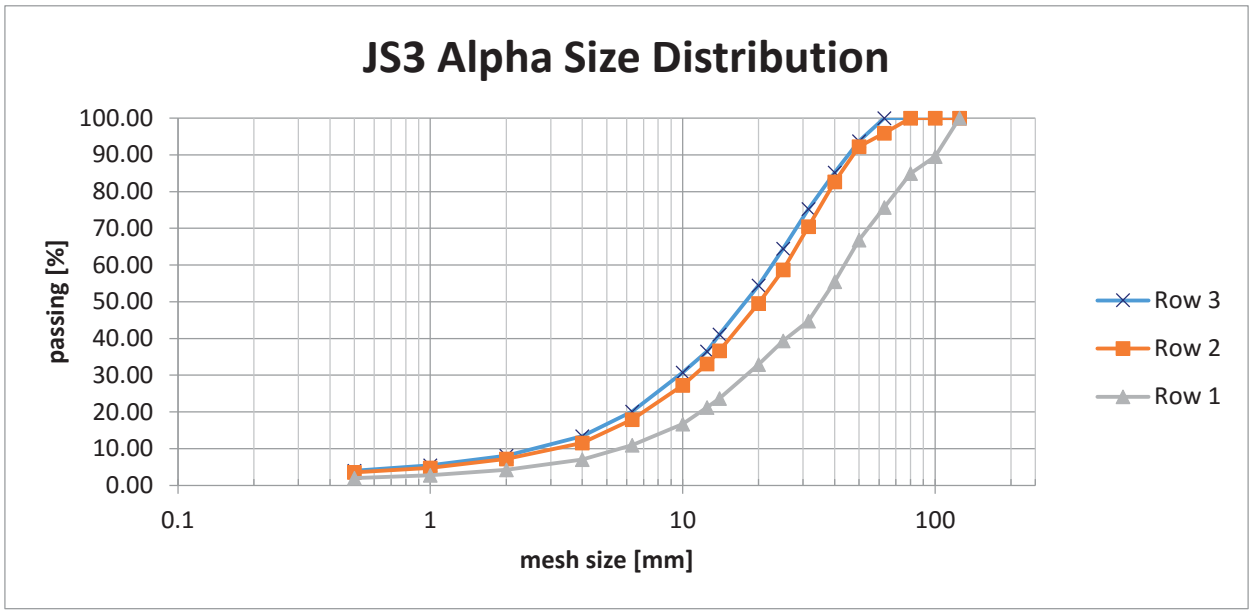

Figure 4-71 JS3 Alpha size distribution

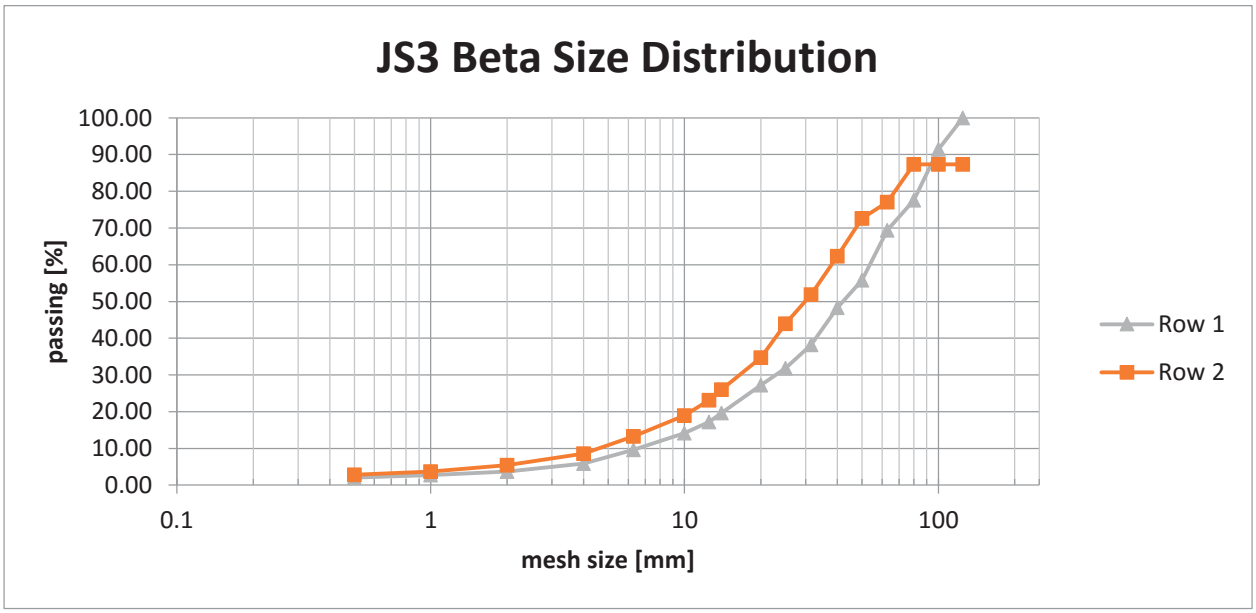

Figure 4-72 JS3 Beta size distribution

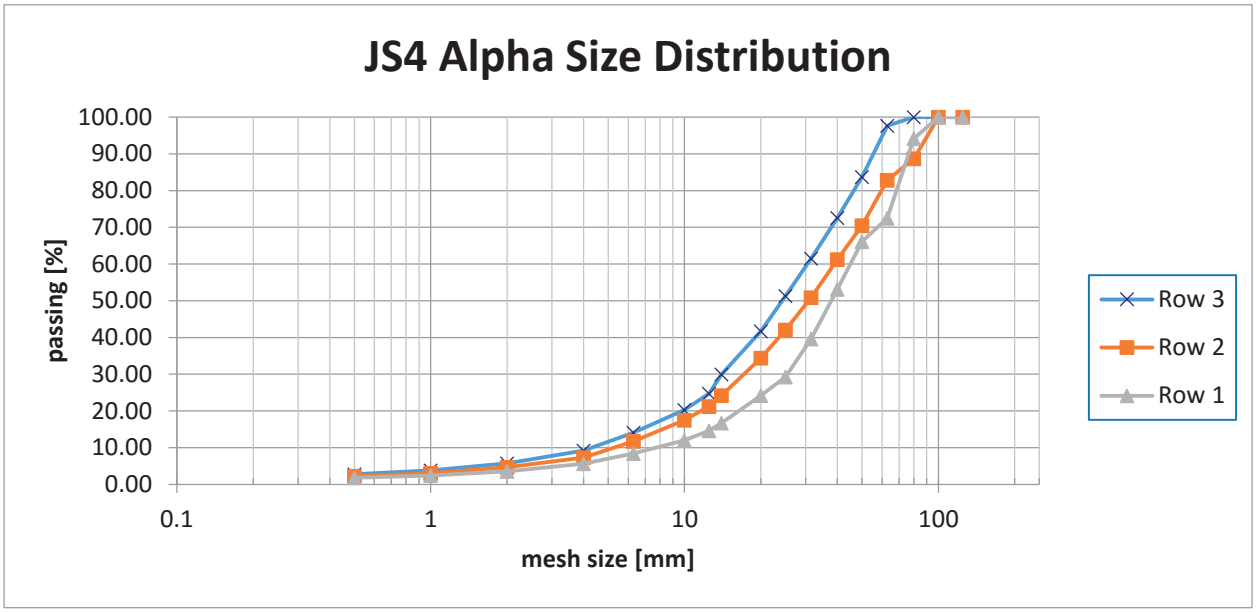

Figure 4-73 JS4 Alpha size distribution

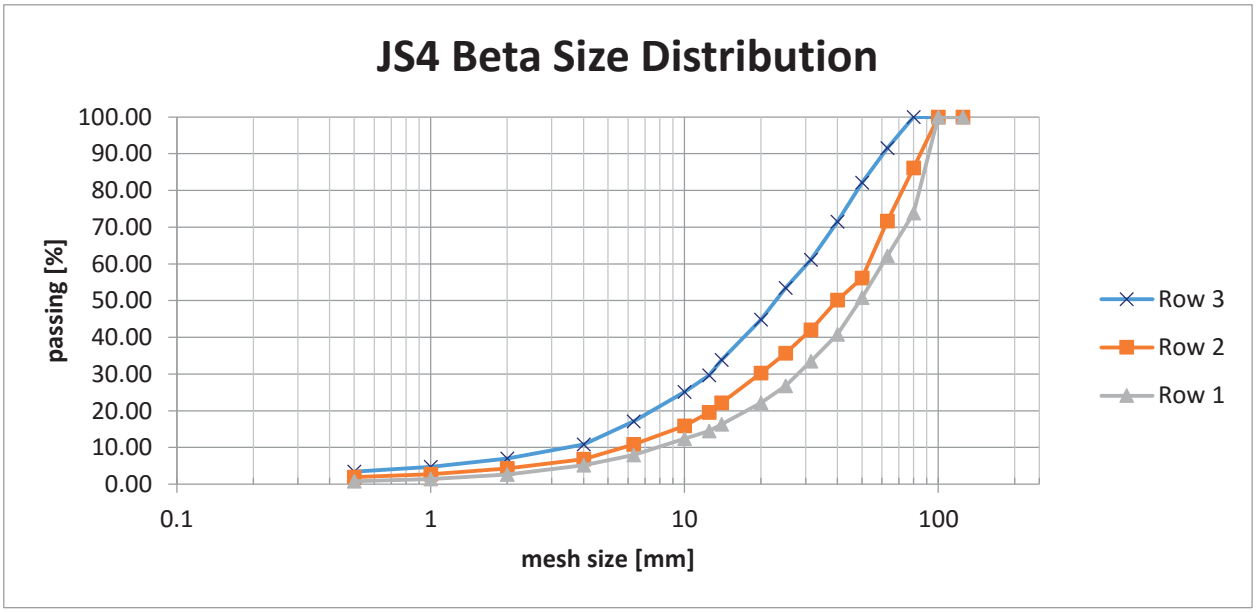

Figure 4-74 JS4 Beta size distribution

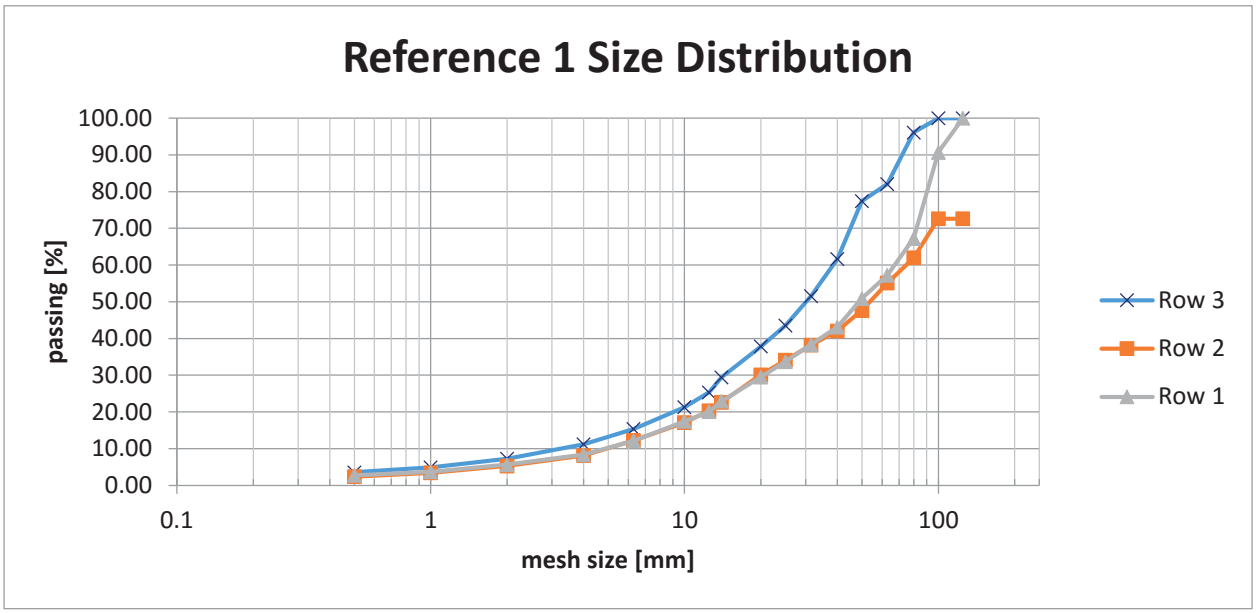

Figure 4-75 Reference 1 size distribution

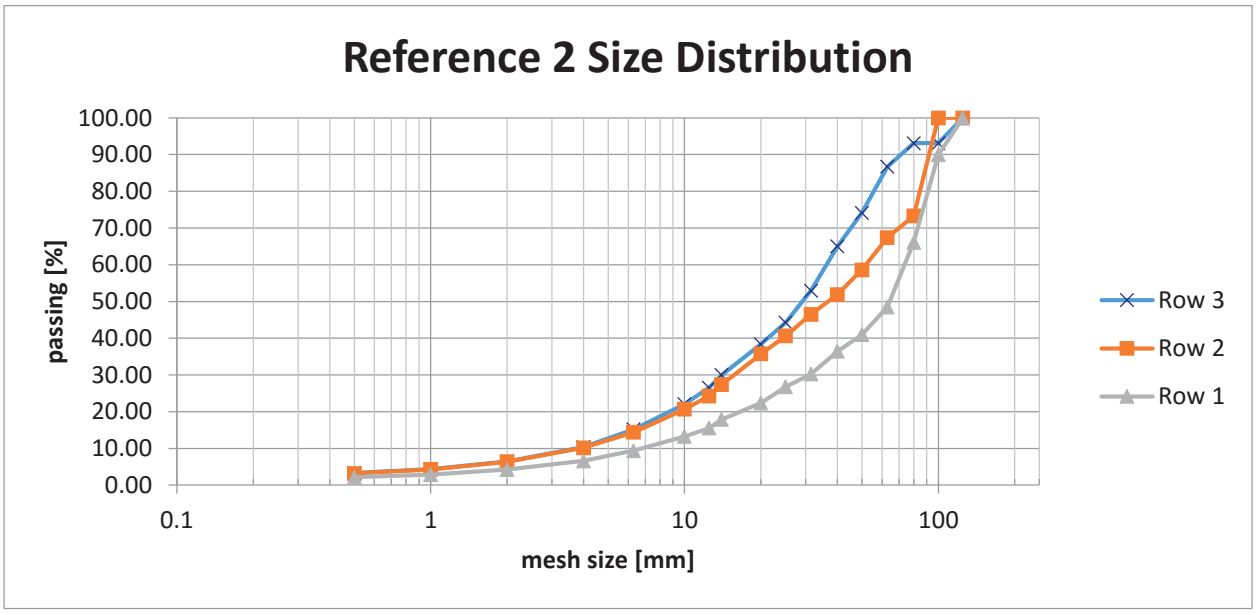

Figure 4-76 Reference 2 size distribution

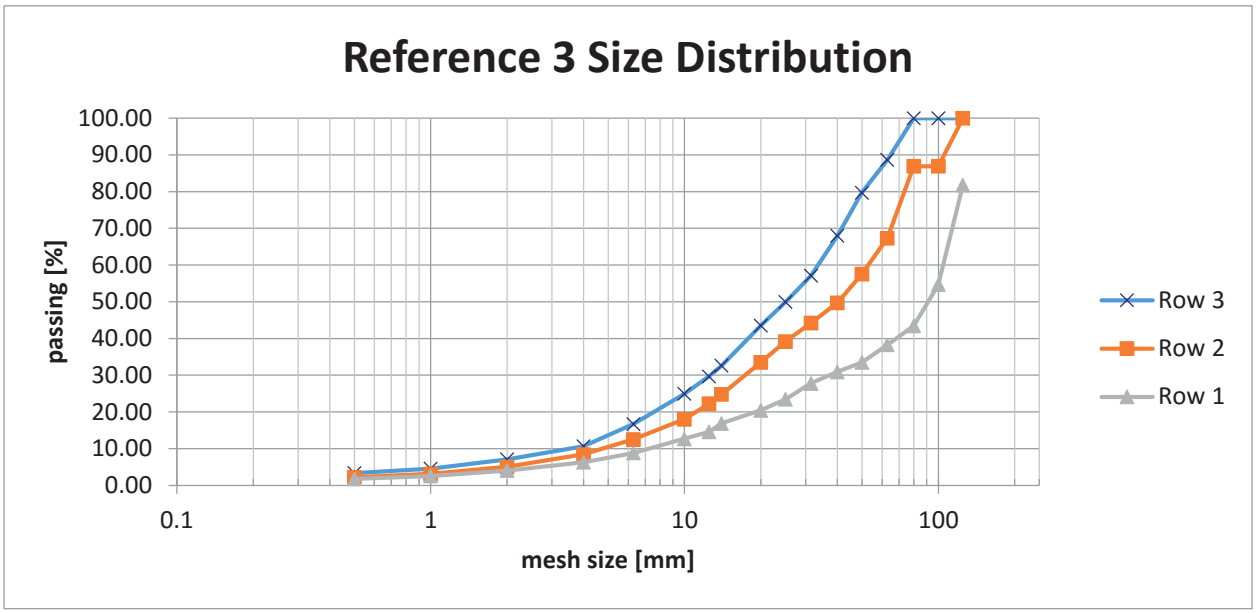

Figure 4-77 Reference 3 size distribution

The K_{30}, K_{50}, K_{80} values of the blocks are shown in Table 4-19 K values of the blocks.

JS1 Alpha	Row 1	Row 2	Row 3	JS4 Alpha	Row 1	Row 2	Row 3
K_{30}	17.17	9.57	8.80	K_{30}	25.47	17.39	14.02
K_{50}	30.86	19.89	16.43	K_{50}	38.04	30.86	24.34
K_{80}	56.83	52.83	33.09	K_{80}	68.90	60.04	46.69
JS1 Beta	**Row 1**	**Row 2**	**Row 3**	**JS4 Beta**	**Row 1**	**Row 2**	**Row 3**
K_{30}	25.71	11.34	-	K_{30}	28.13	19.83	12.62
K_{50}	66.79	21.05	-	K_{50}	49.22	39.86	23.02
K_{80}	91.24	50.53	-	K_{80}	84.70	72.81	48.05
JS1 Gamma	**Row 1**	**Row 2**	**Row 3**	**Reference 1**	**Row 1**	**Row 2**	**Row 3**
K_{30}	22.01	15.2	8.80	K_{30}	20.56	19.87	14.40
K_{50}	39.87	36.35	20.83	K_{50}	48.85	54.10	30.25
K_{80}	83.07	69.50	47.22	K_{80}	90.87	124.55	57.18
JS2 Beta	**Row 1**	**Row 2**	**Row 3**	**Reference 2**	**Row 1**	**Row 2**	**Row 3**
K_{30}	22.1	17.98	13.16	K_{30}	31.06	15.89	14.01
K_{50}	37.25	35.14	24.31	K_{50}	64.46	36.98	29.29
K_{80}	59.78	55.20	46.81	K_{80}	91.66	85.03	56.09
JS3 Alpha	**Row 1**	**Row 2**	**Row 3**	**Reference 3**	**Row 1**	**Row 2**	**Row 3**
K_{30}	18.10	11.18	8.80	K_{30}	37.48	17.57	12.64
K_{50}	35.64	20.23	18.02	K_{50}	91.70	40.33	25.02
K_{80}	70.94	38.17	35.53	K_{80}	123.31	73.99	50.38
JS3 Beta	**Row 1**	**Row 2**	**Row 3**				
K_{30}	23.02	16.76	-				
K_{50}	42.23	29.98	-				
K_{80}	83.48	67.85	-				

Table 4-19 K values of the blocks

4.3 Statistical Analysis

4.3.1 Methods of Analysis

The crack density and sieving data were analyzed with the help of statistical methods to find significant effects. Some statistical methods are restricted in that the populations have to be normally distributed. According to the small amount of data which we used for comparison, the distribution of the population couldn't be determined. Therefore to make a comparison between block properties including their density, P and S wave speeds, crack families and numbers, sieving outputs, two non-parametric (distribution free) statistical analysis methods (Kruskal Wallis and Mann Whitney methods) were used. These analyzes would tell us whether compared samples originate from same distribution or not.

The difference between the two methods is;

Kruskal Wallis Method was used to compare 3 or more data sets.

Mann Whitney Method can be only used to compare 2 independent samples.

Both of these methods are introduced in the sections 4.3.1.1 and 4.3.1.2.

4.3.1.1 Mann Whitney U Test

According to Fay (2010), the Mann Whitney U test is the alternative test to the independent sample t-test. It is a non-parametric test that is used to compare two population means that come from the same population. It can be used for both equal and non-equal sample sizes and it is used to test the median of two populations. Usually the Mann Whitney U test is used when the data is ordinal, the data used in this work is not ordinal however. The Wilcoxon rank sum, Kendall's and the Mann Whitney U test are similar tests.

Assumptions:

Mann Whitney U test is a non-parametric test, hence it does not use any assumptions related to the distribution. There are, however, some assumptions made.

1. The sample drawn from the population is random.

2. Independence within the samples and mutual independence is assumed.

3. An ordinal measurement scale is often used but not obligatory.

The null hypothesis is that, there are no differences between the means of the samples.

The calculation is done as;

- The data belonging to two groups are ranked together.
- The sums of the ranks T_1 and T_2 are calculated.
- The lower quantiles are chosen from the table.
- The upper quantiles are calculated using the formula;

$$Q_U = n(n + m + 1) - Q_L$$

Equation 10 Upper quantile formula

n	*p*	*m=2*	*m=3*	*m=4*	*m=5*
	0.001	3	3	3	3
	0.005	3	3	3	3
2	0.01	3	3	3	3
	0.025	3	3	3	3
	0.05	3	3	3	4
	0.1	3	4	4	5
	0.001	6	6	6	6
	0.005	6	6	6	6
3	0.01	6	6	6	6
	0.025	6	6	6	7
	0.05	6	7	7	8
	0.1	7	8	8	9
	0.001	10	10	10	10
	0.005	10	10	10	10
4	0.01	10	10	10	11
	0.025	10	10	11	12
	0.05	10	11	12	13
	0.1	11	12	14	15
	0.001	15	15	15	15
	0.005	15	15	15	16
5	0.01	15	15	16	17
	0.025	15	16	17	18
	0.05	16	17	18	20
	0.1	17	18	20	21

Table 4-20 Lower quantile table, Schimek (2015)

In order to pick the lower quantiles Q_L, Table 4-20 is used.

The hypothesis of equal population means would be rejected if following conditions were obtained;

$$Q_L > T_{1or2} \; or \; T_{1or2} > Q_U$$

Equation 11 Conditions of Mann Whitney test

Where;

T_1 is sum of the ranks of first group.

T_2 is sum of the ranks of second group.

n is the number of data in first group.

m is the number of data in second group.

Too few data points in the groups (lesser than 2) may lead to the sum of the ranks of the individual groups fall below the lower quantiles. This may cause inconsistent results of Mann Whitney U test.

4.3.1.2 Kruskal Wallis Analysis of Variance

The Kruskal Wallis Test was developed by Kruskal and Wallis (1952) jointly and is named after them. The Kruskal Wallis test is a nonparametric test, and is used when the assumptions of ANOVA are not met. They both test for significant differences on a continuous dependent variable by a grouping with respect to an independent parameter (with three or more groups). In the ANOVA, we assume that distribution of each group is normally distributed and there is approximately equal variance on the scores for each group. However, in the Kruskal Wallis Test, we do not have any of these assumptions. Like all non-parametric tests, the Kruskal Wallis Test is not as powerful as the ANOVA.

Hypothesis:

Null hypothesis: The samples come from identical populations.

Alternative hypothesis: The samples come from different populations. The assumptions are:

1. The samples drawn from the population are random.

2. The samples of each group are independent.

3. The measurement scale should be at least ordinal.

Procedure:

1. Arrange the data of all samples in a single series in ascending order.

2. Assign rank to them in ascending order. In the case of a repeated value, or a tie, assign ranks to them by averaging their rank position.

3. Then sum up the different ranks, e.g. R_1, R_2, R_3…., for each of the different groups.

4. To calculate the value, apply the following formula to calculate the test statistic H:

$$H = \frac{12}{n(n+1)} . \sum_{i=1}^{k} \frac{R_i^2}{n_i} - 3(n+1)$$

Equation 12 Test statistic H formula

The null hypothesis of equal population would be rejected if

$$\boldsymbol{H \geq X^2_{1-a,k-1}}$$

Equation 13 Null hypothesis condition

Here;

H is test statistic for the KW-ANOVA

k is the number of groups

n is the number of observations

n_i is the number of observations in group 1

R_i^2 is sum of the ranks squared of the groups

α is significance level (0.05)

k-1 is degree of freedom

χ^2 is critical value of the test statistic for KW- ANOVA

The Kruskal Wallis test statistic is approximately a chi-square distribution, with k-1 degrees of freedom where n_i should be greater than 5. If the calculated value of the Kruskal Wallis test is less than the critical chi-square value, then the null hypothesis cannot be rejected. If the calculated value of Kruskal Wallis test is greater than the critical chi-square value, then we can reject the null hypothesis and say that at least one sample comes from the different a population.

4.3.2 Comparisons

The next step following the crack analysis is to present the results using the statistical methods mentioned in the section 4.3.1. Differences between blocks are compared to see whether there is an influence of the joints on crack formation or not. The findings from the statistical analysis are also summarized in the section 5.

4.3.2.1 Normal Distribution Curves

It is informative to see the distribution curves of the cracks before making any comment on the statistical analysis.

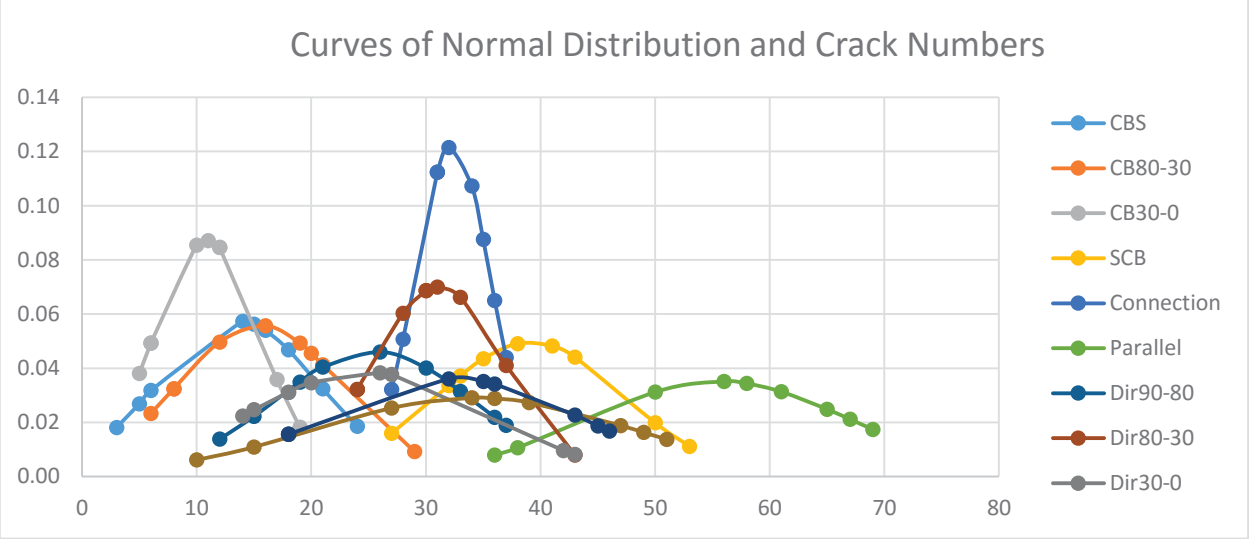

Figure 4-78 Distribution curves of the cracks

Figure 4-78 illustrates that the curves which are more peaked have a smaller variance. The number of connection cracks number is relatively constant in the blocks. On the contrary, the number of cracks in families like Parallel and DIR80-30 have large variances.

Although there is a high variance i.e in Parallel crack numbers, there are data points close to each other as that can be seen. The statistical analysis will allow us to determine which type of blocks have smaller variances and which have larger ones in two, three and four group comparisons.

In the analysis, we expect to see the significant differences and similarities within the block types. In order to make a better interpretation, the analysis has started with every block with other blocks first as single comparison then as a three blocks comparison and then four and five blocks comparison.

4.3.2.2 Comparison of Reference Blocks

Before comparing the reference blocks to the other blocks with Joint sets, the similarity of reference blocks is checked. The Kruskal Wallis test was applied to the slice data for the Reference blocks. In the analysis, k indicates the number of blocks compared while n is the slice number. When using the Mann Whitney U test, first Q_L should be picked from the Table 4-20, in this case n and m are both 4 because each block have 4 slices. After Q_L is found, then Q_U is calculated using the Equation 10. Q_L is found to be 12 while Q_U is calculated as 24. See Equation 11.

When calculating the data for the block groups which have more than one block, the average values of the blocks were used. I.e. the JS1 block set have 2 members which are JS1 Alpha and JS1 Gamma. Therefore the average crack numbers of these blocks were calculated and subjected to statistical analysis.

REF1-REF2-REF3				
Crack Family	H	p value	X^2	Significant Difference
Total Crack Values	2.33	0.31	5.99	No
CB90-80	1.07	0.58	5.99	No
CB80-30	1.03	0.59	5.99	No
CB30-0	0.47	0.79	5.99	No
SCB	4.39	0.11	5.99	No
CONNECT	0.50	0.78	5.99	No
PARALLEL	3.96	0.13	5.99	No
DIR90-80	5.66	0.05	5.99	No
DIR80-30	1.88	0.38	5.99	No
DIR30-0	3.57	0.16	5.99	No
SC	1.06	0.58	5.99	No
VCB	5.27	0.07	5.99	No

Table 4-21 Kruskal Wallis test application to the Reference blocks

The analysis shows that there is no significant differences between reference blocks regarding the number of cracks in the different families. See Table 4-21.

REF -JS1			
Crack Family	T_1	T_2	Significant Difference
Total Crack Values	18	18	No
CB90-80	26	10	**Yes**
CB80-30	26	10	**Yes**
CB30-0	26	10	**Yes**
SCB	11	25	**Yes**
CONNECT	17	19	No
PARALLEL	22	14	No
DIR90-80	18	18	No
DIR80-30	25	11	**Yes**
DIR30-0	26	10	**Yes**
SC	10	26	**Yes**
VCB	23	13	No

Table 4-22 Comparison of block average data of three Reference blocks and two JS1 blocks with Mann Whitney test (n=4 m=4 p=0.05) and Q_L = 12 and Q_U =24

The Mann Whitney test used to compare the average crack numbers in the JS1 blocks with those in the Reference blocks. Table 4-22 shows that the crack numbers have a high variance for the CB, SCB, DIR90-80, DIR30-0 and SC families of cracks. This is also the joint configuration with the largest number of significant variations.

REF-JS2			
Crack Family	T_1	T_2	Significant Difference
Total Crack Values	14.0	22.0	No
CB90-80	10.0	26.0	Yes
CB80-30	10.0	26.0	Yes
CB30-0	12.5	23.5	No
SCB	24.0	12.0	Yes
CONNECT	20.0	16.0	No
PARALLEL	13.0	23.0	No
DIR90-80	25.5	10.5	Yes
DIR80-30	17.5	18.5	No
DIR30-0	19.0	17.0	No
SC	21.0	15.0	No
VCB	12.5	23.5	No

Table 4-23 Comparison of block average data of three Reference blocks and one JS2 block with Mann Whitney test (n=4 m=4 p=0.05) and Q_L = 12 and Q_U =24

When the Mann Whitney test is applied to the average crack numbers in the Reference and JS2 blocks, the results in Table 4-23 show that there are significant differences in crack numbers only for CB90-80, CB80-30 and DIR90-80 families. The crack number of the other families are not significantly different.

REF-JS3			
Crack Family	T_1	T_2	Significant Difference
Total Crack Values	20.0	16.0	No
CB90-80	10.5	25.5	Yes
CB80-30	11.5	24.5	Yes
CB30-0	12.0	24.0	Yes
SCB	11.0	25.0	Yes
CONNECT	20.0	16.0	No
PARALLEL	22.0	14.0	No
DIR90-80	23.5	12.5	No
DIR80-30	14.0	22.0	No
DIR30-0	14.0	22.0	No
SC	25.0	11.0	Yes
VCB	15.0	21.0	No

Table 4-24 Comparison of block average data of three Reference blocks and JS3 block with Mann Whitney test (n=4 m=4 p=0.05) and Q_L = 12 and Q_U =24

A comparison of the average crack numbers in the JS3 block with the ones in the Reference blocks is shown in Table 4-24. This shows that the numbers in families CB90-80, CB80-30, SCB and SC are significantly different. If we check the T_1 and T_2 numbers, CB90-80 family has the largest variation among all however CB80-30 and SCB families have also relatively large variations.

REF-JS4			
Crack Family	T_1	T_2	Significant Difference
Total Crack Values	12.0	24.0	Yes
CB90-80	10.0	26.0	Yes
CB80-30	10.0	26.0	Yes
CB30-0	12.0	24.0	Yes
SCB	20.0	16.0	No
CONNECT	20.0	16.0	No
PARALLEL	13.5	22.5	No
DIR90-80	15.5	20.5	No
DIR80-30	12.0	24.0	Yes
DIR30-0	16.0	20.0	No
SC	21.0	15.0	No
VCB	24.5	11.5	Yes

Table 4-25 Comparison of block average data of three Reference blocks and two JS4 blocks with Mann Whitney test (n=4 m=4 p=0.05) and Q_L = 12 and Q_U =24

A comparison of the average crack numbers in the JS4 blocks with those in the reference blocks is then made, Table 4-25 shows that the numbers in families VCB, CB90-80 and CB80-30 differ significantly while for the other families they don't.

4.3.2.3 Comparison of the Blocks with Joint Sets

In previous section, comparisons between the joint free reference blocks and the jointed JS blocks were made. In this section, the block tests with different types of jointing will be compared.

JS1-JS2			
Crack Family	T_1	T_2	Significant Difference
Total Crack Values	14.5	21.5	No
CB90-80	10.0	26.0	Yes
CB80-30	15.0	21.0	No
CB30-0	23.5	12.5	No
SCB	19.5	16.5	No
CONNECT	19.0	17.0	No
PARALLEL	15.5	20.5	No
DIR90-80	24.0	12.0	Yes
DIR80-30	22.0	14.0	No
DIR30-0	25.0	11.0	Yes
SC	11.5	24.5	Yes
VCB	16.5	19.5	No

Table 4-26 Comparison of block average data of two JS1 blocks and one JS2 Block with Mann Whitney test (n=4 m=4 p=0.05) and Q_L = 12 and Q_U =24

Table 4-26 shows that JS1 and JS2 have significant differences only of SC, DIR30-0 and CB90-80 families of cracks unlike the comparison of these blocks with Reference blocks.

JS1-JS3			
Crack Family	T_1	T_2	Significant Difference
Total Crack Values	18.0	18.0	No
CB90-80	19.5	16.5	No
CB80-30	23.5	12.5	No
CB30-0	26.0	10.0	Yes
SCB	10.0	26.0	Yes
CONNECT	21.0	15.0	No
PARALLEL	25.0	11.0	Yes
DIR90-80	22.0	14.0	No
DIR80-30	24.0	12.0	Yes
DIR30-0	22.5	13.5	No
SC	12.0	24.0	No
VCB	21.0	15.0	No

Table 4-27 Comparison of block average data of JS1 block and JS3 block with Mann Whitney test (n=4 m=4 p=0.05) and Q_L = 12 and Q_U =24

According to the Table 4-27, the JS1 and JS3 blocks have significant differences in CB30-0, SCB and Parallel crack numbers while the rest of the crack family numbers are not.

JS1-JS4			
Crack Family	T_1	T_2	Significant Difference
Total Crack Values	15.0	21.0	No
CB90-80	12.0	24.0	Yes
CB80-30	12.5	23.5	No
CB30-0	22.0	14.0	No
SCB	14.0	22.0	No
CONNECT	18.0	18.0	No
PARALLEL	16.5	19.5	No
DIR90-80	18.0	18.0	No
DIR80-30	22.0	14.0	No
DIR30-0	26.0	10.0	Yes
SC	10.0	26.0	Yes
VCB	25.0	11.0	Yes

Table 4-28 Comparison of block average data of JS1 block and two JS4 blocks with Mann Whitney test (n=4 m=4 p=0.05) and Q_L = 12 and Q_U =24

In this comparison (See Table 4-28) significant differences of DIR30-0, SC and VCB were detected. As distinct from the JS3 comparison, the Parallel, SCB and CB30-0 counts show no significant difference.

JS2-JS3			
Crack Family	T_1	T_2	Significant Difference
Total Crack Values	21.0	15.0	No
CB90-80	19.5	16.5	No
CB80-30	22.0	14.0	No
CB30-0	18.5	17.5	No
SCB	10.0	26.0	Yes
CONNECT	19.0	17.0	No
PARALLEL	25.5	10.5	Yes
DIR90-80	16.5	19.5	No
DIR80-30	17.0	19.0	No
DIR30-0	14.5	21.5	No
SC	21.0	15.0	No
VCB	22.0	14.0	No

Table 4-29 Comparison of block average data of JS2 block and JS3 block with Mann Whitney test (n=4 m=4 p=0.05)

JS2-JS4			
Crack Family	T_1	T_2	Significant Difference
Total Crack Values	16.0	20.0	No
CB90-80	12.0	24.0	Yes
CB80-30	14.5	21.5	No
CB30-0	17.0	19.0	No
SCB	15.0	21.0	No
CONNECT	17.0	19.0	No
PARALLEL	19.0	17.0	No
DIR90-80	10.5	25.5	Yes
DIR80-30	16.0	20.0	No
DIR30-0	16.5	19.5	No
SC	17.0	19.0	No
VCB	25.5	10.5	Yes

Table 4-30 Table 4 30 Comparison of block average data of JS2 block and two JS4 blocks with Mann Whitney test (n=4 m=4 p=0.05) and QL = 12 and QU =24

The Mann Whitney Test results show that JS2 and JS3 blocks have significant differences in SCB and Parallel crack numbers and JS2-JS4 comparison give the results that the VCB and DIR90-80 numbers are significantly different.

According to the evaluated results, no same crack family difference among the distinct blocks were found. The Connection, CB80-30 and CB30-0 crack numbers always show insignificant variations when is compared with the other block groups.

JS3-JS4			
Crack Family	T_1	T_2	Significant Difference
Total Crack Values	14.0	22.0	No
CB90-80	12.0	24.0	Yes
CB80-30	10.5	25.5	Yes
CB30-0	16.0	20.0	No
SCB	26.0	10.0	Yes
CONNECT	15.5	20.5	No
PARALLEL	10.0	26.0	Yes
DIR90-80	11.5	24.5	Yes
DIR80-30	14.0	22.0	No
DIR30-0	22.5	13.5	No
SC	12.0	24.0	Yes
VCB	25.0	11.0	Yes

Table 4-31 Comparison of block average data of JS3 block and two JS4 blocks with Mann Whitney test (n=4 m=4 p=0.05) and QL = 12 and QU =24

If we consider all of the comparisons above, it can be observed that the crack families of JS3 blocks have the most variations except the differences between the JS1 and the Reference blocks. When JS3 is compared with JS4 blocks, five families with significantly different crack numbers can be seen (See Table 4-31).

It´s observed that the CB80-30, SCB, Parallel, DIR90-80 and VCB crack families are significantly different in these two block sets.

JS1-JS2-JS3-JS4				
Crack Family	H	p value	X^2	Significant Difference
Total Crack Values	2.12	0.54	7.81	No
CB90-80	4.41	0.21	7.81	No
CB80-30	6.42	0.09	7.81	No
CB30-0	5.00	0.17	7.81	No
SCB	9.30	0.02	7.81	Yes
CONNECT	0.78	0.85	7.81	No
PARALLEL	7.82	0.05	7.81	Yes
DIR90-80	6.64	0.08	7.81	No
DIR80-30	3.64	0.30	7.81	No
DIR30-0	7.25	0.06	7.81	No
SC	8.01	0.04	7.81	Yes
VCB	7.76	0.05	7.81	No

Table 4-32 Comparison of all JS blocks with Kruskal Wallis test

After comparing all of the block sets to one another pair wise, comparing them all as a whole gives a different perspective on the influence of joints on crack formation. As different results were obtained from the pair wise comparisons, the overall comparison indicates that the numbers of SCB, Parallel and SC family of cracks vary. See Table 4-32.

REF-JS1-JS2-JS3-JS4				
Crack Family	H	p value	X^2	Significant Difference
Total Crack Values	3.40	0.48	9.49	No
CB90-80	11.80	0.01	9.49	Yes
CB80-30	10.67	0.03	9.49	Yes
CB30-0	11.75	0.01	9.49	Yes
SCB	12.00	0.01	9.49	Yes
CONNECT	0.92	0.90	9.49	No
PARALLEL	9.04	0.06	9.49	No
DIR90-80	3.16	0.53	9.49	No
DIR80-30	6.27	0.17	9.49	No
DIR30-0	8.79	0.06	9.49	No
SC	10.91	0.02	9.49	Yes
VCB	9.76	0.04	9.49	Yes

Table 4-33 Comparison of all blocks with Kruskal Wallis test

Thereafter JS blocks were put into the comparison, the results in the Table 4-33 shows that the CB90-80, CB80-30, CB30-0, SCB, SC, VCB families of cracks have significant difference if reference blocks were also considered in the comparison.

The Kruskal Wallis and Mann Whitney test results and normal distribution curves are related to each other (see Figure 4-78). Families with wide normal distribution curves also have significant differences in crack numbers between block sets in the statistical tests.

Note: Single and multiple comparisons show differences according to sample sizes. When the sample size increases, it is expected to observe this result.

5. RESULTS

In this research, the dye penetration technique was utilized for crack detection to obtain a better interpretation of the crack development and how it influenced the rock fragmentation while trying to keep all the test parameters the same but for the joint sets in the blocks.

The dye penetration method let us to trace the crack developments on the slice surfaces. These traced surfaces were then used to generate 3D models in AutoCAD in order to illustrate the crack formations.

In order to generate the 3D model, the remaining parts of the blocks after blasting were cut into the horizontal slices. The dye penetration method was applied to those slices and the visualized crack pattern photographed. The photos were then used for crack tracing in AutoCAD.

The models created in AutoCAD were used to classify the cracks which occurred in the blocks after blasting into crack families. These crack families were also used in the past researches (Navarro 2014, Schimek 2015) and they are expected to occur both in small scale and in full scale blasts.

After identifying and distinguishing the cracks of different families, the counted numbers of those cracks were used in further analysis to make a basic correlation between jointing and the block fragmentation. The analyses and their outcomes are listed below.

5.1 The Kruskal Wallis and Mann Whitney tests results

The comparison of slice based numbers of cracks in the reference blocks with the Kruskal Wallis test shows that there is no significant difference between the crack numbers in the reference blocks even though reference 1 block had a different burden distance in the first row. However slight differences were sometimes detected between the block Reference 1 and other two Reference blocks.

When the different sets of jointed blocks were compared separately with the set of reference blocks, significant differences in crack numbers were detected.

Those differences are described for every crack family as follows;

5.1.1 Cracks from the borehole in sectors between 90°-80°:

This comparison of the CB90-80 family of cracks with that in the set of reference blocks shows that, joints in the blocks cause this crack family to be more numerous than in the reference blocks without joints. Every set of blocks with joints has shown a significant increase in the number of these cracks. Thus the joints in the blocks have a direct influence on formation of CB90-80 cracks. See Figure 4-45 for the CB90-80 comparison.

5.1.2 Cracks from borehole in sectors between 80°-30°:

When the comparisons were made, significant differences were detected in the REF-JS1, REF-JS2, REF-JS3 and REF-JS4 comparisons (See Figure 4-46). This analysis can be interpreted as that joint sets on the blocks have an important influence on formation of new crack families (section 4.2.3) which were counted as CB80-30 cracks.

5.1.3 Cracks from borehole in sectors between 30°-0°:

Like the other families of cracks emanating from the boreholes, the influence of joints on the number of cracks in family CB30-0 is also significant. See Figure 4-47. There is a significant difference between the crack numbers in the reference blocks and those in either of JS1, JS3 and JS4 but not JS2 blocks. In conclusion, blocks with joints are forming

more cracks from boreholes than the blocks without any joints. This might also have an effect on particle distributions which will be discussed later.

5.1.4 Straight cracks from back side:

The Mann Whitney tests applied to the different blocks for this crack family indicates that, the number of cracks in JS1-JS3 blocks is significantly smaller than in the Reference blocks. The number of cracks in the JS4 blocks is not significantly different from the number in the reference blocks. See Figure 4-49.

5.1.5 Connection cracks:

The comparisons of the number of cracks in the jointed blocks, compared with that of the reference blocks show no significant difference according to Mann Whitney tests. Combining the observations of the Connection cracks from the crack counting graphs, it seems that the joints have no great influence on this crack family because the numbers lie in similar ranges for all blocks. When the normal distribution curve in Figure 4-78 is assessed, the Connection cracks seem to have the lowest variance.

5.1.6 Parallel Cracks:

Just as the analysis made for the connection cracks, no significant differences of numbers of Parallel cracks between the reference blocks and jointed blocks were detected as indicated in Figure 4-48. Parallel cracks thus seem to be formed in the blocks independent of the influences of joints. On the other hand, during the blasting procedure, it happened that large parallel cracks between the joints may cause breakings of big particles along the joint or forming boulders in other words. These oversized particles influence the sieving analysis, increasing the K_{30}-K_{50}-K_{80} values of the sieving curves dramatically.

5.1.7 Cracks with direction to the boreholes in sectors between 90°-80°:

In this analysis, block set JS2 has significantly fewer DIR90-80 cracks than the reference blocks. When we check the related DIR90-80 graph in Figure 4-51, the JS3 block has also a smaller number of cracks of this family. However, according to the Mann Whitney Test the decrease was not big enough to be significant.

5.1.8 Cracks with direction to the boreholes in sectors between 80°-30°:

According to the Mann Whitney test only the set of JS1 blocks has a significantly more cracks of the DIR80-30 family than the set of reference blocks. The reason for this result can be explained as that the pressure occurring from the blasts tend the reach the free space which joints form. The JS1 blocks have enough space between the boreholes and the joints so they fill the requirement for DIR80-30 to form easily. When the boreholes are

closer to the joints, it is very likely that we would observe different families of cracks due to the geometry of the borehole and joint design.

5.1.9 Cracks with direction to the boreholes in sectors between 30°-0°:

The probable reason that is mentioned for the DIR80-30 family would also explain why significantly more cracks of the DIR30-0 family are formed in the JS1 block than in the other blocks. The JS1 block jointing is suitable for the formation of DIR families of cracks when we consider that the DIR family cracks are created under similar circumstances.

5.1.10 Short Cracks from boreholes:

The numbers of short cracks are the highest in the reference blocks. The statistical analysis tells that the JS1 and JS3 blocks have significantly lower numbers of SC family cracks than the reference blocks without joints. See Figure 4-54. This absence of joints may allow short cracks to occur more often for there is then no influence of joints which is possibly changing the pressure distribution inside the block.

5.1.11 Vertical Cracks between boreholes:

The number of VCB family cracks in the JS4 blocks was significantly lower than in the other blocks. See Figure 4-55. The joints in the JS1, JS2 and JS3 sets on the other hand seem to have an influence by increasing them compared to the reference blocks.

After the comparisons of the individual crack families in the jointed blocks with the crack families in the reference blocks an overall joint analysis was made.

The Kruskal Wallis test was applied to compare the crack families in all jointed blocks by themselves and together with the reference blocks.

Without involving the reference blocks, there are some significant differences in crack numbers for the SCB, Parallel and SC families. It is observed that JS1 has less than half of the number of SC family cracks than the other jointed blocks. When comparing the SCB family of cracks, the JS3 block has a significantly larger number of SCB family cracks than the other jointed blocks. However, unlike the SCB comparison, the JS3 block has fewer Parallel family cracks compared to the other jointed blocks, roughly half.

When the reference blocks are involved in the comparison, then the outcome changes. In this case significant differences in the number of cracks of families CB90-80, CB80-30, CB30-0, SCB, SC and VCB were observed. Basically, when joints are involved it is quite highly possible to see significant changes in crack numbers for the families mentioned.

5.2 MCD and MCID analysis results

The presence of joints have a direct influence on the formation of different crack families inside the blocks. This also means that there will be a change of damage distribution inside the blocks. To be able to understand the damage formation inside the blocks, MCD and MCID values were analyzed.

The MCD and MCID graphs in Figure 4-40 and Figure 4-41 show that highest MCD value belongs to the JS4 blocks while JS3 has the lowest value. If we look into the total cracks graph in Figure 4-43, it can be seen that JS4 blocks have the largest number of long cracks of all block types while the JS3 block has the lowest number of total cracks.

We expect an increase of MCD and MCID when more long cracks are present in the block. Related with that assumption, the MCID values of JS4 blocks are higher than those for the rest of the blocks with exception of JS1 and Reference 1. However including the Reference 1 into the comparisons wouldn't be right because of the significantly smaller burden distance in row 1 and correspondingly larger width of the block remains.

When a comparison is made between the JS1 and JS2 blocks, it is observed that their total crack numbers are similar which lead them to have similar MCD values.

Connection cracks would be the least effective crack family for crack intersection because they have the least possibility to meet with other cracks. However the graph (Figure 4-50) which is related with this crack family doesn't allow us to make an interpretation over it for the crack number values of the blocks are similar to each other.

5.3 Sieving results

Sieving outcomes are a very important side of the effects of joints on rock fragmentation. The findings about K_{30}, K_{50}, K_{80} are summarized below;

According to the obtained values in Table 4-19, it can be observed that the jointed blocks have finer fragmentation than the reference blocks.

The figures Figure 5-1 to Figure 5-3 show the average K_{30}-K_{50}-K_{80} values of the blocks. The average K values of JS1 have been calculated from the K values of JS1 Alpha and JS1 Gamma which are illustrated at the Table 4-19.

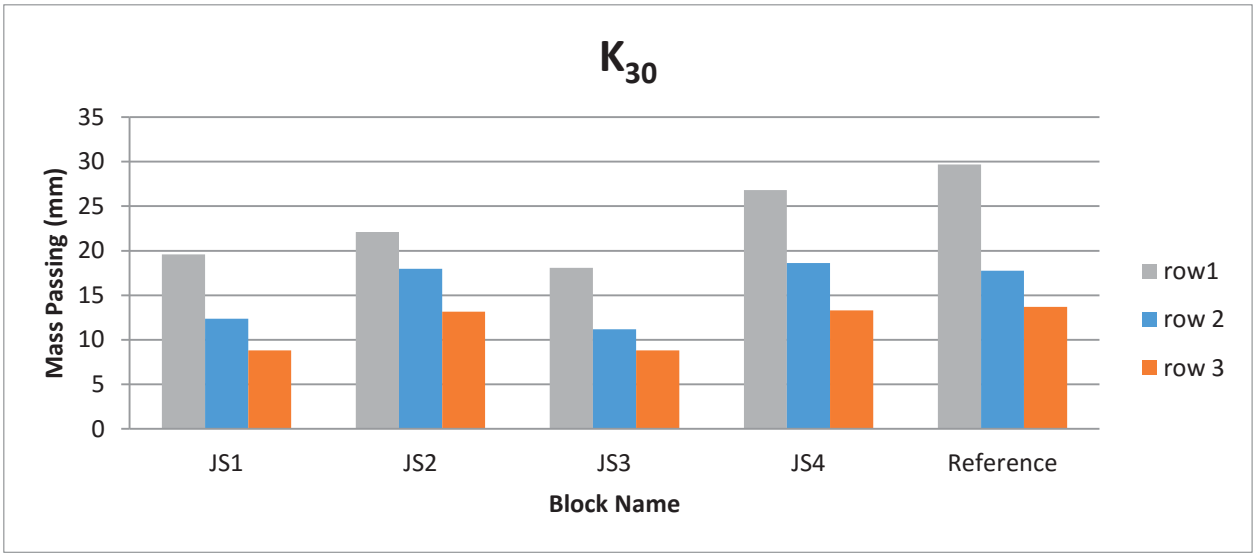

Figure 5-1 K_{30} Values of the blocks

The K_{30} values obtained from the sieving tests show that jointed blocks have a finer fragmentation in all cases except the second row of the JS4 blocks. In addition to that, reference blocks show a large change in fragmentation values between the first row and the second row while the changes in values for the jointed blocks are smaller. The JS3 block with 30° striking joints show the finest fragmentation in K_{30} values.

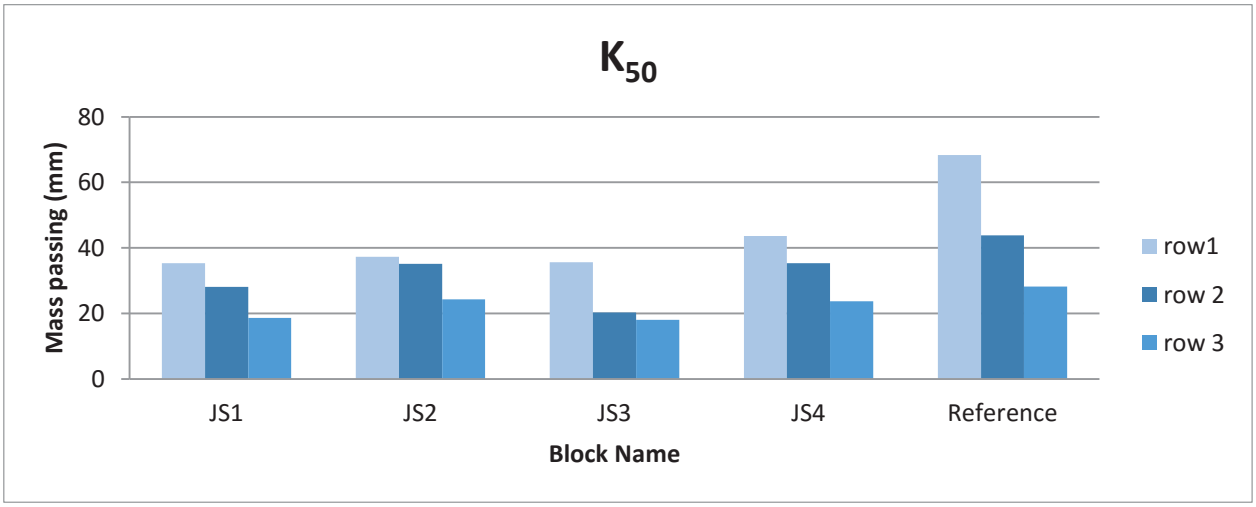

Figure 5-2 K_{50} values of the blocks

The K_{50} values show similar results as the K_{30} values. The reference blocks have the coarsest fragmentation compared to the others. It can be summarized that jointed blocks will have a finer fragmentation after blasting.

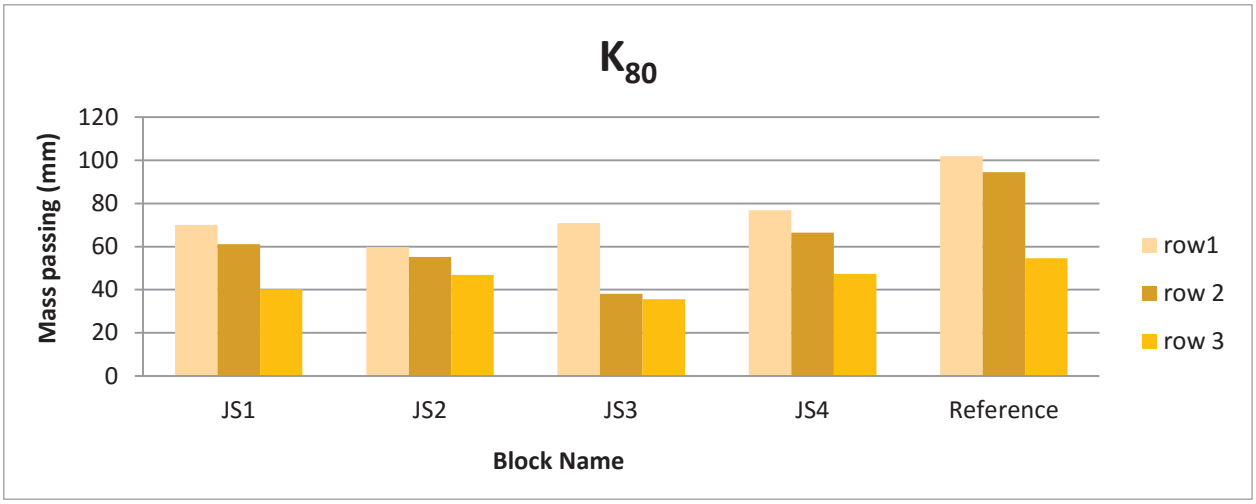

Figure 5-3 K_{80} values of the blocks

Just as for the K_{30} and K_{50} results, the K_{80} values of the reference blocks has the coarsest fragmentation. The joint presence inside the blocks increases the fragmentation after blasting.

To conclude the sieving results, the mean fragmentation values of the jointed blocks can be summarized as;

K_{30} JS3<JS1<JS2<JS4<Reference, i.e JS3 block has the smallest fragments.

K_{50} JS3<JS1<JS2<JS4<Reference

K_{80} JS3<JS1≈JS2<JS4<Reference

Blasting of more samples can be done in order to increase the reliability of the results obtained.

New crack families were found which were related to the joints. According to the observations on the photographs, these JRC cracks occur in the jointed blocks. At first look, they look similar to the existing crack families however their positions, initiation and ending locations make them special. The JRC cracks are more visible and thicker than the other cracks. They can cause serious breakage in the blocks as Figure 5-4 shows.

Figure 5-4 JRC influence in the block JS3 Beta

6. BIBLIOGRAPHY

Alekseychuk, O. (2006). Detection of crack-like indications in digital radiography by global optimization of a probabilistic estimation function. Berlin, Germany: BAM-Dissertationsreihe.

Andriev, G. E. (1995). *Brittle failure of rock materials.* Roterdam: A.A. Balkema.

Ashby, M. F., & Hallam, D. (1986). The failure of brittle solids containing small cracks under compressive stress. *Acta Metallurgica 34(3)*, 497-510.

Buckley, J. M. (2015). *An Introduction to Eddy Current Testing Theory and Technology.*

Cai, M., Kaiser, P. K., & Martin, C. D. (1988). A tensile model for interpretation of microseismic events near underground openings. *Pure and Applied Geophysics 153*, 67-92.

Cunningham, C. (1983). The Kuz-Ram model for prediction of fragmentation from blasting. *International Symposium of Rock Fragmentation by Blasting* (pp. 439-453). Tehnical Universty Lulea.

dal Farra, E. (2012). Initiation delay effects on fragmentation and face geometry in small scale blasting tests. *Tesi di Laurea Magistrale*. Politecnico di Torina.

Fay, M. P., & Proschan, M. A. (2010). *Wilcoxon-Mann_Whitney or t-test? On assumptions for hypothesis tests and multiple interpretations of decision rules.* Statistical Surveys.

Germanovich, J. N.; Dyskin, A. V. (1988). A model of brittle failure for material with cracks in uniaxial loading. (pp. 111-123). Mechanics of Solids, 23 (2).

Griffith, A. A. (1924). Theory of rupture. *Proceedings of the 1st international Congress of applied mechanics* (pp. 55-63). Delft: Tech. Boekhandel en Drukkerij J Walter Jr.

Güven, U. (2011). *Nondestructive Testing Techniques in Engineering.* University of petroleum & energy studies Aerospace: American Society fo Mechanical Engineers (ASME) Student Chapter.

Hariri, M. M. (2011, April). Advantages of Using Technology in Teaching Geosciences, Case Study of Structural Geology. Dubai, Saudi Arabia: Hmadan Ben Mohamad e University .

Hoek, E. (1965). Rock fracture under static stress conditions. Pretoria, South Africa: Council for Scientific and Industrial Research Report MEG 383.

Hoek, E., & Martin, C. (2014). Fracture initiation and propagation in intact rock. *Journal of Rock Mechanics and Geotechnical Engineering*, 287-300.

Hyldahl, J. (2015, September). Effects of jointing on fragmentation. Civil Engineering, Luleå University of Technology.

Kemeny, J. M., & Cook, N. G. (1987). Crack models for the failure of rock under compression. *Proceedings of the 2nd international conference constitutive laws for engineering materials, theory and applications* (pp. 879-887). London: vol.1 Elsevier Science Publishing Co.

Kohan, A. L. (1997). Boiler operator's guide (4th ed). (p. 240). McGraw-Hill Professional, ISBN 978-0-07-036574-2.

Kuznetsov, V. M. (1973). The mean diameter of the fragments formed by blasting rock. Soviet Mining Science.

Martin, C. D. (1997). The effect of cohesion loss and stress path on brittle rock strength. *Canadian Geotechnical Journal 34 (5)*, 698-725.

McClintock, F. A., & Walsh, J. B. (1962). Friction on Graffith cracks in rock under pressure. (pp. 219-228). New York: Proceedings of the 4th US national Congress on appliend mechanics, vol.2Am. Soc. Mech. Eng.

McNulty, J. F. (1962). *USA Patent No. 3,260,105 for Ultrasonic Testing Apparatus and Method at lines 37-48 and 60-72 of Column 1 and lines 1-4 of Column 2.*

Morros, C. (2013). Model-scale tests on the influence of drillhole deviation on blasting fragmentation. Leoben, Austria: MSc Thesis at Chair of Mining Engineering, Montanuniversität Leoben.

Murrell, S. A. (1958). The strength of coal under tri-axial compression. *Mechanical properties of non-metallic brittle materials* (pp. 123-145). London: Butterworth Scientific Publications.

Navarro, J. M. (2014). Detection and Quantification of Blast-Induced Cracks in Small Scale Bench Blasting. Leoben, Austria: MSc Thesis at Chair of Mining Engineering, Montanuniversität Leoben.

Ouchterlony, F. (2005). The Swebrec function: linking fragmentation by blasting and crushing. *Mining Technologies (Trans. Inst. Min. Metal. A), vol 114*, (pp. A29-A44).

Ouchterlony, F. (2009). Fragmentation characterization, the Swebrec function and its use in blast engineering. *Porc Fragblast9, Proc 9th International Symposium on Rock Fragmentation by Blasting 3-22.* London: J Sanchidrián ed. Taylor & Francis Group.

Ouchterlony, F. (2014-2015). Basics and Principles of Mining Rock Fragmentation. *VO 200.001*. Leoben, Austria: Chair of Mining Engineering, Montanuniversität Leoben.

Ouchterlony, F., & Moser, P. (2013-2014). Basics of Explosive Engineering. *VO 200.189*. Leoben, Austria: Chair of Mining Engineering, Montanuniversität Leoben.

Paterson, M. S., & Wong, T. F. (2005). Experimental rock deformation- the brittle field. New York, USA: (2nd ed.) Springler- Verlag.

Persson, P.-A., Holmberg, R., & Lee, J. (1994). *Rock Blasting and Explosives Engineering.* Boca Raton, London, New York, Washington D.C.: CRC Press.

Rummel, W. D., & Matzkanin, G. A. (1997, November). Nondestructive Evaluation (NDE) Capabilities Data Book. Texas, Austin, USA: Nondestructive Testing Information Analysis Center(NTIAC).

Schimek, P. (2015, September). Improvement of Fragmentation by Blasting. Leoben, Austria: Chair of Mining Engineering, Montanuniversität Leoben.

Wishaw, M. (2001). Notes on the Industrial Technologies for Crack Detection and Condition Monitoring. WA, Bessendean: Structural Monitoring Systems Limited.

Zhu, G. (2015). Quantification of Cracks in Model Bench Blasting. Leoben, Austria: Chair of Mining Engineering, Montanuniversität Leoben.

Zuo, J. P., Li, H. T., Xie, H. P., Ju, Y., & Peng, S. P. (2008). A nonlinear strength criterion for rock-like materials based on fracture mechanics. *International Journal of Rock Mechanics and Mining Sciences,45 (4)*, (pp. 594-599).

LIST OF FIGURES

LIST OF TABLES

ANNEX I: CRACK INITIATION AND PROPAGATION

According to Hoek and Martin (2014), to understand the characteristics of rock and rock masses, it is necessary to study the behavior of intact rocks.

"*The characteristics that will be discussed in the following text are the strength and deformation characteristics of intact rock. As it is illustrated in Figure I-2, a number of stress states need to be considered and, it will be assumed that these stress states can be considered in two dimensions. In other words, it is assumed that the intermediate principal stress σ_2 has a minimal influence on the initiation and propagation of failure in the samples*."

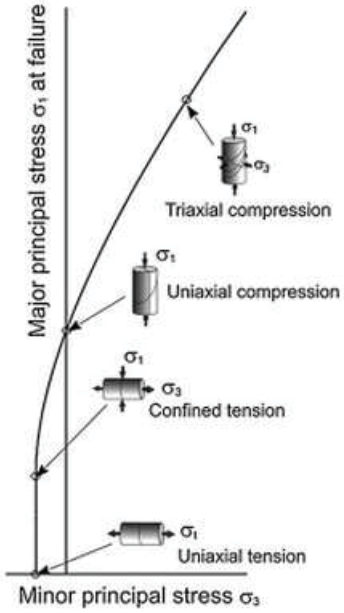

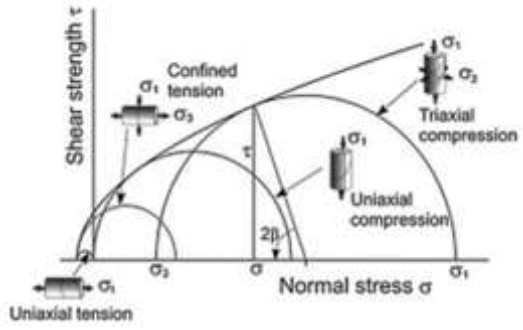

Figure I-1 Crack Propagation Mohr Circle

Figure I-2 Major principal stress- Minor principal stress

According to Hoek and Martin (2014), the theoretical fracture can be explained as;

Griffith tensile theory

"Griffith (1921) proposed that tensile failure in brittle materials such as glass initiates at the tips of minute defects which he represented by flat elliptical cracks. His original work dealt with fracture in material subjected to tensile stress but later he extended this concept to include biaxial compression loading (Griffith, 1924). The equation governing tensile failure initiation in a biaxial compressive stress field is;

$$\sigma_1 = \frac{-8\sigma_t(1+\frac{\sigma_3}{\sigma_1})}{(1-\frac{\sigma_3}{\sigma_1})^2}$$

Equation 14 Tensile failure initiation in a biaxial compressive stress field

Where σ_t is the uniaxial tensile strength of the material. Note that tensile stresses are defined as negative in rock mechanics.

Murrell (1958) proposed the application of Griffith theory to rock. In the 1960s, Griffith's two-dimensional theory was extended to three dimensions by a number of authors including Murrell (1958), Sack and Kouznetsov whose work was summarized in books on brittle failure of rock materials by Andriev (1995) and Paterson and Wong (2005). These extensions involve examining the stresses induced around open penny-shaped cracks in a semi-infinite body subjected to tri-axial compressive stresses σ_1, σ_2 and σ_3. It was shown that the intermediate principal stress σ_2 has no significant influence on the crack tip stresses inducing tensile failure initiation. Hence, this criterion is essentially equivalent to loading a penny-shaped crack in a biaxial stress field, as shown below;

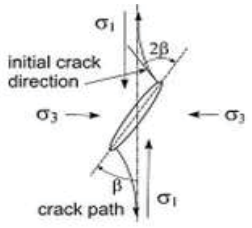

Figure I-3 Crack initiation in a stress field

The equation governing tensile failure initiation is

$$\boldsymbol{\sigma_1 = \frac{-12\sigma_t(1+2\frac{\sigma_3}{\sigma_1})}{(1-\frac{\sigma_3}{\sigma_1})^2}}$$

Equation 15 Tensile failure initiation

Note that, whereas the original Griffith theory predicts a ratio of compressive to tensile strength $\sigma_c/|\sigma_t|=8$, the penny-shaped crack version predicts $\sigma_c/|\sigma_t|=12$. The corresponding Mohr envelope for the penny-shaped crack version is;

$$\tau^2 = |\sigma_t|(|\sigma_t| + \sigma)\left(\sqrt{\frac{\sigma_c}{|\sigma_t|} + 1} - 1\right)^2$$

Equation 16 Mohr envelope for the penny-shaped crack version

Where σ_c is the uniaxial compressive strength of the material.

The Griffith theory deals only with the initiation of tensile failure. It cannot be extended to deal with failure propagation and eventual shear failure in compression. However, under certain conditions when tensile stresses exceed the tensile strength, tensile failure initiation under compression can lead to crack propagation."

Modifications to Griffith theory for closed cracks

"The original Griffith theory was derived from analyses of crack initiation at or near the tips of open elliptical cracks. In the case of rocks, most of the defects from which tensile cracks originate are grain boundaries which are usually cemented and have to be considered as closed cracks. McClintock and Walsh (1962) proposed that tensile fracture from closed Griffith cracks can be predicted on the basis of the conventional Mohr–Coulomb equation: where ϕ is the angle of friction and τ_0 is the shear strength at zero normal stress.

$$\boldsymbol{\tau = \tau_0 + \sigma tan\phi}$$

Equation 17 Mohr-Coulomb equation

Hoek (1965) discussed the transition from the Griffith theory for open cracks, which applies for confining stresses $\sigma_3 < 0$, and the modified theory for closed cracks which applies for compressive confining stresses. For the principal stress plot, this transition occurs at $\sigma_3 = 0$, while for the Mohr envelope, the transition occurs at the tangent points on the Mohr circle representing the uniaxial compressive strength σ_c of the intact rock. The transition is illustrated in the Figure 0-4 in which the principal stress plots are shown for friction angles of 35°, 45° and 55°.

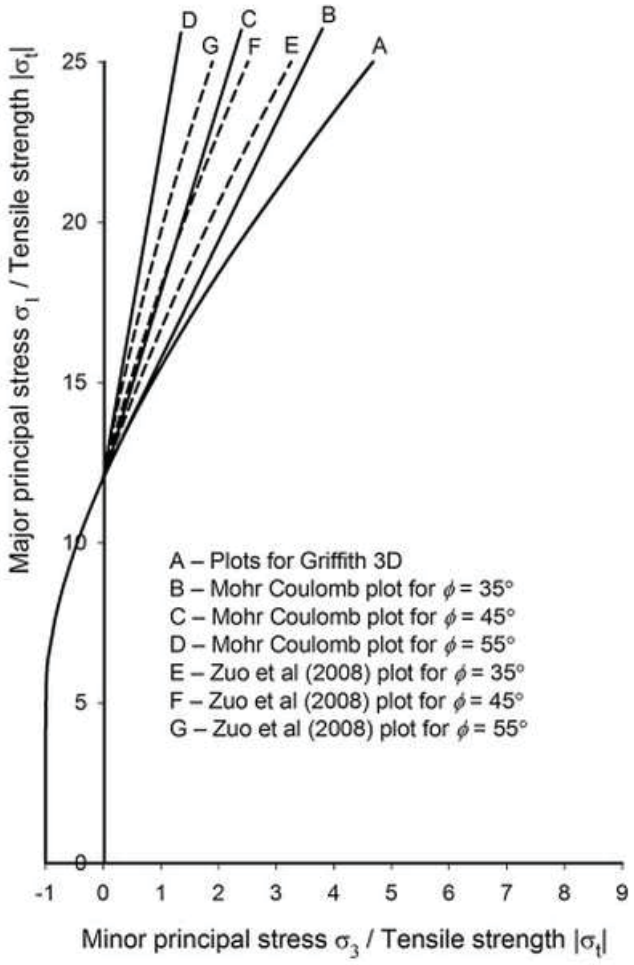

Figure I-4 Major principal stress-Minor principal stress graph

A much more comprehensive discussion on this topic is given in Paterson and Wong (2005) but the plotted results are essentially the same as those shown before. Hence, for the purpose of this discussion, equation following is adequate.

$$\tau = \tau_0 + \sigma_{tan\phi}$$

Equation 18 Mohr-Coulomb equation

Zuo et al. (2008) examined the growth of micro cracks in rock-like materials on the basis of fracture mechanics considerations. They assumed a sliding-crack model which generates wing cracks, similar to those shown in Figure I-4, from close to the crack tips when the frictional strength of the sliding surfaces is overcome. They found that the failure initiation criterion can be expressed by the following equation;

$$\sigma_1 = \sigma_3 + \sqrt{\frac{\mu}{\kappa}\frac{\sigma_c}{|\sigma_t|}\sigma_c\sigma_3 + \sigma_c^2}$$

Equation 19 Failure initiation criterion

Where μ is the coefficient of friction which is equal to the tangent of the friction angle, i.e.

$$\mu = tan\phi.$$

Equation 20 Coefficient of friction

The coefficient κ is used for mixed mode fracture and it can be derived from various approximations based on a maximum stress criterion or a maximum energy release criterion (Zuo et al., 2008). when μ = 0.7, 1 and 1.43 (ϕ = 35°, 45° and 55°), κ = 1 and σc/|σt|=12 .Note that the same transition from open to closed crack behavior has been assumed as for the Mohr–Coulomb criterion discussed above."

Length of induced tensile cracks

“Hoek (1965) carried out experiments in which flat open “cracks” were machined ultrasonically into annealed glass plates which were then loaded biaxially. The initiation of tensile cracks from near the tips of these simulated cracks, as predicted by Griffith's original theory, was confirmed. However, it was found that the length of the tensile cracks was limited by the ratio of the applied biaxial stresses σ3/σ1. As reported by Cho et al. (2007), theoretical studies on closed cracks have been carried out by several authors including Ashby and Hallam (1986), Kemeny and Cook (1987), Germanovich and Dyskin (1988) and Martin (1997) and Cai et al. (1998). These studies, the results of which are plotted in Figure I-5, confirm the importance of confinement in limiting the length of induced tensile cracks from pre-existing flaws in brittle materials subjected to compressive loading. Figure I-5 summarizes some of this information in a different form and shows a principal stress plot and Mohr's diagram for open penny-shaped cracks subjected to different biaxial compressive stress loadings.”

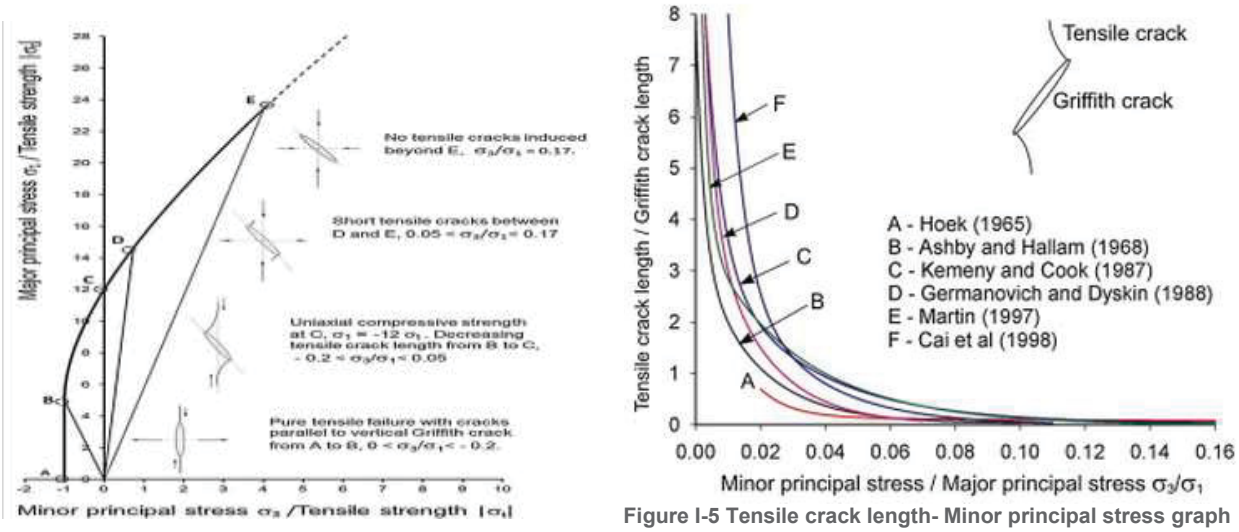

Figure I-5 Tensile crack length- Minor principal stress graph

Figure I-6 Major principal stress- Minor principal stress graph

ANNEX II: BLOCK AND SLICE PICTURES

JS1 Alpha

Picture of JS1 Alpha before blasting

Figure II-1 JS1 Alpha before blasting

Top view of the JS1 Alpha after blasting

Figure II-2 JS1 Alpha top view after blasting of 1st row

Figure II-3 JS1 Alpha top view after blasting of 2nd row

Figure II-4 JS1 Alpha top view after blasting of 3rd row

Slice Pictures of JS1 Alpha

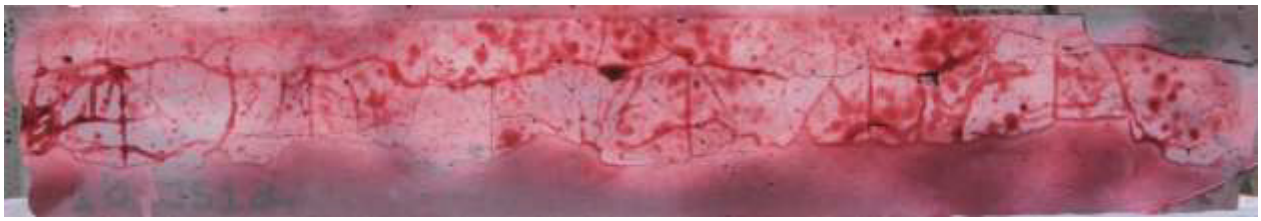

Figure II-5 JS1 Alpha. Slice 1B

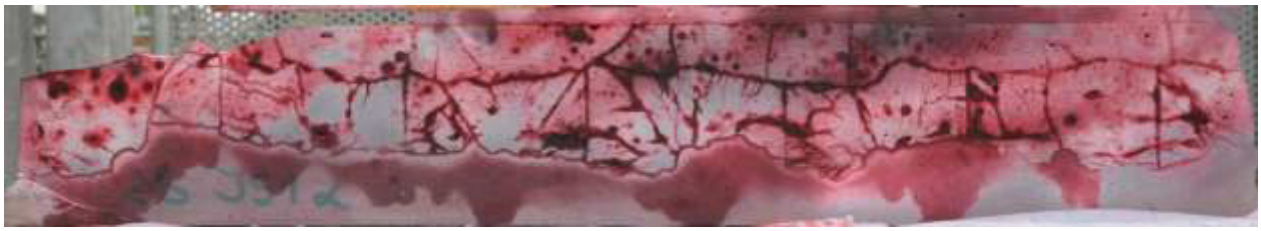

Figure II-6 JS1 Alpha. Slice 2B

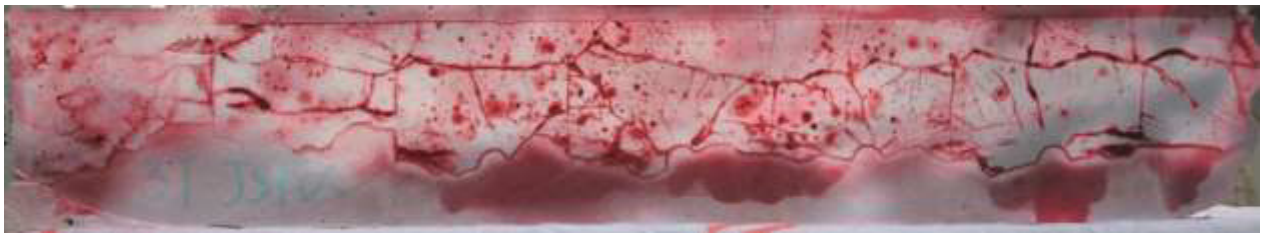

Figure II-7 JS1 Alpha slice 3T

Figure II-8 JS1 Alpha. Slice 4T

AutoCAD drawings of JS1 Alpha

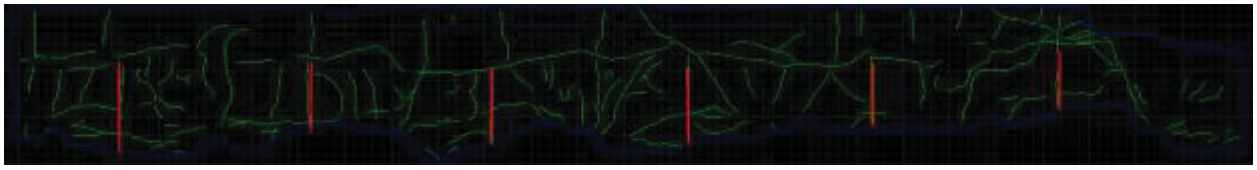

Figure II-9 JS1 Alpha. Slice surface 1B

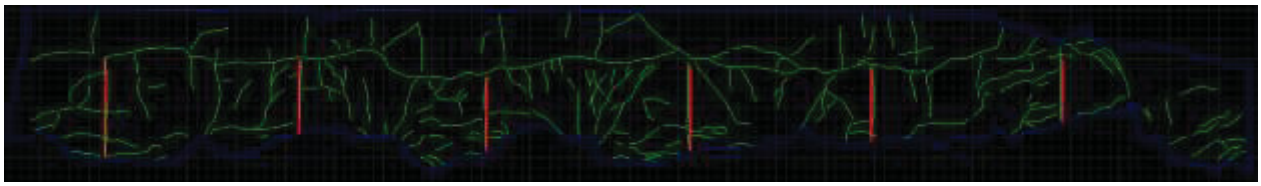

Figure II-10 JS1 Alpha. Slice surface 2B

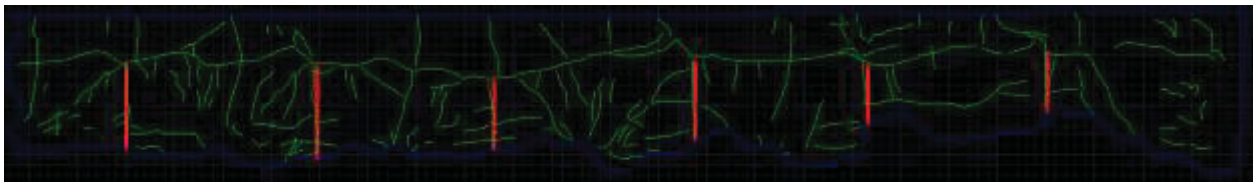

Figure II-11 JS1 Alpha. Slice surface 3T

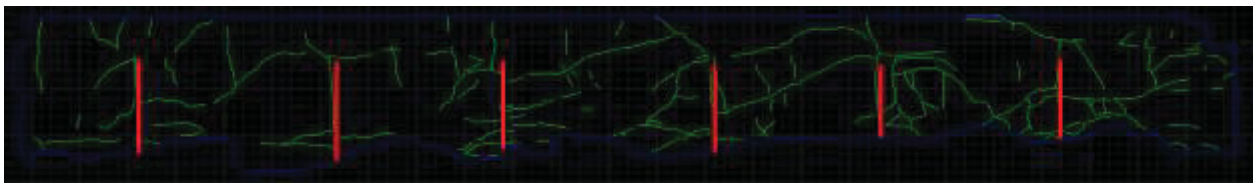

Figure II-12 JS1 Alpha. Slice surface 4T

JS1 Beta

Picture of JS1 Beta before blasting

Figure II-13 JS1 Beta before blasting

Top view of the JS1 Beta after blasting

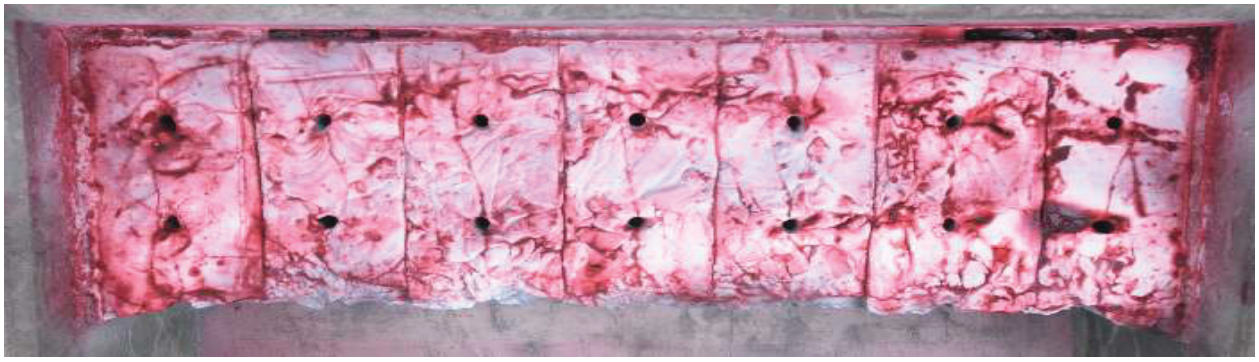

Figure II-14 JS1 Beta top view after blasting of 1st row

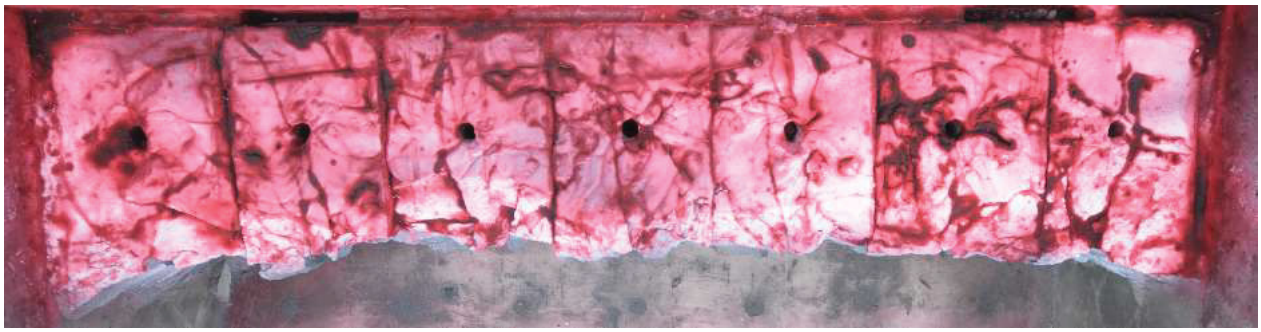

Figure II-15 JS1 Beta top view after blasting of 2nd row

The slice and AutoCAD pictures of JS1 Beta don't exist because 3rd row was not blasted and the block was broken while cutting it into slices.

JS1 Gamma

Picture of JS1 Gamma before blasting

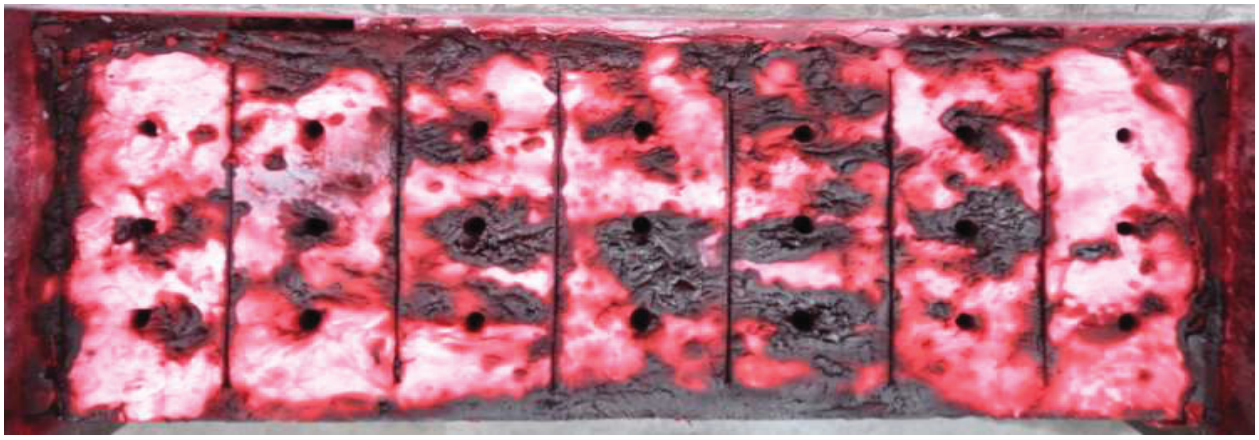

Figure II-16 JS1 Gamma before blasting

Top view of the JS1 Gamma after blasting

Figure II-17 JS1 Gamma top view after blasting of 1st row

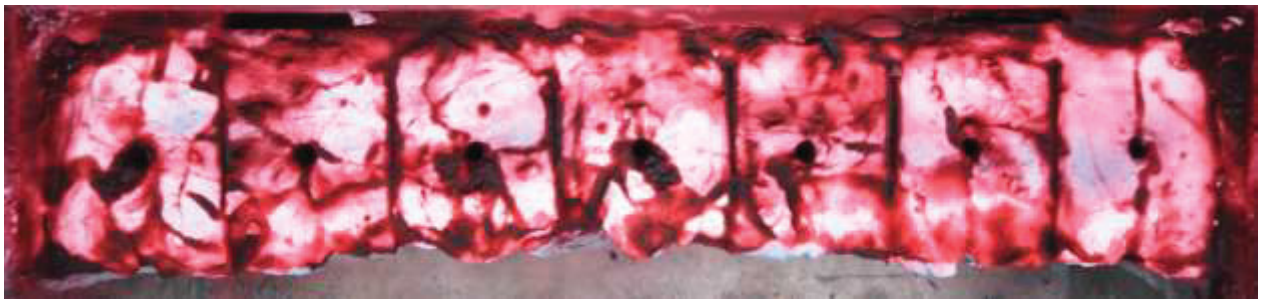

Figure II-18 JS1 Gamma top view after blasting of 2nd row

Figure II-19 JS1 Gamma top view after blasting of 3rd row

Slice Pictures of JS1 Gamma

Figure II-20 JS1 Gamma. Slice 1B

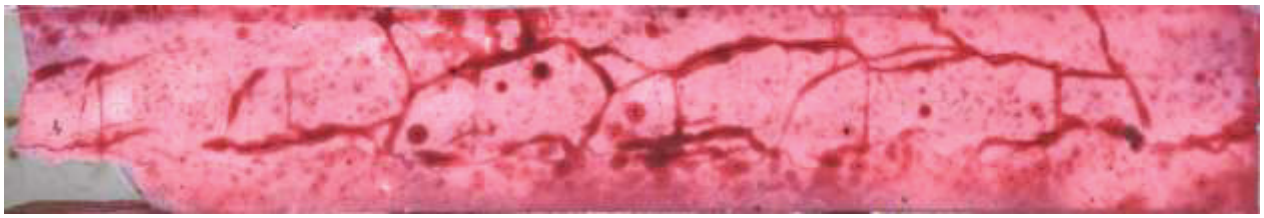

Figure II-21 JS1 Gamma. Slice 2B

Figure II-22 JS1 Gamma. Slice 3B

Figure II-23 JS1 Gamma. Slice 4T

AutoCAD drawings of JS1 Gamma

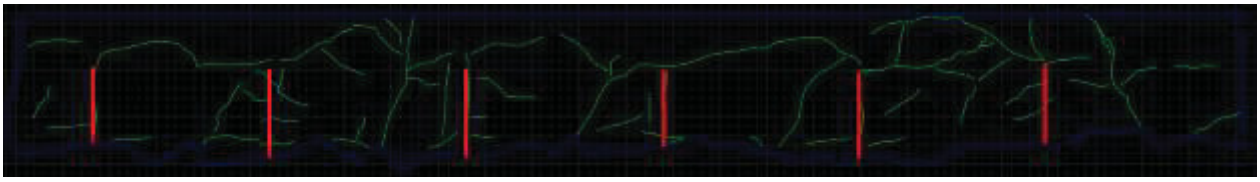

Figure II-24 JS1 Gamma. Slice surface 1B

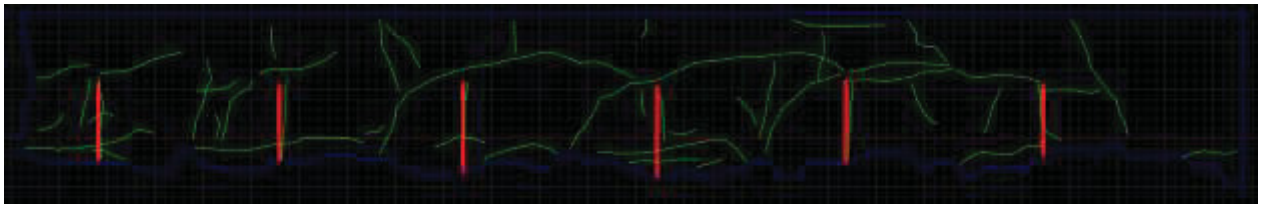

Figure II-25 JS1 Gamma. Slice surface 2B

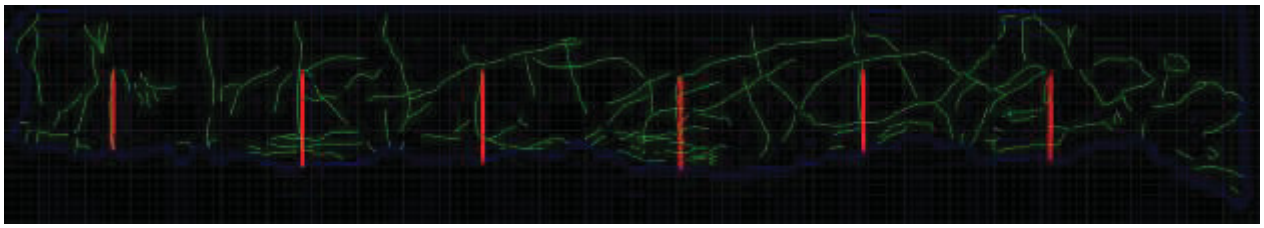

Figure II-26 JS1 Gamma. Slice surface 3B

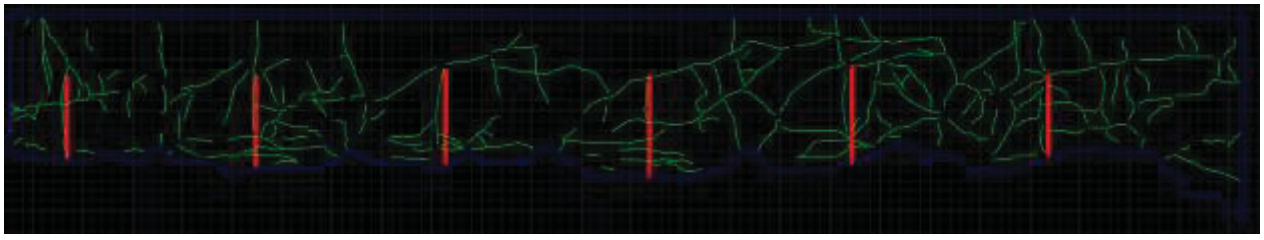

Figure II-27 JS1 Gamma. Slice surface 4T

JS2 Beta

Picture of JS2 Beta before blasting

Figure II-28 JS2 Beta before blasting

Top view of the JS2 Beta after blasting

Figure II-29 JS2 Beta top view after blasting of 1st row

Figure II-30 JS2 Beta top view after blasting of 2nd row

Figure II-31 JS2 Beta top view after blasting of 3rd row

Slice Pictures of JS2 Beta

Figure II-32 JS2 Beta. Slice 1B

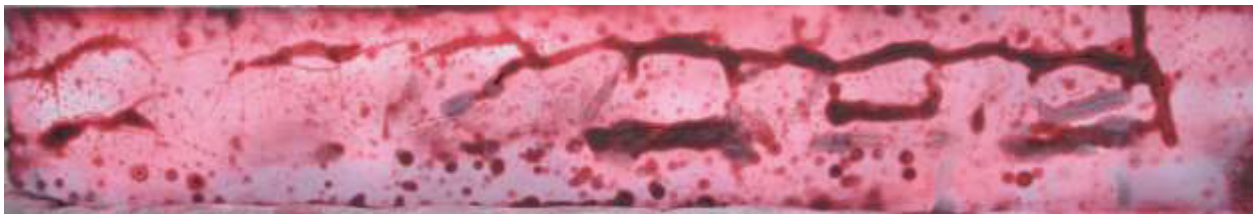

Figure II-33 JS2 Beta. Slice 2B

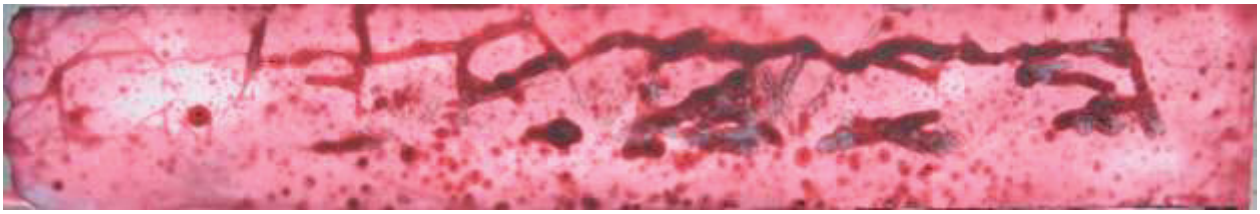

Figure II-34 JS2 Beta. Slice 3B

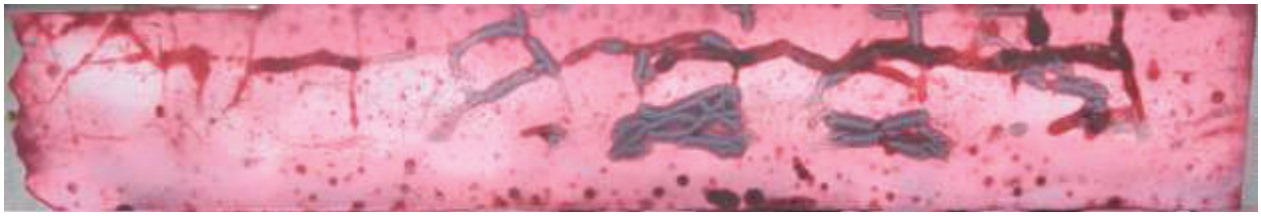

Figure II-35 JS2 Beta. Slice 4T

AutoCAD drawings of JS2 Beta

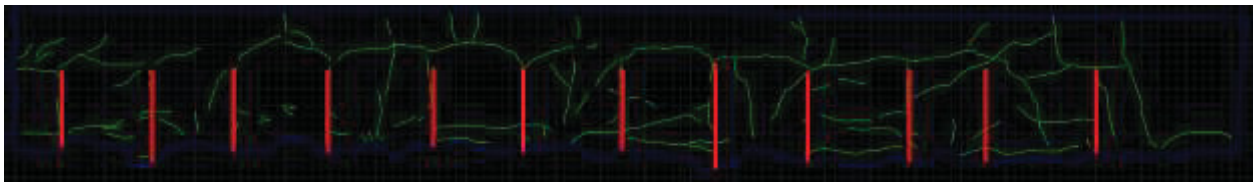

Figure II-36 JS2 Beta. Slice surface 1B

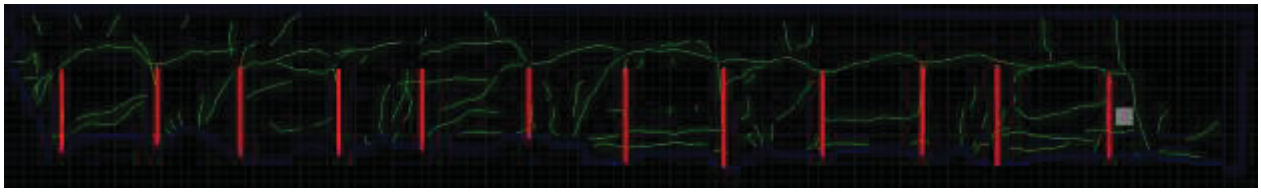

Figure II-37 JS2 Beta. Slice surface 2B

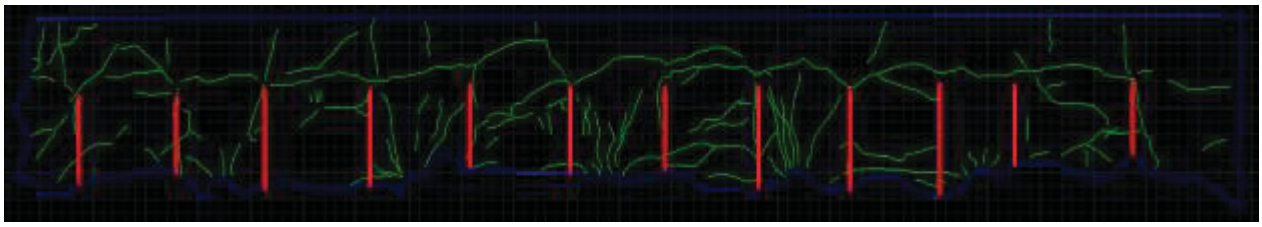

Figure II-38 JS2 Beta. Slice surface 3B

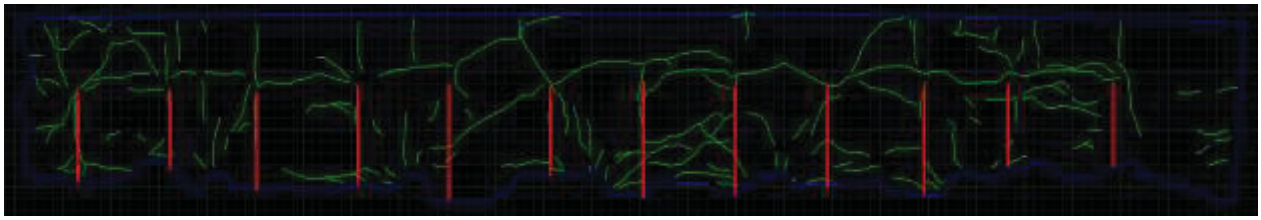

Figure II-39 JS2 Beta. Slice surface 4T

JS3 Alpha

Picture of JS3 Alpha before blasting

Figure II-40 JS3 Alpha before blasting

Top view of the JS3 Alpha after blasting

Figure II-41 JS3 Alpha top view after blasting of 1st row

Figure II-42 JS3 Alpha top view after blasting of 2nd row

Figure II-43 JS3 Alpha top view after blasting of 3rd row

Slice Pictures of JS3 Alpha

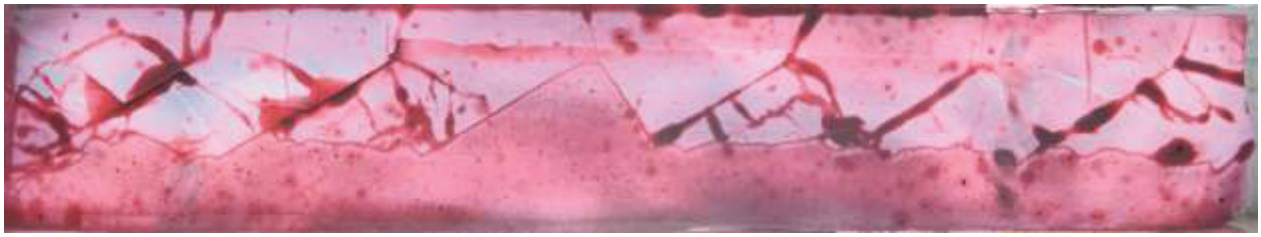

Figure II-44 JS3 Alpha. Slice 1B

Figure II-45 JS3 Alpha. Slice 2B

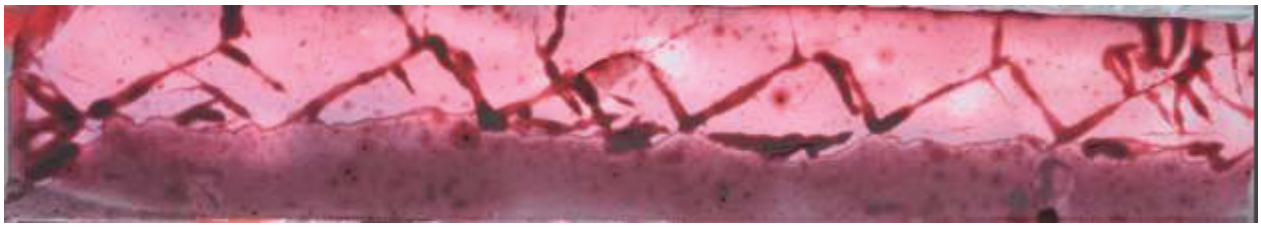

Figure II-46 JS3 Alpha. Slice 3B

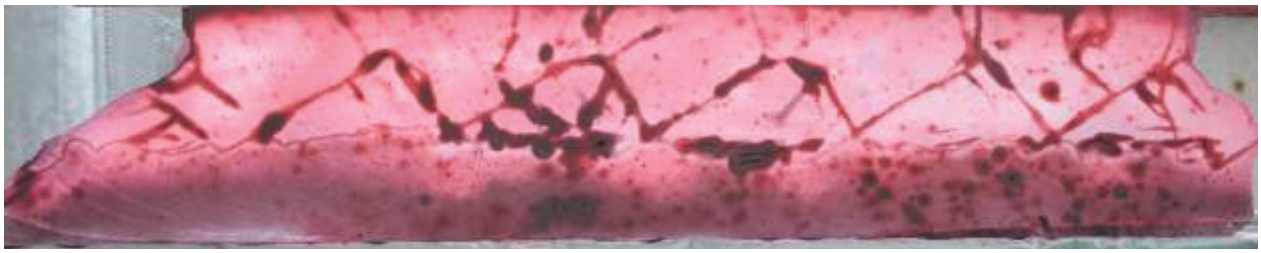

Figure II-47 JS3 Alpha. Slice 4T

AutoCAD drawings of JS3 Alpha

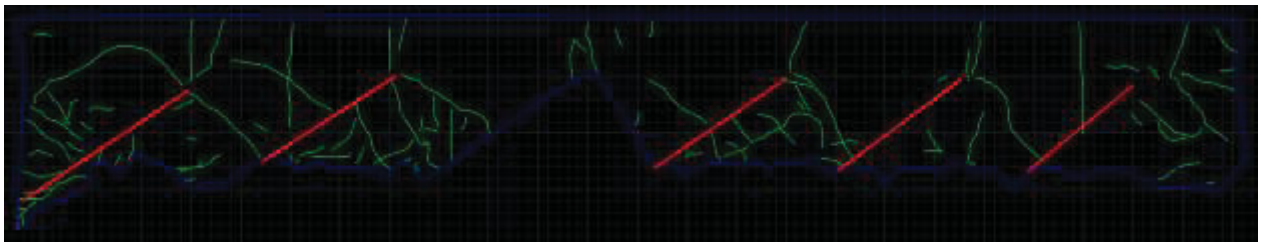

Figure II-48 JS3 Alpha. Slice surface 1B

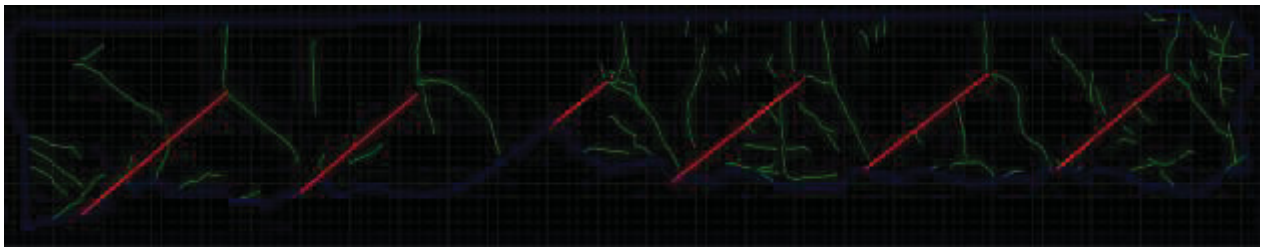

Figure II-49 JS3 Alpha. Slice surface 2B

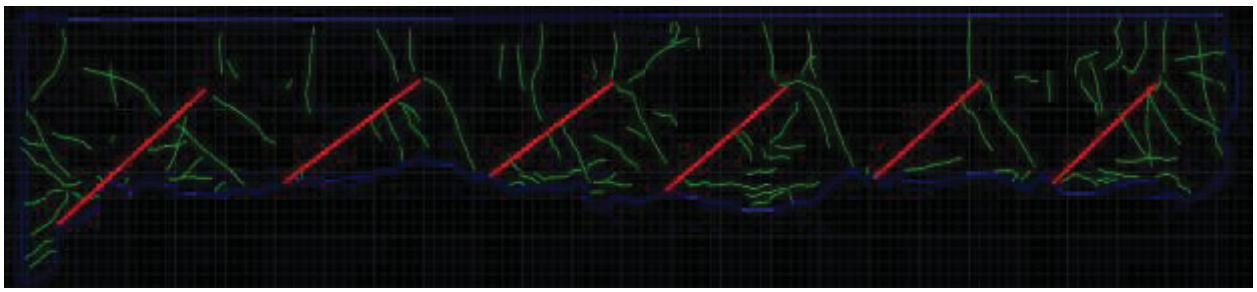

Figure II-50 JS3 Alpha. Slice surface 3B

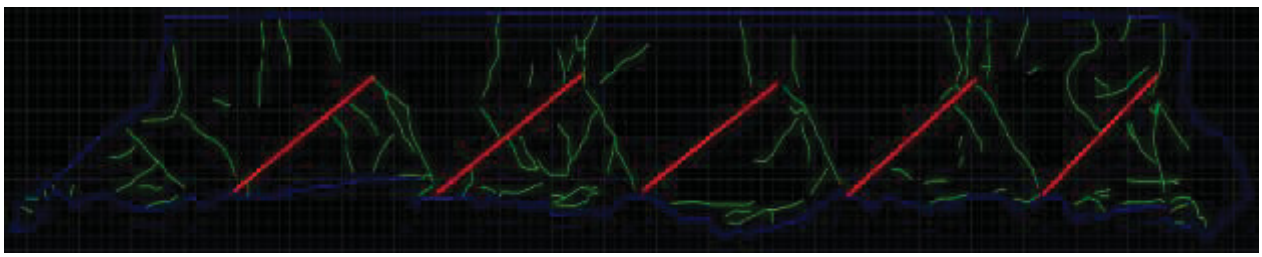

Figure II-51 JS3 Alpha. Slice surface 3T

JS3 Beta

Picture of JS3 Beta before blasting

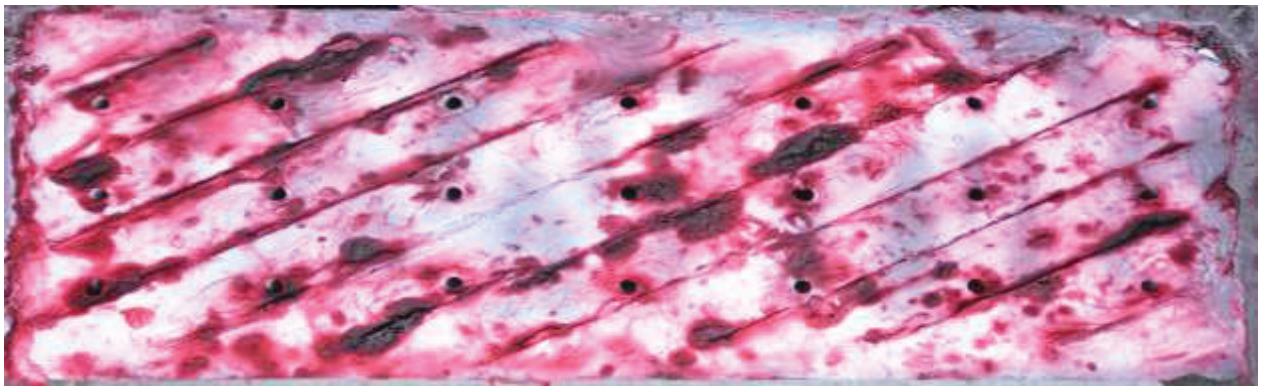

Figure II-52 JS3 Beta before blasting

Top view of the JS3 Beta after blasting

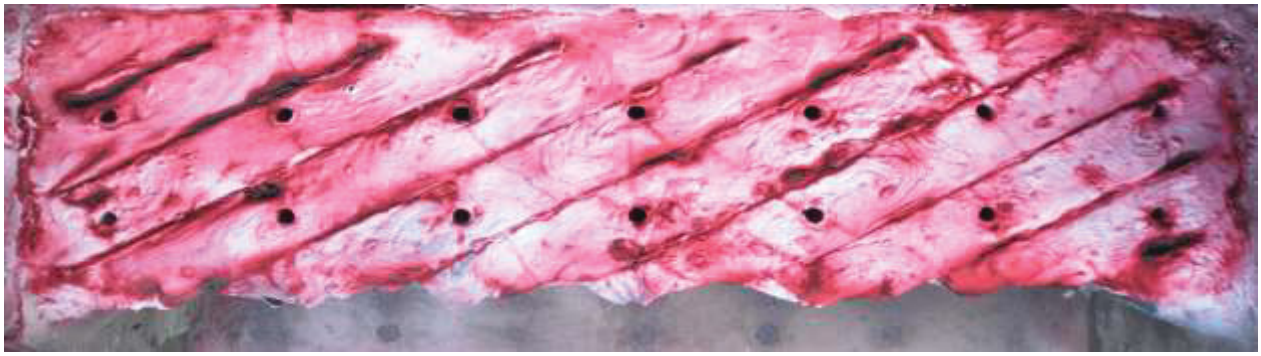

Figure II-53 JS3 Beta top view after blasting of 1st row

Figure II-54 JS3 Beta top view after blasting of 2nd row

JS4 Alpha

Picture of JS4 Alpha before blasting

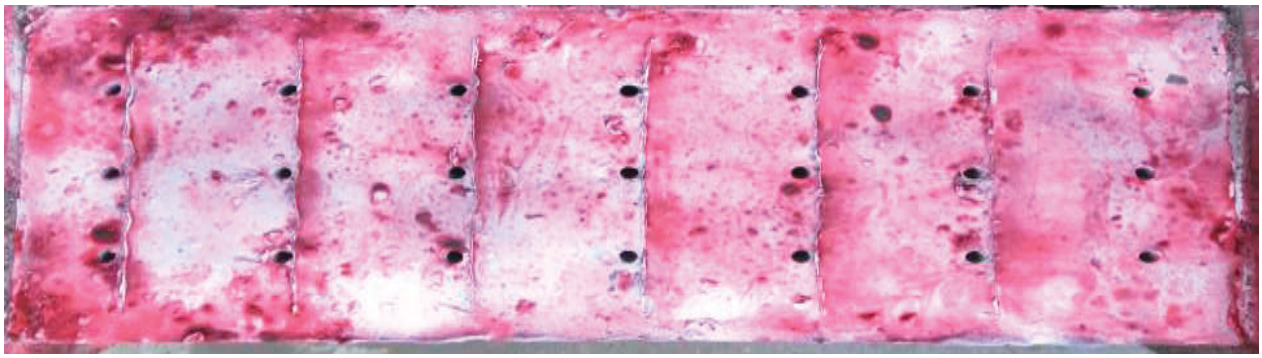

Figure II-55 JS4 Alpha before blasting

Top view of the JS4 Alpha after blasting

Figure II-56 JS4 Alpha top view after blasting of 1st row

Figure II-57 JS4 Alpha top view after blasting of 2nd row

Figure II-58 JS4 Alpha top view after blasting of 3rd row

Slice Pictures of JS4 Alpha

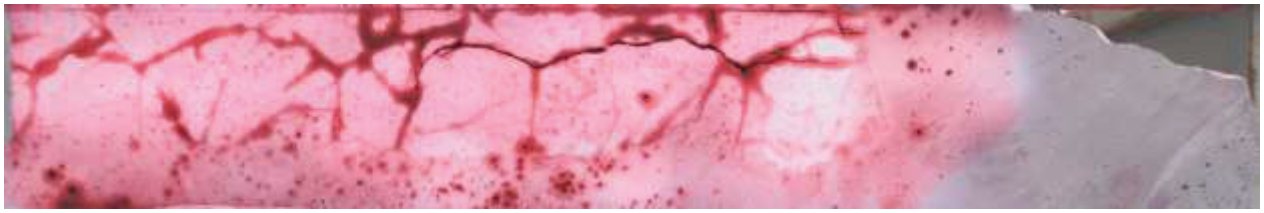

Figure II-59 JS4 Alpha. Slice 1B

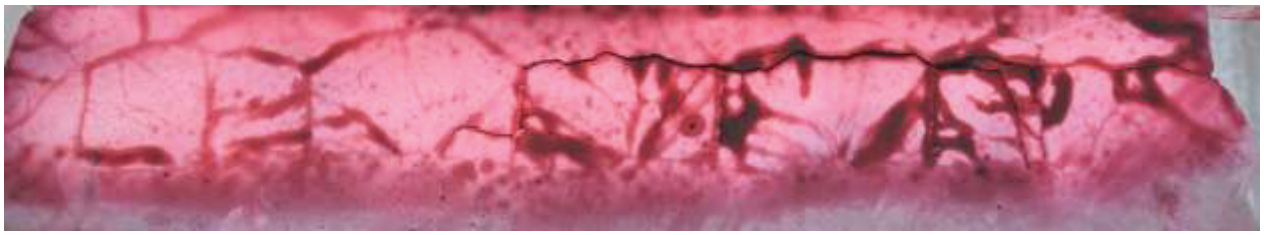

Figure II-60 JS4 Alpha. Slice 2B

Figure II-61 JS4 Alpha. Slice 3T

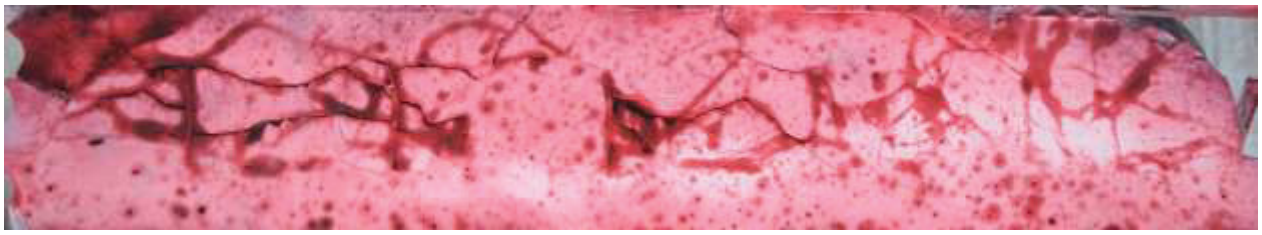

Figure II-62 JS4 Alpha .Slice 4T

AutoCAD drawings of JS4 Alpha

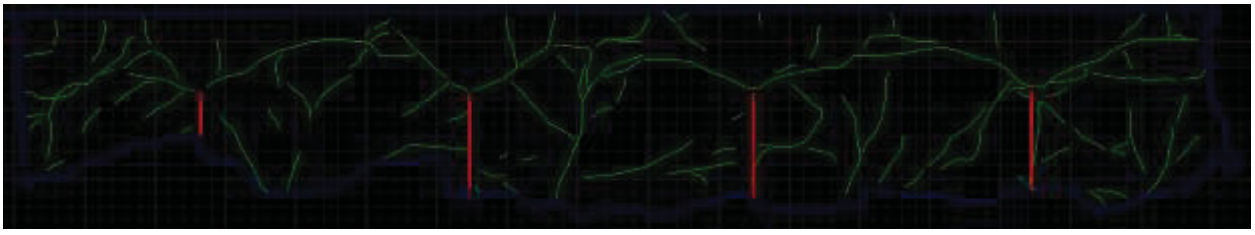

Figure II-63 JS4 Alpha. Slice surface 1B

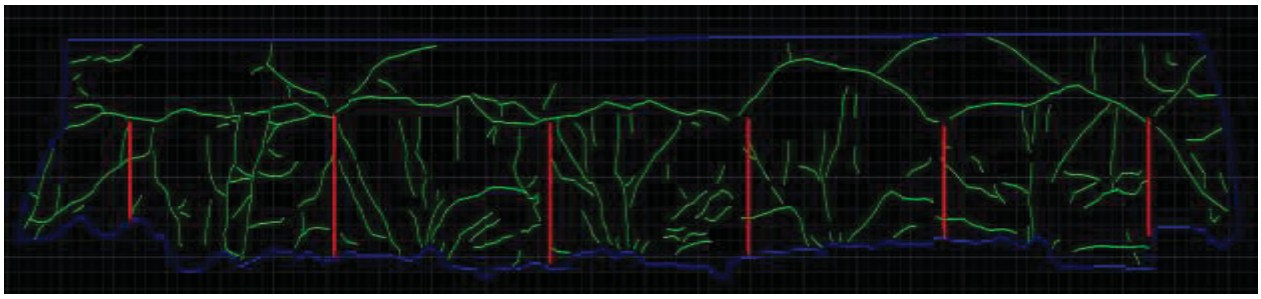

Figure II-64 JS4 Alpha. Slice surface 2B

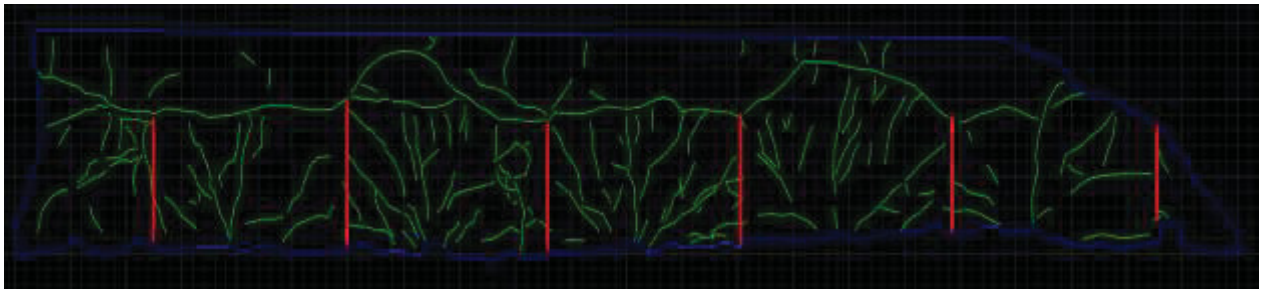

Figure II-65 JS4 Alpha. Slice surface 3B

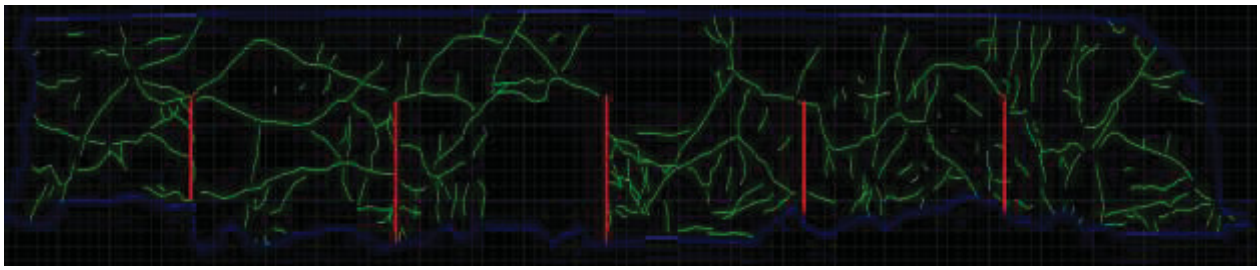

Figure II-66 JS4 Alpha. Slice surface 4T

JS4 Beta

Picture of JS4 Beta before blasting

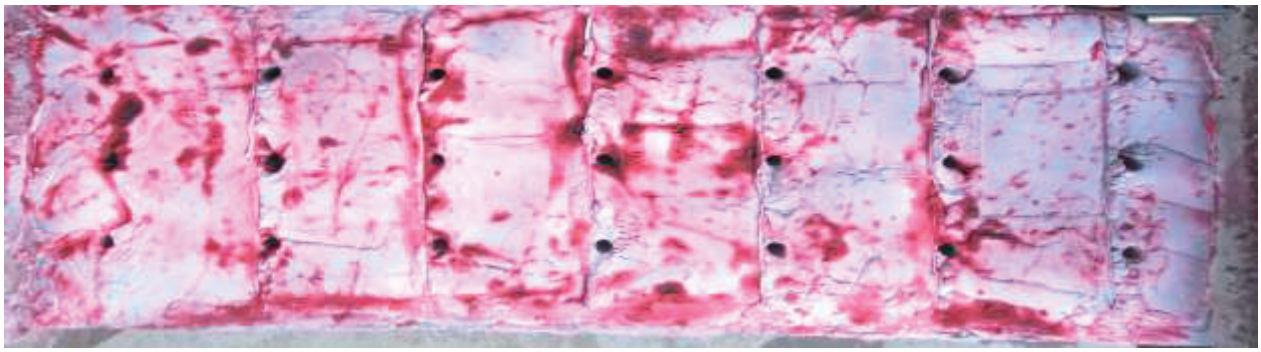

Figure II-67 JS4 Beta before blasting

Top view of the JS4 Beta after blasting

Figure II-68 JS4 Beta top view after blasting of 1st row

Figure II-69 JS4 Beta top view after blasting of 2nd row

Figure II-70 JS4 Beta top view after blasting of 3rd row

Slice Pictures of JS4 Beta

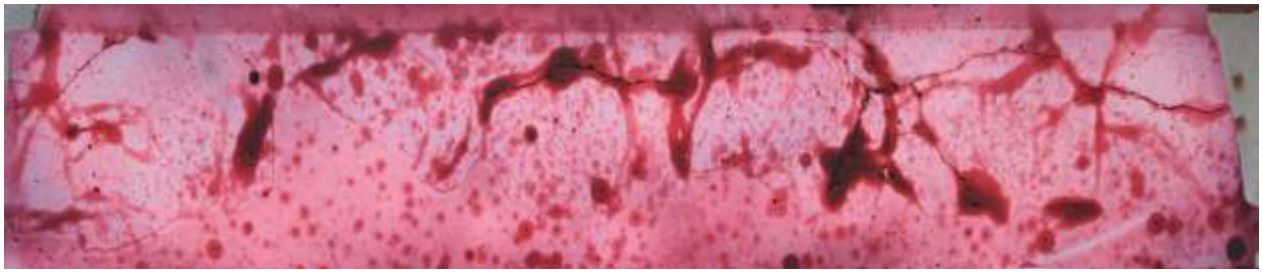

Figure II-71 JS4 Beta. Slice 1B

Figure II-72 JS4 Beta. Slice 2B

Figure II-73 JS4 Beta. Slice 3B

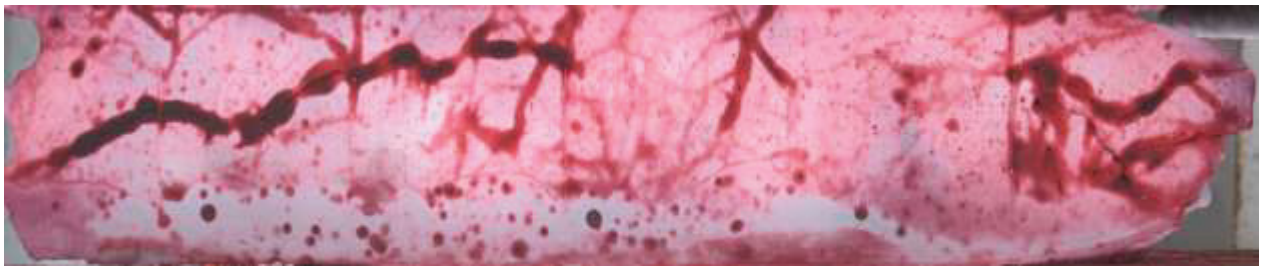

Figure II-74 JS4 Beta. Slice 4T

AutoCAD drawings of JS4 Beta

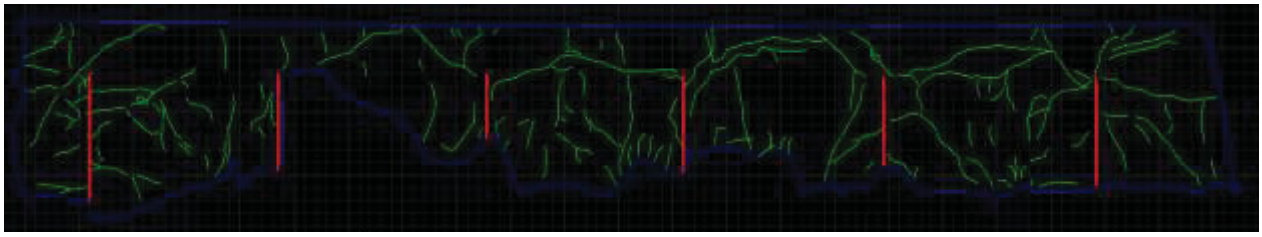

Figure II-75 JS4 Beta. Slice surface 1B

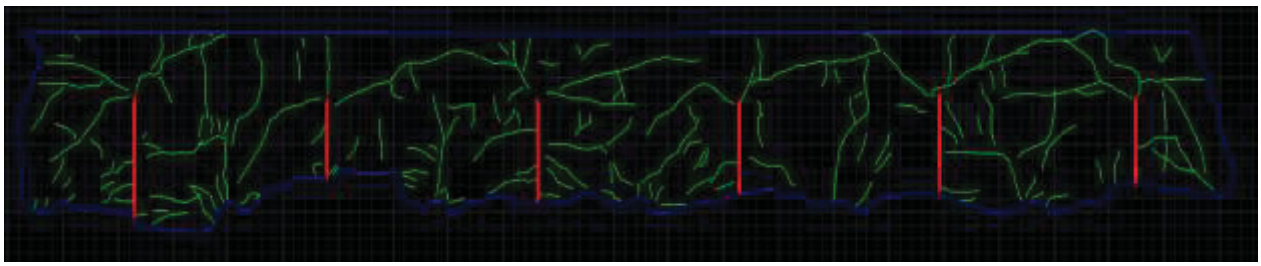

Figure II-76 JS4 Beta. Slice surface 1B

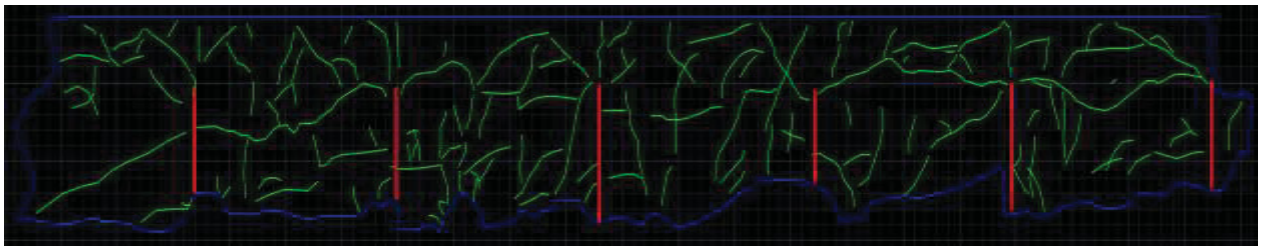

Figure II-77 JS4 Beta. Slice surface 3B

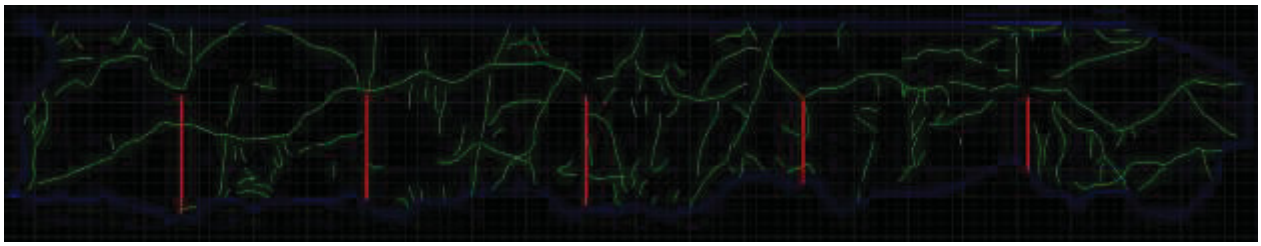

Figure II-78 JS4 Beta. Slice surface 4T

Reference 1

Picture of Reference 1 before blasting

Figure II-79 Reference 1 before blasting

Top view of the Reference 1 after blasting

Figure II-80 Reference 1 top view after blasting of 1st row

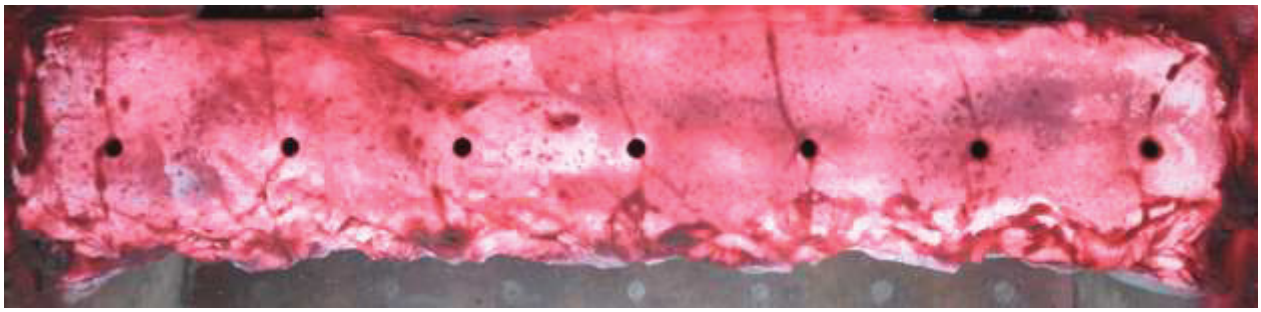

Figure II-81 Reference 1 top view after blasting of 2nd row

Figure II-82 Reference 1 top view after blasting of 3rd row

Slice Pictures of Reference 1

Figure II-83 Reference 1. Slice 1B

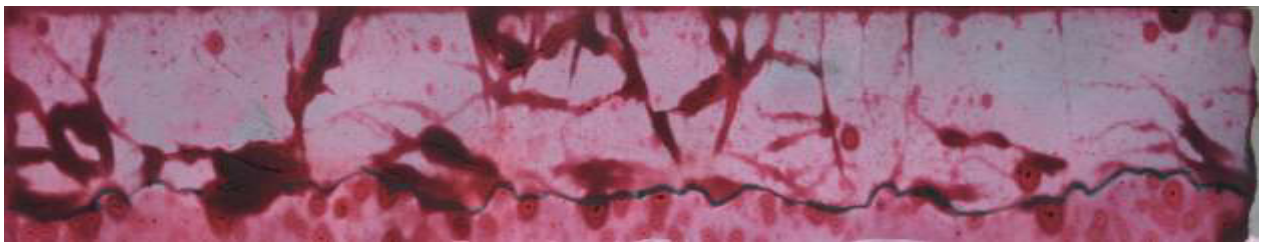

Figure II-84 Reference 1. Slice 2T

Figure II-85 Reference 1. Slice 3T

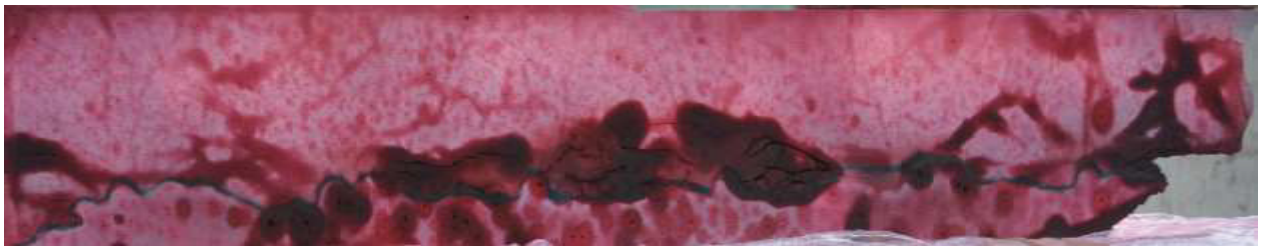

Figure II-86 Reference 1. Slice 4T

AutoCAD drawings of Reference 1

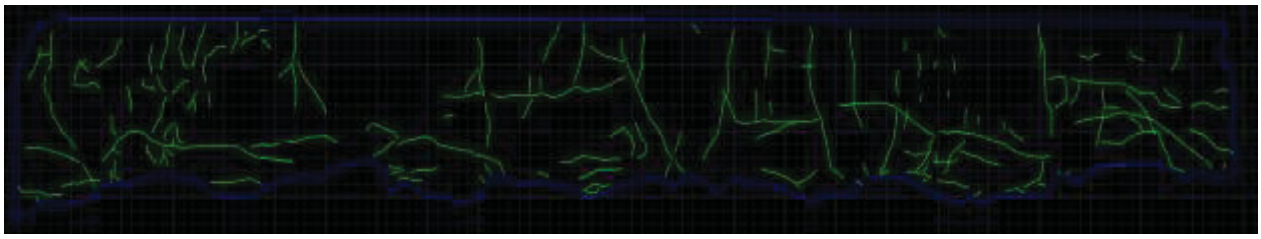

Figure II-87 Reference 1. Slice surface 1B

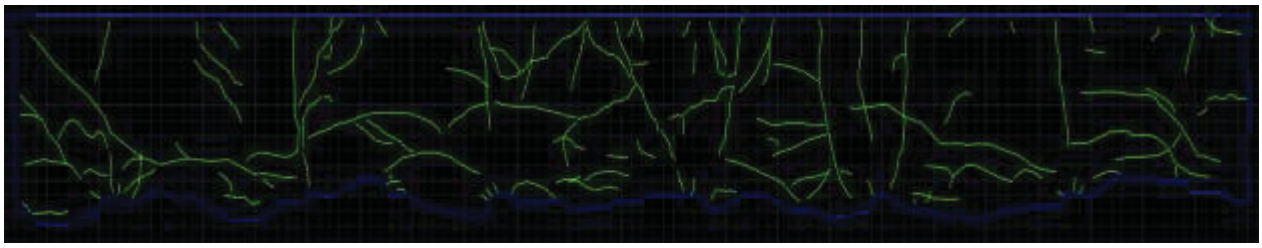

Figure II-88 Reference 1. Slice surface 2T

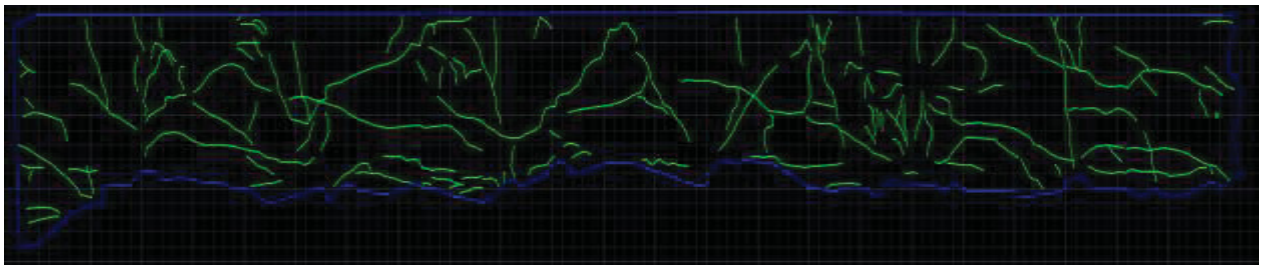

Figure II-89 Reference 1. Slice surface 3T

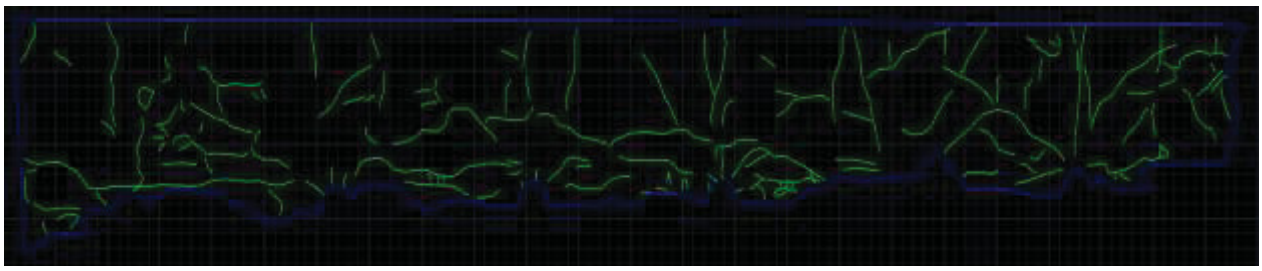

Figure II-90 Reference 1. Slice surface 4T

Reference 2

Picture of Reference 2 before blasting

Figure II-91 Reference 2 before blasting

Top view of the Reference 2 after blasting

Figure II-92 Reference 2 top view after blasting of 1st row

Figure II-93 Reference 2 top view after blasting of 2nd row

Figure II-94 Reference 3 top view after blasting of 3rd row

Slice Pictures of Reference 2

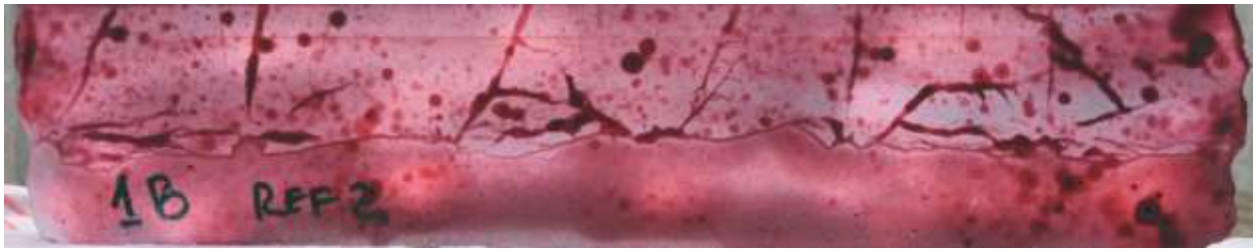

Figure II-95 Reference 2. Slice 1B

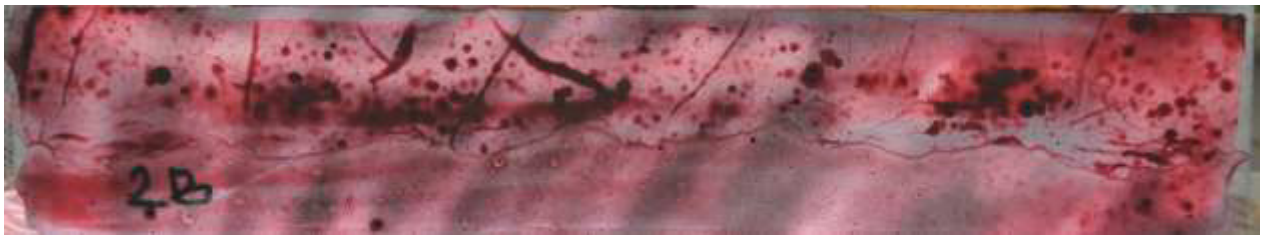

Figure II-96 Reference 2. Slice 2B

Figure II-97 Reference 2. Slice 3T

Figure II-98 Reference 2. Slice 4T

AutoCAD drawings of Reference 2

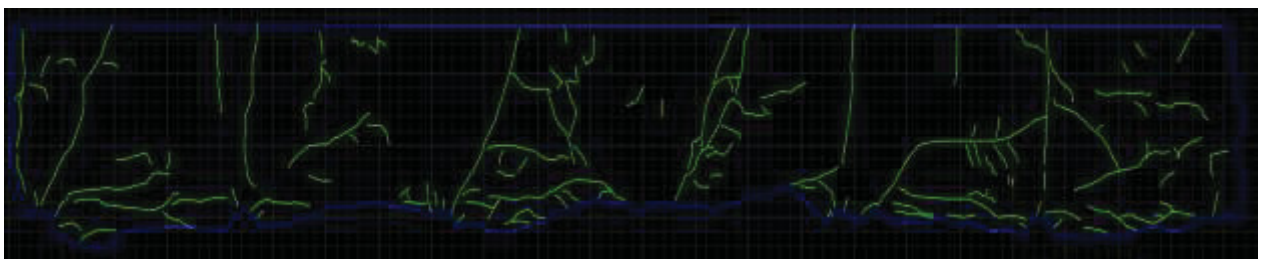

Figure II-99 Reference 2. Slice surface 1B

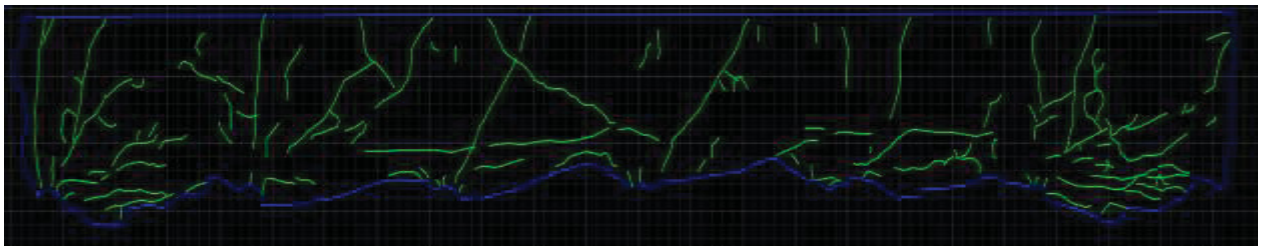

Figure II-100 Reference 2. Slice surface 2B

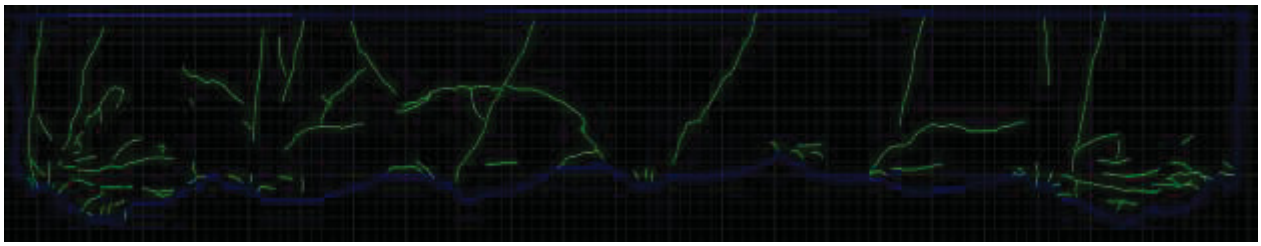

Figure II-101 Reference 2. Slice surface 3T

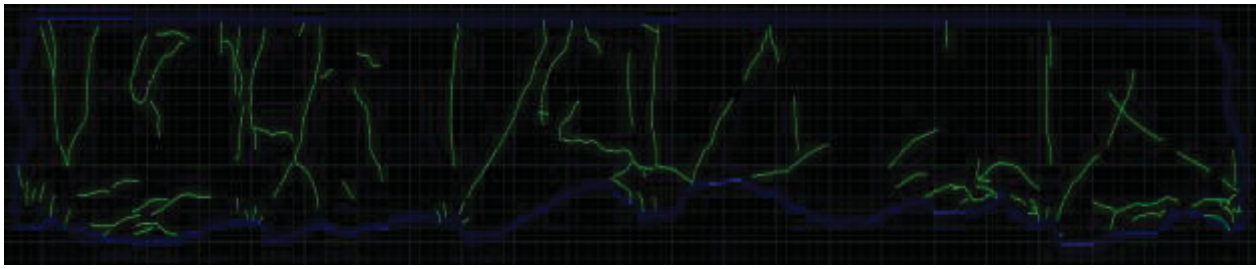

Figure II-102 Reference 2. Slice surface 4T

Reference 3

Picture of Reference 3 before blasting

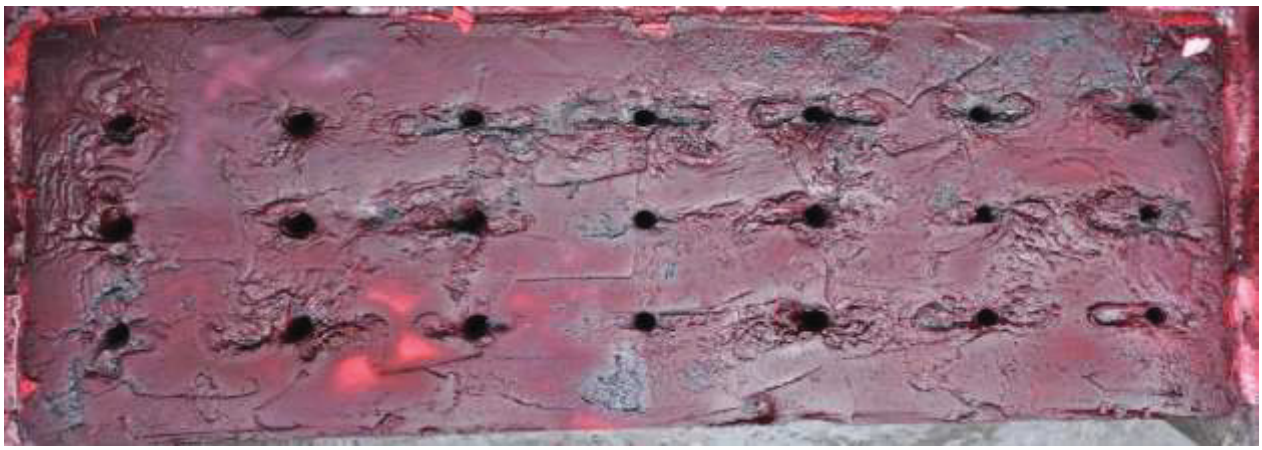

Figure II-103 Reference 3 before blasting

Top view of the Reference 3 after blasting

Figure II-104 Reference 3 top view after blasting of 1st row

Figure II-105 Reference 3 top view after blasting of 2nd row

Figure II-106 Reference 3 top view after blasting of 3rd row

Slice Pictures of Reference 3

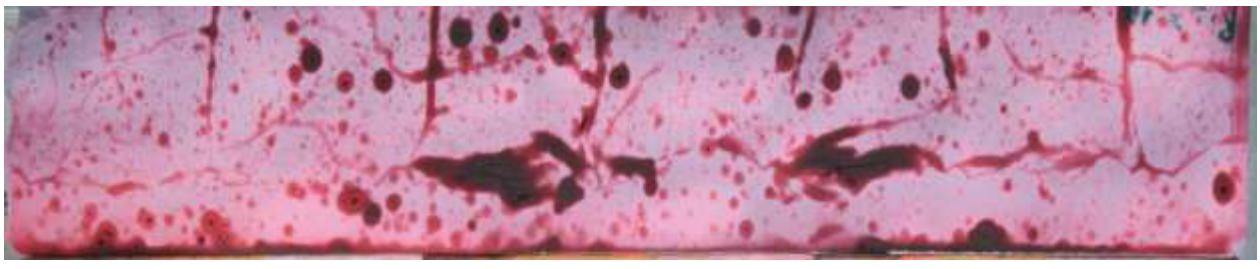

Figure II-107 Reference 3. Slice 1B

Figure II-108 Reference 3. Slice 2B

Figure II-109 Reference 3. Slice 3B

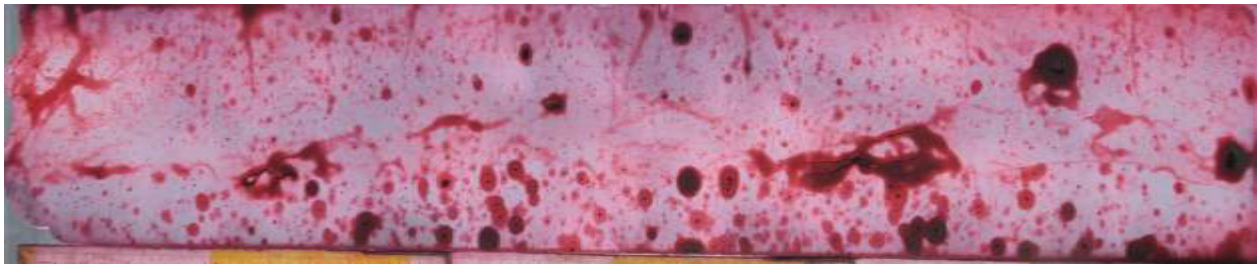

Figure II-110 Reference 3. Slice 4T

AutoCAD drawings of Reference 3

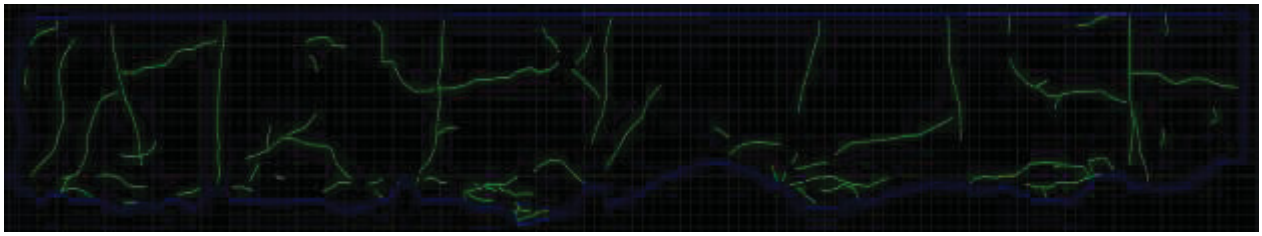

Figure II-111 Reference 3. Slice surface 1B

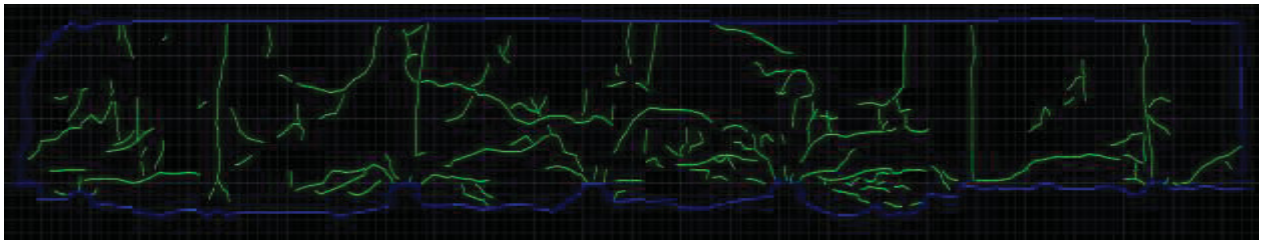

Figure II-112 Reference 3. Slice surface 2B

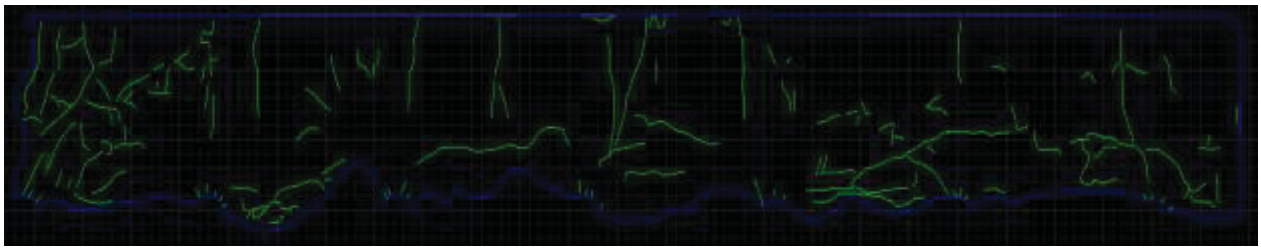

Figure II-113 Reference 3. Slice surface 4T

Cylinder Pictures

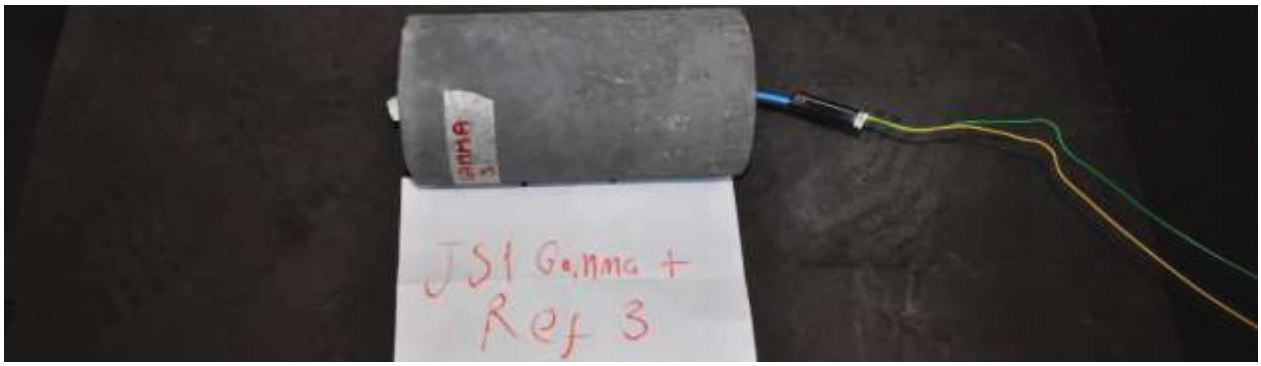

Figure II-114 Cylinder JS1 Gamma- Reference 3

Figure II-115 Cylinder JS1 Gamma- Reference 3 fragments.

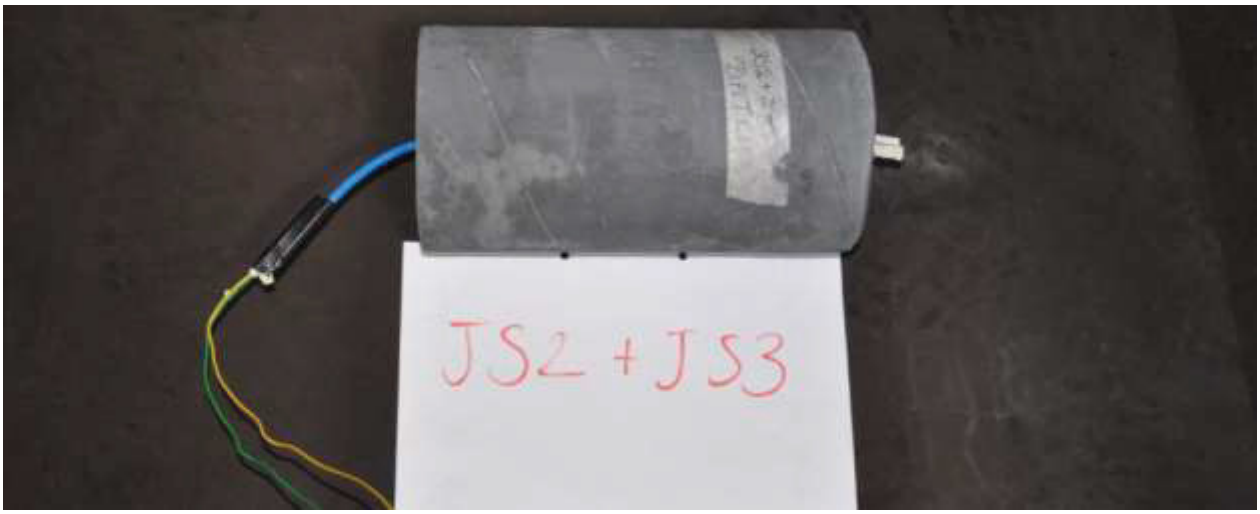

Figure II-116 Cylinder JS2 + JS3

Figure II-117 Cylinder JS2 + JS3 fragments.

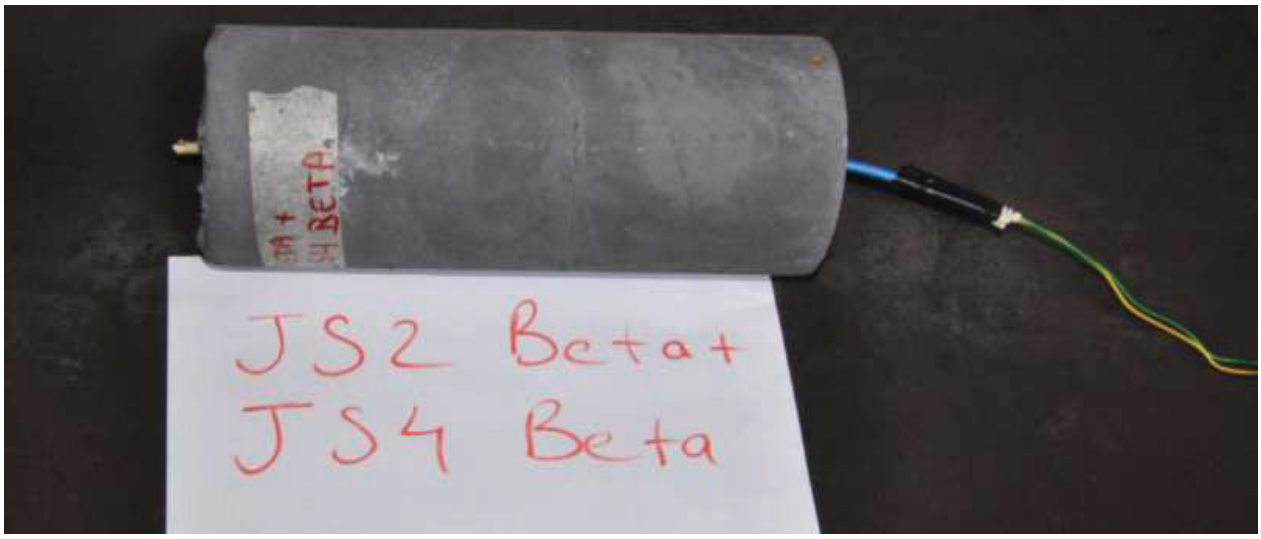

Figure II-118 Cylinder JS2 Beta + JS4 Beta

Figure II-119 Cylinder JS2 Beta + JS4 Beta fragments.

Figure II-120 Cylinder JS3 Beta

Figure II-121 Cylinder JS3 Beta fragments.

ANNEX III: SIEVING DATA OF THE BLOCKS AND CYLINDERS

JS1 Alpha

Row 1

Date of Blast:		28/05/2015		Date of Sieve Analysis:	02/06/2015	
Explosive	**Length**	147.0	[cm]	**Total Mass:**	25450.0	[g]
	Type	20	[g/m]	**Total Mass < 14 mm:**	6266.0	[g]
	Amount	29.40	[g]	**Screen Feed < 14 mm:**	3173.1	[g]
Specific Charge		1155.21	[g/t]	**Other:**	205.5	[g]
				Loss:	115.8	[g]

Mesh Size [mm]	**Mass [g]**		**Mass [%]**	**Retained [%]**	**Passing [%]**	**Local Gradient**
125	0.0		0.00	0.00	100.00	
100	1075.1		4.24	4.24	95.76	0.194
80	822.0		3.24	7.49	92.51	0.154
63	2587.2		10.21	17.70	82.30	0.490
50	1172.3		4.63	22.32	77.68	0.250
40	3071.5		12.12	34.44	65.56	0.760
31.5	3691.7		14.57	49.01	50.99	1.052
25	2551.8		10.07	59.08	40.92	0.952
20	1570.6		6.20	65.28	34.72	0.736
14	2531.7		9.99	75.27	24.73	0.951
12.5		249.5	2.08	77.36	22.64	0.776
10		483.8	4.04	81.39	18.61	0.880
6.3		698.4	5.83	87.22	12.78	0.814
4		493.8	4.12	91.35	8.65	0.858
2		381.6	3.19	94.53	5.47	0.662
1		222.3	1.86	96.39	3.61	0.598
0.5		116.2	0.97	97.36	2.64	0.451
0.25		202.2	1.69	99.05	0.95	
<0,25		114.1	0.95			
Total	**19073.9**	**2961.9**	100.00			

Table III-1 JS1 Alpha row 1 sieving table

Row 2

Date of Blast:		28/05/2015		Date of Sieve Analysis:	02/06/2015	
Explosive	**Length**	147.0	[cm]	**Total Mass:**	24220.0	[g]
	Type	20	[g/m]	**Total Mass < 14 mm:**	9776.0	[g]
	Amount	29.40	[g]	**Screen Feed < 14 mm:**	4917.0	[g]
Specific Charge		1213.87	[g/t]	**Other:**	276.7	[g]
				Loss:	214.8	[g]

Mesh Size [mm]	**Mass [g]**		**Mass [%]**	**Retained [%]**	**Passing [%]**	**Local Gradient**
125	0.0		0.00	0.00	100.00	
100	0.0		0.00	0.00	100.00	0.000
80	0.0		0.00	0.00	100.00	0.000
63	1953.9		8.17	8.17	91.83	0.357
50	3615.3		15.12	23.29	76.71	0.778
40	993.0		4.15	27.44	72.56	0.249
31.5	2197.9		9.19	36.63	63.37	0.567
25	1615.4		6.75	43.38	56.62	0.488
20	1540.8		6.44	49.82	50.18	0.541
14	2225.2		9.30	59.13	40.87	0.575
12.5		477.9	4.13	63.26	36.74	0.940
10		673.3	5.82	69.08	30.92	0.773
6.3		922.5	7.98	77.05	22.95	0.646
4		801.9	6.93	83.99	16.01	0.792
2		682.8	5.90	89.89	10.11	0.663
1		395.4	3.42	93.31	6.69	0.595
0.5		234.6	2.03	95.34	4.66	0.521
0.25		333.5	2.88	98.22	1.78	
<0,25		206.1	1.78			
Total	**14141.5**	**4728.0**	100.00			

Table III-2 JS1 Alpha row 2 sieving table

Row 3

Date of Blast:		28/05/2015		Date of Sieve Analysis:	03/06/2015	
Explosive	**Length**	147.0	[cm]	**Total Mass:**	25060.0	[g]
	Type	20	[g/m]	**Total Mass < 14 mm:**	11230.0	[g]
	Amount	29.40	[g]	**Screen Feed < 14 mm:**	5691.0	[g]
Specific charge		1173.18	[g/t]	**Other:**	230.8	[g]
				Loss:	11.7	[g]

Mesh Size [mm]	**Mass [g]**		**Mass [%]**	**Retained [%]**	**Passing [%]**	**Local Gradient**
125	0.0		0.00	0.00	100.00	
100	0.0		0.00	0.00	100.00	0.000
80	0.0		0.00	0.00	100.00	0.000
63	0.0		0.00	0.00	100.00	0.000
50	1750.6		6.97	6.97	93.03	0.313
40	1034.0		4.12	11.09	88.91	0.203
31.5	2750.8		10.96	22.05	77.95	0.551
25	2678.6		10.67	32.73	67.27	0.637
20	2400.6		9.56	42.29	57.71	0.687
14	3255.0		12.97	55.26	44.74	0.714
12.5		591.8	4.90	60.15	39.85	1.022
10		774.3	6.40	66.56	33.44	0.785
6.3		1286.1	10.64	77.20	22.80	0.829
4		782.8	6.48	83.67	16.33	0.735
2		746.6	6.18	89.85	10.15	0.686
1		422.0	3.49	93.34	6.66	0.608
0.5		211.8	1.75	95.09	4.91	0.440
0.25		215.2	1.78	96.87	3.13	
<0,25		378.3	3.13			
Total	**13869.6**	**5408.9**	100.00			

Table III-3 JS1 Alpha row 3 sieving table

JS1 Beta

Row 1

Date of Blast:		19/05/2015		Date of Sieve Analysis:	21/05/2015	
Explosive	**Length**	147.0	[cm]	**Total Mass:**	24340.0	[g]
	Type	20	[g/m]	**Total Mass < 14 mm:**	4960.0	[g]
	Amount	29.40	[g]	**Screen Feed < 14 mm:**	2495.7	[g]
Specific charge		1207.89	[g/t]	**Other:**	130.4	[g]
				Loss:	-42.3	[g]

Mesh Size [mm]	**Mass [g]**		**Mass [%]**	**Retained [%]**	**Passing [%]**	**Local Gradient**
125	0.0		0.00	0.00	100.00	
100	1479.9		6.05	6.05	93.95	0.280
80	7787.6		31.85	37.90	62.10	1.855
63	3809.2		15.58	53.47	46.53	1.209
50	342.2		1.40	54.87	45.13	0.132
40	1107.6		4.53	59.40	40.60	0.474
31.5	1603.2		6.56	65.96	34.04	0.737
25	1109.9		4.54	70.50	29.50	0.619
20	933.6		3.82	74.32	25.68	0.621
14	1320.7		5.40	79.72	20.28	0.662
12.5		289.7	2.56	82.28	17.72	1.191
10		341.8	3.02	85.30	14.70	0.838
6.3		516.5	4.57	89.87	10.13	0.805
4		358.0	3.17	93.03	6.97	0.825
2		301.1	2.66	95.70	4.30	0.695
1		167.3	1.48	97.18	2.82	0.608
0.5		88.3	0.78	97.96	2.04	0.467
0.25		71.7	0.63	98.59	1.41	
<0,25		159.3	1.41			
Total	**19493.9**	**2293.7**	100.00			

Table III-4 JS1 Beta row 1 sieving table

Row 2

Date of Blast:		19/05/2015		Date of Sieve Analysis:	21/05/2015	
Explosive	**Length**	147.0	[cm]	**Total Mass:**	23790.0	[g]
	Type	20	[g/m]	**Total Mass < 14 mm:**	8700.0	[g]
	Amount	29.40	[g]	**Screen Feed < 14 mm:**	4419.3	[g]
Specific Charge		1235.81	[g/t]	**Other:**	150.5	[g]
				Loss:	114.0	[g]

Mesh Size [mm]	**Mass [g]**		**Mass [%]**	**Retained [%]**	**Passing [%]**	**Local Gradient**
125	0.0		0.00	0.00	100.00	
100	0.0		0.00	0.00	100.00	0.000
80	0.0		0.00	0.00	100.00	0.000
63	863.3		3.62	3.62	96.38	0.154
50	4076.2		17.08	20.70	79.30	0.844
40	1551.8		6.50	27.20	72.80	0.383
31.5	1797.6		7.53	34.74	65.26	0.457
25	2111.6		8.85	43.59	56.41	0.631
20	1938.2		8.12	51.71	48.29	0.697
14	2822.8		11.83	63.54	36.46	0.788
12.5		379.8	3.39	66.93	33.07	0.861
10		740.7	6.61	73.54	26.46	1.000
6.3		961.0	8.58	82.13	17.87	0.849
4		666.6	5.95	88.08	11.92	0.891
2		501.9	4.48	92.56	7.44	0.680
1		297.2	2.65	95.21	4.79	0.636
0.5		150.6	1.34	96.56	3.44	0.476
0.25		121.5	1.08	97.64	2.36	
<0,25		264.0	2.36			
Total	**15161.5**	**4083.3**	100.00			

Table III-5 JS1 Beta row 2 sieving table

JS1 Gamma

Row 1

Date of Blast:		18/06/2015		Date of Sieve Analysis:	08/07/2015	
Explosive	**Length**	147.0	[cm]	**Total Mass:**	26060.0	[g]
	Type	20	[g/m]	**Total Mass < 14 mm:**	5400.0	[g]
	Amount	29.40	[g]	**Screen Feed < 14 mm:**	2723.0	[g]
Specific charge		1128.17	[g/t]	**Other:**	207.2	[g]
				Loss:	0.2	[g]

Mesh Size [mm]	**Mass [g]**		**Mass [%]**	**Retained [%]**	**Passing [%]**	**Local Gradient**
125	0.0		0.00	0.00	100.00	
100	3111.0		11.99	11.99	88.01	0.572
80	2455.0		9.46	21.45	78.55	0.510
63	3567.2		13.75	35.20	64.80	0.805
50	1652.3		6.37	41.57	58.43	0.448
40	2138.4		8.24	49.81	50.19	0.681
31.5	3286.7		12.67	62.48	37.52	1.218
25	1124.2		4.33	66.81	33.19	0.531
20	1382.8		5.33	72.14	27.86	0.784
14	1829.4		7.05	79.19	20.81	0.818
12.5		397.0	3.14	82.33	17.67	1.445
10		335.3	2.65	84.99	15.01	0.730
6.3		567.8	4.50	89.48	10.52	0.770
4		466.1	3.69	93.17	6.83	0.951
2		335.2	2.65	95.83	4.17	0.710
1		210.3	1.67	97.49	2.51	0.734
0.5		119.3	0.94	98.44	1.56	0.681
0.25		112.1	0.89	99.32	0.68	
<0,25		85.5	0.68			
Total	**20547.0**	**2628.6**	100.00			

Table III-6 JS1 Gamma row 1 sieving table

Row 2

Date of Blast:		18/06/2015		Date of Sieve Analysis:	08/07/2015	
Explosive	**Length**	147.0	[cm]	**Total Mass:**	24300.0	[g]
	Type	20	[g/m]	**Total Mass < 14 mm:**	6800.0	[g]
	Amount	29.40	[g]	**Screen Feed < 14 mm:**	3427.7	[g]
Specific Charge		1209.88	[g/t]	**Other:**	243.5	[g]
				Loss:	7.3	[g]

Mesh Size [mm]	**Mass [g]**		**Mass [%]**	**Retained [%]**	**Passing [%]**	**Local Gradient**
125	0.0		0.00	0.00	100.00	
100	0.0		0.00	0.00	100.00	0.000
80	2894.4		12.02	12.02	87.98	0.574
63	3111.0		12.92	24.94	75.06	0.665
50	4389.4		18.23	43.17	56.83	1.204
40	1188.9		4.94	48.11	51.89	0.407
31.5	1062.4		4.41	52.52	47.48	0.372
25	1257.8		5.22	57.74	42.26	0.504
20	1257.4		5.22	62.96	37.04	0.591
14	2117.7		8.79	71.76	28.24	0.760
12.5		301.7	2.51	74.27	25.73	0.820
10		512.6	4.26	78.53	21.47	0.811
6.3		788.4	6.55	85.08	14.92	0.788
4		670.9	5.58	90.66	9.34	1.030
2		379.3	3.15	93.81	6.19	0.594
1		247.0	2.05	95.86	4.14	0.581
0.5		129.0	1.07	96.93	3.07	0.433
0.25		112.0	0.93	97.86	2.14	
<0,25		257.0	2.14			
Total	**17279.0**	**3397.9**	100.00			

Table III-7 JS1 Gamma row 2 sieving table

Row 3

Date of Blast:		18/06/2015		Date of Sieve Analysis:	08/07/2015	
Explosive	**Length**	147.0	[cm]	**Total Mass:**	24210.0	[g]
	Type	20	[g/m]	**Total Mass < 14 mm:**	8680.0	[g]
	Amount	29.40	[g]	**Screen Feed < 14 mm:**	4276.0	[g]
Specific Charge		1214.37	[g/t]	**Other:**	278.2	[g]
				Loss:	28.8	[g]

Mesh Size [mm]	**Mass [g]**		**Mass [%]**	**Retained [%]**	**Passing [%]**	**Local Gradient**
125	0.0		0.00	0.00	100.00	
100	0.0		0.00	0.00	100.00	0.000
80	0.0		0.00	0.00	100.00	0.000
63	667.4		2.78	2.78	97.22	0.118
50	2783.5		11.60	14.38	85.62	0.550
40	2832.3		11.80	26.18	73.82	0.664
31.5	1745.7		7.27	33.45	66.55	0.434
25	2126.1		8.86	42.31	57.69	0.618
20	2249.3		9.37	51.68	48.32	0.794
14	2919.1		12.16	63.84	36.16	0.813
12.5		402.9	3.49	67.33	32.67	0.895
10		636.7	5.51	72.84	27.16	0.828
6.3		1011.4	8.76	81.60	18.40	0.843
4		780.4	6.76	88.36	11.64	1.008
2		476.7	4.13	92.49	7.51	0.632
1		289.9	2.51	95.00	5.00	0.587
0.5		151.4	1.31	96.31	3.69	0.439
0.25		141.0	1.22	97.53	2.47	
<0,25		285.2	2.47			
Total	**15323.4**	**4175.6**	100.00			

Table III-8 JS1 Gamma row 3 sieving table

JS2 Beta

Row 1

Date of Blast:		22/06/2015		Date of Sieve Analysis:	23/06/2015	
Explosive	**Length**	147.0	[cm]	**Total Mass:**	25420.0	[g]
	Type	20	[g/m]	**Total Mass < 14 mm:**	4850.0	[g]
	Amount	29.40	[g]	**Screen Feed < 14 mm:**	2450.0	[g]
Specific Charge		1156.57	[g/t]	**Other:**	286.3	[g]
				Loss:	96.7	[g]

Mesh Size [mm]	**Mass [g]**		**Mass [%]**	**Retained [%]**	**Passing [%]**	**Local Gradient**
125	0.0		0.00	0.00	100.00	
100	0.0		0.00	0.00	100.00	0.000
80	2273.2		9.00	9.00	91.00	0.423
63	1912.4		7.57	16.57	83.43	0.364
50	3498.5		13.85	30.42	69.58	0.785
40	3963.5		15.69	46.11	53.89	1.145
31.5	3040.5		12.04	58.15	41.85	1.058
25	1901.0		7.53	65.67	34.33	0.858
20	1882.0		7.45	73.13	26.87	1.097
14	1938.4		7.67	80.80	19.20	0.943
12.5		311.9	2.69	83.49	16.51	1.331
10		345.0	2.97	86.46	13.54	0.890
6.3		531.3	4.58	91.04	8.96	0.894
4		333.5	2.87	93.92	6.08	0.852
2		273.8	2.36	96.28	3.72	0.708
1		152.4	1.31	97.59	2.41	0.628
0.5		78.4	0.68	98.27	1.73	0.475
0.25		73.1	0.63	98.90	1.10	
<0,25		128.1	1.10			
Total	**20409.5**	**2227.5**	100.00			

Table III-9 JS2 Beta row 1 sieving table

Row 2

Date of Blast:		22/06/2015		Date of Sieve Analysis:	23/06/2015	
Explosive	**Length**	147.0	[cm]	**Total Mass:**	24500.0	[g]
	Type	20	[g/m]	**Total Mass < 14 mm:**	5950.0	[g]
	Amount	29.40	[g]	**Screen Feed < 14 mm:**	2950.0	[g]
Specific Charge		1200.00	[g/t]	**Other:**	203.0	[g]
				Loss:	634.5	[g]

Mesh Size [mm]	**Mass [g]**		**Mass [%]**	**Retained [%]**	**Passing [%]**	**Local Gradient**
125	0.0		0.00	0.00	100.00	
100	0.0		0.00	0.00	100.00	0.000
80	0.0		0.00	0.00	100.00	0.000
63	2059.0		8.44	8.44	91.56	0.369
50	4702.0		19.28	27.72	72.28	1.023
40	4219.1		17.30	45.01	54.99	1.226
31.5	2129.0		8.73	53.74	46.26	0.723
25	1633.6		6.70	60.44	39.56	0.677
20	1640.0		6.72	67.16	32.84	0.835
14	2061.4		8.45	75.61	24.39	0.834
12.5		287.7	3.16	78.77	21.23	1.226
10		454.2	4.99	83.77	16.23	1.202
6.3		66.2	0.73	84.49	15.51	0.099
4		467.3	5.14	89.63	10.37	0.886
2		366.1	4.03	93.66	6.34	0.709
1		212.0	2.33	95.99	4.01	0.661
0.5		102.6	1.13	97.12	2.88	0.476
0.25		84.3	0.93	98.04	1.96	
<0,25		178.0	1.96			
Total	**18444.1**	**2218.4**	100.00			

Table III-10 JS2 Beta row 2 sieving table

Row 3

Date of Blast:		22/06/2015		Date of Sieve Analysis:	23/06/2015	
Explosive	**Length**	147.0	[cm]	**Total Mass:**	23830.0	[g]
	Type	20	[g/m]	**Total Mass < 14 mm:**	7510.0	[g]
	Amount	29.40	[g]	**Screen Feed < 14 mm:**	3789.0	[g]
Specific Charge		1233.74	[g/t]	**Other:**	177.2	[g]
				Loss:	38.5	[g]

Mesh Size [mm]	**Mass [g]**		**Mass [%]**	**Retained [%]**	**Passing [%]**	**Local Gradient**
125	0.0		0.00	0.00	100.00	
100	0.0		0.00	0.00	100.00	0.000
80	0.0		0.00	0.00	100.00	0.000
63	0.0		0.00	0.00	100.00	0.000
50	3852.4		16.23	16.23	83.77	0.766
40	2803.5		11.81	28.04	71.96	0.681
31.5	2844.2		11.98	40.03	59.97	0.763
25	2109.7		8.89	48.91	51.09	0.694
20	1870.4		7.88	56.79	43.21	0.751
14	2745.0		11.57	68.36	31.64	0.873
12.5		339.0	2.92	71.28	28.72	0.856
10		512.1	4.42	75.70	24.30	0.749
6.3		926.2	7.99	83.69	16.31	0.863
4		616.3	5.32	89.01	10.99	0.868
2		440.9	3.80	92.81	7.19	0.613
1		287.5	2.48	95.29	4.71	0.610
0.5		142.6	1.23	96.52	3.48	0.437
0.25		132.0	1.14	97.66	2.34	
<0,25		271.5	2.34			
Total	**16225.2**	**3668.1**	100.00			

Table III-11 JS2 Beta row 3 sieving table

JS3 Alpha

Row 1

Date of Blast:		11/06/2015		Date of Sieve Analysis:	15/06/2015	
Explosive	**Length**	147.0	[cm]	**Total Mass:**	28630.0	[g]
	Type	20	[g/m]	**Total Mass < 14 mm:**	6830.0	[g]
	Amount	29.40	[g]	**Screen Feed < 14 mm:**	3617.9	[g]
Specific Charge		1026.89	[g/t]	**Other:**	293.1	[g]
				Loss:	24.8	[g]

Mesh Size [mm]	**Mass [g]**		**Mass [%]**	**Retained [%]**	**Passing [%]**	**Local Gradient**
125	0.0		0.00	0.00	100.00	
100	3019.4		10.48	10.48	89.52	0.496
80	1317.4		4.57	15.05	84.95	0.235
63	2674.2		9.28	24.33	75.67	0.484
50	2552.3		8.86	33.19	66.81	0.539
40	3251.7		11.29	44.48	55.52	0.829
31.5	3100.7		10.76	55.24	44.76	0.902
25	1566.5		5.44	60.68	39.32	0.560
20	1844.2		6.40	67.08	32.92	0.796
14	2654.3		9.21	76.29	23.71	0.920
12.5		324.5	2.47	78.76	21.24	0.969
10		597.4	4.54	83.30	16.70	1.078
6.3		761.1	5.78	89.08	10.92	0.920
4		511.1	3.88	92.97	7.03	0.968
2		368.9	2.80	95.77	4.23	0.734
1		198.5	1.51	97.28	2.72	0.637
0.5		98.5	0.75	98.03	1.97	0.465
0.25		92.5	0.70	98.73	1.27	
<0,25		166.8	1.27			
Total	**21980.7**	**3119.3**	100.00			

Table III-12 JS3 Alpha row 1 sieving table

Row 2

Date of Blast:		11/06/2015		Date of Sieve Analysis:	15/06/2015	
Explosive	**Length**	147.0	[cm]	**Total Mass:**	23120.0	[g]
	Type	20	[g/m]	**Total Mass < 14 mm:**	8400.0	[g]
	Amount	29.40	[g]	**Screen Feed < 14 mm:**	4160.0	[g]
Specific Charge		1271.63	[g/t]	**Other:**	222.0	[g]
				Loss:	35.0	[g]

Mesh Size [mm]	**Mass [g]**		**Mass [%]**	**Retained [%]**	**Passing [%]**	**Local Gradient**
125	0.0		0.00	0.00	100.00	
100	0.0		0.00	0.00	100.00	0.000
80	0.0		0.00	0.00	100.00	0.000
63	937.3		4.09	4.09	95.91	0.175
50	833.6		3.64	7.72	92.28	0.167
40	2213.1		9.65	17.38	82.62	0.495
31.5	2792.5		12.18	29.56	70.44	0.668
25	2686.6		11.72	41.28	58.72	0.787
20	2097.0		9.15	50.42	49.58	0.759
14	2966.1		12.94	63.36	36.64	0.848
12.5		393.9	3.52	66.88	33.12	0.892
10		657.8	5.88	72.77	27.23	0.876
6.3		1038.2	9.29	82.05	17.95	0.902
4		710.2	6.35	88.40	11.60	0.962
2		488.7	4.37	92.77	7.23	0.682
1		270.7	2.42	95.19	4.81	0.589
0.5		137.3	1.23	96.42	3.58	0.426
0.25		132.0	1.18	97.60	2.40	
<0,25		268.0	2.40			
Total	**14526.2**	**4096.8**	100.00			

Table III-13 JS3 Alpha row 2 sieving table

Row 3

Date of Blast:		11/06/2015		Date of Sieve Analysis:	15/06/2015	
Explosive	**Length**	147.0	[cm]	**Total Mass:**	24600.0	[g]
	Type	20	[g/m]	**Total Mass < 14 mm:**	10180.0	[g]
	Amount	29.40	[g]	**Screen Feed < 14 mm:**	5250.0	[g]
Specific Charge		1195.12	[g/t]	**Other:**	311.7	[g]
				Loss:	1.5	[g]

Mesh Size [mm]	**Mass [g]**		**Mass [%]**	**Retained [%]**	**Passing [%]**	**Local Gradient**
125	0.0		0.00	0.00	100.00	
100	0.0		0.00	0.00	100.00	0.000
80	0.0		0.00	0.00	100.00	0.000
63	0.0		0.00	0.00	100.00	0.000
50	1562.0		6.30	6.30	93.70	0.282
40	2103.6		8.49	14.79	85.21	0.425
31.5	2458.6		9.92	24.70	75.30	0.518
25	2698.4		10.88	35.59	64.41	0.676
20	2477.8		9.99	45.58	54.42	0.756
14	3310.1		13.35	58.94	41.06	0.789
12.5		530.9	4.59	63.53	36.47	1.047
10		663.5	5.74	69.27	30.73	0.767
6.3		1226.4	10.61	79.88	20.12	0.917
4		776.0	6.71	86.59	13.41	0.894
2		613.0	5.30	91.90	8.10	0.726
1		301.5	2.61	94.51	5.49	0.561
0.5		173.7	1.50	96.01	3.99	0.461
0.25		158.1	1.37	97.38	2.62	
<0,25		303.2	2.62			
Total	**14610.5**	**4746.3**	100.00			

Table III-14 JS3 Alpha row 3 sieving table

JS3 Beta

Row 1

Date of Blast:		01/07/2015		Date of Sieve Analysis:	06/07/2015	
Explosive	**Length**	147.0	[cm]	**Total Mass:**	27960.0	[g]
	Type	20	[g/m]	**Total Mass < 14 mm:**	5600.0	[g]
	Amount	29.40	[g]	**Screen Feed < 14 mm:**	2826.2	[g]
Specific Charge		1051.50	[g/t]	**Other:**	89.2	[g]
				Loss:	-572.9	[g]

Mesh Size [mm]	**Mass [g]**		**Mass [%]**	**Retained [%]**	**Passing [%]**	**Local Gradient**
125	0.0		0.00	0.00	100.00	
100	2440.0		8.56	8.56	91.44	0.401
80	3947.4		13.85	22.41	77.59	0.736
63	2343.8		8.22	30.64	69.36	0.469
50	3865.9		13.57	44.20	55.80	0.942
40	2127.3		7.46	51.67	48.33	0.644
31.5	2889.0		10.14	61.80	38.20	0.985
25	1817.6		6.38	68.18	31.82	0.790
20	1307.0		4.59	72.77	27.23	0.697
14	2161.0		7.58	80.35	19.65	0.915
12.5		347.3	2.46	82.81	17.19	1.182
10		428.5	3.04	85.85	14.15	0.872
6.3		642.7	4.56	90.41	9.59	0.842
4		523.1	3.71	94.12	5.88	1.077
2		304.7	2.16	96.28	3.72	0.661
1		141.0	1.00	97.28	2.72	0.452
0.5		91.0	0.65	97.93	2.07	0.391
0.25		124.2	0.88	98.81	1.19	
<0,25		168.4	1.19			
Total	**22899.0**	**2770.9**	100.00			

Table III-15 JS3 Beta row 1 sieving table

Row 2

Date of Blast:		01/07/2015		Date of Sieve Analysis:	06/07/2015	
Explosive	**Length**	147.0	[cm]	**Total Mass:**	30740.0	[g]
	Type	20	[g/m]	**Total Mass < 14 mm:**	7900.0	[g]
	Amount	29.40	[g]	**Screen Feed < 14 mm:**	3993.4	[g]
Specific Charge		956.41	[g/t]	**Other:**	391.6	[g]
				Loss:	43.4	[g]

Mesh Size [mm]	**Mass [g]**		**Mass [%]**	**Retained [%]**	**Passing [%]**	**Local Gradient**
125	3857.7		12.69	12.69	87.31	
100	0.0		0.00	12.69	87.31	0.000
80	0.0		0.00	12.69	87.31	0.000
63	3110.4		10.23	22.92	77.08	0.522
50	1360.5		4.47	27.39	72.61	0.259
40	3115.3		10.25	37.64	62.36	0.682
31.5	3195.1		10.51	48.15	51.85	0.773
25	2401.8		7.90	56.05	43.95	0.715
20	2811.5		9.25	65.30	34.70	1.059
14	2651.0		8.72	74.02	25.98	0.811
12.5		433.3	2.89	76.91	23.09	1.041
10		628.2	4.19	81.10	18.90	0.897
6.3		849.3	5.67	86.76	13.24	0.771
4		706.3	4.71	91.47	8.53	0.969
2		464.4	3.10	94.57	5.43	0.651
1		258.4	1.72	96.30	3.70	0.551
0.5		131.9	0.88	97.18	2.82	0.391
0.25		127.3	0.85	98.03	1.97	
<0,25		296.0	1.97			
Total	**22503.3**	**3895.1**	100.00			

Table III-16 JS3 Beta row 2 sieving table

L

JS4 Alpha

Row 1

Date of Blast:		25/06/2015		Date of Sieve Analysis:	08/07/2015	
Explosive	**Length**	147.0	[cm]	**Total Mass:**	24900.0	[g]
	Type	20	[g/m]	**Total Mass < 14 mm:**	4140.0	[g]
	Amount	29.40	[g]	**Screen Feed < 14 mm:**	2035.7	[g]
Specific Charge		1180.72	[g/t]	**Other:**	239.0	[g]
				Loss:	12.9	[g]

Mesh Size [mm]	**Mass [g]**		**Mass [%]**	**Retained [%]**	**Passing [%]**	**Local Gradient**
125	0.0		0.00	0.00	100.00	
100	0.0		0.00	0.00	100.00	0.000
80	1447.3		5.85	5.85	94.15	0.270
63	5368.3		21.68	27.53	72.47	1.095
50	1575.6		6.36	33.89	66.11	0.398
40	3223.3		13.02	46.91	53.09	0.983
31.5	3329.7		13.45	60.35	39.65	1.223
25	2573.4		10.39	70.75	29.25	1.315
20	1253.5		5.06	75.81	24.19	0.852
14	1850.0		7.47	83.28	16.72	1.036
12.5		243.7	2.12	85.40	14.60	1.196
10		296.7	2.58	87.98	12.02	0.871
6.3		415.0	3.61	91.59	8.41	0.773
4		319.1	2.77	94.36	5.64	0.881
2		236.4	2.06	96.42	3.58	0.654
1		135.6	1.18	97.60	2.40	0.576
0.5		68.8	0.60	98.20	1.80	0.413
0.25		62.8	0.55	98.74	1.26	
<0,25		144.6	1.26			
Total	**20621.1**	**1922.7**	100.00			

Table III-17 JS4 Alpha row 1 sieving table

Row 2

Date of Blast:		25/06/2015		Date of Sieve Analysis:	08/07/2015	
Explosive	**Length**	147.0	[cm]	**Total Mass:**	24540.0	[g]
	Type	20	[g/m]	**Total Mass < 14 mm:**	5900.0	[g]
	Amount	29.40	[g]	**Screen Feed < 14 mm:**	2895.3	[g]
Specific Charge		1198.04	[g/t]	**Other:**	297.6	[g]
				Loss:	20.7	[g]

Mesh Size [mm]	**Mass [g]**		**Mass [%]**	**Retained [%]**	**Passing [%]**	**Local Gradient**
125	0.0		0.00	0.00	100.00	
100	0.0		0.00	0.00	100.00	0.000
80	2753.6		11.31	11.31	88.69	0.538
63	1433.1		5.89	17.20	82.80	0.288
50	2995.7		12.31	29.51	70.49	0.696
40	2251.1		9.25	38.76	61.24	0.630
31.5	2523.9		10.37	49.13	50.87	0.777
25	2155.1		8.85	57.98	42.02	0.827
20	1848.4		7.59	65.57	34.43	0.893
14	2479.5		10.19	75.76	24.24	0.984
12.5		340.9	2.98	78.74	21.26	1.156
10		429.8	3.75	82.49	17.51	0.870
6.3		661.0	5.77	88.26	11.74	0.865
4		504.7	4.41	92.67	7.33	1.036
2		301.5	2.63	95.30	4.70	0.641
1		191.0	1.67	96.96	3.04	0.632
0.5		93.6	0.82	97.78	2.22	0.452
0.25		86.8	0.76	98.54	1.46	
<0,25		167.3	1.46			
Total	**18440.4**	**2776.6**	100.00			

Table III-18 JS4 Alpha row 2 sieving table

Row 3

Date of Blast:		25/06/2015		Date of Sieve Analysis:	08/07/2015	
Explosive	**Length**	147.0	[cm]	**Total Mass:**	25700.0	[g]
	Type	20	[g/m]	**Total Mass < 14 mm:**	7600.0	[g]
	Amount	29.40	[g]	**Screen Feed < 14 mm:**	3883.6	[g]
Specific Charge		1143.97	[g/t]	**Other:**	499.3	[g]
				Loss:	12.6	[g]

Mesh Size [mm]	**Mass [g]**		**Mass [%]**	**Retained [%]**	**Passing [%]**	**Local Gradient**
125	0.0		0.00	0.00	100.00	
100	0.0		0.00	0.00	100.00	0.000
80	0.0		0.00	0.00	100.00	0.000
63	591.2		2.33	2.33	97.67	0.099
50	3543.0		13.97	16.30	83.70	0.668
40	2834.1		11.17	27.47	72.53	0.642
31.5	2806.0		11.06	38.53	61.47	0.693
25	2590.8		10.21	48.74	51.26	0.786
20	2426.2		9.56	58.31	41.69	0.926
14	2975.9		11.73	70.04	29.96	0.926
12.5		642.8	5.20	75.24	24.76	1.682
10		556.9	4.50	79.74	20.26	0.900
6.3		767.3	6.21	85.95	14.05	0.792
4		600.5	4.86	90.80	9.20	0.934
2		425.5	3.44	94.25	5.75	0.676
1		245.2	1.98	96.23	3.77	0.610
0.5		125.2	1.01	97.24	2.76	0.451
0.25		115.7	0.94	98.18	1.82	
<0,25		225.4	1.82			
Total	**17767.2**	**3704.5**	100.00			

Table III-19 JS4 Alpha row 3 sieving table

JS4 Beta

Row 1

Date of Blast:		03/07/2015		Date of Sieve Analysis:	06/07/2015	
Explosive	**Length**	147.0	[cm]	**Total Mass:**	24340.0	[g]
	Type	20	[g/m]	**Total Mass < 14 mm:**	3950.0	[g]
	Amount	29.40	[g]	**Screen Feed < 14 mm:**	1951.8	[g]
Specific Charge		1207.89	[g/t]	**Other:**	89.1	[g]
				Loss:	138.0	[g]

Mesh Size [mm]	**Mass [g]**		**Mass [%]**	**Retained [%]**	**Passing [%]**	**Local Gradient**
125	0.0		0.00	0.00	100.00	
100	0.0		0.00	0.00	100.00	0.000
80	6345.0		26.15	26.15	73.85	1.358
63	2848.0		11.74	37.88	62.12	0.724
50	2753.0		11.34	49.23	50.77	0.873
40	2419.8		9.97	59.20	40.80	0.980
31.5	1775.5		7.32	66.51	33.49	0.827
25	1632.7		6.73	73.24	26.76	0.970
20	1125.1		4.64	77.88	22.12	0.853
14	1418.7		5.85	83.72	16.28	0.860
12.5		201.7	1.83	85.55	14.45	1.051
10		228.8	2.07	87.62	12.38	0.694
6.3		490.0	4.44	92.06	7.94	0.961
4		310.6	2.81	94.87	5.13	0.963
2		270.8	2.45	97.33	2.67	0.940
1		138.2	1.25	98.58	1.42	0.912
0.5		73.1	0.66	99.24	0.76	0.906
0.25		70.6	0.64	99.88	0.12	
<0,25		13.1	0.12			
Total	**20317.8**	**1796.9**	100.00			

Table III-20 JS4 Beta row 1 sieving table

Row 2

Date of Blast:		03/07/2015		Date of Sieve Analysis:	06/07/2015	
Explosive	**Length**	147.0	[cm]	**Total Mass:**	27060.0	[g]
	Type	20	[g/m]	**Total Mass < 14 mm:**	5950.0	[g]
	Amount	29.40	[g]	**Screen Feed < 14 mm:**	2984.0	[g]
Specific Charge		1086.47	[g/t]	**Other:**	223.0	[g]
				Loss:	11.7	[g]

Mesh Size [mm]	**Mass [g]**		**Mass [%]**	**Retained [%]**	**Passing [%]**	**Local Gradient**
125	0.0		0.00	0.00	100.00	
100	0.0		0.00	0.00	100.00	0.000
80	3731.6		13.88	13.88	86.12	0.670
63	3889.8		14.47	28.35	71.65	0.770
50	4164.7		15.49	43.85	56.15	1.054
40	1618.3		6.02	49.87	50.13	0.508
31.5	2190.0		8.15	58.01	41.99	0.742
25	1711.8		6.37	64.38	35.62	0.712
20	1447.5		5.38	69.77	30.23	0.735
14	2177.1		8.10	77.87	22.13	0.874
12.5		340.9	2.58	80.44	19.56	1.092
10		484.5	3.66	84.10	15.90	0.929
6.3		666.4	5.04	89.14	10.86	0.825
4		536.9	4.06	93.20	6.80	1.030
2		331.3	2.50	95.70	4.30	0.662
1		214.5	1.62	97.32	2.68	0.683
0.5		103.7	0.78	98.11	1.89	0.500
0.25		80.9	0.61	98.72	1.28	
<0,25		169.4	1.28			
Total	**20930.8**	**2928.5**	100.00			

Table III-21 JS4 Beta row 2 sieving table

Row 3

Date of Blast:		03/07/2015		Date of Sieve Analysis:	06/07/2015	
Explosive	**Length**	147.0	[cm]	**Total Mass:**	24700.0	[g]
	Type	20	[g/m]	**Total Mass < 14 mm:**	8600.0	[g]
	Amount	29.40	[g]	**Screen Feed < 14 mm:**	4854.7	[g]
Specific Charge		1190.28	[g/t]	**Other:**	323.3	[g]
				Loss:	8.6	[g]

Mesh Size [mm]	**Mass [g]**		**Mass [%]**	**Retained [%]**	**Passing [%]**	**Local Gradient**
125	0.0		0.00	0.00	100.00	
100	0.0		0.00	0.00	100.00	0.000
80	0.0		0.00	0.00	100.00	0.000
63	2150.0		8.46	8.46	91.54	0.370
50	2402.1		9.46	17.92	82.08	0.472
40	2702.3		10.64	28.56	71.44	0.622
31.5	2624.2		10.33	38.89	61.11	0.654
25	1958.0		7.71	46.60	53.40	0.583
20	2185.7		8.61	55.21	44.79	0.787
14	2777.7		10.94	66.14	33.86	0.785
12.5		472.4	4.18	70.33	29.67	1.164
10		518.5	4.59	74.92	25.08	0.753
6.3		903.8	8.00	82.92	17.08	0.832
4		701.6	6.21	89.14	10.86	0.996
2		436.9	3.87	93.01	6.99	0.635
1		260.1	2.30	95.31	4.69	0.576
0.5		142.0	1.26	96.57	3.43	0.450
0.25		112.9	1.00	97.57	2.43	
<0,25		274.6	2.43			
Total	**16800.0**	**3822.8**	100.00			

Table III-22 JS4 Beta row 3 sieving table

Reference 1

Row 1

Date of Blast:		10/07/2015		Date of Sieve Analysis:	22/04/2015	
Explosive	**Length**	147.0	[cm]	**Total Mass:**	22950.0	[g]
	Type	20	[g/m]	**Total Mass < 14 mm:**	5200.0	[g]
	Amount	29.40	[g]	**Screen Feed < 14 mm:**	2494.2	[g]
Specific Charge		1281.05	[g/t]	**Other:**	325.8	[g]
				Loss:	33.9	[g]

Mesh Size [mm]	**Mass [g]**		**Mass [%]**	**Retained [%]**	**Passing [%]**	**Local Gradient**
125	0.0		0.00	0.00	100.00	
100	2107.8		9.30	9.30	90.70	0.438
80	5309.5		23.44	32.74	67.26	1.340
63	2273.1		10.03	42.77	57.23	0.676
50	1434.5		6.33	49.11	50.89	0.507
40	1755.3		7.75	56.85	43.15	0.740
31.5	1086.0		4.79	61.65	38.35	0.493
25	1052.4		4.65	66.29	33.71	0.559
20	946.6		4.18	70.47	29.53	0.593
14	1490.0		6.58	77.05	22.95	0.706
12.5		304.6	2.88	79.93	20.07	1.182
10		275.0	2.60	82.52	17.48	0.621
6.3		561.8	5.31	87.83	12.17	0.784
4		404.0	3.82	91.65	8.35	0.829
2		282.7	2.67	94.32	5.68	0.556
1		210.3	1.99	96.31	3.69	0.621
0.5		99.3	0.94	97.24	2.76	0.423
0.25		99.5	0.94	98.18	1.82	
<0.25		192.1	1.82			
Total	**17455.2**	**2429.3**	100.00			

Table III-23 Reference 1 row 1 sieving table

Row 2

Date of Blast:		10/07/2015		Date of Sieve Analysis:	22/07/2015	
Explosive	**Length**	147.0	[cm]	**Total Mass:**	26350.0	[g]
	Type	20	[g/m]	**Total Mass < 14 mm:**	5900.0	[g]
	Amount	29.40	[g]	**Screen Feed < 14 mm:**	2886.8	[g]
Specific Charge		1115.75	[g/t]	**Other:**	238.7	[g]
				Loss:	2.0	[g]

Mesh Size [mm]	**Mass [g]**		**Mass [%]**	**Retained [%]**	**Passing [%]**	**Local Gradient**
125	7132.0		27.37	27.37	72.63	
100	0.0		0.00	27.37	72.63	0.000
80	2774.0		10.65	38.02	61.98	0.710
63	1791.3		6.87	44.89	55.11	0.492
50	1944.8		7.46	52.36	47.64	0.630
40	1448.2		5.56	57.91	42.09	0.556
31.5	1008.0		3.87	61.78	38.22	0.404
25	1066.0		4.09	65.87	34.13	0.490
20	1032.5		3.96	69.84	30.16	0.553
14	1959.3		7.52	77.36	22.64	0.804
12.5		301.4	2.32	79.68	20.32	0.954
10		414.7	3.19	82.87	17.13	0.766
6.3		635.0	4.89	87.76	12.24	0.728
4		530.8	4.09	91.85	8.15	0.895
2		369.0	2.84	94.69	5.31	0.619
1		242.3	1.87	96.56	3.44	0.625
0.5		138.4	1.07	97.62	2.38	0.535
0.25		129.7	1.00	98.62	1.38	
<0.25		178.7	1.38			
Total	**20156.1**	**2940.0**	100.00			

Table III-24 Reference 1 row 2 sieving table

Row 3

Date of Blast:		10/07/2015		Date of Sieve Analysis:	23/07/2015	
Explosive	**Length**	147.0	[cm]	**Total Mass:**	25180.0	[g]
	Type	20	[g/m]	**Total Mass < 14 mm:**	7350.0	[g]
	Amount	29.40	[g]	**Screen Feed < 14 mm:**	3630.2	[g]
Specific Charge		1167.59	[g/t]	**Other:**	211.6	[g]
				Loss:	13.1	[g]

Mesh Size [mm]	**Mass [g]**		**Mass [%]**	**Retained [%]**	**Passing [%]**	**Local Gradient**
125	0.0		0.00	0.00	100.00	
100	0.0		0.00	0.00	100.00	0.000
80	975.0		3.91	3.91	96.09	0.179
63	3496.2		14.01	17.91	82.09	0.659
50	1163.6		4.66	22.58	77.42	0.253
40	3932.6		15.76	38.33	61.67	1.020
31.5	2530.7		10.14	48.47	51.53	0.752
25	1984.0		7.95	56.42	43.58	0.725
20	1431.5		5.74	62.15	37.85	0.632
14	2096.6		8.40	70.55	29.45	0.704
12.5		503.5	4.09	74.64	25.36	1.319
10		500.0	4.06	78.70	21.30	0.782
6.3		730.0	5.93	84.63	15.37	0.706
4		513.3	4.17	88.80	11.20	0.697
2		485.9	3.95	92.75	7.25	0.627
1		288.3	2.34	95.09	4.91	0.563
0.5		165.5	1.34	96.44	3.56	0.462
0.25		205.4	1.67	98.10	1.90	
<0.25		233.4	1.90			
Total	**17610.2**	**3625.3**	100.00			

Table III-25 Reference 1 row 3 sieving table

Reference 2

Row 1

Date of Blast:		12/05/2015		Date of Sieve Analysis:	15/05/2015	
Explosive	**Length**	147.0	[cm]	**Total Mass:**	24640.0	[g]
	Type	20	[g/m]	**Total Mass < 14 mm:**	4385.4	[g]
	Amount	29.40	[g]	**Screen Feed < 14 mm:**	2400.0	[g]
Specific Charge		1193.18	[g/t]	**Other:**	655.1	[g]
				Loss:	-51.0	[g]

Mesh Size [mm]	**Mass [g]**		**Mass [%]**	**Retained [%]**	**Passing [%]**	**Local Gradient**
125	0.0		0.00	0.00	100.00	
100	2469.4		10.06	10.06	89.94	0.475
80	5850.8		23.83	33.89	66.11	1.379
63	4328.1		17.63	51.51	48.49	1.298
50	1852.0		7.54	59.06	40.94	0.732
40	1109.9		4.52	63.58	36.42	0.524
31.5	1518.5		6.18	69.76	30.24	0.779
25	857.7		3.49	73.26	26.74	0.531
20	1075.5		4.38	77.64	22.36	0.802
14	1105.6		4.50	82.14	17.86	0.630
12.5		248.2	2.35	84.49	15.51	1.247
10		237.5	2.25	86.75	13.25	0.703
6.3		408.8	3.88	90.62	9.38	0.749
4		295.5	2.80	93.43	6.57	0.782
2		247.1	2.34	95.77	4.23	0.636
1		144.8	1.37	97.14	2.86	0.566
0.5		75.7	0.72	97.86	2.14	0.418
0.25		64.7	0.61	98.48	1.52	
<0,25		160.7	1.52			
Total	**20167.5**	**1883.0**	100.00			

Table III-26 Reference 2 row 1 sieving table

Row 2

Date of Blast:		12/05/2015		Date of Sieve Analysis:	18/05/2015	
Explosive	**Length**	147.0	[cm]	**Total Mass:**	23990.0	[g]
	Type	20	[g/m]	**Total Mass < 14 mm:**	6600.6	[g]
	Amount	29.40	[g]	**Screen Feed < 14 mm:**	3367.5	[g]
Specific Charge		1225.51	[g/t]	**Other:**	258.7	[g]
				Loss:	50.0	[g]

Mesh Size [mm]	**Mass [g]**		**Mass [%]**	**Retained [%]**	**Passing [%]**	**Local Gradient**
125	0.0		0.00	0.00	100.00	
100	0.0		0.00	0.00	100.00	0.000
80	6449.5		26.73	26.73	73.27	1.394
63	1418.2		5.88	32.60	67.40	0.350
50	2115.6		8.77	41.37	58.63	0.603
40	1619.3		6.71	48.08	51.92	0.545
31.5	1304.4		5.41	53.49	46.51	0.460
25	1420.0		5.88	59.37	40.63	0.585
20	1179.0		4.89	64.26	35.74	0.574
14	2024.0		8.39	72.65	27.35	0.750
12.5		329.2	3.09	75.73	24.27	1.056
10		383.6	3.60	79.33	20.67	0.719
6.3		669.8	6.28	85.61	14.39	0.783
4		453.0	4.25	89.85	10.15	0.770
2		402.8	3.78	93.63	6.37	0.671
1		224.3	2.10	95.73	4.27	0.578
0.5		117.5	1.10	96.83	3.17	0.430
0.25		89.4	0.84	97.67	2.33	
<0,25		248.6	2.33			
Total	**17530.0**	**2918.2**	100.00			

Table III-27 Reference 2 row 2 sieving table

Row 3

Date of Blast:		12/05/2015		Date of Sieve Analysis:	18/05/2015	
Explosive	**Length**	147.0	[cm]	**Total Mass:**	24260.0	[g]
	Type	20	[g/m]	**Total Mass < 14 mm:**	7311.5	[g]
	Amount	29.40	[g]	**Screen Feed < 14 mm:**	3725.6	[g]
Specific Charge		1211.87	[g/t]	**Other:**	86.6	[g]
				Loss:	21.2	[g]

Mesh Size [mm]	**Mass [g]**		**Mass [%]**	**Retained [%]**	**Passing [%]**	**Local Gradient**
125	0.0		0.00	0.00	100.00	
100	1679.8		6.89	6.89	93.11	0.320
80	0.0		0.00	6.89	93.11	0.000
63	1562.0		6.41	13.30	86.70	0.298
50	3072.4		12.60	25.90	74.10	0.680
40	2214.1		9.08	34.98	65.02	0.586
31.5	2943.6		12.07	47.06	52.94	0.860
25	2108.9		8.65	55.71	44.29	0.772
20	1435.7		5.89	61.59	38.41	0.639
14	2051.6		8.42	70.01	29.99	0.693
12.5		401.2	3.44	73.45	26.55	1.075
10		523.8	4.49	77.94	22.06	0.830
6.3		803.4	6.89	84.83	15.17	0.810
4		559.2	4.79	89.62	10.38	0.836
2		456.2	3.91	93.53	6.47	0.682
1		251.4	2.16	95.69	4.31	0.585
0.5		116.8	1.00	96.69	3.31	0.381
0.25		97.0	0.83	97.52	2.48	
<0,25		289.2	2.48			
Total	**17068.1**	**3498.2**	100.00			

Table III-28 Reference 2 row 3 sieving table

Reference 3

Row 1

Date of Blast:		29/06/2015		Date of Sieve Analysis:	**07/07/2015**	
Explosive	**Length**	147.0	[cm]	**Total Mass:**	24980.0	[g]
	Type	20	[g/m]	**Total Mass < 14 mm:**	4200.0	[g]
	Amount	29.40	[g]	**Screen Feed < 14 mm:**	2093.0	[g]
Specific Charge		1176.94	[g/t]	**Other:**	205.2	[g]
				Loss:	22.5	[g]

Mesh Size [mm]	**Mass [g]**		**Mass [%]**	**Retained [%]**	**Passing [%]**	**Local Gradient**
125	4515.5		18.17	18.17	81.83	
100	6756.0		27.18	45.35	54.65	1.809
80	2786.9		11.21	56.56	43.44	1.029
63	1277.8		5.14	61.70	38.30	0.527
50	1192.9		4.80	66.50	33.50	0.579
40	637.1		2.56	69.06	30.94	0.357
31.5	787.2		3.17	72.23	27.77	0.452
25	1069.7		4.30	76.53	23.47	0.729
20	746.9		3.00	79.54	20.46	0.614
14	886.0		3.56	83.10	16.90	0.537
12.5		270.5	2.30	85.40	14.60	1.290
10		220.4	1.87	87.27	12.73	0.615
6.3		457.4	3.89	91.16	8.84	0.788
4		296.2	2.52	93.67	6.33	0.737
2		266.8	2.27	95.94	4.06	0.640
1		175.1	1.49	97.43	2.57	0.658
0.5		91.8	0.78	98.21	1.79	0.521
0.25		99.7	0.85	99.05	0.95	
<0,25		111.4	0.95			
Total	**20656.0**	**1989.3**	100.00			

Table III-29 Reference 3 row 1 sieving table

Row 2

Date of Blast:		29/06/2015		Date of Sieve Analysis:	07/07/2015	
Explosive	**Length**	147.0	[cm]	**Total Mass:**	25200.0	[g]
	Type	20	[g/m]	**Total Mass < 14 mm:**	6220.0	[g]
	Amount	29.40	[g]	**Screen Feed < 14 mm:**	3023.3	[g]
Specific Charge		1166.67	[g/t]	**Other:**	136.5	[g]
				Loss:	14.4	[g]

Mesh Size [mm]	**Mass [g]**		**Mass [%]**	**Retained [%]**	**Passing [%]**	**Local Gradient**
125	0.0		0.00	0.00	100.00	
100	3279.7		13.08	13.08	86.92	0.628
80	0.0		0.00	13.08	86.92	0.000
63	4907.3		19.57	32.65	67.35	1.068
50	2458.4		9.80	42.45	57.55	0.681
40	1956.7		7.80	50.26	49.74	0.653
31.5	1385.9		5.53	55.78	44.22	0.493
25	1254.3		5.00	60.79	39.21	0.519
20	1424.5		5.68	66.47	33.53	0.701
14	2188.5		8.73	75.19	24.81	0.845
12.5		306.5	2.54	77.73	22.27	0.952
10		512.4	4.24	81.97	18.03	0.947
6.3		661.8	5.48	87.45	12.55	0.784
4		497.3	4.12	91.57	8.43	0.875
2		406.7	3.37	94.93	5.07	0.735
1		236.1	1.95	96.89	3.11	0.703
0.5		107.5	0.89	97.78	2.22	0.485
0.25		151.9	1.26	99.03	0.97	
<0,25		116.9	0.97			
Total	**18855.3**	**2997.1**	100.00			

Table III-30 Reference 3 row 2 sieving table

Row 3

Date of Blast:		29/06/2015		Date of Sieve Analysis:	07/07/2015	
Explosive	**Length**	147.0	[cm]	**Total Mass:**	24980.0	[g]
	Type	20	[g/m]	**Total Mass < 14 mm:**	7600.0	[g]
	Amount	29.40	[g]	**Screen Feed < 14 mm:**	3766.7	[g]
Specific Charge		1176.94	[g/t]	**Other:**	144.5	[g]
				Loss:	1663.8	[g]

Mesh Size [mm]	**Mass [g]**		**Mass [%]**	**Retained [%]**	**Passing [%]**	**Local Gradient**
125	0.0		0.00	0.00	100.00	
100	0.0		0.00	0.00	100.00	0.000
80	0.0		0.00	0.00	100.00	0.000
63	2641.4		11.34	11.34	88.66	0.504
50	2076.2		8.92	20.26	79.74	0.459
40	2733.7		11.74	32.00	68.00	0.714
31.5	2536.6		10.89	42.89	57.11	0.731
25	1662.1		7.14	50.02	49.98	0.578
20	1490.1		6.40	56.42	43.58	0.614
14	2548.3		10.94	67.37	32.63	0.811
12.5		325.5	2.91	70.28	29.72	0.824
10		533.7	4.77	75.05	24.95	0.784
6.3		921.0	8.23	83.28	16.72	0.867
4		678.6	6.07	89.35	10.65	0.993
2		397.6	3.55	92.90	7.10	0.586
1		282.9	2.53	95.43	4.57	0.636
0.5		138.3	1.24	96.67	3.33	0.456
0.25		113.4	1.01	97.68	2.32	
<0,25		259.0	2.32			
Total	**15688.4**	**3650.0**	100.00			

Table III-31 Reference 3 row 3 sieving table

JS1 Gamma + Reference 3 Cylinder

Date of Blast:		16/07-2015		Date of Sieve Analysis:		
Explosive	**Length**	147.0	[cm]	**Total Mass:**	10510.0	[g]
	Type	20	[g/m]	**Total Mass < 14 mm:**	3600.0	[g]
	Amount	29.40	[g]	**Screen Feed < 14 mm:**	1695.9	[g]
Specific Charge		2797.34	[g/t]	**Other:**	15.2	[g]
				Loss:	164.8	[g]

Mesh Size [mm]	**Mass [g]**		**Mass [%]**	**Retained [%]**	**Passing [%]**	**Local Gradient**
125	0.0		0.00	0.00	100.00	
100	0.0		0.00	0.00	100.00	0.000
80	0.0		0.00	0.00	100.00	0.000
63	0.0		0.00	0.00	100.00	0.000
50	390.8		3.83	3.83	96.17	0.169
40	159.5		1.56	5.40	94.60	0.073
31.5	526.6		5.16	10.56	89.44	0.235
25	1565.4		15.35	25.91	74.09	0.815
20	2106.8		20.66	46.57	53.43	1.465
14	1849.0		18.13	64.70	35.30	1.162
12.5		327.5	6.33	71.02	28.98	1.742
10		281.7	5.44	76.46	23.54	0.932
6.3		468.8	9.05	85.52	14.48	1.051
4		319.3	6.17	91.69	8.31	1.221
2		188.7	3.64	95.33	4.67	0.832
1		96.6	1.87	97.20	2.80	0.736
0.5		47.6	0.92	98.12	1.88	0.573
0.25		46.8	0.90	99.02	0.98	
<0,25		50.8	0.98			
Total	**6598.1**	**1827.8**	100.00			

Table III-32 JS1 Gamma + Reference 3 sieving table

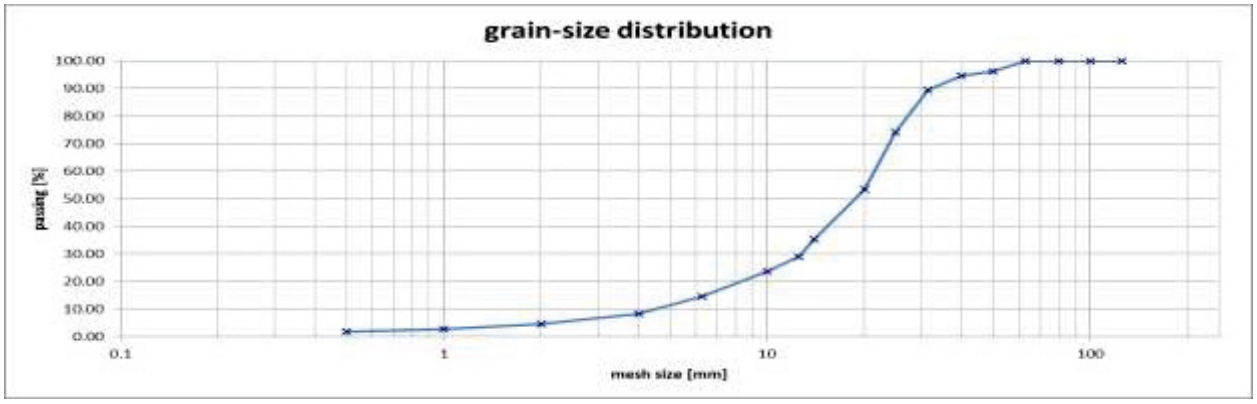

Figure III-1 Grain-Size distribution of the cylinder JS1 Gamma+ Reference 3

JS2 + JS3 Cylinder

Date of Blast:		16/07/2015		Date of Sieve Analysis:	23/07/2015	
Explosive	**Length**	147.0	[cm]	**Total Mass:**	9970.0	[g]
	Type	20	[g/m]	**Total Mass < 14 mm:**	3900.0	[g]
	Amount	29.40	[g]	**Screen Feed < 14 mm:**	1930.3	[g]
Specific Charge		2948.85	[g/t]	**Other:**	1.5	[g]
				Loss:	2.4	[g]

Mesh Size [mm]	**Mass [g]**		**Mass [%]**	**Retained [%]**	**Passing [%]**	**Local Gradient**
125	0.0		0.00	0.00	100.00	
100	0.0		0.00	0.00	100.00	0.000
80	0.0		0.00	0.00	100.00	0.000
63	0.0		0.00	0.00	100.00	0.000
50	0.0		0.00	0.00	100.00	0.000
40	481.9		4.84	4.84	95.16	0.222
31.5	567.0		5.69	10.53	89.47	0.258
25	1754.4		17.61	28.14	71.86	0.948
20	1439.1		14.45	42.59	57.41	1.006
14	1819.7		18.27	60.85	39.15	1.074
12.5		234.1	4.74	65.59	34.41	1.138
10		289.3	5.86	71.44	28.56	0.836
6.3		511.7	10.36	81.80	18.20	0.975
4		346.7	7.02	88.82	11.18	1.072
2		231.7	4.69	93.51	6.49	0.784
1		130.1	2.63	96.14	3.86	0.750
0.5		61.1	1.24	97.38	2.62	0.557
0.25		55.4	1.12	98.50	1.50	
<0,25		74.2	1.50			
Total	**6062.1**	**1934.3**	100.00			

Table III-33 JS2 + JS3 Cylinder sieving table

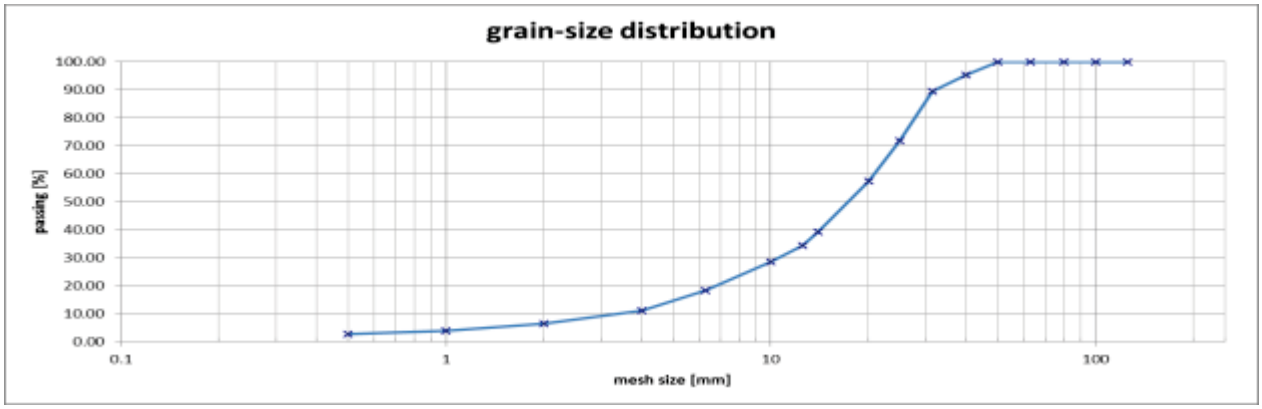

Figure III-2 Grain-Size distribution of the cylinder JS2+JS3

JS2 Beta + JS4 Beta Cylinder

Date of Blast:		16/07/2015		Date of Sieve Analysis:	23/07/2015	
Explosive	**Length**	147.0	[cm]	**Total Mass:**	10460.0	[g]
	Type	20	[g/m]	**Total Mass < 14 mm:**	4000.0	[g]
	Amount	29.40	[g]	**Screen Feed < 14 mm:**	1894.7	[g]
Specific Charge		2810.71	[g/t]	**Other:**	2.3	[g]
				Loss:	-28.2	[g]

Mesh Size [mm]	**Mass [g]**		**Mass [%]**	**Retained [%]**	**Passing [%]**	**Local Gradient**
125	0.0		0.00	0.00	100.00	
100	0.0		0.00	0.00	100.00	0.000
80	0.0		0.00	0.00	100.00	0.000
63	0.0		0.00	0.00	100.00	0.000
50	0.0		0.00	0.00	100.00	0.000
40	352.2		3.37	3.37	96.63	0.154
31.5	630.3		6.04	9.41	90.59	0.270
25	1741.3		16.68	26.09	73.91	0.880
20	1650.8		15.81	41.90	58.10	1.079
14	2066.0		19.79	61.69	38.31	1.167
12.5		239.2	4.72	66.41	33.59	1.161
10		323.5	6.39	72.80	27.20	0.945
6.3		490.3	9.68	82.48	17.52	0.952
4		360.0	7.11	89.59	10.41	1.146
2		217.6	4.30	93.89	6.11	0.768
1		125.0	2.47	96.36	3.64	0.747
0.5		61.0	1.20	97.56	2.44	0.579
0.25		47.8	0.94	98.51	1.49	
<0,25		75.6	1.49			
Total	**6440.6**	**1940.0**	100.00			

Table III-34 JS2 Beta + JS4 Beta cylinder sieving table

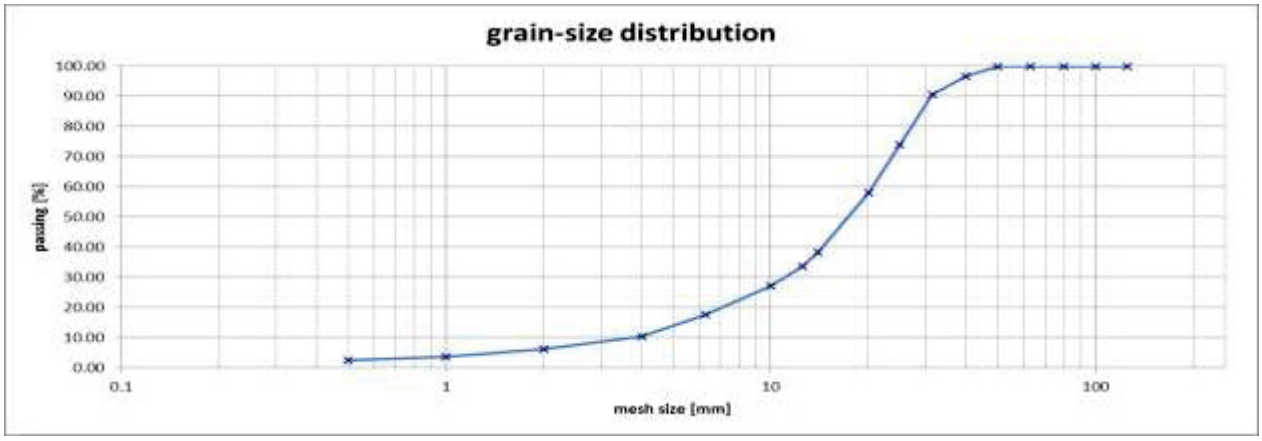

Figure III-3 Grain-Size distribution of the cylinder JS2 Beta+JS4 Beta

JS3 Beta Cylinder

Date of Blast:		16/07/2015		Date of Sieve Analysis:	23/07/2015	
Explosive	**Length**	147.0	[cm]	**Total Mass:**	10640.0	[g]
	Type	20	[g/m]	**Total Mass < 14 mm:**	4160.0	[g]
	Amount	29.40	[g]	**Screen Feed < 14 mm:**	2307.6	[g]
Specific Charge		2763.16	[g/t]	**Other:**	0.3	[g]
				Loss:	267.1	[g]

Mesh Size [mm]	**Mass [g]**	**Mass [%]**	**Retained [%]**		**Passing [%]**	**Local Gradient**
125	0.0		0.00	0.00	100.00	
100	0.0		0.00	0.00	100.00	0.000
80	0.0		0.00	0.00	100.00	0.000
63	0.0		0.00	0.00	100.00	0.000
50	308.4		2.91	2.91	97.09	0.128
40	555.7		5.24	8.16	91.84	0.249
31.5	650.7		6.14	14.30	85.70	0.290
25	1985.4		18.74	33.04	66.96	1.068
20	1495.4		14.11	47.15	52.85	1.061
14	1439.5		13.59	60.74	39.26	0.833
12.5		415.6	7.83	68.56	31.44	1.961
10		321.3	6.05	74.61	25.39	0.958
6.3		462.2	8.70	83.32	16.68	0.909
4		333.3	6.28	89.59	10.41	1.039
2		230.7	4.34	93.94	6.06	0.779
1		125.3	2.36	96.30	3.70	0.711
0.5		58.3	1.10	97.39	2.61	0.507
0.25		56.7	1.07	98.46	1.54	
<0,25		81.7	1.54			
Total	**6435.1**	**2085.1**	100.00			

Table III-35 JS3 Beta cylinder sieving table

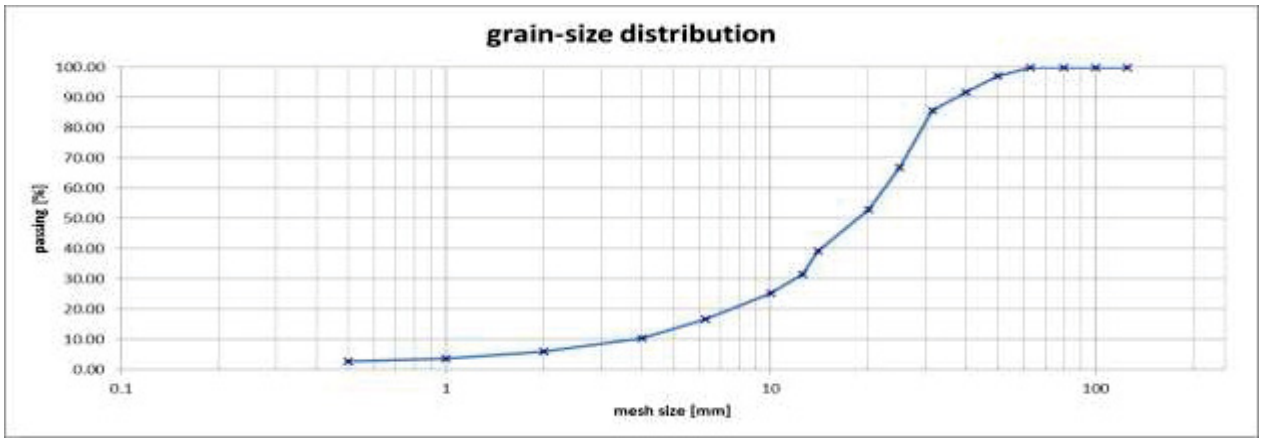

Figure III-4 Grain-Size distribution of the JS3 Cylinder

ANNEX IV: MCD AND MCID TABLES

JS1 ALPHA/ Crack number in a cell	TOTAL/MEAN	SLICE 1	SLICE 2	SLICE 3	SLICE 4
0	76	19	17	18	22
1	133	37	25	30	41
2	254	84	42	54	74
3	234	66	60	45	63
4	124	20	72	16	16
5	30	10	10	5	5
6	6	0	0	0	6
CELLS	452	127	103	95	127
CRACKS	781	217	209	150	205
MCD	1.73	1.71	2.03	1.58	1.61
MCID	0.12	0.11	0.10	0.19	0.09

Table IV-1 MCD and MCID table of JS1 Alpha

JS1 GAMMA/ Crack number in a cell	TOTAL/MEAN	SLICE 1	SLICE 2	SLICE 3	SLICE 4
0	127	39	43	30	15
1	173	56	52	36	29
2	268	50	54	88	76
3	181	30	13	57	81
4	104	8	8	52	36
5	25	0	5	5	15
6	42	0	0	12	30
CELLS	532	132	129	145	126
CRACKS	793	144	132	250	267
MCD	1.49	1.09	1.02	1.72	2.12
MCID	0.08	0.05	0.07	0.11	0.10

Table IV-2 MCD and MCID table of JS1 Gamma

JS2 BETA/ Crack number in a cell	TOTAL/MEAN	SLICE 1	SLICE 2	SLICE 3	SLICE 4
0	81	39	12	12	18
1	150	37	42	31	40
2	246	80	54	52	60
3	219	54	48	45	72
4	124	20	8	44	52
5	50	0	5	30	15
6	18	0	6	12	0
CELLS	471	139	101	103	128
CRACKS	807	191	163	214	239
MCD	1.71	1.37	1.61	2.08	1.87
MCID	0.08	0.07	0.07	0.08	0.09

Table IV-3 MCD and MCID table of JS2 Beta

JS3 ALPHA/ Crack number in a cell	TOTAL/MEAN	SLICE 1	SLICE 2	SLICE 3	SLICE 4
0	131	36	41	28	26
1	149	35	48	35	31
2	198	48	42	60	48
3	189	48	39	45	57
4	74	20	12	30	12
5	25	0	5	10	10
6	12	12	0	0	0
CELLS	470	118	127	120	105
CRACKS	647	163	146	180	158
MCD	1.38	1.38	1.15	1.50	1.50
MCID	0.06	0.06	0.04	0.07	0.08

Table IV-4 MCD and MCID table of JS3 Alpha

JS4 ALPHA/ Crack number in a cell	TOTAL/MEAN	SLICE 1	SLICE 2	SLICE 3	SLICE 4
0	43	10	10	10	13
1	70	17	21	21	11
2	194	46	58	60	30
3	297	63	102	54	78
4	188	28	44	52	64
5	150	10	25	50	65
6	42	0	0	0	42
CELLS	393	80	110	102	101
CRACKS	941	164	250	237	290
MCD	2.39	2.05	2.27	2.32	2.87
MCID	0.09	0.09	0.1	0.08	0.10

Table IV-5 MCD and MCID table of JS4 Alpha

JS4 BETA/ Crack number in a cell	TOTAL/MEAN	SLICE 1	SLICE 2	SLICE 3	SLICE 4
0	41	10	3	14	14
1	69	20	13	12	24
2	206	48	48	54	56
3	279	54	84	87	54
4	240	44	72	56	68
5	115	35	40	5	35
6	54	18	12	12	12
CELLS	398	93	96	99	110
CRACKS	963	219	269	226	249
MCD	2.42	2.35	2.80	2.28	2.26
MCID	0.11	0.11	0.11	0.13	0.09

Table IV-6 MCD and MCID table of JS4 Beta

Reference 1/ Crack number in a cell	TOTAL/MEAN	SLICE 1	SLICE 2	SLICE 3	SLICE 4
0	44	15	12	8	9
1	87	25	20	16	26
2	192	62	46	60	24
3	249	69	66	60	54
4	224	28	52	40	104
5	125	40	25	45	15
6	84	18	12	30	24
CELLS	405	112	97	98	98
CRACKS	961	242	221	251	247
MCD	2.37	2.16	2.28	2.56	2.52
MCID	0.12	0.125	0.11	0.13	0.10
Reference 2/ Crack number in a cell	**TOTAL/MEAN**	**SLICE 1**	**SLICE 2**	**SLICE 3**	**SLICE 4**
0	126	22	25	43	36
1	122	31	30	33	28
2	204	52	52	40	60
3	195	66	45	36	48
4	128	32	72	16	8
5	50	25	0	10	15
6	60	18	6	30	6
CELLS	467	117	115	119	116
CRACKS	759	224	205	165	165
MCD	1.63	1.91	1.78	1.39	1.42
MCID	0.10	0.11	0.10	0.08	0.09
Reference 3/ Crack number in a cell	**TOTAL/MEAN**	**SLICE 1**	**SLICE 2**	**SLICE 3**	**SLICE 4**
0	83	31	26	27	26
1	115	48	31	34	36
2	178	64	48	56	66
3	123	30	63	30	30
4	92	4	40	45	48
5	70	10	30	30	30
6	36	6	18	12	12
CELLS	370	125	120	123	125
CRACKS	614	162	230	207	222
MCD	1.66	1.30	1.92	1.68	1.78
MCID	0.09	0.05	0.08	0.07	0.07

Table IV-7 MCD and MCID table of Reference blocks

ANNEX V: ABBREVIATIONS

Description	Abbreviation
CNU shaped cracks	CNU
Combination of CJB and J90C cracks	CC
Connections between boreholes	Connect
Cracks connecting joints to the boreholes	CJB
Cracks from borehole in sectors between 30-0	CB30-0
Cracks from borehole in sectors between 80-30	CB80-30
Cracks from borehole in sectors between 90-80 and 90-100	CB90-80
Cracks with direction to the boreholes in sectors between 80-30	DIR80-30
Cracks with direction to the boreholes in sectors between 90-80	DIR90-80
Cracks with direction to the boreholes in sectors between 30-0	DIR30-0
Dye penetrant inspection	DPI
Dye penetrant method	DPM
Eddy Current testing	ECT
Inclined cracks	IC
Joint 90° end cracks	J90C
Joint related cracks	JRC
Joint set-system	JS
Liquid penetrant inspection	LPI
Magnetic particle inspection	MPI
Mean crack density	MCD
Mean crack density intersection	MCID
Montanuniversität Leoben	MUL
Non aqueous wet developer	NAWD
Non-destructive testing	NDT
Parallel cracks to the surface	Parallel
Penetrant testing	PT

Description	Abbreviation
Radiography	RT
Reference	REF
Straight cracks from back side	SCB
Ultrasonics	UT
Vertical cracks from the back	VCB

Table V-1 Abbreviations and descriptions